Heterojunction band offset engineering

Alfonso Franciosi
TASC-INFM National Laboratory, Area di Ricerca, I-34012 Trieste, Italy
and
Department of Chemical Engineering and Materials Science, University of Minnesota,
Minneapolis, MN 55455, USA

and

Chris G. Van de Walle
Xerox Palo Alto Research Center, 3333 Coyote Hill Road, Palo Alto, CA 94304, USA

ELSEVIER
Amsterdam–Lausanne–New York–Oxford–Shannon–Tokyo

Contents

ELSEVIER

Surface Science Reports 25 (1996) 1-140

surface science
reports

Heterojunction band offset engineering

Alfonso Franciosi [a,*], Chris G. Van de Walle [b]

[a] *TASC-INFM National Laboratory, Area di Ricerca, I-34012 Trieste, Italy and Department of Chemical Engineering and Materials Science, University of Minnesota, Minneapolis, MN 55455, USA*
[b] *Xerox Palo Alto Research Center, 3333 Coyote Hill Road, Palo Alto, CA 94304, USA*

Manuscript received in final form 3 January 1996

Abstract

Control of band discontinuities in semiconductor heterostructures may introduce a new important degree of freedom in the design of heterojunction devices and allow independent optimization of carrier injection, carrier confinement and ionization thresholds in high speed and optoelectronic devices. We will review recently proposed methods to microscopically control heterojunction parameters by means of local interface dipoles introduced at the heterointerface during growth. A parallel survey of new theoretical models of semiconductor heterojunctions will illustrate our newfound ability to derive from first principles rules of heterojunction behavior. The combination of new empirical methods and theoretical models is establishing the new area of heterojunction engineering in surface and interface science.

1. Introduction

Heterojunction devices have widespread application in modern solid state electronics. In a first broad class of devices, carrier transport is across the interface (HBTs, lasers, photodiodes, LEDs, etc.). In a second class, transport is along the interface (MOSFETs, MODFETs, MESFETs, etc.). Heterojunction parameters such as the valence- and conduction-band discontinuities, and the built-in potentials determine the performance of both classes of devices. For example, they affect carrier confinement on both sides of the active region where radiative recombination occurs in heterojunction lasers, emitter efficiencies in HBTs, as well the gate voltage swing and the gate leakage current in MODFET structures [Kroemer, 1985; Priddy et al., 1987; Cirillo et al., 1986; Malik et al., 1988; Beltram et al., 1991]. Determining heterojunction valence and conduction band offsets and the ability to tune them to a desired application would have an obvious impact on the optimization of both classes of devices. An increasing effort has been devoted in the past few years to in situ analysis of the heterojunction parameters of high quality heterostructures grown by

---

* Corresponding author. Tel.: +39-403756421; fax: 39-40226767; e-mail: franciosi@arts90.area.trieste.it.

SSDI 0167-5729(95)00008-9

state-of-the-art growth methods [Capasso and Margaritondo, 1987; Brillson, 1992; Yu et al., 1992a].

Throughout the 1980s, pioneering studies have focused on the possibility of modulating valence and conduction band offsets by examining the effect of different growth temperatures and sequences on heterojunction band offsets [Kowalczyk et al., 1982; Zurcher and Bauer, 1983; Grant et al., 1985]. Early successes in device-grade materials [Capasso et al., 1985a,b] involved the tuning of the effective potential barriers for electron and hole injection by means of ultrathin ionized donor and acceptor sheets. Such sheets were grown within 10 nm of the metallurgical junction by molecular beam epitaxy (MBE) and gave rise to a sort of microscopic capacitor across the junction [Capasso et al.,1985a]. Other research groups deposited controlled amounts of impurities in the interface region with the target of modifying the local chemical and electrostatic environments and changing the band offsets [Katnani et al., 1985; Niles et al., 1985, 1986; Perfetti et al., 1986].

Such pioneering efforts have had a surprisingly small impact on the device community, because of a number of real or perceived practical difficulties. First, most efforts were limited in scope by the difficulty of reconciling the environment and the mission of existing growth facilities with the target of understanding microscopic junction properties. Secondly, because of the lack of state-of-the-art facilities, few studies involved device-grade materials, or device-compatible impurities. For example, some of the most promising work involved amorphous semiconductor overlayers and alkali metal impurities. Finally, no generally accepted theoretical framework was available to guide the experimental effort. Major questions about the microscopic factors that affected the band offsets and the driving forces behind interface evolution remained largely unanswered.

In the last few years several of these limitations have been removed. Dual purpose MBE facilities devoted to the exploration of interface properties and the fabrication of working devices have been established. These have produced a flurry of new exciting reports, and an unprecedentedly wide range of tunability of band offsets in technologically relevant device materials and structures. In parallel with experiment, a convergence of different theoretical models, including first principles calculations, the theoretical alchemy approach and linear response theory (LRT) results, have finally started to establish a common theoretical framework. The purpose of this review is to illustrate some of these recent experimental and theoretical developments.

Although a brief summary of some of the experimental and theoretical methods will be given in Sections 2 and 3, we will make no attempt at presenting a complete survey of experimental techniques and calculation methods employed in the study of semiconductor heterojunctions. We will mostly focus instead on the techniques that are having the strongest impact on the field, and provide the minimum level of detail required to understand the current literature on the subject. In terms of materials systems, we will focus on a few semiconductor heterojunctions of interest for optoelectronic and high speed device applications, and for which the widest range of tunability for the band offsets has been observed experimentally or predicted theoretically. Most theoretical and experimental studies have identified heterovalent semiconductor junctions with polar orientation as those that exhibit the strongest dependence of interface properties on the local interface environment. Therefore such interfaces may represent a class of highly tunable interface systems, and this review will examine a proportionally large number of heterovalent interface systems (IV/III–V, II–VI/III–V, III–V/IV/III–V, etc.), as compared to isovalent systems (IV/IV, III–V/III–V, etc.).

Electron and hole state energies in solids can be modified by strain and quantum confinement, as extensively observed by optical and transport methods in quantum well (QW) structures. Growing pseudomorphic layers with various amounts of strain (controlled by the lattice constant of the substrate and the composition of the overlayer), for example, can be an effective way of engineering band-lineups. The treatment of quantum confinement is beyond the scope of this paper, but we will briefly discuss the effect of strain on band offsets in Section 3.6, to lay a background for the discussion of some of the experimental results in Section 5.

This review will mostly focus on band-offset modifications that take place in a rather narrow layer (on the order of a few ångström) near the interface. The presence of donors or acceptors in space charge layers on either side of the interface leads to band bending on a length scale of hundreds or even thousands of ångströms (see Fig. 1). These changes in band positions can be calculated by solving Poisson's equation for the system, given appropriate boundary conditions (including the band offsets at the interface), and have also been exploited to vary the effective barrier for electron and hole injection or confinement. We will discuss such doping-related methods briefly in Section 5, but we will emphasize in the rest of the paper band-offset modifications due to dipoles occurring on an atomic length scale in the neighborhood of the interface, i.e., local changes of the band offsets at the metallurgical junction.

Illustration of the theoretical framework that derives from first principles calculations, the theoretical alchemy approach, and LRT results can be found in Section 4, prior to the discussion of most experimental results (Section 5). This was done to better illustrate the relations between the different theoretical models, and simplify comparison of theory and experiment. Most of the experimental results and empirical models proposed in the last few years will be summarized in Section 5. We elected to summarize again when necessary in Section 5 some of the theoretical results described in Section 4 to clarify the discussion of the data. We hope that the reader will forgive us the necessary repetitions that did ensue.

Throughout the text, we adopted the following notation: an A/B or A–B heterojunction implies that an overlayer of semiconductor A is grown on substrate B. Unless noted otherwise, A/B or A–B heterojunctions will be comprised of a crystalline overlayer and a crystalline substrate. We will denote an amorphous semiconductor A as aA, so that a heterojunction involving an amorphous overlayer A and a crystalline substrate B will be denoted as aA/B or aA–B. Doping type in a semiconductor A will be indicated as n-A or p-A. The value of the valence-band discontinuity ΔE_v will be taken as *positive* if the valence-band maximum in A (the overlayer) is *lower* in energy than in B (the substrate), as in AlAs–GaAs, ZnSe–GaAs, or SiO_2–Si heterojunctions. Analogously, the value of the conduction-band discontinuity ΔE_c will be taken as *positive* if the conduction-band minimum in A (the overlayer) is *higher* in energy than in B (the substrate), so that the algebraic sum of the offsets equals the bandgap difference.

2. Experimental methods

2.1. Probing heterojunction interfaces

The performance of any type of heterojunction device is determined by two kinds of interface parameters: the band discontinuities and the built-in potential. A schematic band diagram of a n-isotype semiconductor heterojunction between a semiconductor B and a wider bandgap semiconductor A is shown in Fig. 1. The bandgap difference ΔE_g between the forbidden gaps E_g(A)

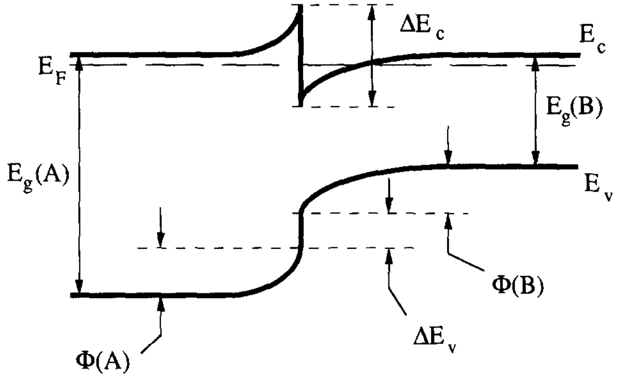

Fig. 1. Heterojunction between two semiconductors A and B with type-I band alignment. The difference between the forbidden gaps of the two semiconductors $\Delta E_g = E_g(A) - E_g(B)$ is distributed between the valence-band discontinuity ΔE_v and the conduction-band discontinuity ΔE_c. Both semiconductors are n-type (n-isotype heterojunction, as can be seen from the position of the Fermi level E_F in the two gaps away from the junction. The barriers due to band bending $\Phi(A)$ and $\Phi(B)$ in each semiconductor give the hetrojunction buit-in potential $\Phi_{bi} = \Phi(A) + \Phi(B)$.

and $E_g(B)$ of the two semiconductors is distributed between the valence-band discontinuity ΔE_v and the conduction-band discontinuity ΔE_c. This type of band alignment, in which the bandgap of the smaller gap material is completely contained within the bandgap of the wider gap material will be referred to as type-I alignment, in analogy with the notation commonly used for the related QW and superlattice structures. Type-I alignment is that encountered in many technologically relevant heterojunction systems, such as AlGaAs–GaAs, SiO_2–Si, HgTe–CdTe, ZnCdSe–ZnSe, ZnSe–GaAs, etc. Different types of alignment, in which the bandgap of one material is only partially contained (type-II alignment) or not contained (type-III alignment) within the bandgap of the other material are also possible. The barriers due to band bending $\Phi(A)$ and $\Phi(B)$ give the heterojunction built-in potential $\Phi_{bi} = \Phi(A) + \Phi(B)$.

Both the band discontinuities and the built-in potential contribute to determine carrier injection or confinement in heterojunction devices, but with important differences. The built-in potential Φ_{bi} is determined by the interface position of the Fermi level E_F, and the problem of finding, predicting or measuring it is related to that of determining the Schottky barrier height in a metal–semiconductor junction. Given an interface position of E_F, the band bending will extend on either side of the metallurgical junction on a length scale that depends on the bulk doping of the two semiconductors. Such a length scale, of the order of the Debye length, can be as long as several thousand ångström in low doped semiconductor, and as short as 50–100 Å for degenerate semiconductors [Sze, 1981]. The band discontinuities, on the other hand, correspond to high electrostatic potential gradients acting on the carriers on the length scale of a single atomic interplanar spacing for ideally abrupt interfaces. Even if one takes into account the gradual evolution of the local electronic density of states that is bound to be present in going from A to B across the heterojunction (see Section 3), or a modicum of atomic intermixing (see Section 5), the corresponding potential gradients will be localized on the scale of a few atomic layers, and mostly independent of doping.

Since knowledge of $\Phi(A)$ and $\Phi(B)$, i.e., of the position of the Fermi level at the interface together with the bulk degeneracies V_A and V_B (the position of E_F in the gap of each semiconductor away from the interface) unequivocally determines the band discontinuities, the two band-bending parameters $\Phi(A)$ and $\Phi(B)$, and the band discontinuities are not strictly independent. Only two experimentally determined independent parameters, in addition to the bulk degeneracies, are required to describe the behavior of the heterojunction. The nature of the band discontinuities and the physical parameters that affect how the bandgap difference is distributed between the valence- and conduction-band offsets have been the subject of an intense experimental and theoretical effort. Good reviews of the experimental situation in this area are available [Capasso and Margaritondo, 1987; Brillson, 1992]. One important issue which has been debated often in the literature is if the band discontinuities are determined by the bulk properties of the two semiconductors comprising the junctions, or if they are affected by the local interface environment. Since only in the former case the band offsets would be expected to be strictly commutative and transitive, a number of authors have attempted to verify the so-called commutativity and transitive rules of heterojunction band offsets. Given three semiconductors A, B and C, the two rules can be stated for the valence band offsets as follows:

$$\Delta E_v(A/B) = -\Delta E_v(B/A), \tag{1}$$

$$\Delta E_v(A/B) + \Delta E_v(B/C) = \Delta E_v(A/C). \tag{2}$$

Similar expressions would hold for the conduction band offsets. Before 1978, band discontinuities were mostly estimated from transport measurements [Milnes and Feucht, 1972; Henisch, 1984]. However, transport measurements are essentially space-averaging techniques in the direction perpendicular to the interface, while the band offsets are spatially localized at the interface [Margaritondo and Franciosi, 1984]. Transport measurements are therefore affected by contact performance, unintentional doping, leakage currents, and have sometimes produced a wide scatter of results for a given interface system [Margaritondo and Perfetti, 1987; Brillson, 1992; Yu et al., 1992a].

A few poineering papers in the late 1970s and early 1980s showed that photoemission spectroscopy techniques could be used to measure valence-band offsets locally, as illustrated in a number of early reviews [Margaritondo and Franciosi, 1984; Capasso and Margaritondo, 1987]. The local character of the measurements derives from the very short inelastic mean free path for photoexcited electrons in solids, which is of the order of 5–10 Å for photoelectron kinetic energies in the 40–100 eV range, and of 20–30 Å in the 1–1.4 keV range. This limits the photoemission sampling depth to a few tens of ångströms even in the X-ray photoemission spectroscopy (XPS) range. Sampling heterojunction band offsets by photoemission therefore requires fabrication of the heterojunction by sequential deposition of thin layers of one semiconductor on top of the other semiconductor. An additional simplification is that, although not strictly a contactless technique, since the sample is grounded to avoid charging, photoemission is relatively unaffected by contact performance.

Photoemission spectroscopy is a powerful local probe that has produced in the past few years reliable offset determinations for over 50 heterojunction systems [Brillson,1992; Yu et al., 1992a], and most of the band-offset engineering experiments described in this review exploited photoemission spectroscopy for in situ analysis of the band offsets. Nevertheless this technique requires careful consideration of the possible effect of chemical shifts, band bending and strain in affecting the data analysis procedure, and has a few intrinsic limitations. First, the uncertainty of present photoemission determinations of the band offsets is of the order of 0.05–0.07 eV, and therefore quite substantial as compared to optical and transport determinations. Secondly, the technique cannot sample interfaces buried below the photoemission sampling depth, and therefore cannot probe directly most device structures. Finally, the photoionization process leaves the system in an excited state. If the resulting many-body effects differ in the two semiconductors comprising the junction, the apparent valence-band offset in photoemission may in principle differ somewhat from the ground-state valence-band offset.

Since the mid-1980s a number of optical measurements of superlattice structures have been used to probe the band discontinuities. While such techniques offer unparalleled energy resolution, they require the fabrication of well characterized multiple quantum well structures (MQWS), and often a detailed knowledge of the associated quantum confined states. Another technique that offers some of the advantages of both optical and transport techniques is internal photoemission spectroscopy. This technique involves transport measurements of carrier optical activation over a band offset, and is finding increasing application also in connection with the development of high brightness coherent infrared sources. The energy resolution of the technique is higher than that of conventional photoemission experiments, provided that an appropriate model for the onset of carrier activation is applied to the data analysis, and one can sample interfaces buried well below the conventional photoemission sampling depth. An important limitation is that the technique is applicable only to semiconductor materials on which ohmic contacts can be fabricated.

All of the experimental probes of the band discontinuities listed above are essentially space-averaging techniques along the interface. Scanning tunneling microscopy (STM) has been recently applied to the study of heterojunction cross sections, in a manner reminiscent of cross-sectional transmission electron microscopy (XTEM) but with greatly simplified sample preparation due to the high surface sensitivity of STM. This technique may represent a probe of the band discontinuities with unparalleled resolution along the interface, and in our opinion the next few years will see a dramatic increase in the number of this type of heterojunction studies.

Transport and optical determination of band offsets will be briefly described in Section 2.2. Section 2.3 will be devoted to photoemission spectroscopy. A few selected results of structural studies of engineered interfaces will be discussed in Section 2.4 as an introduction to the issue of interdiffusion and strain at engineered interfaces.

2.2. Transport and optical determination of the offsets

2.2.1. Transport methods

Transport methods have found widespread use for the determination of the band offsets. Before the application of photoemission techniques, they were essentially the only class of methods available to probe the heterojunction built-in potential and band discontinuities, as well as Schottky barriers in metal–semiconductor contacts [Milnes and Feucht, 1972; Sze, 1981; Henisch, 1984]. Transport techniques can be conventionally divided in two broad classes, namely capacitance–voltage (C–V) and current–voltage (I–V) techniques. A description of the equipment and experimental geometries commonly employed can be found in a variety of texts and review articles [Milnes and Feucht, 1972; Sze, 1981; Brillson, 1982; Henisch, 1984].

For example, C–V measurements can extract the built-in potential Φ_{bi} assuming a conventional square-root dependence for C on $\Phi_{\mathrm{bi}} - qV$, where V is the applied voltage and q is the electron charge. If the distance between the Fermi level E_{F} and the band extrema away from the interface are known a priori from bulk doping, one can obtain a measure of ΔE_c and ΔE_v [Brillson, 1992]. Since the square root dependence corresponds to an ideally abrupt transition at the interface between constant doping profiles in two semiconductors, it may or may not be a good approximation of the real junction behavior. Impurity concentration gradients, as well as the presence of localized charge at the interface can complicate the analysis. The same potential complications, together with carrier recombination, tunneling and shunt currents limit the interpretation of I–V measurements [Forrest, 1987; Brillson, 1992]. Conversely, if the doping profile is known a priori, capacitance techniques can be used to probe the presence of an interface charge at the heterojunction interface [Kroemer et al., 1980; Wang et al., 1985; Brillson, 1992]. A summary of recent transport results for several technologically relevant heterojunctions can be found in several reviews [Margaritondo and Perfetti, 1987; Brillson, 1992].

As an example to illustrate the dispersion in the available transport results, we briefly mention recent transport work on heterovalent heterojunctions that will be examined in detail by other techniques in Sections 2.3 and 4. We select the lattice-matched, prototypical heterovalent heterojunctions Ge–GaAs, and ZnSe–GaAs.

Because of the good lattice match of Ge and GaAs (+0.13% mismatch) and the relatively low growth temperature of Ge on GaAs, Ge–GaAs heterojunctions can be fabricated relatively easily. A number of theoretical and experimental studies have focused on this system as a prototypical IV/III–V heterojunction [Margaritondo and Perfetti, 1987; Biasiol et al., 1992]. In technology, the use of heavily doped epitaxial Ge layers as a low resistance base in n–p–n AlGaAs/Ge/GaAs heterojunction bipolar transistors (HBTs) should lead to higher injection efficiencies and lower base contact resistance [Strite et al., 1990a; Ünlü et al., 1990]. The increase in efficiency rests on the increased valence-band offsets expected for AlGaAs/Ge as compared to AlGaAs/GaAs. Early I–V estimates of the valence-band offsets [Ballingall et al., 1983] reportedly yielded $\Delta E = -0.68$ eV and $\Delta E_c = -0.05$ eV. More recent C–V measurements [Ünlü et al., 1990] on p-Ge/n-GaAs(0 0 1) heterojunctions grown by MBE yielded $\Delta E_v = -0.49 \pm 0.05$ eV and $\Delta E_c = 0.28 \pm 0.05$ eV, with very good agreement quoted [Ünlü et al., 1990; Dahmen et al., 1993] with the results of I–V measurements on the same samples ($\Delta E_c = -0.22$ eV). On the other hand, for Ge/GaAs heterojunctions fabricated using an electron beam source for Ge deposition, I–V measurements reportedly yielded $\Delta E_c = -0.04$ eV [Kawanaka and Sone, 1990]. We will see that such a spread of experimental values exists also in photoemission determination of the offsets, and that the situation is further complicated by recent internal photoemission results.

Interest in ZnSe–GaAs heterojunctions has greatly increased in recent years because of its potential applications in a number of high speed and optoelectronic devices. The wide bandgap of ZnSe and related ternary alloys such as $Zn_{1-x}Cd_xSe$ and $ZnSe_{1-y}S_y$ makes them promising materials for optoelectronic device technology in the blue region of the visible spectrum [DePuydt et al., 1987, 1988; Cheng et al., 1987; Gunshor and Kolodziejski, 1988; Haase et al., 1991; Jeon et al., 1991; Vanzetti et al., 1992; Bratina et al., 1993a,b]. In 1991 pulsed operation at 77 K of blue–green lasers comprised of ZnSe–$Zn_{1-x}Cd_xSe$–ZnSe quantum well structures grown by MBE on GaAs was demonstrated for the first time [Haase et al., 1991; Jeon et al., 1991]. The lattice parameter of ZnSe is well matched to that of GaAs (−0.27% mismatch) so that high quality epitaxy of ZnSe on GaAs is possible, and GaAs wafers are presently the substrates of choice for device fabrication. For the same reason, ZnSe has also been proposed as a candidate for wide gap barrier material in GaAs-based high speed devices [Tamargo et al., 1988].

For all of the proposed ZnSe-based heterojunction device applications, the large valence-band offset predicted theoretically [Anderson, 1962; Shay et al., 1976; Ihm and Cohen, 1979; Harrison and Tersoff, 1986; Van de Walle and Martin, 1987; Christensen, 1988a; Eppenga, 1989; Qteisch and Needs, 1991] for ZnSe–GaAs should hinder hole injection from GaAs substrates into ZnSe epitaxial layers. This, together with the difficulty of obtaining ohmic contacts to p-type ZnSe [Shibli et al., 1990; Woodall, 1991], is one of the major obstacles to exploiting the full potential of ZnSe in practical devices.

Recent C–V and I–V measurements [Mazuruk et al., 1988] on n-ZnSe/n-GaAs(0 0 1) heterostructures grown by metal-organic chemical vapor deposition (MOCVD) at 300°C on GaAs(0 0 1), were used to propose a staggered (type-II) model for the band lineup with the conduction-band minimum for ZnSe lying 0.5–0.7 eV below that of GaAs. This would correspond to a valence-band offset in the range of 1.78–1.98 eV. On the other hand, based on C–V and I–V measurements of n-ZnSe/n$^+$-GaAs(0 0 1) heterostructures grown by MBE [Colak et al., 1989], other authors proposed that the conduction-band minimum of ZnSe is to be found 0.2–0.3 eV above that of GaAs, consistent with a valence-band offset in the 1 eV range. Qian et al., along the same lines, argued for an unspecified, small conduction-band discontinuity in (0 0 1)-oriented heterostructures grown by MBE at 320°C [Qian et al., 1989]. We will see in Section 2.2.2 that experimental studies by photoemission spectroscopy tend to support the lower value of the valence-band offset [Kowalkzyk et al., 1985; Bratina et al., 1993a,b], although we emphasize that in principle, as will be illustrated in Sections 4 and 5, a wide range of offsets may derive from the establishment of different interface compositions as a result of different growth conditions.

2.2.2. Optical methods

Optical techniques used to probe the band offsets directly and indirectly include absorption, luminescence, light scattering, and internal photoemission spectroscopies. Optical absorption and luminescence are most effectively performed in MQWS. The conduction and valence band discontinuities define the quantum well depth for electrons and holes, and optical techniques can probe direct transitions between sub-bands within the quantum wells. If the geometry of the structure and the effective masses are accurately known, the experimental transition energy can be used to probe the well depth [Duggan, 1987]. Values of the band offsets are often estimated from the analysis of the optical response as a function of the sample geometrical parameters (quantum well thickness) or intensity of an applied magnetic field [Duggan, 1987; Shahzad et al., 1988; Walecki et al., 1990]. The dependence on hydrostatic pressure of the position of spectral features related to *direct* optical transitions was successfully used to determine the band discontinuities in heterojunctions with type-I band alignment [Wolford et al., 1986, 1987; Wolford, 1987]. The dependence on the applied electric field of the position of spectral features related to *indirect* transitions was used instead to probe the band offsets in heterojunctions with staggered (type-II) band alignment [Wilson, 1988].

Light scattering techniques can also be used to probe band bending, charge densities and energy levels in quantum well structures [Pinczuk, 1984; Abstreiter, 1985; Brillson, 1992]. In recent work on ZnSe–GaAs(0 0 1) heterostructures, for example, the electric-field induced contribution to the intensity of the longitudinal optical phonon Raman features was used to infer the band bending in ZnSe and GaAs. The band bending, in conjunction with a phenomenological model, was then used to estimate a conduction-band offset $\Delta E_c = +0.31 \pm 0.05$ eV [Olego, 1989].

In general, determination of the band discontinuities from the optical spectra does require the formulation of an empirical or theoretical model of the properties of the superlattice or MQWS under consideration, that depend on layer thickness and abruptness [Smith and Mailhiot, 1987; Brillson, 1992], or the experimental determination of all relevant structural parameters (such as superlattice period, interface composition profile, strain) and at least some of the main band parameters (e.g.,the effective masses). Any uncertainty on parameter determination may result in an ambiguous determination of the band offsets. A fairly dramatic and technologically relevant example of this, was the recent controversy about the band offsets in HgTe/CdTe heterojunctions [Yu, 1992].

Short-period superlattices comprised of CdTe and HgTe layers have been attracting attention since they were first proposed as an alternate material to $Hg_{1-x}Cd_xTe$ alloys for infrared applications [Schulman and McGill, 1979]. The coexistence of the Hg–Te and Cd–Te chemical bonds in the ternary alloys yields a Hg–Te bond of lower stability relative to that of HgTe [Harrison, 1983]. A consequence of this is that Hg loss from the alloy surface is observed following a variety of processing steps, together with the formation of Hg-related point defects that may change dramatically the carrier concentration and the optical properties [Nitz et al., 1981; Lastraz-Martinez et al., 1982; Chen et al., 1983; Spicer et al., 1983; Davis, 1986; Wall et al., 1987; Raisanen et al., 1988; Spicer et al., 1988; Carey et al., 1988].

In CdTe–HgTe superlattices the two binary compounds are spatially separated and, therefore, stability problems should be reduced. Transport and optical properties of such heterostructures are strongly dependent on interface abruptness and the band offsets [Arch et al., 1986a,b; Reno and Faurie, 1986; Reno et al., 1986, 1987; Otsuka et al., 1987; Leopold et al., 1988; Simon et al., 1990] and several experimental studies have explored the composition profile and band discontinuities achievable in practice in the superlattice [Arch et al., 1986a; Leopold et al., 1988; Faurie et al., 1982; Zanio, 1986; Zanio and Massopust, 1986]. It has been shown that appreciable interdiffusion of Hg, Cd, and Te atoms across the interface occurs at growth temperatures as low as 110°C [Arch et al., 1986a]. Such an interdiffusion process modifies the composition profile and may affect the electronic properties of the heterostructure. For example, interdiffusion could change the effective HgTe layer thickness in short period HgTe–CdTe superlattices and therefore modify the superlattice bandgap [Reno et al., 1986; Simon et al., 1990].

A valence-band offset $\Delta E_v \sim 40$ meV was first estimated in CdTe–HgTe superlattices grown with (1 1 1) orientation through an analysis of low-temperature magneto-optical measurements [Guldner et al., 1983; Berroir et al, 1986a,b]. Photoluminescence and resonant Raman scattering were also applied to investigate the electronic properties of CdTe–HgTe heterostructures, and the results of these studies were said to imply an upper limit of 120 meV for the valence-band offset [Olego et al., 1985; Olego and Faurie, 1986]. However, room temperature XPS measurements (see Section 2.2.3) yielded a much larger value of 0.35 eV for ΔE_v at both CdTe–HgTe $(\bar{1}\,\bar{1}\,\bar{1})$B and CdTe$(\bar{1}\,\bar{1}\,\bar{1})$B–HgTe heterojunctions [Kowalczyk et al., 1986; Duc et al., 1987a,b; Faurie et al., 1987]. Since the XPS results were obtained at room temperature, while the optical measurements were performed at low temperature, it was suggested that the discrepancy might reflect a temperature dependence of the valence-band offset [Faurie et al., 1987; Chow et al., 1987]. However, lower temperature (50 K) photoemission measurement of ΔE_v for CdTe–HgTe (1 1 1) [Sporken et al., 1989] showed only small changes of ΔE_v from the room temperature value.

New optical and transport studies of CdTe–HgTe superlattices also ended up supporting the larger value of ΔE_v [Schulman and Chang, 1986; Wagner et al., 1988; Perez et al., 1988]. In an effort to solve this controversy, a theoretical investigation [Johnson et al., 1988] examined in detail the dependence of the superlattice bandgap and electron cyclotron effective mass on the valence-band offset and pointed out that the early magneto-optical data [Berrior et al., 1986] could also be consistent with a valence-band offset ≥ 350 meV. In fact the larger offset reportedly yielded even better agreement between theory and experiment. In other words, at the time of this writing the origin of the apparent discrepancy appears to be an insufficient analysis of the influence of the effective mass parameters on the original optical results.

2.2.3. *Internal photoemission*

The internal photoemission technique is an optical method to sample the band offsets that does not require a detailed knowledge of the band parameters, or the fabrication of quantum well structures with ideal geometry. The principle of the technique has been well known for many years [Fowler, 1931; Williams, 1965; Kane, 1966], although recent improvements have followed the introduction of new methods to detect the photon energy threshold [Abstreiter et al., 1985; Heiblum et al., 1985, 1986a,b; Eizenberg et al., 1987] and infrared sources with high brightness [Coluzza et al., 1992a; McKinley et al., 1993].

A simplified experimental scheme is depicted in Fig. 2 [Coluzza et al., 1992a]. The bottom-most section of Fig. 2 illustrates an internal photoemission experiment performed using a conventional

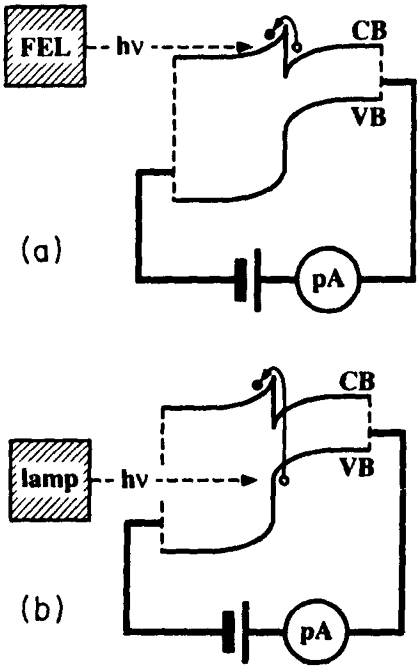

Fig. 2. Simplified schematics of internal photoemission measurements of heterojunction band offsets using a free-electron laser (FEL) or a conventional source. (a) FEL induced optical pumping across the conduction band (CB) discontinuity is detected by measuring the corresponding external current. (b) Similar experiments with a conventional photon source usually involve pumping from the top of the valence band (VB) in one material to the bottom of the CB in the other [Coluzza et al., 1992a].

photon source [Haase et al., 1987; Dahmen et al., 1993]. Photons of suitable wavelength travel across the wider gap material with little adsorption and are adsorbed within the lower gap material near the heterojunction. The optical pumping of interest is from the top of the valence band in one material to the bottom of the conduction band in the other, and gives rise to a corresponding threshold in the optical absorption spectra. The detection is obtained by biasing the junction at low temperature (77 K), amplifying and measuring the external photocurrent, and identifying the threshold corresponding to the band discontinuity in the plot of the measured photocurrent as a function of photon energy.

The topmost section of Fig. 2 illustrates the recent experimental scheme which exploits as a photon source a free-electron laser operating in the 2–10 μm wavelength range. Optical pumping occurs directly across the conduction-band discontinuity. Initial state electrons are provided by the junction forward bais and the ensuing steady-state carrier injection into the lower gap material [Coluzza et al., 1992a; McKinley et al., 1993]. The high brightness of the free-electron laser allows one to work with lower injected carrier densities and reduced space-charge problems [Coluzza et al., 1992a]. Experiments performed on AlGaAs/GaAs heterojunctions showed a well-defined optical threshold in the current–photon energy characteristics, corresponding to the conduction-band discontinuity.

A major source of uncertainty in band offset determination using internal photoemission is the method used to determine the numerical value of the optical threshold. Most authors use a square-root lineshape as predicted by Fowler for Schottky barriers, and by Kane and Williams for heterostructures [Fowler, 1931; Williams, 1965; Kane, 1966]. In principle, quantum confinement of the electron and hole states in the triangular quantum well created by band bending near the interface, and interdiffusion effects that change the band gap of the semiconductors near the junction may also affect the determination of the offsets, although by far the major limitation of the technique is bound to be the requirement of good ohmic contact fabrication to both of the materials comprising the junction.

Some of the most recent internal photoemission measurments have targeted heterovalent heterojunctions, of special interest to us because of the expected tunability of the band offsets (see Section 4). A very surprising result was recently obtained with a conventional photon source on p-Ge/n-GaAs(0 0 1) heterojunctions grown by MBE at 500°C and 300°C [Dahmen et al., 1993]. A conduction-band discontinuity $\Delta E_c = -0.33 \pm 0.04$ eV was reported for heterostructures in which the Ge overlayer was grown at 500°C, while a conduction-band offset ~ 0.3 eV lower was found for a Ge growth temperature of 300°C. Transport measurements of the same samples reportedly confirmed the trend ($\Delta E_c = -0.48 \pm 0.07$ eV and $+0.025 \pm 0.07$ eV for the two samples were obtained from the C–V data). The authors attributed such a drastic variation of the offset to the establishment of different microscopic configurations at the two interfaces as a result of the different growth temperature.

Although it will be shown in the next sections that different interface configurations for heterovalent heterojunctions may influence the band offsets, the result by Dahmen et al. remains surprising in the light of other recent experimental work. In an internal photoemission study exploiting a free-electron laser, aGe–GaAs(1 1 0) heterojunctions fabricated at room temperature were found to exhibit $\Delta E_c = -0.34 \pm 0.01$ eV [McKinley et al., 1993]. Recent photoemission spectroscopy studies of Ge layers grown by MBE on GaAs(0 0 1) epitaxial substrates yielded $\Delta E_v = -0.54 \pm 0.05$ eV ($\Delta E_c = -0.22 \pm 0.05$ eV) for Ge growth at 360°C, and $\Delta E_v = -0.57 \pm 0.05$ eV

($\Delta E_c = -0.19 \pm 0.05$ eV) for Ge growth at 480°C [Sorba et al., 1993b]. Other photoemission studies of Ge/GaAs(0 0 1) junctions grown by MBE in the 300–40°C temperature range, to be discussed in Section 5.2.3, reported conduction-band offsets in the -0.21 to -0.29 eV range. Therefore, except for the internal photoemission result by Dahmen et al., there is little evidence of a dependence of the band offset on Ge growth temperature in the 500°C to room temperature range for Ge/GaAs(0 0 1) heterojunctions.

2.3. Photoemission spectroscopy

In view of the relatively small sampling depth of photoemission spectroscopy, most photoemission determinations of the offsets focus on heterostructures comprised of relatively thin semiconductor overlayers grown in situ or ex situ on top of a suitable substrate. Typical overlayer thicknesses employed vary from 5 to 30 Å, depending on the photon energy and the corresponding photoelectron escape depth. In favorable cases, the valence-band offset can be measured directly from the valence band emission as a function of overlayer thickness.

If the valence-band offset is large as compared to the experimental energy resolution, which is sometimes the case when synchrotron photoemission is employed, the individual valence band maxima of the two semiconductors may be apparent in the photoelectron energy distribution curves (EDCs). This is shown in Fig. 3 for aSi/CdS heterojunctions fabricated by depositing 3.5 Å of aSi at room temperature on cleaved CdS surface [Katnani and Margaritondo, 1983]. A least squares

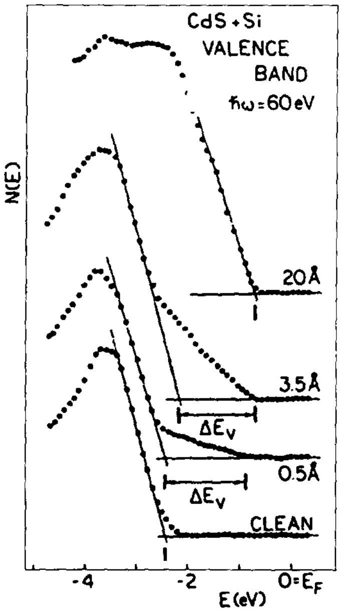

Fig. 3. Photoemission spectra from aSi/CdS($10\bar{1}0$) heterojunction comprised of an aSi overlayer of increasing thickness deposited at room temperature on a substrate cleaved in situ (center), are compared to the initial CdS ($10\bar{1}0$) emission prior to aSi deposition (bottom). The heterojunction spectra exhibit two edges directly reflecting the valence-band offset of 1.55eV [Katnani and Margaritondo, 1983].

linear extrapolation was used to estimate the positions of the individual valence maxima in Fig. 3 and calculate the corresponding valence-band offset $\Delta E_v = -1.55 \pm 0.10$ eV. This heterojunction exhibits a type-II alignment, with staggered gaps and a conduction-band offset of + 0.24 eV. Note the relatively thin value of the overlayer thickness employed, corresponding to just a few monolayers. This was mandated by the photoemission sampling depth, that is of the order of 3–5 Å in Si at the photon energy employed (60 eV). On the other hand, in such a photon energy range the experimental energy resolution available is typically 0.1–0.2 eV, and therefore better suited to direct determinations of the band offsets.

Even in such favorable cases, to reduce the experimental uncertainty on ΔE_v it may be desirable to perform a less arbitrary analysis of the valence band EDCs and decompose the valence band emission from the interface in terms of individual substrate and overlayer contributions. This was discussed in detail in a recent study of nonmagnetic/semimagnetic semiconductor heterostructures [Yu et al., 1993]. Such heterostructures have attracted attention since the original suggestion of a spin-superlattice [von Ortenberg, 1982], i.e., MQWS where a semimagnetic semiconductor is coupled with a nonmagnetic counterpart of similar energy gap and conduction band electron effective mass.

Nonmagnetic/semimagnetic structures will exhibit strong modification of the electronic properties in a magnetic field due to the large difference in the electronic g-factors of the two materials [Wu et al., 1986; Furdyna, 1988]. For example, the spin splitting of electronic states in semimagnetic semiconductors may be two orders of magnitude greater than in the adjacent nonmagnetic layer [Wu et al., 1986; Furdyna and Kossut, 1988] and comparable to the ionization energy of shallow impurities. The consequent tunability of the depth of the quantum wells by the magnetic field may give rise to phenomena such as enhancement of electronic g-factors in shallow nonmagnetic wells surrounded by semimagnetic barriers, magnetically induced transitions from type-I to type-II superlattice [Deleporte et al., 1990], boil-off and freeze out of electrons to and from quantum wells, and selective spin tunneling across the barriers [Wu et al., 1986; Furdyna, 1988].

Fig. 4 shows synchrotron radiation photoemission results at a photon energy of 80 eV for aGe–CdTe(1 1 0), aGe–$Cd_{0.65}Mn_{0.35}Te$(1 1 0) and aGe–$Cd_{0.4}Mn_{0.6}Te$(1 1 0) interfaces fabricated by Ge deposition at room temperature on single crystal substrate surfaces cleaved in situ [Yu et al., 1993]. Qualitative trends in the valence band emission from the interface as a function of overlayer thickness suggest that the valence band emission from the interface is, to a first approximation, simply a superposition of substrate-related and overlayer-related valence band spectra. The exponential attenuation observed for all substrate core features as a function of Ge coverage (not shown) also argued against interface reactions and the formation of new mixed phases. It was therefore justified to fit the experimental interface spectra to a superposition of $Cd_{1-x}Mn_xTe$ and elemental Ge emission. The results are shown in Fig. 4 for the three interfaces at a Ge coverage of 5 Å. EDCs prior to Ge deposition (dashed line) were selected for each interface to represent the substrate emission. EDCs at Ge coverages $\theta > 20$ Å were selected to represent the bulk Ge emission (dotted line). The experimental data in the region of the leading valence band edge (solid circle) were fitted to a superposition of substrate and overlayer spectra. A nonlinear least squares fit, implementing a modified Levenberg–Marquardt algorithm [Raisanen et al., 1991], was performed as a function of two parameters, namely the relative amplitude and energy offset of substrate and overlayer EDCs. The result of the best fit is also shown in Fig. 4 as the solid line superimposed to the data.

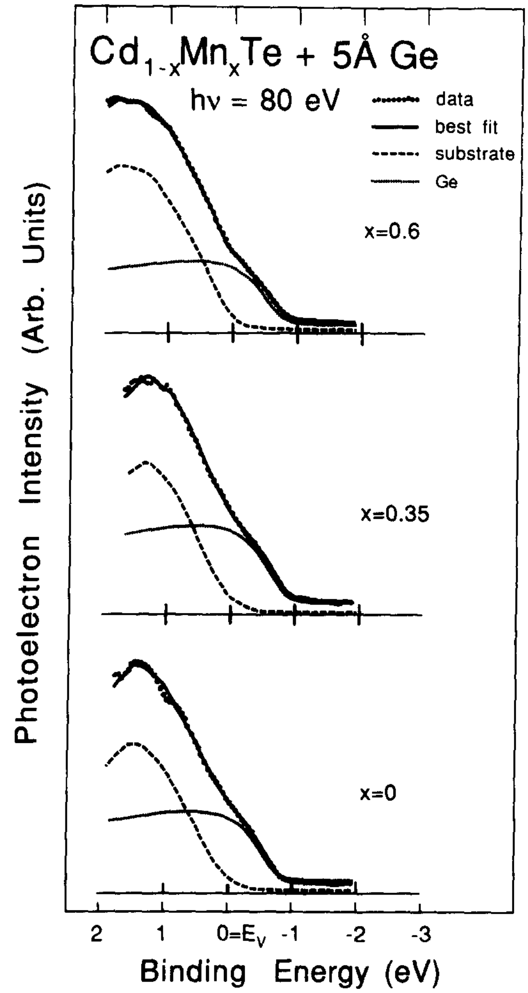

Fig. 4. Fit of photoemission spectra from aGe–$Cd_{1-x}Mn_x$ Te(110) heterojunctions (solid circles) in terms of a superposition of $Cd_{1-x}Mn_xTe$ (dashed line) and elemental aGe (dotted line) valence band spectra. The Ge coverage was 5 Å. The result of the best fit is shown by the solid line superimposed to the experimental data for each interface. The offset between the linearly extrapolated values of the valence band maxima for substrate and overlayer spectra gives directly the valence-band offset ΔE_v, which was found to be −0.80 eV for aGe–CdTe(110), −0.83eV for aGe–$Cd_{0.65}Mn_{0.35}Te(110)$, and −0.81eV for aGe–$Cd_{0.40}Mn_{0.60}Te(110)$. The uncertainty in the systematic variation of the offset in the series is 0.03eV, while in each individual value the uncertainty is 0.07eV [Yu et al., 1993].

The offset between the linearly extrapolated values of E_v for substrate and overlayer spectra was found to be −0.80 eV for aGe–CdTe, −0.83 eV for aGe–$Cd_{0.65}Mn_{0.35}Te$, and −0.81 eV for aGe–$Cd_{0.40}Mn_{0.60}Te$. The reliability of the results was demonstrated by the consistent value of the offset obtained for each sample at different Ge coverages [Yu et al., 1993]. The reliability of the procedure was also supported by the values of the Ge/substrate relative intensity obtained from the fit, which closely matched (within ± 5%) the values expected from the observed Ge 3d/Cd 4d and Ge 3d/Te 4d integrated core intensity ratios.

The experimental uncertainty in the valence-band offsets determined through the above methods has two components. First, there is the uncertainty deriving from the fitting procedure, which is of the order of the smallest variation in parameter space which gives comparable total least squares differences (± 0.02 eV). In addition, there is a substantial experimental uncertainty which derives from the determination of the position of E_v through a linear extrapolation of the leading valence band edge of substrate and overlayer spectra. The corresponding combined uncertainty in high-resolution, synchrotron radiation photoemission studies has been estimated at ± 0.07 eV [Wall et al., 1991]. Such a higher uncertainty affects the numerical value of each single offset, but does not affect the variation of the offset in the series depicted in Fig. 4, because of the cancellation of possible systematic errors due to the linear extrapolation method.

When the magnitude of the valence-band offset is comparable or smaller than the experimental energy resolution, photoemission spectroscopy can still be used to gauge the band offsets by determining first the position in energy of the valence band edge of the clean surface of the substrate, then of a thin overlayer of the second semiconductor, and correcting for substrate band bending changes during deposition [Katnani and Margaritondo, 1983; Margaritondo and Franciosi, 1984]. For semiconductor overlayers which are thin compared to the Debye length of the material, band bending in the overlayer can be neglected. In general, the band-bending correction is extracted from the observed variation of the position of the substrate core levels during deposition, and this can limit the reliability of the photoemission estimates of ΔE_v [Margaritondo and Franciosi, 1984]. The substrate core level selected to monitor band bending has to be unaffected by interface chemistry, segregation or interdiffusion, so that core level shifts reflect band bending only. The dependence of core level intensities on overlayer thickness is often used to rule out interdiffusion and segregation [Brillson, 1982; Katnani et al., 1983], and cation core levels are most often selected for compound semiconductors.

Another powerful photoemission technique to gauge band offsets was proposed in the early 1980s [Waldrop and Grant, 1979; Kraut et al., 1980] to exploit the comparatively longer sampling depth of XPS while overcoming its limited experimental energy resolution as compared to synchrotron radiation photoemission techniques. As an example of the application of this technique we review here results for the best known isovalent heterojunction system, namely AlAs/GaAs (0 0 1) and GaAs/AlAs(0 0 1). In XPS the valence-band offset ΔE_v is usually obtained [Waldrop et al., 1987; Katnani and Bauer, 1986; Yu et al., 1989; Hashimoto et al., 1990; Sorba et al., 1992a] from the photoemission-determined position of the Ga 3d or Al 2p core levels relative to the valence-band maximum in bulk standards, and the energy difference of the Al 2p and Ga 3d core levels at the interface in the actual heterojunction. Upon growing an AlAs overlayer on top of a GaAs substrate to fabricate AlAs–GaAs(0 0 1) heterojunctions, for example, the valence-band offset is given by

$$\Delta E_v = [E_{cl}(\text{Ga 3d}) - E_v(\text{GaAs})] - [E_{cl}(\text{Al 2p}) - E_v(\text{AlAs})] + \Delta E_{cl} = -\Delta E_b + \Delta E_{cl}, \tag{3}$$

where the subscripts cl and v denote binding energies pertaining to the core levels and valence-band maximum in the bulk semiconductor constituents, such energies are taken to be positive and referred to the spectrometer Fermi level, and ΔE_{cl} is the apparent Al 2p–Ga 3d core-level separation across the heterojunction.

Determination of the core binding energy difference in the two bulk materials ΔE_b, requires separate measurements of the core and valence-band maximum positions in each bulk standard. The uncertainty on the numerical value of the offset derives mostly from the uncertainty in the determination of the position of the valence-band maximum relative to the Fermi level for each bulk material. The position of E_v is usually determined either from a linear extrapolation of the leading valence band edge [Katnani and Margaritondo, 1983], or through a least squares fit of the data [Waldrop et al., 1987] to a suitably broadened theoretical electronic density of states (DOS) near E_v. The first method is in principle less accurate, although it is likely to be adequate for deriving the valence-band offset for common anion systems such as AlAs–GaAs due to the cancellation of systematic errors that follows from the similarity of the anion-derived DOS features. Most authors who use the second method [Katnani and Bauer, 1986; Yu et al., 1989] employ the same theoretical GaAs DOS to fit both GaAs and AlAs data, and therefore make an assumption equivalent to that implicit in the first method. In general, sources of uncertainty in the determination of E_v with the second method are related to matrix elements and surface related effects, the accuracy of the theoretical DOS, as well as the numerical value of the broadening parameter [Wall et al., 1991]. Values of ΔE_b obtained for AlAs/GaAs with monochromatized XPS, using the centroid of the core-level doublet to mark the core position, vary from 54.00 ± 0.05 eV [Sorba et al., 1992a], to 53.95 eV [Waldrop et al., 1987], 53.99 eV [Yu et al., 1989], and 53.97 eV [Hashimoto et al., 1990], that is they are all quantitatively consistent.

The interface core separation $\Delta E_{cl} = E_{cl}(\text{Al 2p}) - E_{cl}(\text{Ga 3d})$ can be measured with high accuracy, and is independent of overlayer and substrate doping if band bending is negligible over the short photoemission sampling depth. The XPS photoemission escape depth is typically ~ 15 Å for an average photoelectron collection angle of 55°, and is often small as compared to the Debye lengths of the two semiconductors comprising the junction. It will also be independent of overlayer thickness if the overlayer is thick enough so that the contribution from the first layer atoms is negligible. The apparent core position reflects then the average "bulk" electrostatic potential of the overlayer rather than possible chemical shifts. One should, in principle, verify that such conditions are met. Variations in the apparent value of ΔE_{cl} with doping or overlayer thickness, as well as asymmetric broadening of the substrate or overlayer core level lineshapes are expected if one or the other of the two conditions are not met.

Determination of ΔE_v for an AlAs–GaAs(0 0 1) heterojunction is exemplified in Fig. 5 [Sorba et al., 1992a]. The valence band spectra in the rightmost inset of Fig. 5 were obtained from a 0.5 μm thick GaAs epitaxial substrate (top) and a 200 Å thick AlAs epitaxial layer (bottom). The binding energy scale is referenced to the valence-band maximum E_v as derived from a least squares linear fit of the leading valence band edge. EDCs for the Al 2p and Ga 3d core emission from these two samples are shown below the inset in Fig. 5(a). The core binding energies were measured relative to E_v for each sample, and the zero of the energy scale was taken at the position of the Ga 3d centroid in GaAs. The corresponding core binding energy difference is that expected from a hypothetical heterojunction with zero valence-band offset, i.e., ΔE_b. Core EDCs from an AlAs–GaAs(0 0 1) heterostructure fabricated by growing a 15 Å thick AlAs overlayer at 580°C on top of the GaAs substrate are shown in Fig. 5(b). The corresponding interface core level separation, ΔE_{cl} is 54.42 ± 0.03 eV. The core separation is independent of overlayer thickness in the coverage range 10–25 Å. This is illustrated in the leftmost inset of Fig. 5 where the Al 2p–Ga 3d core separation at the interface is plotted as a function of overlayer thickness for an AlAs–GaAs(0 0 1) heterostructure (squares). Using the experimental values of ΔE_{cl} and ΔE_b in Eq. (3) and Fig. 5 the valence-band offset is $\Delta E_v = +0.42 \pm 0.07$. The corresponding result for GaAs–AlAs(0 0 1) heterojunctions was $\Delta E_v = -0.46 \pm 0.06$ eV [Sorba et al., 1992a].

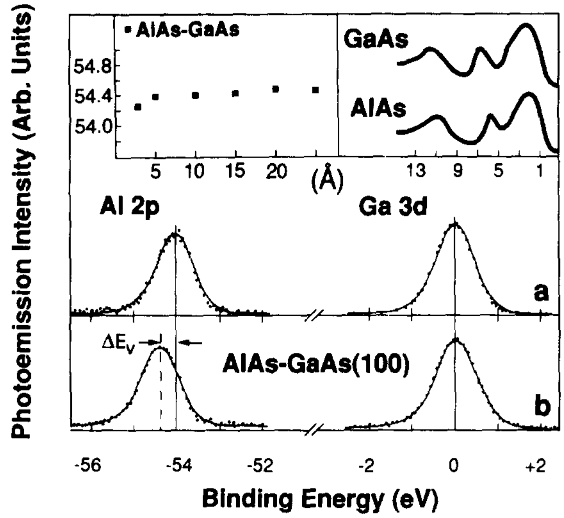

Fig. 5. Photoemission measurements of band offsets for AlAs–GaAs(001) heterojunctions grown by molecular beam epitaxy (MBE). Rightmost inset: valence band emission from thick AlAs(001) and GaAs(001) epitaxial layers. (a) Al 2p and Ga 3d core level emission from bulk AlAs(001) and GaAs(001) samples. The zero of the energy scale was taken at the position of the Ga 3d cores in GaAs and the apparent core separation is that expected for a hypothetical heterojunction with zero valence-band offset. (b) Core emission from an actual AlAs–GaAs(001) heterostructure. The observed variation in the core separation relative to (a) is independent of AlAs coverage (see leftmost inset), and gives directly ΔE_v [Sorba et al., 1992a].

Recent determinations of the band offsets for AlAs/GaAs heterojunctions with (0 0 1) orientation are shown in Table 1. Quantitatively consistent results have been obtained on interfaces with (1 1 0), (1 1 1)B, and (3 1 1) A orientation [Hirakawa et al., 1990]. The results indicate that within experimental uncertainty the band offsets are commutative (see Eq. (2)) with magnitude in the 0.39–0.46 eV range [Katnani and Bauer, 1986; Waldrop et al., 1987; Yu et al., 1989; Hashimoto et al., 1990; Sorba et al., 1992a]. This is in agreement with recent linear response theory results [Baroni et al., 1989; Peressi et al., 1991; Baldereschi et al., 1993a] that will be illustrated in Section 3.3, which indicate that in isovalent heterostructures the band offsets are essentially a bulk property of the two semiconductors involved, and largely independent of orientation, interdiffusion and defect formation.

Optical determinations of the valence-band offset support a somewhat larger value of 0.56 eV [Wolford et al., 1986, 1987; Wolford, 1987; Dawson et al., 1987; Moore et al., 1987]. The issue is further complicated by the existence of different theoretical predictions. The most recent predictions of ΔE_v from first-principles calculations within the local density approximation yielded values of 0.37 eV [Van de Walle and Martin, 1986a], 0.41 eV [Zhang et al., 1990] and 0.48 eV [Baroni et al., 1989]. Recent work on many-body corrections to the local density approximation, however, indicate that the inclusion of such effects should modify the offset, and new corrected values of 0.53 eV [Zhang et al., 1990] and 0.58 eV [Baroni et al., 1989] have been proposed.

The systematic discrepancy of up to 0.10 eV between the lower, photoemission-determined value of the offset and the value derived from optical studies was tentatively associated to the different final

Table 1
Literature results for the valence-band offset in AlAs–GaAs(001) and GaAs–AlAs(001) heterostructures. First column: number of samples examined. Second column: overlayer-substrate type. Third column: overlayer/substrate doping type. Fourth column: Al 2p–Ga 3d interface core level separation (in eV). Fifth column: bulk core binding energy difference (in eV). Sixth column: valence-band offset (in eV). Last column: reference

Number of meas.	Growth sequence	Doping	ΔE_{cl}	ΔE_b	ΔE_v	Ref.
4	AlAs–GaAs(001)	—	54.41	53.95	+ 0.46	a
4	GaAs–AlAs(001)	—	54.31	53.95	− 0.36	a
3	AlAs–GaAs(001)	—	54.65	54.27	+ 0.39	b
2	GaAs–AlAs(001)	—	54.65	54.27	− 0.39	b
2	AlAs–GaAs(001)	n/n	54.45	53.99	+ 0.46	c
3	GaAs–AlAs(001)	n/n	54.43	53.99	− 0.44	c
2	AlAs–GaAs(001)	i/n	54.42	53.97	+ 0.45	d
2	GaAs–AlAs(001)	-/n	54.42	53.97	− 0.45	d
40	AlAs–GaAs(001)	p/p, n/n, n/p, p/i, n/i, i/n, i/i/i	54.42	54.00	+ 0.42	e
9	GaAs–AlAs(001)	i/i	54.46	54.00	− 0.46	e

[a] Waldrop et al., 1987; [b] Katnani and Bauer, 1989; [c] Yu et al., 1989; [d] Hashimoto et al., 1990; [e] Sorba et al., 1992a.

state involved in the two processes [Sorba et al., 1992a]. In principle, the effect of the core hole potential on the photoemission electron states may modify such states relative to the ground state of the system and affect differently GaAs and AlAs derived states [Zhang et al., 1990].

We mention also that from the apparent position of the Ga 3d and Al 2p core levels relative to the Fermi level, in the absence of appreciable photovoltage effects, one can extract in principle the position of the Fermi level at the interface using the measured core binding energies relative to the valence-band maximum. Often, a relatively wide scatter in the values of the interface position of the Fermi level contrasts with the very limited scatter in the values of the interface core separation ΔE_{cl}. The position of the Fermi level at the interface is therefore likely to be strongly affected by small differences in the growth procedure, while the band offsets are quite insensitive to the same variations.

We emphasize that the pinning position of the Fermi level at the interface is not a bulk property of the two materials and may therefore be affected by the details of the growth procedure. The apparent Fermi level pinning positions in AlAs/GaAs ranged from about 0.1 eV above the top of the valence band in GaAs (or about 0.6 eV above the top of the valence bands in AlAs) to about the mid-gap position in GaAs and AlAs, indicating that a wide range of defect concentrations or types may be generated for small variations in the growth parameters [Sorba et al., 1992a].

To conclude this brief survey of photoemission techniques used to measure heterojunction band offsets, we mention that the use of photoemission spectromicroscopy with synchrotron radiation will offer the possibility to study the spatial homogeneity of the band offsets with a lateral resolution that depends on the instrument employed, but that may reach 0.1 μm with the best soft-X-ray photoemission microscopes available today. A recent pioneering study of aGe–GaSe heterojunctions [Gozzo et al., 1995] prepared by depositing a 0.5 ML of Ge at room temperature on substrates cleaved in situ, exploited the soft-X-ray microscope MAXIMUM [Ray-Chaudhuri et al., 1993]. The results have been used to propose that inhomogeneities as large a 0.4 eV in the valence band offsets may exist in these heterojunctions on the scale of several microns, and go undetected by spatially averaging techniques.

Although this surprising result remains to be verified at overlayer coverages above the submonolayer range, and in ordered epitaxial systems, it represents a challenge that will certainly stimulate further work in this area. Inhomogeneities of the order of 0.4 eV in the band offsets can be easily ruled out in device grade heterostructures (e.g. quantum wells) since they would give rise to large variations in confinement energies, emission wavelengths, etc., If the lateral inhomogeneities recently observed by ballistic electron emission microscopy (BEEM) in Schottky barriers [Kaiser et al., 1991; Palm et al., 1993; Niedermann et al., 1993; Ludeke and Bauer, 1994] are any guide to the behavior of heterojunctions, we may very well expect variations in the band offsets of the order of 50 meV on a lateral scale of 100 Å.

2.4. Structural aspects

2.4.1. Room-temperature deposition

In the early 1980s many studies of band offsets in semiconductor heterojunctions were performed by depositing a semiconductor overlayer on top of a semiconductor substrate cleaved in situ and kept at room temperature (RT) during overlayer deposition [Katnani and Margaritondo, 1983; Capasso and Margaritondo, 1987]. In these conditions the overlayers were often described as amorphous, although often no attempt was made to characterize the overlayer structure by means of in situ diffraction techniques such as reflection high energy electron diffraction (RHEED) or low energy electron diffraction (LEED). Performing deposition at room temperature, however, does not guarantee that an amorphous overlayer will be obtained.

For example, several authors have recently reported that low rate deposition of ZnSe onto GaAs (1 1 0) substrates cleaved in situ gives rise to epitaxy at room temperature with the formation of a well defined 1 × 1 RHEED pattern [Meng et al., 1990; Vanzetti et al., 1992; Bratina et al., 1993a,b]. Other authors [Kowalczyk et al., 1982] could not detect long-range order by LEED in ZnSe overlayers deposited at RT on GaAs (1 1 0) substrates. Annealing of the interface at 300°C after deposition, reportedly yielded a LEED pattern of undisclosed type. The same authors observed long-range order (with undisclosed periodicity) immediately after deposition if ZnSe was deposited on GaAs (1 1 0) substrates kept at 300 °C [Kowalczyk et al., 1982].

The discrepancy between such results may stem from the dependence of overlayer morphology on substrate preparation and deposition conditions, that should be especially critical in RT experiments. Low temperature epitaxy is bound to be influenced by the average separation of cleavage steps, and by overlayer deposition conditions such as rate, evaporator to sample distance, etc. In particular, steps due to intentional substrate misorientation are known to play an important role in promoting compound semiconductor epitaxy on GaAs (0 0 1) surfaces, and the deposition rate and radiated power may affect the nucleation rate away from the steps [Herman and Sitter, 1989]. All of these factors may contribute in general to determine the type and location of the overlayer nucleation sites, and their role should be even more important when the surfaces are prepared by cleavage, and the low growth temperature corresponds to comparatively low surface diffusion lengths.

2.4.2. Amorphous overlayers

When an amorphous overlayer is actually fabricated, several types of conceptual problems arise in the analysis of the band offsets. The dependence of the overlayer band structure on long-range order is poorly known for most materials. Electronic structure calculations for a few semiconductors have shown that several characteristics of the electron energy spectrum of semiconductors are sensitive to topological disorder [Wearie and O'Reilly, 1987]. In particular, it is possible to define a valence and a conduction band for amorphous semiconductors, but the corresponding DOS may differ substantially from those of the corresponding crystalline semiconductors. The general trend, as observed by photoemission spectroscopy, is a smearing of the DOS structure [Wearie and O'Reilly, 1987]. For the valence band of amorphous Ge (and similarly for amorphous Si and C), this results mainly in a broadening of the double structure occurring some 7–10 eV below the top of the valence-band maximum of crystalline Ge [Ley et al., 1972; Shevchik, 1974], and associated with the six-membered rings in the diamond structure [Shevchik, 1974]. In addition, it is difficult to define unequivocally a bandgap in the amorphous material, because of the existence of states in the gap, that above a characteristic energy are increasingly delocalized in r-space [Wearie and O'Reilly, 1987].

Photoemission measurements have indeed shown that the electron density of states of amorphous Ge depends on growth conditions such as the substrate temperature and the angle between the source and the sample normal [Ribbing et al., 1971, Orlowski et al., 1974]. Therefore the magnitude of the bandgap is not a well-defined physical constant. The presence of dangling bond states in the gap, with density that varies widely with annealing, has been associated by List and Spicer with large *apparent* variations (~ 0.7 eV) in the valence-band offset for aSi–GaAs(1 1 0) heterojunctions as determined by photoemission spectroscopy [List and Spicer, 1988].

A second type of problem in using results from amorphous overlayers to infer heterojunction band offsets in technologically relevant heterostructures concerns the effect of elastic strain on the overlayer band structure and overlayer/substrate band offsets. For ideally amorphous overlayers the substrate lattice parameter should have no influence on the overlayer atomic structure, so that one could consider the overlayer fully relaxed. However, the technologically relevant version of the same heterojunction is likely to be elastically strained, if the substrate and overlayer lattice parameters are different, and the thickness of the overlayer is below a critical thickness that depends on the elastic constants of the two materials [Matthews and Blakeslee, 1974, 1975, 1976]. As will be illustrated in Section 3.6, any residual strain in the overlayer may change the crystal symmetry, remove band degeneracies, vary the bandgaps, and change the substrate/overlayer band offsets. Even from a purely phenomenological point of view, any determination of the band offsets through Eq. (3) may in principle require corrections when residual strains are present in the overlayer. Tersoff and Van de Walle pointed out that the effect of strain on the position of the core levels relative to the valence-band maximum should be carefully evaluated [Tersoff and Van de Walle, 1987].

2.4.3. Interlayer structure

As will be shown in Section 5, most changes in heterojunction band offsets have been achieved by modifying the growth conditions or fabricating thin heterovalent layers in the junction region. To identify the physical mechanisms responsible for the change in offsets it would be of paramount importance to determine the location of the different atomic species at the interface. Theoretical predictions in this area are of little use. The problem resides with the wide variety of possible microscopic configurations that may exist and give rise to a given offset, and the kinetic aspects of interface formation. Such issues should be addressed theoretically within a molecular dynamics framework that is not yet available for such complex systems.

To identify the detail of the interface atomic structure experimentally is also quite difficult. Surface diffraction techniques, including the widely available RHEED and LEED probes, provide information on surface reconstruction and long-range order during growth, but this information may have little bearing on the actual atomic structure of the buried interface. For example, the many surface reconstructions that can be observed during MBE growth of GaAs on GaAs wafers as a function of the growth temperature and As/Ga flux ratio [Herman and Sitter, 1989] have a bearing on the growth rate, but not on the bulk crystal structure of the epitaxial layer. Cross sectional techniques, in which two dimensional sections of the heterojunction normal to the interface plane are imaged by microscopy techniques such as TEM or STM have been applied to very few heterojunctions. Such techniques are very powerful probes of long-range order, strain, and the presence of second phases [Lee et al., 1990; Wright and Williams, 1991] or extended defects (dislocations, twins, antiphase domains, etc.) near the interface, but can identify isoelectronic substitutional defects and point defects only in favorable cases [Ourmazd et al., 1989], often through complex data analysis and numerical simulations.

The reduced sensitivity to substitutional disorder is a serious limitation since in most technologically relevant heterostructures disorder is likely to take place through the formation of substitutional defects. For isovalent heterojunctions, and for heterovalent heterojunctions with (1 1 0) orientation, ideally abrupt interfaces would be electrically neutral, so that there should be no electrostatic energy gain for the system in establishing a mixed interface configuration [Harrison et al., 1978; Harrison, 1979; Baroni et al., 1989; Baldereschi et al., 1993a]. For lattice-matched interfaces, such as AlGaAs/GaAs, there should be also little elastic energy gain in atomic intermixing [Dandrea et al., 1992]. Therefore any driving force toward the formation of a nonabrupt interface should be purely entropic in character. Even in such a favorable case, chemical roughness of the interface has been observed by TEM [Ourmazd et al., 1989].

For heterovalent heterojunctions with polar orientation, ideally abrupt interfaces would actually be charged, and therefore thermodynamically unstable [Harrison et al., 1978; Kunc and Martin, 1981]. Neutral interfaces with lower free energy may be established as a result of the formation of a variety of substitutional defects [Kunc and Martin, 1981], and the resulting different types of local interface atomic structure in principle may give rise to widely different band discontinuities [Harrison et al., 1978; Baroni et al., 1989; Dandrea and Zunger, 1990; Biasiol et al., 1992]. For such interfaces there is therefore a well-defined enthalpic driving force toward the formation of substitutional disorder. The closest we have come experimentally to verify the above theoretical picture is a recent report that ZnSe–Si(0 0 1) heterojunctions fabricated by ZnSe deposition at room temperature followed by crystallization at 500°C gave rise to large areas of twinned ZnSe, while the presence of an As monolayer on the Si(0 0 1) surface prior to ZnSe growth was found to prevent reaction between Si and Se and yield epitaxial growth without any significant twinning [Bringans et al., 1992].

As far as heterojunctions in which a metal or nonmetal (e.g. Cs, Al, H) layer has been fabricated at the interface in an attempt to modify the band offsets (see Section 5.4), relatively little information is available about the atomic location of the constituents of the interface layer. No information is available about the atomic sites occupied by metallic impurities nor about the atomic structure of interface species fabricated through reaction with gaseous species. The lack of such structural information is a severe handicap for any attempt to identify the microscopic mechanism responsible for the change in band offset.

2.4.4. Pseudomorphic interlayers

A subset of results for which some structural information has been obtained, includes interface layers comprised of Si and Ge in III–V/III–V heterojunctions and homojunctions (see Section 4.4). For such systems the situation is simpler than in the previous case, since Si and Ge are known to occupy substitutional sites in most III–V semiconductors. Secondly, since such heterostructures can be grown epitaxially in appropriate conditions, they lend themselves to analysis by means of X-ray interference, transmission electron microscopy, and channeling methods. Finally, since an extensive literature exists on the optical properties of Si and Ge impurities in III–V materials, important information about the atomic sites can be obtained in principle also by optical and transport methods. In spite of these potential simplifications, III–V/IV/III–V heterostructures remain affected by phenomena such as interdiffusion [Herman and Sitter, 1989], segregation [Brandt et al., 1991], antiphase domain formation [Neave et al., 1983; Strite et al., 1990a, b, c]; and – in the case of III–V/Si/III–V heterostructures – strain-induced defect formation.

Fig. 6 shows high resolution cross sectional TEM micrographs of the interface region of AlAs–Si–GaAs (0 0 1) heterostructures for nominal Si interlayer thicknesses of 2, 4 and 8 ML [Sorba et al., 1992a]. Only limited contrast between the III–V and Si lattice could be achieved, but the pseudomorphic character of the interlayer is quite clear for coverages of 2 and 4 ML, with no evidence of twins, or of the edge and 60° dislocations observed during GaAs growth on Si (0 0 1)

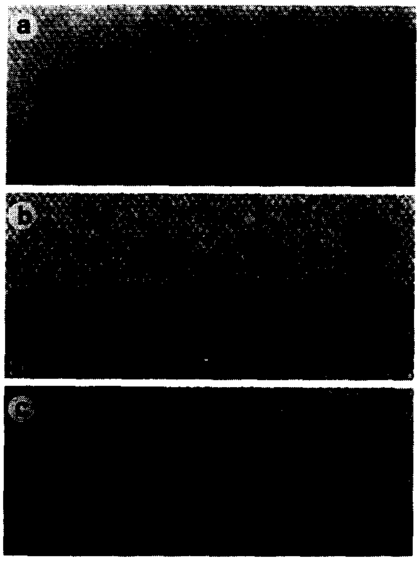

Fig. 6. High resolution transmission electron microscopy photographs [(1 1 0) cross section] of AlAs–Si–GaAs (0 0 1) heterostructures with a Si interface layer thickness of 2 ML (top), 4 ML (center) and 8 ML (bottom) [Sorba et al., 1992a].

wafers [Zhu and Carter, 1990; Xing et al., 1992]. In the case of the sample with 8 ML Si interlayer thickness, the micrograph shows the presence of microtwins on the (1 1 1) planes, indicating that partial strain relaxation may have begun. For Si interlayer thicknesses of 14 ML strain relaxation is complete and a large defect density is observed in the III–V overlayer [Sorba et al., 1992a, 1993a].

Fig. 7 shows cross sectional TEM photographs of two fifteen-period Si–GaAs(0 0 1) SLs. The average superlattice composition, as derived from XRD results [Sorba et al., 1992a, b; Scamarcio et al., 1992a,b] was $(Si)_{2.1}(GaAs)_{27.6}$ and $(Si)_{3.2}(GaAs)_{50.5}$ for the SLs in the bottommost and uppermost sections of Fig. 7, respectively. Although a limited waviness of the layers in Fig. 2 complicates a quantitative comparison of TEM and XRD values for the Si layer thickness, the results of Figs. 6 and 7 clearly demonstrate the absence of dislocations and antiphase domains in III–V/Si/III–V structures for Si layer thicknesses in the 2–4 ML range. TEM results for GaAs–Ge–GaAs single quantum wells for Ge layer thicknesses of 4–14 ML also show well defined, spatially

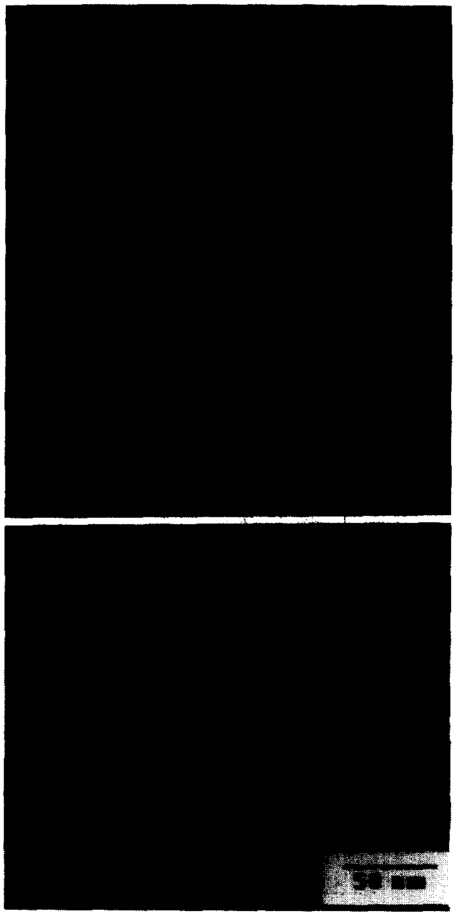

Fig. 7. Cross sectional TEM photographs [(1 1 0) cross section] of two fifteen-period Si–GaAs (0 0 1) SLs. The average superlattice composition, as derived from a comparison of XRD results and dynamical scattering simulations, was $(Si)_{2.1}(GaAs)_{27.6}$ (bottom) and $(Si)_{3.2}(GaAs)_{50.5}$ (top) [Franciosi et al., 1993].

localized group-IV layers, with no evidence of antiphase domain formation within the III–V overlayer [Franciosi et al., 1993]. The results of Figs. 6 and 7 are consistent with recent TEM studies of GaAs–Si–GaAs (0 0 1) heterostructures [Adomi et al., 1991; Liu et al., 1992]. For example, a 9 Å thick Si interface layer was found to be pseudomorphic, while an 18 Å thick interlayer was reportedly at least partially relaxed [Adomi et al., 1991]. Other authors observed defect formation at lower Si thicknesses [Sudersena Rao et al., 1992].

Fig. 8 illustrates how X-ray diffraction (XRD) techniques can be brought to bear on the determinations of the structure of interface layers. XRD patterns recorded in the vicinity of the symmetric (4 0 0) GaAs reflection are shown for GaAs–Si–GaAs (0 0 1) heterostructures involving Si interface layers with nominal thickness of 1 and 2 ML (Figs. 8 (a) and (b), respectively, solid circles) and GaAs overlayers about 2000 Å thick [Sorba et al., 1992a]. Similar patterns were also obtained by other authors [Sudersena Rao et al., 1992]. Due to the different lattice constant of the Si and GaAs crystals, the Si unit cell in the samples is tetragonally distorted, so that the wave field scattered by the GaAs lattice planes in the overlayer is not exactly in phase with that scattered by the lattice planes of the GaAs substrate. The interference between the two waves gives rise to characteristic fringes in the X-ray diffraction pattern, in which the intensity of the fringes depends strongly on the

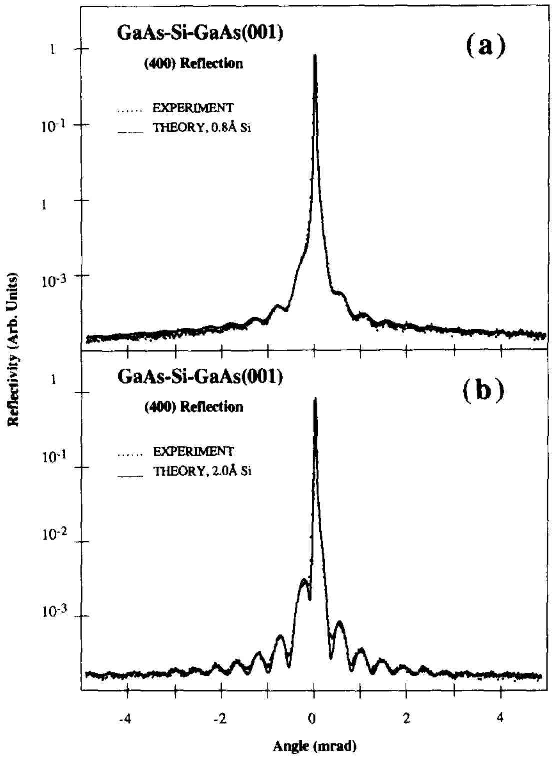

Fig. 8. Cu Kα X-ray diffraction (XRD) patterns (solid circles) near the symmetric (400) GaAs reflection from GaAs–Si–GaAs (001) heterostructures for nominal Si interlayer thicknesses of 1 (a) and 2 (b) monolayers. The result of a dynamical scattering simulation is also shown (solid line). Best agreement with experiment was found for a Si interface layer thickness of 0.8 Å (top) and 2 Å (bottom) [Sorba et al., 1992a].

product of thickness and strain of the embedded Si layer, and the angular distance between the fringes depends on the thickness of the GaAs overlayer [Tapfer and Ploog, 1986, 1989; Tapfer, 1989; Tapfer et al., 1990; Holloway, 1990].

For Si pseudomorphic layers (+4.1% in-plane strain) the strain normal to the interface plane can be calculated from elastic theory as −3.07%, and it is therefore possible to determine the average thickness of the embedded Si layer and of the GaAs overlayer by comparing the experimental diffraction pattern and simulated patterns obtained from dynamical scattering theory for distorted crystals (see solid line in Figs. 8(a) and (b)). The closest match in Fig. 8(a) was obtained for a Si interface layer thickness of 0.8 Å (0.6 ML) and a GaAs overlayer thickness of 1900 Å, and in Fig. 8(b) for a Si thickness of 2 Å (1.4 ML) and a GaAs thickness of 2050 Å. Since no Debye–Waller broadening or smoothing was used in the comparisons of Fig. 8, the agreement between theory and experiment is especially significant and supports an abrupt and coherent nature of the interfaces and good crystalline quality of the overlayers [Tapfer et al., 1992].

Fig. 9 depicts the experimental (Fig. 9a) and simulated (Fig. 9b) diffraction pattern in the vicinity of the symmetric (400) GaAs reflection from a fifteen period Si–GaAs(001) superlattice. The dominant feature is the GaAs substrate peak. The experimental pattern exhibits satellite peaks up to the third order. The closest match between experiment and dynamical simulations was obtained for an average superlattice composition $(\mathrm{Si})_{3.2}(\mathrm{GaAs})_{50.5}$, where the noninteger number of monolayers for Si reflects thickness fluctuations across the structure. We emphasize that satellite peaks are affected by interface disorder, and high order peaks are more sensitive than low order peaks [Tapfer and Ploog, 1986, 1989; Tapfer, 1989; Tapfer et al., 1990; Holloway, 1990]. The remarkable agreement between experiment and the dynamical simulation for ideal structures underscores that ideal pseudomorphic strain and fairly abrupt interfaces can be achieved with appropriate growth protocols even for systems in which some degree of interdiffusion is expected [Sorba et al., 1992b; Gillespie et al., 1992].

We emphasize that the above studies indicate only that *most* of the group-IV atoms can be localized in well-defined pseudomorphic layers with relatively abrupt interfaces by an appropriate growth protocol. It is certainly likely that a minority fraction of the deposited group-IV atoms diffuse in the III–V layers [Brandt et al., 1991]. For example, comparison of the numerical values of Si-layer thicknesses derived from XRD and flux calibrations suggests actual layer thicknesses ranging from 70% to 90% of the nominal values [Sorba et al., 1992a]. Extensive atomic intermixing, as well as any type of nonsubstitutional disorder can be ruled out based on TEM, XRD and on the results of recent Rutherford/backscattering channeling studies [Sudersena Rao et al., 1992; Schmiedeskamp, 1993], but limited substitutional disorder within one or two atomic layers from the interface is more difficult to rule out. In fact, based on high energy photoelectron diffraction studies of Si monolayers on GaAs(001), it was proposed that Si indiffusion results in Si occupancies of 0.6, 0.3 and 0.15 in the first, second and third layer, respectively [Tran and Chambers, 1993a, b].

Raman studies of Si–GaAs(001) SLs were also used to investigate the nature of the sites occupied by the Si atoms in the interface layer. The SL Raman spectra show folded acoustic doublets, together with confinement- and strain-induced shifts of the Si-like optical phonon modes in remarkable agreement with the predictions of lattice dynamics calculations for ideal SL structures [Sorba et al., 1992b, 1993a; Scamarcio et al., 1992a, b]. Fig. 10 shows Ar^+ excited Raman results for a $(\mathrm{Si})_{3.2}(\mathrm{GaAs})_{50.5}$ SL in the optical range ($z(yz)\bar{z}$ polarization). The spectrum is dominated by two asymmetric bands at 291.4 and 476.5 cm^{-1} while a weaker broad band is barely detected at about

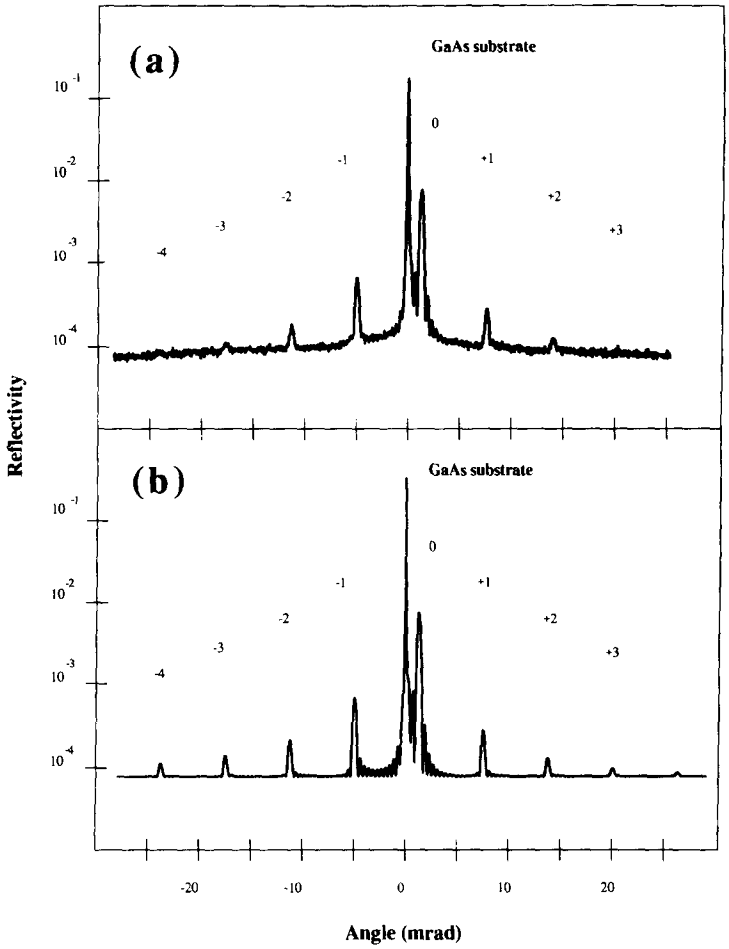

Fig. 9. Experimental (a) and calculated (b) Cu Kα XRD pattern in the vicinity of the symmetric (400) GaAs reflection for a fifteen period Si–GaAs superlattice. Satellite peaks up to the third order are clearly observed. Best agreement between the experimental and calculated patterns was obtained for an average superlattice composition $(\mathrm{Si})_{3.2}(\mathrm{GaAs})_{50.5}$ [Sorba et al., 1992b].

385 cm^{-1}. The Raman feature at 291.4 cm^{-1} in Fig. 10 was attributed to phonon modes quasi-confined [Fasolino et al., 1989; Jusserand and Cardona, 1989] within the GaAs layers. The band at 476.5 cm^{-1} was assigned to confined optical modes in strained Si on the basis of its position, polarization dependence, and variation with SL parameters. This band derives from the majority of the Si atoms, spatially localized in the pseudomorphic interface layers. The weak broad band at about 385 cm^{-1} is likely to reflect chemical roughness of the interface, since it corresponds to a superposition of several local vibrational modes of Si-related defects in GaAs [Ramsteiner et al., 1988; Talwar and Vandevyver, 1989]. The frequencies associated with two such modes, namely $\mathrm{Si}_{\mathrm{As}}$ and $\mathrm{Si}_{\mathrm{Ga}}$ substitutional defects, are shown for comparison by vertical arrows in Fig. 10.

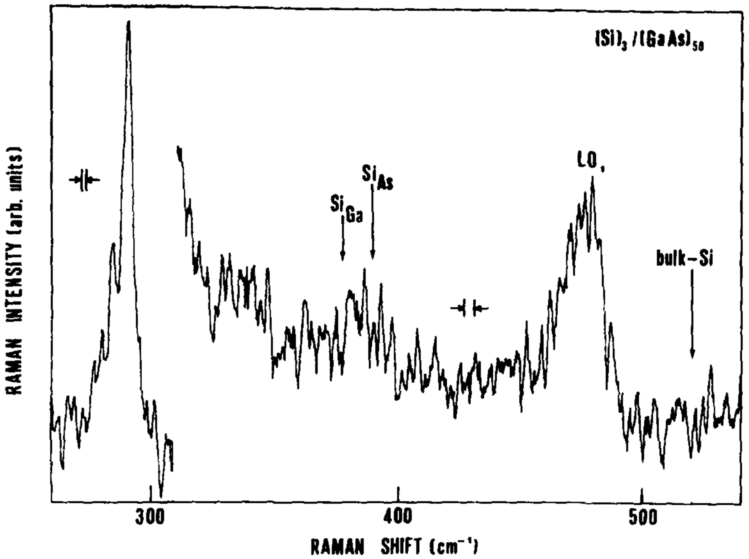

Fig. 10. Raman measurements (off-resonance) in backscattering geometry from the (001) surface for a fifteen period (Si)$_{3.2}$ (GaAs)$_{50.5}$ superlattice excited with the 487.9nm Ar$^+$ line in the optical range ($z(yx)\bar{z}$ polarization). The experimental resolution is shown by horizontal arrows. The major feature at 291.4 cm^{-1} is attributed to phonon modes quasiconfined within the GaAs layers. The band at 476.5cm^{-1} is assigned to confined longitudinal optical (LO$_1$) modes in the pseudomorphic Si layers, while the smaller, broad feature near 385 cm^{-1} reflects the superposition of several local vibrational modes of Si-related defects in GaAs. For comparison, we show (vertical arrows) frequencies associated with Si$_{As}$ and Si$_{Ga}$ substitutional defects in GaAs, and LO modes in unstrained bulk Si [Sorba et al., 1992b].

The intensity of the different local vibrational modes in Raman was correlated to the free carrier density and used to infer the Si site occupation in a recent study of Si δ-doping in GaAs [Ashwin et al., 1993]. This is well illustrated by the results in Fig. 11. When relatively low temperatures were used during Si deposition (400°C), a correspondence between the Raman derived density of Si$_{Ga}$ donor atoms, the free carrier density and the total Si coverage exists up to a Si coverage of ~ 0.02 ML. Above this value, the electron density falls and the Si$_{Ga}$ saturates, indicating the onset of self-compensation, to remain constant up to a coverage of ~ 0.1 ML. At higher Si coverage the intensity of the Si$_{Ga}$ feature falls rapidly, and becomes undetectable for 0.5 ML coverage. This last effect was interpreted as the result of Si aggregation in an elemental Si layer, leading to extensive self-compensation.

All of the results for III–V/Si/III–V structures (III–V = AlAs, GaAs) discussed in this paragraph were obtained for relatively low Si growth temperatures 400°C–500°C, and we believe are starting to paint a consistent picture. During low-temperature growth aggregation of Si atoms in the III–V matrix yields layers that are pseudomorphic for thicknesses below 4–8 ML, and relatively defect free. The Si atoms are predominantly localized in these layers, although some chemical roughness at the interface may exist on the scale of a couple of atomic layers, with the formation of both Si$_{Ga}$ and Si$_{As}$ defects. Indiffusion of Si atoms to yield selective n-type doping of the III–V matrix can involve no more than ~ 0.1 ML of Si at the growth temperatures employed in these studies.

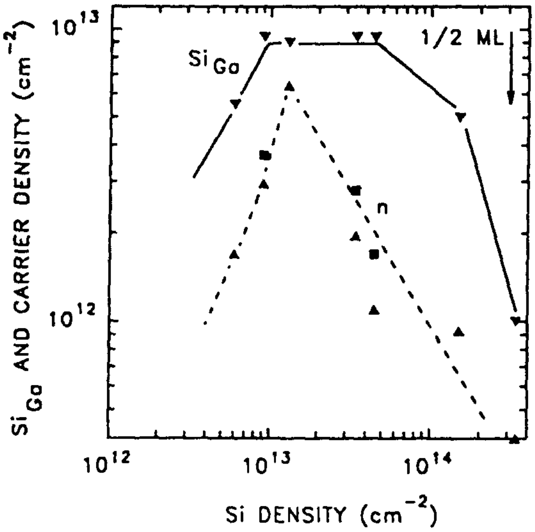

Fig. 11. Self-compensation in periodic (100 periods) Si δ-doping structures grown by MBE at 400°C in GaAs(001). The measured free carrier concentration and the apparent density of Si_{Ga} defects is plotted as a function of the total Si coverage per δ-doped layer, as determined by secondary ion mass spectrometry. The data for the free carrier concentration were obtained from Hall effect (solid triangles pointing downward) and infrared absorption (solid squares) measurements. The concentration of Si_{Ga} sites (solid triangles pointing upward) was deduced from the intensity of the related local vibrational mode in Raman spectroscopy. Solid and dashed lines are intended as a guide to the eye only [Ashwin et al., 1993].

3. Theoretical methods

In order to appreciate the issues involved in band offset engineering, it is helpful to review some theoretical notions about the mechanisms that determine band discontinuities. In this section we present a brief summary of various theories that address the atomic and electronic structure of semiconductor interfaces, and band offsets in particular. An excellent review of theoretical approaches has been given in [Tersoff, 1987], to which we refer the interested reader for a fuller discussion.

One important piece of information we would like to obtain from such theoretical treatments is whether the band offsets are *intrinsic* (i.e., determined solely by properties of the bulk materials) or not (i.e., dependent on specific properties of the interface). If the band offsets are intrinsic, then they cannot be changed by variations at the interface. If they are not intrinsic, then there are (in principle) ways to "engineer" the offset [Martin, 1989]. It will turn out that the answer depends on the type of interface. There are certain classes of interfaces for which the band offsets, to a high degree of accuracy, can be considered intrinsic. Nonetheless, there exist other types of interfaces where the band offsets can definitely be modified by manipulating the interfacial structure. Theory provides guidance as to the determining factors.

We will be considering an interface between two lattice-matched semiconductors A and B; relaxation of atoms around the interface is taken into account, but discussion of more complicated reconstructions, and of the effect of impurities or interlayers will be postponed until Section 4.

3.1. Formulation of the band-lineup problem

We can formulate the band-lineup problem as follows: we start with two semiconductors, A and B, with different bandgaps E_g^A and E_g^B, and bring them together at an interface. Since the bandgap is discontinuous, it is clear that the valence and/or conduction bands will also be discontinuous, as illustrated in Fig. 12. Note that the bands on either side of the interface are depicted as flat, corresponding to the notion (see Sections 2.1 and 2.3) that we are only interested in a region on the order of a few atomic distances around the interface, and that band bending is negligible on this length scale.

Various theoretical methods are capable of calculating the band structure of a semiconductor; the interface problem amounts to finding a way to line up the two band structures across the interface. The band structure of semiconductor A can be calculated relative to a reference level (usually an average of the electrostatic potential) $\bar{V}_A$. Similarly, the band structure of semiconductor B is referred to a level $\bar{V}_B$. For instance, the position of the valence-band maximum, E_v, is a distance $E_v - \bar{V}$ above the position of the average electrostatic potential (see Fig. 12). The band offset problem then consists of determining the difference in average electrostatic potentials between A and B, i.e. $\Delta\bar{V}$. The problem would thus be solved *if* we could determine the positions of the average electrostatic potentials inside A and B on an absolute energy scale, e.g. with respect to the vacuum level. "Energy" refers here to the "potential energy", which is (to within a constant factor) equivalent to the potential.

It may seem that if one is able to carry out the band structure calculations for the two semiconductors, then the problem is solved, since these calculations will provide information about

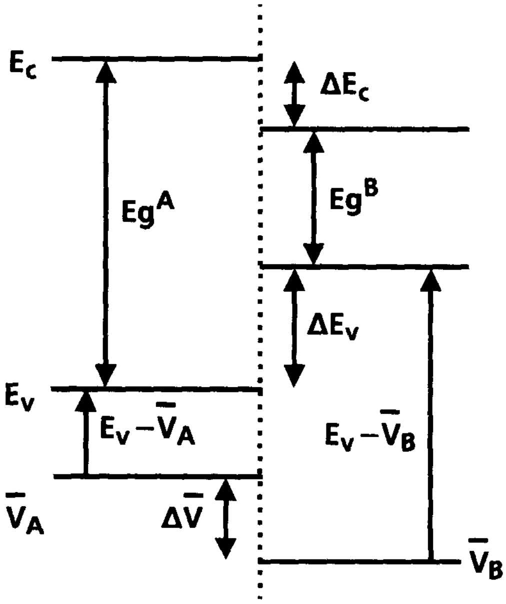

Fig. 12. Schematic illustration of the band structure lineup problem between semiconductors A and B. The positions of valence and conduction bands are indicated, all referred to their appropriate reference level $\bar{V}$ in each semiconductor. The distance between $\bar{V}_A$ and $\bar{V}_B$ determines the band lineup.

the position of $\bar{V}_A$ and $\bar{V}_B$. Unfortunately this is not so. The problem is that there is no absolute reference for the average potential in an infinite solid. This problem is caused by the long-range nature of the Coulomb interaction, which makes the average potential of an infinite system ill-defined [Kleinman, 1981]. The fact that the average potential in an infinite solid is ill-defined is often described associating single particle-energies with "removal energies". Since in an infinite system there is no "elsewhere" (e.g., a vacuum level) to remove an electron to, it would seem to follow that the single-particle energies in the infinite semiconductor cannot be put on an absolute energy scale. This argument is incomplete, if not wrong, as was pointed out by Baroni [Baroni et al., 1989]. If the interactions were finite in range, the average potential inside a macroscopic but finite sample would actually *not* depend on the shape of the solid or surface effects, and would therefore have a well-defined thermodynamic limit. It is precisely the long-range nature of the Coulomb interaction that causes the removal energies to depend on the detailed structure of the surface. Or, in the case of an interface, it is the long-range nature of the Coulomb interaction that causes the presence of a dipole at an interface to shift the energy levels throughout the semi-infinite solid on either side.

It follows that a band structure calculation for an individual solid cannot provide information about the absolute position of the average potential. To calculate a band lineup, one has to obtain additional information about the behavior of the potentials in the neighborhood of the interface. This indicates that, at least *in principle*, the details of the atomic structure near the interface may affect the potentials far away, and hence the band-lineup.

We thus have to accept that when we study a bulk semiconductor, the average electrostatic potential inside the solid is not known on an absolute energy scale, but is defined only to within an arbitrary constant. This arbitrary constant can be fixed by making specific assumptions about the boundary conditions. In order to solve the heterojunction problem, an obvious approach is to specify the boundary condition to be exactly that at the semiconductor interface, i.e., to perform a calculation in which both semiconductors are present and joined at the junction. This ensures that the electrostatic potentials of both materials are expressed with respect to the same reference, and allows direct extraction of $\Delta\bar{V}$ and thus of the band discontinuities. Various theoretical approaches have addressed the problem from this angle, with considerable success for a number of important interfaces. However, there are some problems associated with this approach: each new interface requires a new calculation (which is usually quite time-consuming). Also, even though the calculations provide quantitative answers, they do not directly provide any information about the mechanisms that determine the lineups. Various model theories have therefore been developed to address the problem.

Following Martin [Martin, 1989], we categorize theoretical work in four classes: (1) fully self-consistent ab initio calculations for particular interface structures; (2) linear-response theory, applied to ab initio calculations; (3) calculations based on simplified, approximate Hamiltonians; and (4) simple models. We discuss these approaches one by one.

3.2. *Self-consistent first-principles calculations*

"First-principles" refers to the fact that methods in this category are aimed at solving the quantum-mechanical equations for the system under study, without any input from experiment. Density-functional theory is a first-principles technique that has been widely applied to the study of semiconductor heterojunctions. The density-functional method allows the calculation of the ground-state energy of a system of atoms through self-consistent solution of a one-particle Schrödinger equation [Hohenber and Kohn, 1964; Kohn and Sham, 1965]. Electron–electron interactions are included by adding an exchange and correlation (XC) term to the Hartree potential; the XC term is expressed as a functional of the charge density. In the local-density approximation (LDA), this functional is reduced to a function of the local charge density. Calculating the ground-state energy of a system is an important aspect of the study of interfaces, since a determination of the stable structure should be the first step in the theoretical analysis. By calculating the energy of the system as a function of atomic positions one can determine the stable structure, including relaxations and reconstructions, and derive formation energies. But, as we will see below, density-functional calculations also provide information about the electronic structure of the system, and yield information about band offsets.

Density-functional theory can be applied to all-electron calculations, for instance in augmented-plane-wave (APW) methods [Massidda et al., 1987], or in the more tractable linearized-muffin-tin-orbital (LMTO) method [Christensen, 1988a]. However, in calculations for semiconductors it is usually unnecessary to carry around information about the core electrons; an efficient way to eliminate the core electrons from the problem is provided by the use of pseudopotentials. Ab initio, norm-conserving pseudopotentials are used in all state-of-the-art pseudopotential calculations [Hamann et al., 1979].

The mathematical approach used in the self-consistent solution of the variational problem typically assumes periodicity. For an interface problem, periodicity can be maintained by considering a superlattice structure, in which layers of the two semiconductors are periodically repeated. Besides directly providing useful information about actual superlattice structures, this approach also yields results for isolated interfaces, provided the layers are sufficiently thick to ensure adequate separation between adjacent interfaces. Experience has shown that to extract band offsets layers of four to six atoms thick typically suffice [Christensen, 1988a; Van de Walle and Martin, 1987]; charge densities and potentials indeed typically converge quite rapidly to their bulk value away from the interface. It is then possible to identify a "bulk-like" region in the middle of each superlattice layer, where the value of an average potential can be determined. The procedure is illustrated in Fig. 13 for the case of a Si–Ge interface. For the purpose of deriving the band-lineup, we are only interested in the behavior of the potential as we move perpendicular to the interface; the remaining two coordinates can be eliminated by averaging in planes parallel to the interface:

$$\bar{V}(z) = \frac{1}{S} \int_S V(x, y, z) \mathrm{d}x \mathrm{d}y, \tag{4}$$

where S represents the area of a unit cell in the plane of the interface. We are then left with a one-dimensional function, which still exhibits periodic variations in the direction perpendicular to the interface. As illustrated in Fig. 13, this function rapidly recovers its bulk behavior in each of the two materials comprising the junction as one moves away from the interface; however, the positions of the average potentials in the bulk-like regions are shifted with respect to one another, providing exactly the quantity $\Delta\bar{V}$ that we needed, according to Fig. 12, to obtain the band-lineup. Indeed, separate bulk calculations for the two semiconductors (Si and Ge in our example) can be carried out, providing information about individual band positions with respect to the average potential $\bar{V}$.

This procedure for obtaining band offsets is actually similar to that followed empirically in XPS determinations of the offsets (see Section 2.3). In XPS, typically, the separation between two

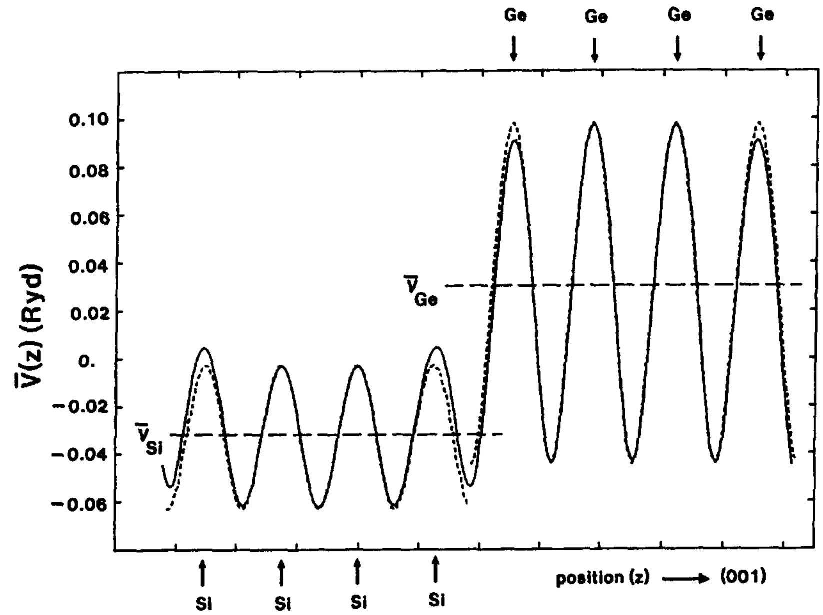

Fig. 13. Variation of the plane-averaged potential $\bar{V}$ (as defined in Eq. (4) across a Si–Ge (001) interface, calculated in a 4 + 4 superlattice (with unstrained Si and strained Ge). The dashed lines show the corresponding potentials for bulk Si and (strained) bulk Ge (shifted so that their average values coincide with $\bar{V}_{Si}$ and $\bar{V}_{Ge}$. The bulk potentials are seen to coincide with $\bar{V}(Z)$ already at a distance of one atomic layer away from the interface. Note that the average levels $\bar{V}_{Si}$ and $\bar{V}_{Ge}$ are shifted with respect to one another; this shift determines the band lineup [Van de Walle and Martin, 1986b].

representative core levels is measured across the interface; independent measurements on bulk samples are performed to obtain the energy separation between the valence-band maximum and the core levels in each material. The core level separation is then used to line up the valence bands and obtain the band offsets. All-electron calculations can actually mimic this approach, and provide information about core-level lineups as well as band offsets [Massidda et al., 1987]. Some particularly interesting information in this respect was obtained using LMTO calculations to calculate the energy difference between the valence-band maximum and the core levels at a strained Si–Ge heterojunction [Schwartz et al., 1989]. Pseudopotential calculations cannot directly provide core level lineups, since the core electrons are removed from the problem. However, using average potentials for the lineup is very similar in spirit.

It is important to acknowledge that in density-functional theory the calculated eigenvalues do not necessarily correspond to quasiparticle energies. A well-known consequence of this deficiency is the failure of density-functional theory to produce the correct band gaps. It is therefore important to realize that corrections beyond density-functional theory may be necessary to obtain the exact band positions (with respect to the average electrostatic potential). We also note, however, that the calculated potential lineup term ($\Delta \bar{V}$) depends only on the charge density of the heterojunction, and as such is a ground-state property that is reliably given by density-functional theory. The corrections to LDA are therefore limited to the positions of the quasiparticle energy levels that are obtained in bulk calculations for the individual materials. Quasiparticle calculations of this nature have been carried out for a wide variety of semiconductors [Zhu et al., 1991]; by comparing the results with LDA band structures, it was found that the average LDA error in the heterojunction valence-band offset was about 120 meV. For the purposes of the present review, we should bear in mind that these errors do not enter if one is only interested in *changes* in the band offsets (induced by changes in the interfacial composition and structure), which will only affect the potential-lineup term.

Many groups have carried out self-consistent first-principles calculations for a variety of interfaces, and we will not attempt to list all references here. In Section 4 we will list a number of conclusions that have been obtained by examining first principles results for a large number of interfaces, and examine their impact on the issue of heterojunction engineering.

3.2.1. The interface dipole: facts and myths

The concept of an "interface dipole" is often abused. When properly defined, a qualitative and quantitative discussion of an interface dipole can yield important information about the heterojunction interface. Unfortunately, very often no proper definition is given, and many people do not even realize that without such a definition the concept is meaningless.

One definition that is often used, in particular in connection with first-principles pseudopotential calculations, is the following [Bylander and Kleinman, 1988a,b]: suppose one takes the difference between the charge density at the interface (obtained from a supercell calculation, and averaged in planes parallel to the interface), and the charge density in the bulk (similarly averaged). One can then use Poisson's equation to calculate a dipole. The dipole, however, is not unique, since it depends critically on where the mathematical surface representing the interface is chosen. The location of the interface determines that on one side, the bulk charge density of semiconductor A will be subtracted, and on the other side that of semiconductor B. A different choice of the "mathematical" interface can produce a very different dipole. In addition, comparison between different interface orientations makes little sense with this definition. The bottom line is that the concept of interface dipole is best avoided, unless one specifies explicitly which definition is being used, and uses the concept only to identify trends between situations which are sufficiently similar (e.g., same interface orientation) to allow a meaningful comparison.

The issue of defining an interface dipole can be appropriately addressed with the technique of "macroscopic averaging", developed by Baldereschi and co-workers [Baldereschi et al., 1988]. These authors developed an elegant and rigorous technique for analyzing the potentials and charge densities around a semiconductor interface. It is based on the concept of a macroscopic average. As we see in Fig. 13, the microscopic potentials and charge densities around an interface fluctuate with a periodicity imposed by the lattice. Concepts such as the discontinuity in average potentials are actually defined on a macroscopic scale, since they involve the difference in potential on either side of the junction, and far away from the interface. These macroscopic quantities can conveniently be extracted by filtering out the microscopic oscillations, which is most easily accomplished by averaging the microscopic quantities over a volume corresponding to the unit cell.

Looking at a heterojunction, we know that the average potential will undergo a shift as one passes through the interface from one semiconductor to the other. The shift in the average potential is actually a macroscopic quantity, since it can be observed in measurements far away from the junction. On a microscopic level, however, the potential looks very complicated because it exhibits a periodic variation on the atomic scale. This periodic variation is actually irrelevant for the macroscopic quantity (the potential-lineup) that we are interested in, and we would like to "filter out" these rapid fluctuations in the potential, and only take into account the variation on longer length scales. This type of filtering is a familiar concept in classical electromagnetism for instance in the theory of dielectric polarization. Baldereschi and co-workers [Baldereschi et al., 1988] have applied the macroscopic averaging technique to the heterojunction problem.

We already know that to extract dipoles and lineups we may perform an average of the potential in planes parallel to the interface, as defined in Eq. (4). The quantity ($\bar{V}$) is a one-dimensional function, which still exhibits periodic variations in the direction perpendicular to the interface. The macroscopic average is accomplished by averaging this function, at each point, over a distance corresponding to one period:

$$\bar{\bar{V}}(z)=\frac{1}{a}\int_{z-a/2}^{z+a/2}\bar{V}(z')\,\mathrm{d}z', \tag{5}$$

where a is the length of one period in the direction perpendicular to the interface. The same procedure can be applied to the charge density; results for a GaAs–AlAs interface are illustrated in Fig. 14. We see in the figure that the macroscopic average of the potential varies across the interface from one constant value to a different one. The lineup is related to the dipole moment of the charge profile:

$$\Delta\bar{V}=\frac{e^2}{\varepsilon_0}\int z[\bar{n}(z)-n_0]\,\mathrm{d}z, \tag{6}$$

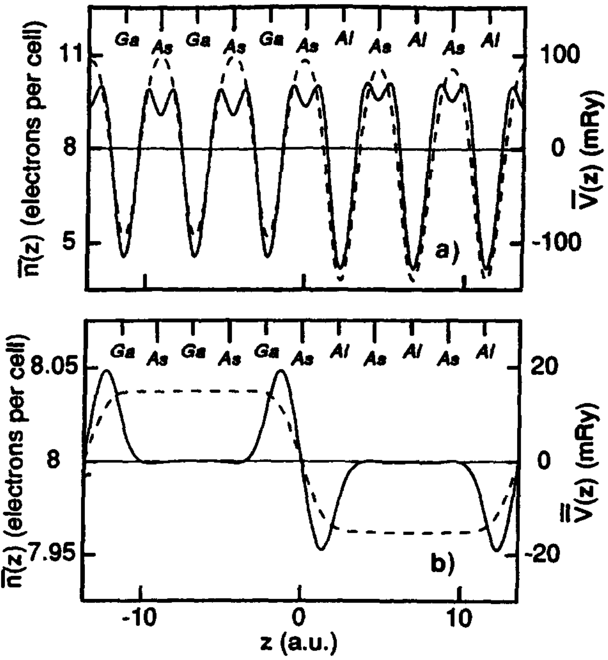

Fig. 14. Planar (a) and macroscopic (b) averages of the change density (solid lines) and the electrostatic potential (dashed lines) of $(GaAs)_3(AlAs)_3$ (001) [Boroni et al., 1989].

where n_0 is the average electronic density of the two bulk materials. This provides an unambiguous definition of the interface dipole, without having to make any assumption about the nature of the interface.

The macroscopic average defined above relied on the fact that the periodicity of the microscopic variations would be the same on both sides of the interface. This assumption obviously is not satisfied in the case of an interface between lattice-mismatched semiconductors. The macroscopic averaging procedure can actually be extended to such applications, as described by Baroni and co-workers [Baroni et al., 1989].

After having stressed that great caution should be exercised in using the concept of an interface dipole, it is worth pointing out that this concept can still be a very useful notion. In particular, one is often interested not in the absolute magnitude, but in changes in the interface dipole, brought about by some modification of the interface (e.g., the presence of an interlayer), while the "semiinfinite" bulk materials on either side remain unmodified. The experimentally measured change in the band offset can then be directly associated with a change in the interface dipole. It is then the task of theoretical analysis to try and ascribe this change to a particular modification of the electronic structure, and in the process of doing so care should be taken in the definition and calculation of any interface dipole.

3.3. Linear-response theory

The first application of linear-response theory to the problem of heterojunction band offsets appeared in Tersoff's study of the role of quantum dipoles in the band-lineup [Tersoff, 1984c]. Tersoff used a (qualitative) linear-response argument to show that interface dipoles cannot be neglected, contrary to the prevailing view at that time. This argument also lead to the 1986 Harrison–Tersoff approach [Harrison and Tersoff, 1986]. These model theories will be discussed in Section 3.5.

A more quantitative application of linear-response theory to heterojunctions, based on first-principles calculations, has been developed by Baroni et al. [Baroni et al., 1988, 1989]. These authors showed that a linear-response approach gives essentially the same results as full-fledged self-consistent calculations, if applied in situations where its use is justified. The band offset can be considered to be the sum of two terms [Baroni et al., 1988]: the first term depends only on bulk properties, and is therefore independent of interface orientation and abruptness; the second term, which vanishes for isovalent and ideally abrupt nonpolar heterojunctions, does depend on the details of the interface geometry, but it can be calculated (once the geometry is known) from simple quantities such as lattice parameters and the dielectric constants of the constituents.

The linear response approach [Baroni et al., 1988, 1989] can be described as follows. The goal is to model the *difference* between the two semiconductors, i.e., the difference with respect to an optimally chosen average (whose contribution to the band offset vanishes). For instance, for the case of GaAs–AlAs (0 0 1) one can construct a virtual crystal of $Ga_{0.5}Al_{0.5}As$, and then introduce the interface; on one side of the interface, a perturbation is added to turn the crystal into pure GaAs, while on the other side the perturbation turns it into pure AlAs. The bare potential describing such a perturbation is the sum of localized potentials that transform the virtual ions ($Ga_{0.5}Al_{0.5}$) into real ones (Ga or Al). It turns out that these perturbations are sufficiently small to be handled within linear-response theory. The electrostatic potential-lineup across the interface can then be obtained to first order from the charge-density response to those localized perturbations. The results for isovalent interfaces such as GaAs–AlAs are quite accurate, as compared with fully self-consistent calculations.

The fact that linear response theory would work well for semiconductors with sufficiently similar potentials was already pointed out by Bylander and Kleinman in 1987 [Bylander and Kleinman 1987, 1988a, b]. However, these authors speculated [Bylander and Kleinman, 1989] that while linear response theory is entirely adequate for a system such as GaAs–AlAs, it would already exhibit inaccuracies for a system such as GaAs–Ge [in the (1 1 0) orientation], because of the larger difference in potentials of the constituents. Baroni and co-workers have shown, however, that even for GaAs–Ge, the predictions of linear response theory coincide exactly with those of full self-consistent calculations [Baroni et al., 1989].

For nonisovalent interfaces, such as GaAs–Ge, one can still apply linear-response theory, but in the case of polar interfaces, and nonabrupt nonpolar interface orientations [Baldereschi et al., 1993a] additional effects must be taken into account. These additional terms can be obtained from simple electrostatics, still within the linear-response approach; we will postpone a discussion until Section 4.2.3.1.

3.4. Calculations based on simplified Hamiltonians

Self-consistent tight-binding calculations have produced interesting information about heterojunction band offsets. One disadvantage of the approach is that in most cases no information about the energy of the system is produced, so that one does not know whether a particular configuration is stable or energetically allowed. Another potential problem resides in the choice of the tight-binding parameters; typically, these parameters are fitted to reproduce certain bulk properties, but their suitability to describe different types of bonding at an interface is not guaranteed. In addition, there is no clear prescription for the choice of the energy level on an absolute energy scale; sometimes the electron affinity is used [Perez et al., 1990], even though this is a surface property which may or may not have any bearing on the interface problem (the failure of the electron affinity rule, to be discussed in Section 3.5.1).

Self-consistent tight-binding calculations have in many instances produced results for band offsets which are close to those obtained with first-principles methods. They can play a valuable role in heterojunction investigations, as long as one is aware of the intrinsic limitations of the method.

3.5. Simple models

All of the model theories have in common that they attempt to associate a reference level with each semiconductor, the reference level being an intrinsic property of the bulk semiconductor; band offsets should then follow from simply lining up the reference levels. This assumption by itself implies that the band offsets resulting from these models will be linear, transitive, and independent of interface orientation (see Section 2.1). One can therefore evaluate how successful one expects such model theories to be by inspecting experimental results (or theoretical results obtained from reliable self-consistent first-principles calculations) for classes of interfaces. If these offsets obey the commutativity and transitivity rules (see Eqs. (1) and (2)), they can at least in principle be described by a linear theory. If transitivity and commutativity are not fulfilled, this is a clear indication that interface-specific effects are occurring that cannot be described by simple models based solely on intrinsic reference levels. (One can still try to keep the simple model as a basis, and add certain features to it, such as effects of electrostatic dipoles at polar interfaces; we will see examples of this in Section 4.)

The model theories based on reference levels usually employ the concept of an interface dipole, with the magnitude and importance attached to the dipole varying widely between different theories. As pointed out by Tersoff [Tersoff, 1987], these different point of views can largely be explained by realizing that, as discussed above, the dipole depends on the choice of reference. Some theories a priori choose a reference so that during the lineup process the interface dipole will be minimized. Other theories choose a different reference (often associated with the particular calculation technique), and then emphasize that a dipole will arise that drives the system towards a particular lineup. The latter approach may have the advantage that it is more similar to treatments of metal/semiconductor junctions, where charge transfer clearly is an important driving force. However, within the field of semiconductor heterojunctions both types of model theories seem capable of success.

We will not attempt here to provide a comprehensive list or description of the various heterojunction theories that have been developed over the years, but confine ourselves to mentioning or discussing certain approaches that are relevant for our understanding of the issues related to heterojunction engineering.

3.5.1. Intrinsic reference levels without a need for additional dipoles

The oldest heterojunction theory is Anderson's electron-affinity rule [Anderson, 1962]. Anderson chose electron affinities as the quantities that would serve as a reference for lining up bands. The problem is that electron affinities are experimental quantities that depend on orientation, relaxation, reconstruction, and other properties of the surface, all of which can introduce extra dipoles that shift the energy bands in the bulk. These details of the surface structure in general bear absolutely no relation to the structure of the semiconductor interface, and hence one should not expect electron affinities to serve as appropriate reference levels. Nonetheless, the fundamental idea is a valuable one, if it were only possible to define some kind of "intrinsic" electron affinity, which would ignore surface effects and only take the "bulk" contribution into account [Van Vechten, 1985]. However, the separation between bulk and surface contributions is not unique, and it is not clear how to determine the "intrinsic" contribution from experimental information alone.

Harrison's theory [Harrison, 1977] attempted to derive intrinsic reference levels for bulk semiconductors, based on atomic energy levels, in the context of (LCAO) Linear Combination of Atomic Orbitals theory. It should be noted that Harrison later took a somewhat different point of view [Harrison and Tersoff, 1986], influenced by the work of Tersoff [Tersoff, 1984b], producing a tight-binding theory of heterojunctions and interface dipoles which is related to the concept of charge neutrality levels discussed in Section 3.5.2. We also mention the approach of Frensley and Kroemer [Frensley and Kroemer, 1977], who were probably the first to take information obtained from band-structure calculations and use it to construct a model for band lineups. They relied on establishing reference levels based upon values of the potential at interstitial sites. The accuracy of the approach was limited (see discussion in [Van de Walle and Martin, 1987]), but it definitely drove the field in the direction of attempting to establish intrinsic reference levels based on bulk calculations.

3.5.1.1. Model-solid approach In Section 3.1 we discussed the fundamental issue of the band-lineup problem, namely the problem of defining the value of the average potential within a solid on an absolute energy scale. We mentioned that once a specific assumption is made about the boundary conditions, the value of the average electrostatic potential is fixed. However, since the correct boundary condition for the semiconductor interface is not known a priori, a specific assumption will produce average potentials that are well defined but not unique, and not necessarily relevant for the band offset problem. Nonetheless, these average potentials can be used as a reference, and the problem then consists of determining the discontinuity in average potentials $\Delta\bar{V}$ that produces the correct band lineups. This $\Delta\bar{V}$ has often been referred to as "the interface dipole"; however, from the discussion above it should be clear that this quantity has no physical meaning, since it depends on the assumptions made to fix the arbitrary constant in the average electrostatic potential. Different assumptions would produce entirely different values of $\Delta\bar{V}$, while still producing the same,correct valence-band offset; in Fig. 12, a different assumption for the boundary conditions would change the values of $\bar{V}$, affecting both $E_V - \bar{V}$ and $\Delta\bar{V}$ such that $E_V(A) - E_V(B)$ remains constant.

One can try to choose the boundary conditions such that the resulting $\bar{V}$ values would produce good band offsets without any additional corrections, i.e., one can attempt to minimize any additional correction $\Delta\bar{V}$. The "model solid theory" of Van de Walle and Martin [Van de Walle and Martin, 1987; Van de Walle, 1989] follows this approach. Van de Walle and Martin analyzed the (self-consistent) charge distribution around a variety of semiconductor interfaces, and compared it with various possible models to generate such a charge density. It was found that a rather simple model, consisting of a superposition of neutral atomic charge densities, produces densities that are a good approximation to the self-consistent densities. Using neutral atoms as a building block has an important advantage: since each building block is neutral, and has no dipole nor quadrupole moment, the average potential in a system consisting of a superposition of these building blocks is completely determined by the average potential in a single building block. (Another way of looking at this, is that, for a superposition of neutral atoms, the details of the surface structure do not affect the average potential, even in the presence of the long-range Coulomb interaction.) It then becomes possible to calculate values of the average potential on a common energy scale for all semiconductors, and band offsets can be directly obtained by taking differences between entries in a table. The advantage of this model-solid approach is that it is very simple, and can be applied to any semiconductor. The price paid for this simplicity and generality is a certain loss of accuracy; the error bar on band-lineups obtained within the model-solid approach has been estimated to be ~0.2 eV.

As discussed by Van de Walle and Martin [Van de Walle and Martin, 1987; Van de Walle, 1989], the model-solid approach is expected to work well for nonpolar interfaces, in cases where no additional dipoles are expected. It is possible to go beyond this class of interfaces and still use the model-solid approach, although additional contributions will then arise, which can be evaluated based on electrostatic theory (see Section 4.2.3.1).

3.5.1.2. Atom-centered Wigner–Seitz cells Other models can be developed that have higher accuracy by providing a better description of the self-consistent charge densities. However, this is usually at the expense of general applicability. Baldereschi and co-workers [Baldereschi et al., 1988] have developed a model in which the elementary building blocks are atom-centered Wigner–Seitz (WS) cells. Within each WS cell, the self-consistent charge density for the bulk semiconductor is used. Once again, these cells are neutral and bear no dipole or quadrupole moments, making the potential sufficiently short range not to produce any shift in the macroscopic potential across the interface. The model thus produces an exact charge density for the bulk material, and it has also been shown to produce a charge density around the GaAs–AlAs interface which is very close to the self-consistent result. This model therefore yields a very good value for the GaAs–AlAs band-lineups. However, it is clear that this model is less easily applicable to interfaces between materials with a lattice mismatch, where the bulk WS cells do not match geometrically anymore.

The approaches discussed in this section are based upon the notion of deriving a reference level in each semiconductor which would be perturbed as little as possible when two semiconductors were joined at the interface; i.e., no additional dipoles would be generated. The models that we discuss next, on the other hand, devote little attention to what the initial, "zeroth-order" reference levels are, and stress that local charge neutrality will generate interface dipoles that drive the system towards a particular type of lineup.

3.5.2. *Alignment of intrinsic reference levels driven by dipoles: charge neutrality levels*

A particular set of model theories is based upon the notion of an induced density of interface states [Tejedor et al., 1977; Tersoff, 1984b,c; Flores et al., 1989, 1993]. The idea is that the proximity of another material at the interface induces a distribution of states in the gap of the semiconductor. In the case of a metal, these states would be related to tails of metal wave functions, and the states are commonly referred to as Metal-Induced Gap States (MIGS). The induced states can carry a certain amount of charge, depending on what fraction of them are filled. The concept of a "charge neutrality level" (CNL) is similar to the Fermi level in a metal; when states below the CNL are filled, local charge neutrality is maintained. In general, the CNL will be close to the metal Fermi energy at a metal–semiconductor junction. At a heterojunction, the band lineup will be (approximately) determined by lining up the CNLs for the two semiconductors. Indeed, if the levels are not aligned, charge would flow between the two materials, which would set up a dipole that would restore the initial situation. The issues relating to CNLs are quite subtle, and intimately related to polarization associated with dielectric screening; a discussion can be found in work by Harrison and Tersoff [Harrison and Tersoff, 1986].

Initial work on CNLs tended to emphasize their intrinsic nature, i.e., the fact that they could be regarded as a bulk property of the semiconductor. Tersoff [Tersoff, 1984b] proposed to calculate a CNL based upon the bulk band structure. Flores and collaborators [Muñoz et al., 1987] carried out self-consistent tight-binding calculations for (1 1 0) interfaces, and found that it was possible to explain the results by invoking local charge neutrality, i.e., the lining up of intrinsic CNLs.

More recently, Flores and co-workers [Flores et al., 1989; Perez et al., 1990] have introduced the concept of an "extrinsic" CNL to emphasize that the CNL can depend on the details of the interface. For a semiconductor interface, the intrinsic CNL would determine the band offsets at ideal junctions with small lattice mismatch. More complicated geometries can lead to modified "extrinsic"CNLs, and hence changes in band offsets. In our opinion, this approach could equally well be formulated in terms of the original "intrinsic" CNL, valid for an ideal, nonpolar interface, and additional dipole contributions (which in many cases are probably easy to determine from elementary electrostatics). The approach would then be similar to that of the model-solid theory, or linear response, which acknowledge that the simple, linear band-offset models can only be valid for a certain class of ideal, nonpolar interfaces, and that additional dipoles can occur in many situations. It seems to us that redefining the concept of the CNL to include these additional dipoles, by introducing "extrinsic" CNLs, complicates the situation rather than simplifying it.

3.6. *The effect of strain*

3.6.1. *Building strain into the layers*

In our discussion of heterojunction engineering we emphasize methods to shift the bands on either side of the interface with respecet to one another; the presence of strain in one or both of the materials is an interesting and widely used method of obtaining this effect. It is well known that hydrostatic or uniaxial strain has the effect of changing the band gap of the semiconductor; it therefore follows that also the band offsets will be affected. The effects of strain on the band structure have been appreciated and investigated since the beginning of semiconductor research. Most experiments have been carried out by external application of hydrostatic or uniaxial stress (see, e.g. the studies by Pollak and Cardona [Pollak and Cardona, 1968]).

With the advent of modern growth techniques such as molecular beam epitaxy it was realized that strain could be built into a given semiconductor by growing it on top of a suitably lattice-mismatched substrate [Osbourn, 1982]. If the lattice mismatch is too large, or if the overlayer is too thick, the strain energy becomes too large, and misfit dislocations are formed to relieve the strain, allowing the overlayer to approach its own lattice constant. But if the lattice mismatch is modest, and the overlayer thin enough (below the so-called critical layer thickness), pseudomorphic growth is achieved. The overlayer assumes then an in-plane lattice constant equal to that of the substrate (which acts as a template) [Van der Merwe, 1963; Van der Merwe and Van der Berg, 1972]. The lattice constant in the perpendicular direction is also affected, since the strained semiconductor strives to conserve its overall volume, although usually it does not quite succeed in doing so; the relationship between parallel and perpendicular strain is given by Poisson's ratio, which is determined by the elastic constants of the semiconductor. Expressions for these strains can be derived in a straightforward fashion by minimizing the expression for elastic strain energy; formulas for different orientations have been derived and can be found in the literature (see, e.g., [Van de Walle, 1989]).

When a thin overlayer is grown on top of a thick substrate, it is safe to assume that only the overlayer will be strained, and the substrate will be relatively unaffected. The situation would be different in a free-standing superlattice, where layers of finite thickness are alternated. In this case the strain will be distributed over both types of layers; once again, formulas can be derived by minimizing the strain energy [Van de Walle, 1989].

Given a particular structure, we can thus determine the strain in each of the semiconductor constituents. We are assuming here that the strains are uniform and homogeneous throughout the layer, as should be the case when the thickness is below the critical layer thickness and perfect pseudomorphic growth is achieved. It is worth remarking that the determination of strains based on the application of macroscopic elastic theory has been shown to be accurate even for very small thicknesses of the semiconductor (down to a few atomic layers) [Van de Walle and Martin, 1986]. In general, the strain condition of the material can be expressed in the form of a strain tensor; in practice, quite often only the strain components parallel or perpendicular to the interface are given, which suffice to construct the strain tensor.

Tuning of strain is often achieved by varying the composition in an alloy overlayer. For example, a $Si_{1-x}Ge_x$ layer can be grown on top of a Si substrate. The lattice constant of the alloy will increase with increasing Ge content x (for most alloys this behavior is adequately described by linear interpolation, i.e., Vegard's law); as the lattice constant of the overlayer increases, the lattice mismatch with the substrate also increases, leading to larger strain in the overlayer, and correspondingly larger effects on the alloy band structure. These strain effects are superimposed on the changes in band structure corresponding to the alloying effect. Strain-induced changes in band -lineups can also be achieved by varying the lattice constant of the substrate. In practice, this may be achieved by first growing a thick, relaxed layer of the alloy with the desired composition. In the $Si_{1-x}Ge_x$ system, such relaxed layers have been grown on Si substrates [Morar and Wittmer, 1988; LeGoues et al., 1991; Fitzgerald et al., 1992].

3.6.2. Deformation potentials

Once the strain condition of the materials on both sides of the interface is known, one can proceed and determine the band offsets. In particular, one can carry out self-consistent first-principles calculations in exactly the same fashion as described in Section 3.2, now simply putting the atoms in the positions appropriate for a strained lattice. Such calculations have been performed for a large number of systems (see, e.g., [Van de Walle and Martin, 1986]). However, the need to find a simpler model is greater than ever here, since it would be totally impractical to have to perform a complete self-consistent calculation for every strain situation that may occur (in addition to all possible materials combinations).

Fortunately, it has been known for a long time that most effects of strain on the band structure of a semiconductor can be described in terms of *deformation potentials*. In the linear regime (to which we limit the present discussion; strains large enough to lead to nonlinear effects will be difficult to obtain under pseudomorphic growth conditions), a particular property of the band structure (e.g., the bandgap) can be expressed as a constant (unstrained) term plus a term which is the product of a deformation potential and a particular strain component (or combination of strain components). For instance, the bandgap in the presence of hydrostatic strain can be expressed as

$$E_g = E_g^0 + a\,\mathrm{Tr}(\varepsilon), \tag{7}$$

where E_g^0 is the value of the bandgap in the absence of strain, and $\mathrm{Tr}(\varepsilon) = \Delta\Omega/\Omega$ is the trace of the strain tensor, which corresponds to the fractional volume change (we denote volume by Ω, to distinguish it from potentials which are labeled V). Hydrostatic deformation potentials for bandgaps can be easily found in the literature (see, e.g., references in [Van de Walle, 1989]).

In addition to hydrostatic components, pseudomorphic growth always introduces uniaxial (or biaxial) components in the strain. These strain components lead to splittings of degenerate bands. Two cases can be distinguished here. In the case of the valence-band maximum at Γ (Fig. 15) there exists an orbital degeneracy, with two bands (the heavy – hole and light-hole bands) having the same energy at the zone center (in the absence of spin–orbit splitting, the degeneracy would be threefold). Because these bands contain different mixtures of p_x, p_y, and p_z orbitals, application of uniaxial strain will affect the relative energies of the bands. The splitting can be expressed in terms of a deformation potential (typically denoted by the symbol b for deformations along $\langle 0\,0\,1 \rangle$, and with d for deformations along $\langle 1\,1\,1 \rangle$, which are well documented in the literature (see [Van de Walle, 1989], and references therein). The other type of degeneracy is spatial in nature, and is found, e.g., in Si where the conduction band minima occur along the $\langle 1\,0\,0 \rangle$ directions (along the line from Γ to X) in reciprocal space; this implies there are six minima, which occur at the same energy in the

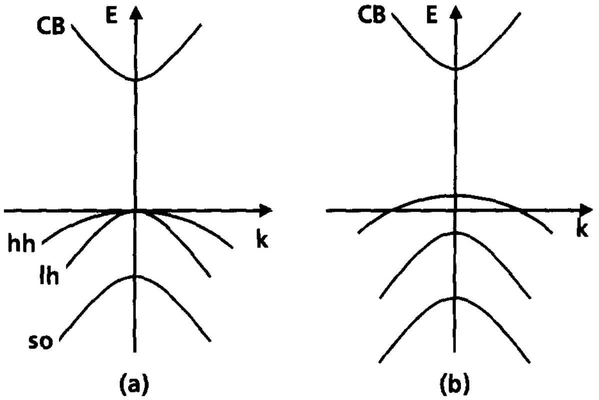

Fig. 15. Schematic representation of the effect of strain on the bands around the zone center in a semiconductor with the zincblende structure. (a) Unstrained material; (b) uniaxially strained material.

unstrained material. Application of a uniaxial strain along [0 0 1] will affect the minimum oriented along [0 0 1] differently from those oriented [1 0 0] and [0 1 0]. Once again, the relevant expressions for splittings are well documented [Van de Walle, 1989], with Ξ_u as a typical notation for the deformation potential.

The deformation potentials discussed so far relate to effects that can be observed (and measured) in the bulk band structure. To evaluate the effect of strain on the band-lineups at the interface, however, one needs additional information, in particular about the effects of hydrostatic strain. (The uniaxial strain effects can always be expressed as a splitting of bands relative to some average value; the position of this average value, in turn, is affected by the hydrostatic component.) The above discussion of hydrostatic strain only alluded to changes in the bandgap, but did not specify how *individual band edges* behave when strain is applied. This problem is actually of high interest in its own right, apart from its relevance for band-lineups. Indeed, the shifts in energy bands due to local deformations caused by acoustic phonons constitute an important scattering mechanism for carriers, as discussed by Bardeen and Shockley [Bardeen and Shockley, 1950].

The deformation potentials that describe the shifts in individual band edges when strain is applied are labeled "absolute" deformation potentials (as opposed to the "relative" deformation potentials which describe shifts in the band edges relative to each orther, such as shifts in the bandgap). A proper formulation of the problem actually requires careful attention [Van de Walle and Martin, 1989; Resta et al., 1990, 1991]; for instance, the absolute deformation potentials may depend on the orientation of the deformation. Here we will not explore these intricacies, and assume (as seems to be supported by first-principles calculations [Van de Walle and Martin, 1989]) that the hydrostatic, orientation-independent terms in the deformation potential dominate, and that an "absolute" deformation potential can be associated with each band edge. We can then write, for instance, for the position of the (nondegenerate, zone-center) conduction band:

$$E_c = E_c^0 + a_c \mathrm{Tr}(\varepsilon), \tag{8}$$

where E_c^0 is the position of the conduction-band minimum in the absence of strain, and a_c is the appropriate absolute deformation potential.

There remains the problem of deciding how to line up the bands across the strained interface. Most model theories do not provide a prescription for incorporating the effect of strain. About the only exception is the model-solid theory of Van de Walle and Martin [Van de Walle, 1986; Van de Walle and Martin, 1987], which provides a natural framework in which the effects of strain can be incorporated. Given the fact that within the model-solid theory the positions of all bands are defined on an absolute energy scale, one can easily incorporate the effects of strain on those absolute energy positions. Since the reference for the "absolute" energy positions is determined by the average potential in a "model solid" which consists of a superposition of neutral atoms, all one has to do is adjust the volume of this model solid in order to find the shift in the reference level. The shifts in individual band positions then follow from a bulk band structure calculation for the strained solid. These calculations can be carried out once and for all, and the results can be expressed (in the linear regime) in terms of "absolute deformation potentials", which have been tabulated [Van de Walle, 1989]. Specific examples of the application of this approach to strained interfaces can also be found in the literature [Van de Walle, 1989]. The approach is supported by first-principles calculations on strained interfaces [Peressi et al., 1993; Tit et al., 1993)], showing that the dependence of the band offsets on strain is due to the band-structure term, and hence to pure bulk effects rather than to interface-specific features.

It should therefore be clear that the model-solid approach to incorporating strain effects will yield good results under the same conditions as those listed for application of the model-solid theory to unstrained interfaces (i.e., nonpolar interfaces, in cases where no additional dipoles are expected). One can of course speculate that at an interface where additional dipolar terms occur (e.g., at a polar interface) the strain may introduce changes in the dipole itself (in addition to changes in the band structure). In our opinion such effects will be small on the scale of the dipole itself, and therefore the model-solid approach should be adequate to evaluate the strain-dependent effects, even in the presence of an additional dipole.

4. Theoretical understanding and predictions

4.1. Isovalent versus heterovalent systems

In Section 3.2 we gave an overview of the fundamentals and accomplishments of first-principles calculations. Here we will review some conclusions that have been obtained by analyzing first-principles results for a wide variety of interfaces.

It has been observed that the band offsets at isovalent interfaces are independent of orientation and interface quality [Baroni et al., 1989, 1993; Baldereschi et al., 1993b]. This applies to interfaces between group-IV elements [Van de Walle and Martin, 1986b], and to III–V/III–V and II–VI/II–VI systems with a common anion (or cation), for which it was found that the (0 0 1) interfaces produce the same offset as the (1 1 0) [Van de Walle and Martin, 1988; Lambrecht and Segall, 1990b]. If the compounds have no component element in common (such as InAs–GaSb), a slight difference in lineup may be present between the two possible (0 0 1) interfaces (In–Sb and Ga–As), but it does not exceed 0.1 eV [Lambrecht and Segall, 1990b; Dandrea et al., 1992]. The study of Dandrea et al. [Dandrea et al., 1992] addressed the effects of variations in interfacial geometry for (0 0 1) interfaces between III–V materials. They found that in the case of a common atom (AC–BC), isovalent A–B intermixing near the interface does not affect the band offset (even for lattice-mismatched systems). For quaternary AB–CD systems, two distinct interfaces are possible (A–D or B–C); these can have offsets differing by up to 0.1 eV. In this case intermixing can lead to changes in the offset, related to the offsets associated with A–D versus B–C bonds. A similar study was carried out by Hybertsen [Hybertsen, 1990a] for the offset at the lattice-matched $Ga_{0.47}$ $In_{0.53}$ As–InP interface; it was found that if the correct interfacial layer spacings are taken into account, the offset is independent of which of the two chemically abrupt interfaces occurs (In–As or $Ga_{0.47}$ $In_{0.53}$–P).

The GaInAs–InP interface was also studied by Peressi et al. [Peressi et al., 1990] as a prototypical case of no-common atom interfaces, not only confirming (using both linear-response theory and full self-consistent calculations) the independence of the offset on the interface termination in (0 0 1) orientation, but also the independence on any other possible orientation, because of the additivity of anionic and cationic effects.

This independence of the offsets on details of the interfacial structure indicates that they depend only on the bulk properties of the constituents. This fact has two important consequences. First, it means that the offsets for this class of interfaces can be described by linear theories. Note that the independence of the offset on interface detail for isovalent interfaces is a *necessary* but *not sufficient* condition for linear response theory to hold. Linear theories are discussed in Section 3.5. Secondly, the independence of the offsets on interfacial details clearly limits the possibilities of "band-offset engineering" for this class of interfaces.

Heterovalent interfaces, on the other hand, offer a much wider variety of possibilities for tuning the offsets. The offsets at *nonpolar* heterovalent interfaces [e.g., (1 1 0)] are once again determined to the first order by bulk properties only, but the offsets at the more common *polar* interfaces [e.g., (1 0 0)] are clearly dependent on the microscopic details of the interface. It is therefore this latter class of interfaces that will offer most challenges but also most promise for band-offset engineering. It will not be possible to describe the band offsets simply with a linear model, although we will see that a linear model can still function to predict one component in the offset, which will then be supplemented by an additional component that can be evaluated based on simple electrostatics. More importantly, the sensitivity details of to the interfacial structure makes this class of interfaces excellent candidates for attempts at band-offset modification.

4.2. Theoretical approaches to band-offset modification

In this section we will discuss theoretical approaches and predictions for band-offset modification. Based upon the discussion in Section 4.1, we know that in order for band-offset modifications to be possible the interface should be polar in character. Despite this general rule, there have been some theoretical predictions about band-offset changes introduced at nonpolar interfaces, and we discuss them in Section 4.2.1. However, band-offset modifications will have the greatest likelihood of success at polar interfaces, which include such popular interface orientations as (0 0 1) and (1 1 1), and are here introduced in Section 4.2.2. We organize the discussion of the theoretical work for polar interfaces along the following lines: Section 4.2.3 deals with the issue of atomic mixing at polar interfaces, while Section 4.2.4 discusses the concept of microscopic capacitors. The boundary between these two approaches is not sharp, and may be largely a matter of different points of view about the same problem. The "atmoic mixing" approach emphasizes the need to avoid nonneutral interfaces, and includes thermodynamic arguments in predictions of acceptable interface structures;

the band offsets for the resulting structures can be calculated and may or may not exhibit modifications related to interfacial structure. In the "microscopic capacitor" approach, the emphasis is on more idealized model structures which clearly produce dipoles at the interface. To what extent these ideal structures can be realized is a topic which is only addressed afterwards.

Most theoretical papers in the field have assumed one or the other of these points of view; this division can therefore be used as a convenient scheme to organize the discussion.

4.2.1. Nonpolar interfaces

Simple arguments, as well as more sophisticated linear response theory [Baroni et al., 1988] indicate that band-offset modification will not be possible at (1 1 0) interfaces. Indeed, each (1 1 0) plane consists of an equal number of cation and anion sites (see Fig. 16). Replacing a complete plane (or several planes) of host atoms with another type of atoms will therefore have no net effect. In order for a dipole to be possible, one would have to substitute (for instance) only the cation sites in one plane, and only the anion sites in a different plane. Changes in band offsets due to such atomic swaps at nonpolar interfaces have also been addressed theoretically by Baldereschi et al. [Baldereschi et al., 1993a], as discussed in Section 5.2.2. While such a scenario may seem unlikely, there are experimental indications that offset modification at nonpolar interfaces can occur (see Section 5.2.2).

A number of explicit first-principles calculations have confirmed that at nonpolar interfaces, interlayers seem to have little or no effect on the band offsets. Christensen and Brey (1988) have carried out self-consistent LMTO calculations on a large number of (1 1 0) interfaces with ultrathin interlayers. They found that for a wide class of interfaces the band offsets are largely insensitive to the presence of the interlayer, i.e., they found the changes in offset to be smaller than 0.05 eV. The only case in which they found a noticeable change in offset was for a CuBr interlayer, which could be

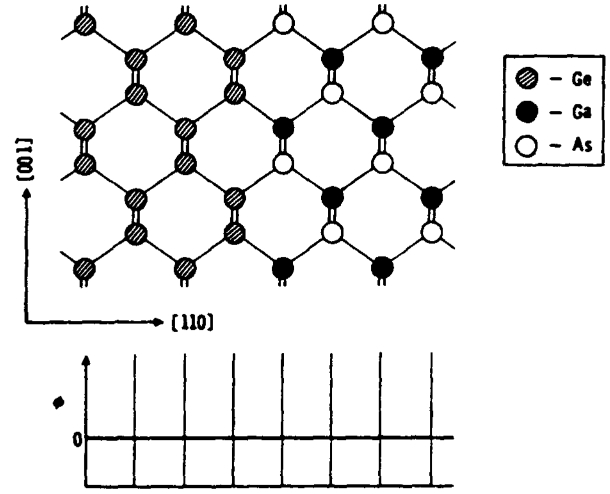

Fig. 16. Schematic representation of a Ge–GaAs (1 1 0) heterojunction. The crystal is viewed along the [$\bar{1}$ 1 0] direction with the (0 0 1) direction vertical. All atoms are tetrahedrally coordinated; the "double bonds" in the figure represent two tetrahedral bonds, separated by the usual 109° angle and projected onto the plane of the figure. Every atomic plane parallel to the junction is neutral on average, corresponding to a nonpolar junction [Harrison et al., 1978].

explained in terms of its tendency to form interface states, which also produce nontransitivity in the band-lineups.

Despite the general rule about the constancy of the offsets at nonpolar interfaces, there have been some theoretical predictions about band-offset changes introduced at nonpolar interfaces. All of these predictions have been based on self-consistent tight-binding calculations. In semiempirical LCAO calculations, Flores and collaborators have found distinct shifts in band offsets due to interlayers at (1 1 0) interfaces; they have analyzed their results in terms of shifts in the extrinsic charge neutrality level (CNL) [Flores et al., 1989, 1993]. They find that the final band-lineup is obtained by lining up the extrinsic CNLs of the two semiconductors; these extrinsic levels have been modified from their intrinsic level by the deposition of Al. As discussed in Section 3.5, this definition of the CNL as a quantity that can depend on the properties of the interface seems in conflict with the original definition of a CNL as a quantity that would be an intrinsic property of the semiconductor, and could be used to predict band offsets at arbitrary interfaces.

Perez et al. [Perez et al., 1990] found that introduction of an ideal, abrupt Al interlayer between ZnSe and Ge modifies the band-offset by a significant amount, which, depending on the geometry, can exceed 1 eV [Perez et al., 1990; Duran et al., 1987]. They showed that the change in offset is already close to its final value for an Al thickness of one monolayer, and changes very little when the thickness of the metal is increased. The resulting band-lineups could be related to the superposition of two Schottky barrier heights (ZnSe–Al and Ge–Al). The fact that the band offset can be changed so significantly seems to conflict with the linear-response arguments for nonpolar interfaces. One can argue, of course, that the fact that the interlayer is metallic introduces qualitative changes that take the problem beyond the regime where linear-response theory is valid. On the other hand, the common formulation of the lineup problem for heterojunctions and Schottky barriers advocated by Tersoff [Tersoff, 1984b,c] would seem to indicate that even with a metallic interlayer one would, to first order, not expect a signi- ficant change in the lineup. Explicit dependence on geometry is not included in this first-order approach, of course. This issue was addressed in part by Perez et al. [Perez et al., 1990], who actually investigated various interface geometries, and obtained dramatically different offsets, with the interlayer-induced changes varying from positive to negative values. This result illustrates that the actual offsets can only be determined if the precise interface geometry is known, an issue which these tight-binding calculations did not address since they do not have the capability of calculating total energies. This leaves open the possibility that the true, stable geometry would be such as to yield only minor changes in the band offset, consistent with the expected insensitivity of the band offset to nonpolar interfaces.

Flores and co-workers [Flores et al., 1993] have also attempted to derive some more general conclusions about the effect of metal interlayers on semiconductor band offsets. They argue that more electronegative metals will tend to reduce the band offset. In our opinion, such conclusions are premature, given the important influence of interface geometry on the results. Since comprehensive calculations of the stable geometries are still lacking, no conclusions should be drawn about effects on lineups.

Muñoz et al. have also investigated the effect of H, Cs, and Al interlayers at GaP–Si (1 1 0) interfaces [Muñoz et al., 1989]. Once again, the atomic structure of the interface was not known, and the tight-binding calculations cannot address this issue. The authors assert [Muñoz et al., 1989] in the case of Cs that different locations of the Cs atom produce changes on the order of ± 0.15 eV in the offset (which is small compared to the overall dipole due to the interlayer); however, it is still not clear to what extent the assumed geometries bear any resemblance to the realistic structures on which experiments have been performed [Perfetti, 1987].

Finally, Muñoz and Rodriguez-Hernandez [Muñoz and Rodriguez-Hernandez, 1992] have published results for Si and Ge interlayers at AlAs–GaAs (1 1 0) interfaces. They obtain significant changes in the offsets (0.2 eV or more) for the case of one and two monolayers, in sharp contrast with the results of previous calculations [Christensen and Brey, 1988]. Given the fact that the self-consistent tight-binding calculations are probably less reliable than the first-principles LMTO method employed by Christensen and Brey, coupled with the fact that Muñoz and Rodriguez-Hernandez do not provide any physical explanation of the unexpected change in offset at a nonpolar interface, we think that there is currently no sufficient theoretical evidence to expect that changes in offsets could be obtained by interlayers at nonpolar interfaces.

4.2.2. *Ideal polar interfaces*

In Sections 3.3 and 3.4.1 we emphasized that simple models can work well for nonpolar interfaces, but that one should expect additional contributions to the band offset at polar interfaces. Fortunately, such contributions can usually be described quite well with a simple electrostatic approach. Let us consider, for example, a polar Ge–GaAs (001) interface, as illustrated in Fig.17. Two structures are actually possible for the ideal, abrupt interface, one in which the first layer of the

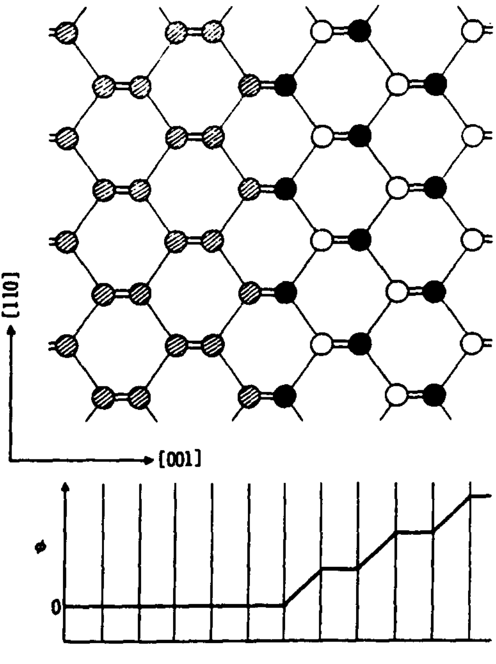

Fig. 17. Schematic representation of a Ge–GaAs(001) heterojunction, viewed along the $[\bar{1}10]$ direction with the $[\bar{1}\bar{1}0]$ direction vertical. The first atomic plane to the right of the junction is entirely made of Ga, which is negatively charged. The potential averaged over planes parallel to the junction is obtained by integrating Poisson's equation from left to right. A nonzero average electric field arises in the GaAs region due to charge accumulation at the junction [Harrison et al., 1978].

III–V compound consists entirely of Ga atoms (as shown in Fig.17), and one in which this first layer would consist entirely of As atoms. Such ideal polar interfaces between heterovalent semiconductors suffer from a problem that was first pointed out by Harrison [Harrison et al., 1978], and that we will discuss in detail in Section 4.2.3: the change in charges across the interface sets up an electric field that would extend throughout the overlayer, a situation which is clearly energetically unfavorable for a thick overlayer. Section 4.2.3 will focus on finding structures which do not suffer from the instability problem, by introducing changes in the atomic structure and composition of the interface (mixing). Another way to avoid the instability is to work with layers of finite thickness, in which the build-up of the electric field would be limited in spatial extent. A discussion of the concepts and calculations relating to finite-thickness interlayers will be given in Section 4.2.4.

In this section, we discuss theoretical work that has focused on the ideal, abrupt, polar interfaces. Bylander and Kleinman [Bylander and Kleinman, 1990] have carried out self-consistent calculations on ideal, abrupt Ge–GaAs (0 0 1) and (1 1 1) interfaces. They found that large electric fields are generated. Localized interface states are formed at the (0 0 1) interfaces, a fact that has been known for a long time [Baraff et al., 1977a,b; Pollmann and Pantelides, 1980]. The electric field generated due to the charge build-up at an abrupt polar heterovalent interface would lead to a high energy in a thick layer. However, one could envision a superlattice in which the thickness of each layer was finite, and the electric fields would change sign in alternate layers, leading to a sawtooth potential [Bylander and Kleinman, 1990]. The (0 0 1) interfaces were found to have a large formation enthalpy, and are thus likely to be unstable. The (1 1 1) interfaces, on the other hand, were found to have a formation enthalpy lower than the (1 1 0) interface, indicating that they may be stable against mixing or reconstruction. Bylander and Kleinman therefore suggested that it should be possible to grow (1 1 1) superlattices containing large electric fields.

Mujica et al. [Mujica et al., 1992] have carried out self-consistent tight-binding calculations for ideal Ge–GaAs and Ge–AlAs interfaces, aimed at deriving results for Ge interlayers at GaAs–AlAs interfaces. They find that interface states are formed that are partially occupied with electrons or holes; a conclusion in agreement with the work of Bylander and Kleinman [Bylander and Kleinman, 1990]. Based on their results for the isolated interface, the authors derive [Mujica et al., 1992] some conclusions for structures with Ge interlayers sandwiched between two semiinfinite semiconductors. They find that the induced band-offset modification saturates at an interlayer thickness of three monolayers. For thick interlayers, the induced dipole should be the sum of the dipoles induced at the individual interfaces. It may therefore make sense to carry out individual calculations for the two interfaces, and then combine the results to obtain results for an interlayer. The results thus derived for the band-offset modification [Mujica et al., 1992] are in qualitative agreement with the results for GaAs–Si–AlAs structures obtained by Peressi et al. [Peressi et al., 1991], to be discussed in Section 4.2.4.

Mujica et al. have discussed the effect of the interface states in terms of "band bending" [Mujica et al., 1992]. Obviously the presence of a partially occupied interface state will give rise to a sharp local fluctuation in the potential (and a strong electric field, as was observed in the calculations of Bylander and Kleinman [Bylander and Kleinman, 1990]). It may be misleading, however, to call this potential fluctuation "band bending". The term band bending is usually employed in connection with potential variations due to space charge layers around a junction (or a surface), an effect in which the bands are bent over distances of several 100 Å (see Fig. 1). In contrast, the local potential fluctuations due to interface states [Mujica et al., 1992] are very different in nature, occurring on a length scale of only a few atomic distances; as such, they are more appropriately included in the value of the band offsets.

Finally, a comment on the use of Fermi-level lineups [Mujica et al., 1992]: the calculations for Ge–GaAs and Ge–AlAs are "joined" by aligning the Fermi-level positions obtained in the separate calculations. While this may be allowed as a mathematical approach, it conveys the misleading impression that Fermi-level alignment would play any role in determining band-lineups. In general, the position of the Fermi level in a semiconductor is determined by the doping level in the bulk, far away from the junction. Knowledge of these Fermi-level positions far away from the interface then provides boundary conditions for the solution of the band profile as a function of the spatial coordinates; the band-lineup at the interface is another *input* to the solution of this problem. The concept of Fermi level as discussed by Mujica et al. [Mujica et al., 1992] (as well as other papers by the same group) may be useful as a mathematical tool in the calculations (determining the energy boundary between filled and unfilled states), but is unrelated to the thermodynamic quantity which is commonly used, and which is meaningful only on more macroscopic length scales.

4.2.3. Atomic mixing at polar interfaces

4.2.3.1. Theory of atomic mixing In 1978, Harrison et al. [Harrison et al., 1978] carried out a study of Ge–GaAs interfaces in different orientations, and concluded that experimentally prepared junctions had to contain deviations from the ideal atomic arrangements [Harrison et al., 1978]. The authors tried to use the experimental data to extract information about geometries and interface dipoles. More importantly, they proposed a model for atomic rearrangements at the interface that forms the basis of much of today's thinking about mixing at polar interfaces. Harrison's formulation of the problem is still very illuminating, and we briefly repeat the arguments here; however, the original paper [Harrison et al., 1978] is to be highly recommended for its clarity and pedagogical presentation. Harrison started with an infinite crystal of pure Ge, in which he imagined a (1 1 0), or (0 0 1), or (1 1 1) plane, which will become the plane of the interface. By definition this system has no dipole shift across the junction. He then proceeded to transfer protons between nuclei to the right of the junction, such as to convert half of the nuclei to Ga, and half to As.

This shift of protons (which Harrison called "theoretical alchemy") produces a calculable change in electrostatic potential, and may produce an accumulation of nuclear charge, as well as a dipole layer at the interface. The electronic charge density will of course adjust to the changes in the nuclear charges; however, a qualitative analysis that brings out the most important features of the system can be carried out without a need to know the details of the electronic structure. If this prescription would be applied to a (1 1 0) interface (see Fig. 16), the transfer of protons between nuclei would occur in planes parallel to the interface, and all such planes are still neutral on average. No charge accumulation or dipole layers can therefore be generated at the interface.

To investigate dipole layers one has no need to know the potential at each point; the value of the potential averaged over planes parallel to the interface suffices. This point was already made in Section 3.2; note that in Section 3.2 we restricted the discussion to the potential generated by electrons alone, whereas in the present discussion we also include the contribution of the ionic cores to the potential. This plane-averaged potential is equivalent to the potential at one point due to charges averaged over planes parallel to the interface [Harrison et al., 1978]. A dipole shift shows up as a discontinuity in the average potential. Charge accumulation would correspond to a discontinuity in the electric field, i.e., a discontinuity in the slope of the average potential.

For the case of the (0 0 1) interface (see Fig. 17), the transfer of protons between nuclei occurs in the direction perpendicular to the interface. Each plane of atoms parallel to the interface is now charged (note the discontinuities in the slope of the average potential). The average potential sketched in Fig. 17 is obtained by integrating Poisson's equation froom left to right. The potential is flat on the Ge side of the junction. Crossing into GaAs, the slope changes discontinuously upon going through a charged plane of atoms; this leads to a potential that contains an average gradient, in addition to a fluctuating component. This average gradient may be thought of as arising from charge accumulation at the interface.

The type of potential depicted in Fig. 17 cannot be sustained in a real system because it would lead (over a distance of a few atomic layers) to potential differences greater than the bandgap, and spontaneous generation of carriers would occur [Bylander and Kleinman, 1990].

Another way of looking at the issue is as follows: at an ideal, abrupt polar III–V/IV interface, IV–V bonds have an excess of 1/4 electron, and IV–III bonds have a deficiency of 1/4 electron; these therefore behave as donor and acceptor states, and give rise to partially occupied localized interface states [Dandrea et al., 1990]. Nonpolar (e.g., (1 1 0)) interfaces contain an equal number of IV–III and IV–V bonds, and therefore charge neutrality can be maintained within the interfacial layer. At polar interfaces (such as (1 0 0) and (1 1 1)), however, each interface contains only one single type of bond, and will therefore carry a net excess of deficiency of charge. Such charged interfaces give rise to an electric field.

Thus far we have glanced over the fact that in the "theoretical alchemy" picture, when protons are transferred between nuclei, there will be a corresponding rearrangement of the electronic charge to screen the perturbation. Even in the presence of a self-consistent electronic charge, the fluctuating component in the potential will be the same as would be generated in a bulk crystal by transferring protons between nuclei. Indeed, Harrison pointed out that putting an extra proton on a Ge atom, and turning it into an As atom, lowers the energy of the electronic states; similarly, removing a proton, leading to a Ga atom, raises the energy of the electronic states. The bonds will therefore become polarized; however, each bond still contains two electrons, and the charge accumulation due to proton transfer is maintained. The bond polarization also does not eliminate the average gradient in the potential. However, this gradient corresponds to an electric field that will be screened by the dielectric constant of GaAs.

The charge density in each plane is $\sigma = 2e/a^2$, since there is one charge per area $a^2/2$; e is the charge of an electron, and a is the lattice constant ($a = 5.65$ Å for GaAs). The corresponding electric field can be obtained from $\varepsilon = -\sigma/\varepsilon\varepsilon_0$, where ε_0 is the permittivity of vacuum, and ε is the relative dielectric constant of the material (in this case, $\varepsilon = 11$ for GaAs, in S.I. units). In Fig. 17 we see that this field acts over half of each period, with a zero field in the other half; the average electric field is therefore obtained by dividing the above quantity in half. This leads to an average field of 5.2×10^9 V/m, corresponding to an increase in the electrostatic potential energy by 2.9 eV for each distance a. Clearly a field of this magnitude cannot be sustained in a realistic structure.

Harrison et al. therefore postulated that the planar, abrupt geometry of the interface must be modified to eliminate the charge accumulation. Looking at Fig. 17, we see that the charge accumulation at the interface (and hence the electric field) could be eliminated if one proton per two atoms would be added to the first plane of Ga atoms at the interface. This is equivalent to having a mixed plane of atoms, with half Ge and half Ga; see Fig. 18. Alternatively, one could add one proton per two Ge atoms to the last layer of Ge, which can be accomplished by having a mixed layer with half Ge and half As. Harrison et al. pointed out that there are "innumerable other ways" to add protons and create a charge-neutral interface, but these are the simplest. Looking at Fig. 18 we see that the neutral interface contains equal numbers of Ga–Ge and As–Ge bonds; the additional electrons associated with As–Ge bonds are exactly compensated by holes associated with Ga–Ge bonds [Martin, 1980]. This simple bond-counting rule must be obeyed by any neutral interface.

Looking at Fig. 18, we see that the electric field within GaAs has been eliminated. However, a shift in the average potential is now present, corresponding to a dipole at the interface. The magnitude of this shift can be determined by imagining that to the right of the GaAs shown in Fig. 18 we construct an analogous junction, this time with a mixed plane of Ge and As atoms; the entire system is then neutral. We find that in this case the Ge potential (energy) on the right would be shifted up by an amount $e/4a\varepsilon\varepsilon_0$, which would be equal to 0.73eV. The potential step δ in Fig. 18 is therefore equal to half this amount, i.e., 0.37eV. These numbers are derived using the dielectric constant of bulk GaAs; of course, near the interface and on the length scales discussed here it is not entirely clear which dielectric constant is the appropriate one to use, and one may expect that the actual value would be influenced by the presence of Ge nearly, which has a dielectric constant $\varepsilon = 16$. This introduces a degree of uncertainty in these simple estimates. The issue has been discussed by Peressi et al. [Peressi et al., 1991].

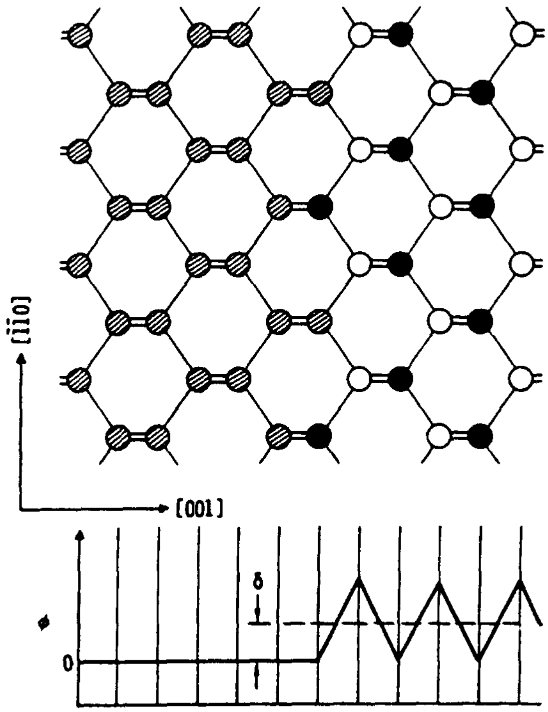

Fig. 18. Ge–GaAs (001) heterojunction as in Fig. 17, but with half of the Ga atoms at the junction replaced by Ge atoms. The average electric field in the GaAs has been eliminated, but there still exists a dipole shift δ which will affect the band offset [Harrison et al., 1978].

Fig. 17 depicted a (001) Ga junction, in which the first atomic plane to the right of the junction consists of Ga atoms. It is of course also possible to have a (001) As junction, in which the first atomic plane to the right of the junction consists of As atoms, and the mixed interface corresponding to this case would then look like Fig. 18 but with the Ga and As atoms interchanged. It is easy to see that there will be a significant difference in band offsets between these two cases [Dandrea et al., 1992]; the first interface ($Ga_{0.5}Ge_{0.5}$) can actually be converted into the second ($As_{0.5}Ge_{0.5}$) by transferring 0.5 protons from right to left between interface planes. The simple estimate described above produces a change in offset of 0.73 eV (or 0.50 eV, depending on whether the GaAs or Ge dielectric constant is used). First-principles calculations (see Section 4.2.3b) have found a value of 0.6eV for this change in offset.

It is actually possible to construct mixed interfaces in which the dipole δ is entirely eliminated. Two transition layers are required in this case, as illustrated in Fig. 19. In this example, the first layer contains 1/4 As, and the second 3/4 Ga, with the remaining atoms Ge. No dipole and no charge accumulation occurs in this case. An alternative structure can be constructed by interchanging Ga and As atoms in Fig. 19. Structures with mixing over more than two atomic layer also exist. It is to be expected (and has been confirmed by first-principles calculations [Biasiol et al., 1992; Nicolini et al., 1994]) that structures in which the dipole has been eliminated in this fashion exhibit band offsets similar to the nonpolar (110) interface.

Similar arguments can be applied to (111) interfaces [Harrison et al., 1978]. A much larger number of potential interface geometries was considered in a later report by Harrison [Harrison,

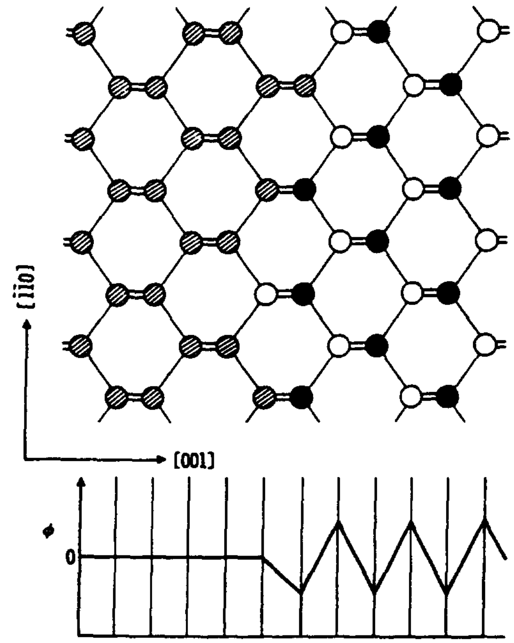

Fig. 19. A Ge–GaAs (001) heterojunction as in Figs. 17 and 18, but with two transition planes,. The first is 1/4 As, the second 3/4 Ga, with the remaining atoms Ge. This is the simplest geometry that eliminates both charge accumulation and dipole shift [Harrison et al., 1978].

1988]. Statistical averages over the various geometries, for which energies were calculated within the bond-orbital approximation, produced dipoles as a function of temperature, which showed qualitative agreement with experiment for different orientations.

Significant contributions to the understanding of mixing at polar interfaces have also been made by Martin [Martin, 1980], who investigated the driving forces for atomic reconstruction at the polar interfaces. A parallel was drawn with self-compensation mechanisms in the bulk. Martin went on to relate the reconstructions to Ising-like models in two dimensions, and to analyze ordering of charges and dipoles in the interface layers.

It has been pointed out that the problem of reconstructions at polar interfaces has a lot in common with the same problem at polar surfaces [Harrison, 1979; Martin, 1980]. Here too ideal, abrupt surfaces would lead to charge accumulation, and reconstructions and stoichiometry changes are driven by charge neutralization. The problem is typically harder to solve at surfaces than it is at interfaces, because large atomic displacements, changes in coordination, vacancy formation, etc., are processes that are likely to occur at surfaces, but not at interfaces.

4.2.3.2. Calculations addressing atomic mixing The arguments of Harrison et al. [Harrison, 1978] and of Martin [Martin, 1980] showed that ideal, abrupt interfaces would be energetically unfavorable, and that mixed interfaces would be formed. However, a more quantitative theoretical approach is required to determine the energy and band offsets for the various possible geometries. The first attempt in this direction was carried out by Kunc and Martin [Kunc and Martin, 1981], who performed density-functional pseudopotential calculations for Ge–GaAs (100) interfaces. Mixing at the interface was handled in a virtual crystal approximation, in which, for instance, a mixed plane with half Ge and half Ga atoms is modeled by a plane of virtual atoms, constructed by averaging the pseudopotentials of Ga and Ge. Since the interface dipole is determined by charge densities and potentials that are averaged over atomic planes, this approximation (which neglects certain potential fluctuations within the plane) should have little effect on the calculated band-offset modification. The energy of the system, however, may depend on the details of the distribution of atoms in the plane, and the virtual crystal approach does not yield information about this aspect of the problem. Relaxations of the atomic planes around the interface were included.

Within the approximations used, Kunc and Martin found the (1/2 Ge + 1/2 As) interface to be lower in energy by 0.3 eV per interface atom. Kunc and Martin found a valence-band offset of 0.57 eV for the (1/2 Ge + 1/2 Ga) case, and −0.03 eV for the (1/2 Ge + 1/2 As) case. They noted that the average of these values is very close to the calculated offset for the (110) interface. The values calculated by Kunc and Martin are listed in Table 2, and compared with results from other calculations to be discussed below. Also note that the difference between these values is quite close to the estimate based upon simple electrostatic arguments outlined in Section 4.2.3.1.

Baroni et al. [Baroni et al., 1989] have shown that linear response theory gives answers that are very similar to the self-consistent result for Ge–GaAs interfaces. They found a valence-band offset of 0.82eV for the (1/2 Ge + 1/2 Ga) case, and 0.22eV for the (1/2 Ge + 1/2 As) case, i.e., values that differ by about 0.2eV from the earlier results [Kunc and Martin, 1981], probably due to improvements in pseudopotentials and convergence of the calculations. But, again the average of these values is very close to the calculated offset for the (110) interface, and the difference between the (001) Ga and (001) As interfaces is 0.6eV, in agreement with the simple electrostatic estimate.

Table 2

Calculated valence-band offsets (in eV) for the GaAs–Ge (110) interface, and for two mixed GaAs–Ge (001) interfaces, in which one atomic layer near the interface is mixed (see Fig. 18 for the mixed $Ge_{0.5}Ga_{0.5}$ interface). The calculations are based on pseudopotential-density functional theory, and discussed in more detail in the text. Note that all calculations predict the same offset difference (0.6 eV) between the two mixed interfaces, and that the average offset is within 0.1 eV of the value for the nonpolar (110) interface

Configuration	a	b	c	d
(110)	—	0.48	0.54	—
(001) $Ge_{0.5}Ga_{0.5}$	0.5	0.70	0.82	0.88
(001) $Ge_{0.5}As_{0.5}$	−0.03	0.10	0.22	0.28

[a] Kunc and Martin, 1981; [b] Dandrea et al., 1990; [c] Baroni et al., 1989; [d] Biasiol et al., 1992.

In the calculations by Kunc and Martin the supercells contained 4 Ge, 2 Ga, and 2 As atoms, which were arranged in different geometries to allow comparison of the resulting energies. For more complicated geometries, one has to carefully consider the stoichiometry of the interface, and appropriately take into account the number of each type of atom present when comparing energies for different interfaces. A general description of the problem requires the careful definition of formation energies, in which chemical potentials appear that represent the energies of the reservoirs from which atoms are taken [Chetti and Martin, 1992; Lambrecht et al., 1992].

Dandrea et al. [Dandrea et al., 1990] carried out first-principles pseudopotential calculations for Si–GaP, Ge–GaAs, and Si–GaAs heterojunctions, deriving information about relative stability of different interface reconstructions (mixing types), as well as the associated band offsets. Their results for Ge–GaAs are listed in Table 2.

Finally, various possible configurations leading to charge-neutral interfaces have been investigated by Biasiol et al. [Biasiol et al., 1992]. The authors first performed calculations for the type of interface depicted in Fig. 18, in which mixing occurs in one atomic layer. Their results for these interfaces were very close to the linear-response results of Baroni et al. (see Table2). Then they also investigated structures in which mixing occurs in two atomic planes, leading to a configuration with no ionic dipole (see Section 4.2.3.1); it was found that the resulting offset is indeed nearly the same as for the nonpolar (1 1 0) interface.

Recently, ZnSe–GaAs(00 1) interfaces have been examined along the same lines by Nicolini et al. [Nicolini et al., 1994; Bratina et al., 1994], who performed calculations for the type of interface depicted in Fig. 18, and for structures in which mixing occurs in two atomic planes. Again, the largest variation in band offsets was found in comparing the cation-mixed and anion-mixed interface terminations (Fig. 18), while the configurations with no ionic dipole (see Section 4.2.3.1) yielded offsets similar to those expected for the nonpolar (1 1 0) interface. The formation enthalpies (and band offsets) corresponding to the same ZnSe–GaAs(00 1) configurations were calculated by Kley and Neugebauer [Kley and Neugebauer, 1994], postulating two different lateral reconstructions for the interfaces. The authors found the two configurations depicted in Fig. 18 to be degenerate, and corresponding to the lowest formation enthalpy. The calculated value of the offsets matched very closely those obtained by Nicolini et al., as well as the predictions of linear-response theory [Nicolini et al., 1994; Bratina et al., 1994; Kley and Neugebauer, 1994].

4.2.4. Microscopic capacitors

4.2.4.1. Electrostatic theory of microscopic capacitors In Section 4.2.3.2 we discussed how abrupt, ideal polar interfaces between heterovalent semiconductors (such as Ge and GaAs) necessarily lead to a build-up of charge at the interface, which induces an electric field extending throughout the overlayer. Such a situation would obviously be unstable in the case of an interface between two semiinfinite solids; this instability forms the driving force for the atomic mixing described above. However, as long as the overlayer remains sufficiently thin, it might be possible to retain an ideal interface without mixing [Bylander and Kleinman, 1990]. This has led to the concept of a thin interlayer of atoms of different valence introduced in an otherwise isovalent interface, a structure that has been labeled a "microscopic capacitor". We caution the reader, however, that the same expression was used earlier by Capasso and co-workers to describe the result of fabricating n^+ and p^+ doped layer on either side of a heterojunction to create an additional electrostatic step in the potential profile [Capasso et al., 1985a,b]. This will be described in Section 5.3. To avoid confusion, here we will use the expression "microscopic capacitor" only to describe the effect of an ideal heterovalent interface layer with charged interfaces. A simple example of such a structure is illustrated in Fig. 20, where we consider an ideal 2-monolayer-thick interlayer of Ge situated between semiinfinite layers of GaAs, grown in the [001] direction.

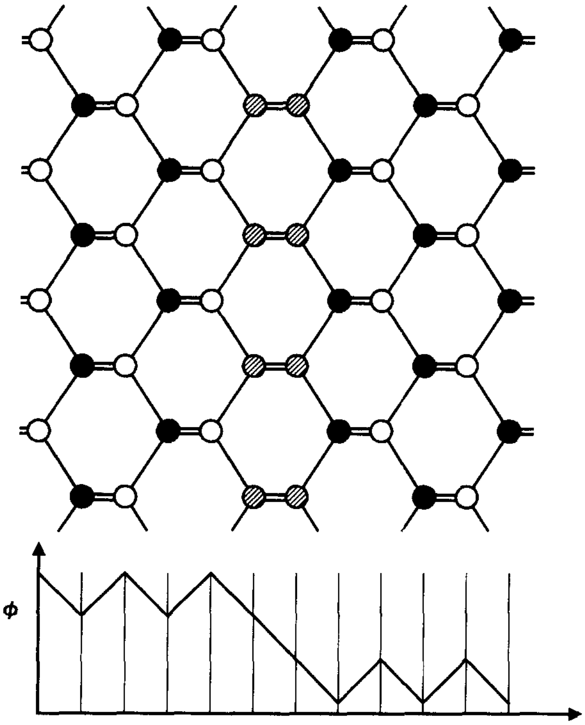

Fig. 20. Schematic representation of a GaAs–Ge–GaAs(001) structure, in which the Ge forms an abrupt, ideal two-atomic-layer thick interlayer between the GaAs semiinfinite semiconductors. The potential averaged over planes parallel to the junction is shown at the bottom.

In the simplest approach [Harrison et al., 1987; Baroni et al., 1989], the effect of a thin interlayer at the semiconductor interface can be modeled by a parallel-plate capacitor. The potential across the capacitor is given by $V = Q/C$ where Q is the total charge, and C the capacitance. We also know that $C = A\varepsilon\varepsilon_0/d$ where A is the area of the capacitor, ε is the relative dielectric constant of the material, ε_0 is the permittivity of vacuum, and d is the distance between the capacitor plates. We then obtain $V = Qd/A\varepsilon\varepsilon_0 = qd/\varepsilon\varepsilon_0$ where $q = Q/A$ is the charge per unit area; for GaAs, we have $d = a/4 = 1.41$ Å (a is the GaAs lattice constant), $A = a^2/2 = 15.96$ Å^2. Assuming that $\varepsilon = 11$, the relative dielectric constant of GaAs, we find $V = 1.46$ eV; if we would take $\varepsilon = 16$, the dielectric constant of Ge, we would obtain $V = 1.00$ eV. Given the very small thickness of the Ge layer, it is not clear which dielectric constant is the appropriate one to use: that of GaAs, that of Ge, or some value in between. In their investigations based on linear response theory, Peressi et al. [Peressi et al., 1991] have used a value corresponding to the interlayer, considered as a bulk material; for incomplete coverages (less than 2 ML), they used an average over the inverse dielectric constants, weighted by the composition; for the purposes of the present estimate the precise choice is not important.

The bottom line is that the presence of the interlayer causes a dipole shift, so that the average potential in the GaAs layer on the right differs from the average potential on the left. This basic dipole shift would be maintained if the GaAs layer on the right were replaced by, say, an AlAs layer; in that case we would accomplish a shift in the band-offset between GaAs and AlAs due to the interlayer of Ge.

There are various other ways to describe or think about such interlayers. For instance, one could consider it as an ideal, abrupt polar interface between GaAs and Ge, followed by a polar interface between Ge and GaAs, each of which contributes a particular dipole shift. For the two-atom thick interlayer, the two interfaces are distinct from each other because one is a (001) Ga interface, while the other is a (001) As interface, producing different dipole shifts. We caution the reader, however, that since for ideal, abrupt polar interface each individual interface would have a nonzero net charge, and give rise to a long-range electrostatic field, the total dipole shift associated with the interlayer would depend on the interlayer thickness. This can be easily visualized in terms of a microscopic capacitor in which the charge on each plate is kept constant while the plate separation is varied. Since the capacity is inversely proportional to the plate separation, the dipole shift would be directly proportional to interlayer width. While a two-atom thick layer may seem rather thin to carry out this division into two separate interfaces, there are indications from theoretical studies that the approximation may be justified. For very thick interlayers it is obvious that the total dipole shift will simply be the sum of the shifts at individual interfaces. It has also been shown that the dipole shifts introduced by an interlayer are close to converged for a two-atom thick layer [Mujica et al., 1992]; adding additional Ge layers has little effect on the offset.

The formation of a Ge interlayer in a GaAs crystal can also be conceived in terms of "theoretical alchemy" [McKinley et al., 1991]. For instance, focusing upon the (001) orientation, one can transfer a proton from the As nuclei to the Ga nuclei in an adjacent plane; the result is a two-monolayer thick interlayer of Ge imbedded in the GaAs crystal. This imaginary charge transfer clearly sets up a dipole; the sign of which can be determined by the following argument: the Ge atoms located on As sites would act (if they were isolated impurities) as acceptor atoms, which would be negatively charged if ionized. The Ge atoms on Ga sites, on the other hand, behave as donors and carry positive charge. Note that these signs actually agree with those of the simple "proton transfer" picture. These charges determine the direction of the electric field, and hence the sign of the dipole. This point of view establishes a clear link with the concept of using doping interface dipoles to tune band offsets [Capasso et al., 1985a,b], where the dipole would be formed by including a sheet of donors and a sheet of acceptors within ~ 100 Å of the junction. The difference in the microscopic capacitor is that the sheets of dopants are constrained to a one-atom thick layer each, and that they occur right at the interface. More detail will be provided in Section 5.1.

4.2.4.2. Calculations of microscopic capacitors at heterojunction interfaces In Section 3.2 we discussed how first-principles calculations for heterojunction interfaces are carried out. The procedure for addressing structures with interlayers is very similar; inserting a thin interlayer at a heterojunction will affect only the potential lineup $\Delta\bar{V}$; indeed, the position of the valence-band maximum with respect to $\bar{V}$ in each individual semiconductor remains unaffected by the interlayer. We will now discuss a number of first-principles calculations on various interlayer systems. Most of these results qualitatively support the simple electrostatic capacitance approach. The precise numerical values of the induced dipoles deviate from the simple estimate mainly because of the uncertainty about which dielectric constant to use, and Peressi et al. [Peressi et al., 1991] have actually provided a prescription for the dielectric constant which works quite well. We will also see, however, that most of the calculated numbers do not agree with experimental observations. This may be an indication of the fact that the structures which have been assumed in the theoretical approach are not representative of the real experimental structures.

Muñoz, Chetty and Martin [Muñoz et al., 1990] have carried out pseudopotential-density-functional calculations for double layers of Ge in bulk GaAs (i.e., at a GaAs–GaAs homojunction), in the (001) and (111) orientations. The (001) case corresponds exactly to the situation described in Section 4.2.4.1 and depicted in Fig. 20. At such a homojunction, any band offset obtained must be totally due to the interlayer-induced dipole. For the (100) case the dipole-induced shift in the band offset was found to be about 1 eV, in rough agreement with the simple electrostatic estimate based on the capacitance of an interlayer. The authors also found that the charge transfer per Ge atom (prior to dielectric screening) is about −1 electron per Ge atom sitting on a Ga site, and + 1 electron per Ge sitting on an As site, so that the bilayer will effectively act as a n^{+}–p^{+} layer at the junction.

In the (111) orientation, two interfacial structures are possible: one which carries a maximum number of Ge–Ge bonds, and one with a minimum number of Ge–Ge bonds. Muñoz et al. [Muñoz et al., 1990] found that the configuration with the maximum number of Ge–Ge bonds had the lowest formation enthalpy (in qualitative agreement with results of Bylander and Kleinman [Bylander and Kleinman, 1990]), and the smallest dipole. The planar-averaged self-consistent potential for the (111)-near configuration (the configuration with the maximum number of Ge–Ge bones) is shown in Fig. 21. The induced dipole, $\Delta\bar{V} = 0.74$ eV, is clearly visible across the Ge interlayer. Also notice the slope of the macroscopic average of the potential in the GaAs layer, corresponding to the electric field that is set up in the structure. This electric field arises because the calculation is effectively carried out on a $(GaAs)_5(Ge)_2$ superlattice, with imposition of periodic boundary conditions.

Peressi et al. [Peressi et al., 1991] have investigated the effects of thin Si interlayers between GaAs and AlAs, using fully self-consistent calculations as well as linear response theory. They first carried out pseudopotential-density functional calculations for Si and Ge interlayers at GaAs and AlAs homojunctions. To ensure local charge neutrality, they used a mixed interface structure in which the Ge atoms are spread over at least two monolayers, even for coverages of less than two monolayers.

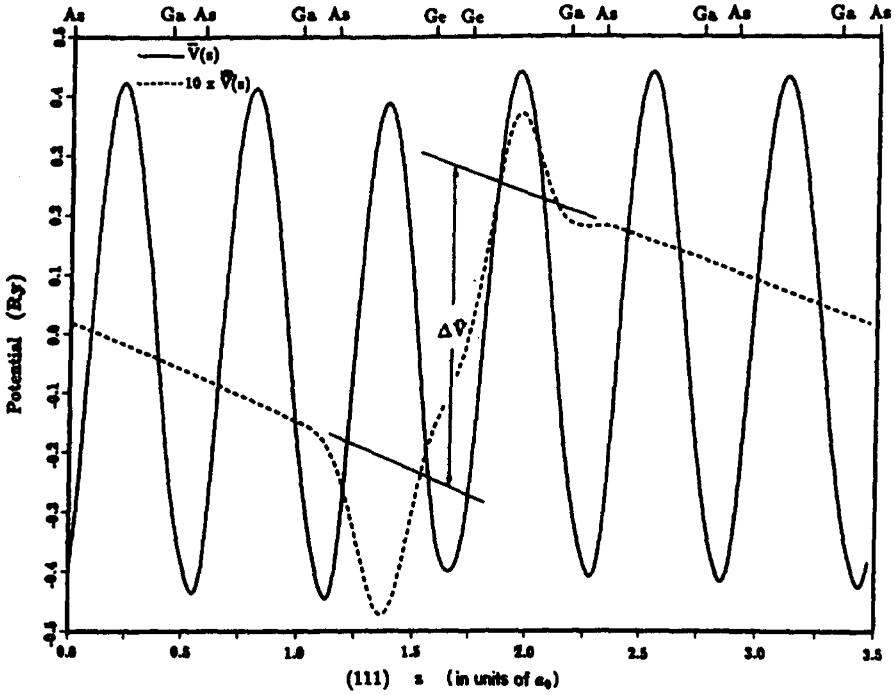

Fig. 21. Planar-averaged self-consistent potential Δ $\bar{V}$ for a Ge interlayer at a GaAs–GaAs homojunction, calculated for a $(GaAs)_5(Ge)_2$(1 1 1)-near structure. The macroscopic average of the potential $\bar{\bar{V}}$ shows the macroscopic electric field with microscopic variations at the interface; the discontinuity $\Delta\bar{\bar{V}} = 0.74$ eV across the Ge interlayer is also indicated [Muñoz et al., 1990].

This arrangement ensures that the number of Ge atoms on As sites still equals the number of Ge atoms on Ga sites, i.e., the interlayer atoms occur in pairs, each of which carries a dipole. Virtual ions were used to describe the layers for coverages below two monolayers. The authors found that for a two-monolayer thick interlayer of Ge, the induced dipole is 1.22 eV. Their results for homojunctions are displayed in Fig. 22. The microscopic capacitor model would simply predict a linear behavior as a function of coverage; instead, the self-consistent calculations show that the linear behavior is only followed at low coverage, and that at higher coverage (above 0.5 ML) the dipole increases less rapidly. The results of Peressi et al. [Peressi et al., 1991] for Si interlayers at GaAs–AlAs heterojunctions are shown in Fig. 23. For GaAs–AlAs, their results compare favorably with experiment up to coverages of 0.5 ML; the theoretically predicted dipole keeps rising for higher coverages, whereas the experimental value saturates. Relaxation of the atomic positions had only small effects on the theoretical offsets. The authors speculated that below 0.5 ML all interlayer atoms stay confined in a bilayer, whereas at higher coverages significant interdiffusion might occur [Peressi et al., 1991].

Finally, we mention that Shen and Matthai [Shen and Matthai, 1992] have carried out similar (pseudopotential-density-functional) calculations for Ge bilayers at the InAs–GaAs interface. They find that the bilayer shifts the band offsets by 1.06 eV, which once again is quite close to the value one would obtain from the microscopic capacitor model. Analogous results have been recently obtained

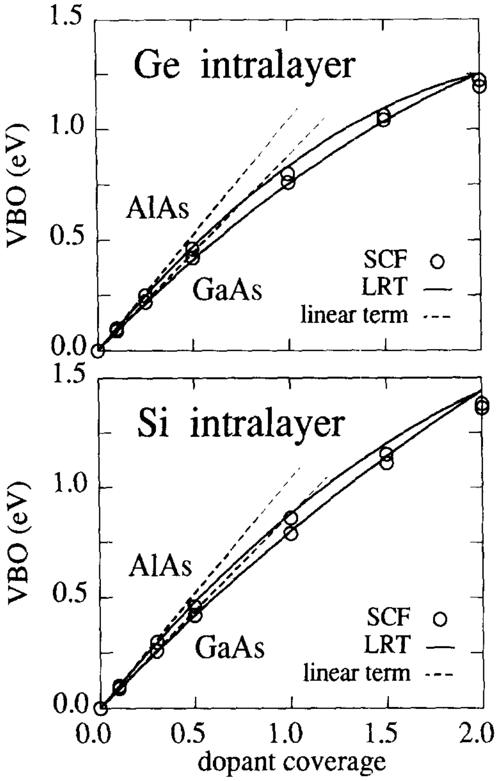

Fig. 22. Valence-band offsets at GaAs–GaAs and AlAs–AlAs homojunctions as a function of the thickness of a Ge or Si interlayer. Results from self-consistent calculations (SCF) are indicated by circles; results from linear response theory (LRT) are indicated by the solid lines. The dashed lines represent the linear behavior predicted by linear response theory for low coverages [Peressi et al., 1991].

by Saito et al. for Si bilayers in GaAs–AlAs (311)A interfaces by means of a self-consistent tight-binding method [Saito et al., 1994a,b].

4.2.5. *Calculations for interlayers including deviations from ideality*

One can question to what extent it is realistic to expect a two-atom thick interlayer (microscopic capacitor) to assume the ideal, abrupt structure discussed in Section 4.2.4.1. For instance, one may envision a driving force for the interlayer atoms to diffuse into the substrate or the overlayer, leading to a much broader profile. On a more local scale, the polar interface between the interlayer and the substrate and/or the overlayer may be subject to the type of atomic mixing that is expected at polar interfaces. There are experimental indications that in the case of a Si interlayer the Si atoms would be distributed over several atomic layers. In the case of a Si monolayer on GaAs (001), X-ray photoelectron diffraction studies by Tran and Chambers [Tran and Chambers, 1993] found that a ratio of Si fractional occupancies in the first, second, and third layers of 1.0: 0.5: 0.25 agreed best with the experimental observations. In Section 4.2.4.1 we mentioned that for sufficiently thin interlayers in principle it might be possible to retain an ideal interface without mixing, since such

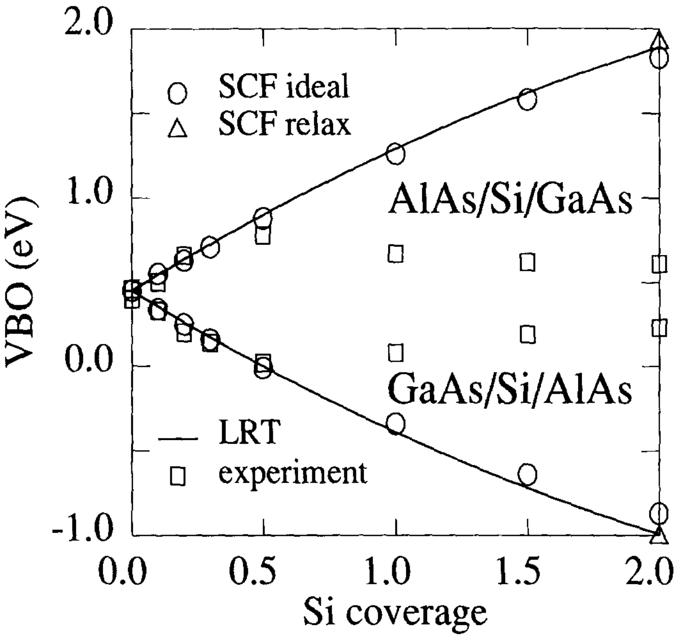

Fig. 23. Valence-band offsets at GaAs–AlAs heterojunctions as a function of the thickness of a Si interlayer. Results from self-consistent calculations (SCF) for ideal unrelaxed structures are indicated by circles; SCF results including microscopic relaxation are indicated by triangles; predictions from linear response theory (LRT) are indicated by the solid lines. The squares represent experimental data from [Sorba et al., 1991]. Note that the notation in this figure differs from the convention used throughout the present paper, so that AlAs/Si/GaAs refers to a structure fabricated on an AlAs substrate [Peressi et al., 1991].

layers do not lead to a build-up of the potential over large distances. However, even for thin layers it might be favorable to undergo the mixing process, because the mixed interface may be lower in energy. The problem then becomes one of a microscopic capacitor in which the interlayer is no longer abrupt, but has interfaces that are spread out over a number of atomic layers; this of course ties in with the discussion of atomic mixing presented in Section 4.2.3.1. One can then envision the problem as one consisting of mixed interfaces between the substrate and the interlayer on one side and the interlayer and the overlayer on the other side. If these two interfaces were identical, the net change in offset would be zero. However, one may expect these two interfaces to be inequivalent, in which case they will lead to different band offsets which do not cancel out, and which will lead to a shift in the overall band offset.

Rodriguez-Hernandez and Muñoz [Rodriguez-Hernandez and Muñoz, 1993] have explicitly investigated the effect of interdiffusion for Ge interlayers at GaAs and AlAs homojunctions, using the pseudopotential-density-functional approach. Ge atoms were allowed to spread out over up to four layers. The atoms were placed in their ideal lattice positions, i.e., no relaxation was allowed. Many different configurations were investigated, most yielding very similar energy values. This result suggests that the real interface will probably consist of a mixture of these various possibilities [Rodriguez-Hernandez and Muñoz, 1993]. The authors do not specify the atomic structures, but only mention that for each coverage value (ranging 0.5–2.5 ML) the configuration with the lowest energy was chosen to calculate the band offset. It is then found that the interlayer-induced change in offset initially increases, up to 1 ML of coverage, and then decreases to zero. While this calculation confirms the qualitative point that the Ge atoms do not stay fixed in an ideal, abrupt interface, it does not yet provide quantitative information about the precise structures that would occur experimentally. In particular, the calculation predicts that the offset would continue to rise until a coverage of 1 ML is reached,while the experimental change in offset saturates at 0.5 ML (see Section 5.5). In addition, the calculation indicates that for larger coverages the change in offset should go to zero, while experimentally a finite saturation value is obtained.

The experiments of Biasiol et al. [Biasiol et al., 1992], to be described in Section 5.5.2, indicate that for the case of a Ge interlayer between GaAs and AlAs the observed change in band offset is not related to a dipole due to a microscopic capacitor, but can be explained by adding the offsets for the individual GaAs–Ge and Ge–AlAs junctions, with the caveat that those offsets are not commutative, i.e., they depend on the growth sequence. The theoretical results of Biasiol et al. [Biasiol et al., 1992] for mixed interfaces were discussed in Section 4.2.3.1; the authors suggested that by combining the calculated offsets for two inequivalent mixed interfaces one could obtain results for the interlayer-induced offset that are consistent with experiment. Results consistent with experiment were obtained by assuming that when the III–V compound is grown on top of a group-IV material, the resulting interface is of the type with one mixed layer, in which the anion is mixed with the group-IV element. On the other hand, when the group-IV element is grown on top of the III–V compound, the results are consistent with an interface in which two layers are mixed (i.e., an interface that carries no dipole, and has an offset close to that of the (110) interface). This simple rule also seems to apply to the ZnSe/Ge(001) interface [Bratina et al., 1994]: when the compound semiconductor is grown on top of a group-IV substrate, the measured offset is close to the theoretical prediction for an interface with one anion-mixed layer. Biasiol et al. [Biasiol et al., 1992] did emphasize, however, that the structures examined in their study are only some of the simplest ones, and that additional defects may also play a role.

The results of Biasiol et al. [Biasiol et al., 1992] were obtained from experimental studies on Ge layers up to 16 ML thick, but it was found that well-defined neutral interfaces were established for coverages as low as 1–2 ML. It is therefore tempting to suggest that this tendency to form inequivalent interfaces depending on the growth sequence is also responsible for the saturation of the induced dipole that was observed in the "microscopic capacitor" experiments. The theoretical values quoted for the individual Ge–GaAs and Ge–AlAs interfaces [Biasiol et al., 1992], combined with the prescription for dependence on growth sequence mentioned above, produce a value of -0.86 eV for the offset in a GaAs–Ge–AlAs structure, and of 0.21 eV for the offset in an AlAs–Ge–GaAs structure. These values agree very well with the reported saturation values [Biasiol et al., 1992].

To further test this hypothesis, one could try and apply it to the case of Si interlayers at GaAs–AlAs heterojunctions. Unfortunately, the lattice mismatch makes growth of thick layers very difficult here, so that less experimental information is available than in the Ge case. However, we can attempt to deduce the required values from calculations reported in the literature. The strain in the Si layer will lead to splitting of the Si valence band; however, for the present purposes we do not need to concern ourselves with these splittings, and only focus attention on the position of the average valence band. Some of the values we need have been calculated by Dandrea et al. [Dandrea et al., 1990]: for the Si–GaAs nonpolar interface the offset is 0.06 eV; for the GaAs–Si interface, with a mixed-anion layer, the valence-band offset is -0.5 eV. To our knowledge the equivalent values for the interfaces between AlAs and Si have not been calculated; here we estimate these values by making some assumptions.

For the nonpolar Si–AlAs interface, we can use an estimate based on the model-solid theory [Van de Walle, 1989], leading to -0.58 eV. For the anion-mixed (001) interface, we can observe from the values calculated in [Biasiol et al., 1992] that both for the GaAs–Ge and the AlAs–Ge interface the value differs by an equal amount from the value for the nonpolar interface. Applying this assumption to the AlAs–Si interface, we find that the offset at the As-mixed (001) interface should be $0.58 - 0.44 = 0.14$ eV. Combining all this information, we obtain an offset for a GaAs–Si–AlAs structure of $-0.50 \; -0.58 \; = -1.08$ eV, and for an AlAs–Si–GaAs structure of $0.14 + 0.06 = 0.20$eV. The latter value is in good agreement with the saturation value reported in [Sorba et al., 1992a]. The value for the GaAs–Si–AlAs structure seems to be somewhat higher than the experimental result in [Sorba et al., 1992a] (~ 0.8eV); still, considering the roughness of the estimates, and the neglect of strain, it seems like this simple approach provides a reasonably good prediction for the offset. The agreement may indicate that the mechanism of inequivalent mixed interface formation proposed [Biasiol et al., 1992] is a general one.

Finally, we remark that a further deviation from abrupt, ideal interfaces for the interlayer would occur if not only atomic mixing were present, but additional defects would occur. Some authors have speculated on the role of antisites [Peressi et al., 1991; Biasiol et al., 1992]. A few first-principles investigations of formation energies of intrinsic point defects at the GaAs–AlAs have already been carried out, but the effect on the band offset has not been analyzed so far [Heinemann and Scheffler, 1992].

5. Empirical control of heterojunction band offsets

5.1. Strain and band offset modification

5.1.1. Strain and the experimental determination of the offset

The conceptually simplest method to vary the band offsets is to fabricate heterostructures in elastically strained conditions, using appropriate substrates for epitaxy. If the strain configuration is known, one can then apply the arguments presented in Section 3.6 to predict the effect that strain will have on the band offsets. From the experimental point of view, however, there is comparatively little information available about the experimental dependence of the heterojunction band offsets on strain. This probably reflects the fact that most of the semiconductor heterojunction systems used today in high speed and optoelectronic technology are essentially lattice-matched.

Many important systematic studies of heterojunction band offsets [Margaritondo and Perfetti, 1987] have relied on the formation of large classes of heterojunctions by deposition of disordered and possibly amorphous Ge or Si overlayers on cleaved, nonpolar semiconductor substrates. In a typical example of such experiments, Mahowald et al. conducted a detailed synchrotron radiation photoemission study of Si/InP(110) interfaces for overlayer thicknesses up to 12 ML [Mahowald et al., 1986]. The authors reported laminar grow both at 280°C and 20°C, a low energy electron diffraction (LEED) pattern indicative of largely disordered growth, and used the core level separation ΔE_{cl} (see Eq. (3)) at the interface to derive a valence-band discontinuity of -0.46 ± 0.1 eV and -0.56 ± 0.1 eV for the two growth temperatures, respectively. We remind the reader that, with the convention used here, the sign of the valence-band offset is taken positive when the valence-band maximum in the substrate is above that in the overlayer. However, the in-plane mismatch for Si–InP interfaces is 8.1%, so that the strain configuration of the Si overlayer could vary dramatically in the coverage range explored. The strain configuration has to be known, and the effect of the strain has to be properly taken into account to accurately derive the band offsets. Even if an ideally amorphous overlayer is formed at all coverages, so that it can be presumed unstrained, the interface parameters should be re-examined to establish new systematic trends for well characterized, ordered interfaces.

Only very recently, a few experimental studies have examined the pseudomorphic growth of strained epitaxial interface systems. Unfortunately, the analysis of the experimental results has not always taken advantage of the theoretical developments described in Section 3.6. For example, when photoemission is used to determine band offsets at strained-layer interfaces, particular care has to be taken in the interpretation of the results. When using core levels to lineup the band edges, it is not sufficient to only perform the core-level lineup measurements on the strained heterojunction system; one also has to measure the energy difference between valence band maximum and core level in the strained semiconductor (which may not be easy to accomplish) [Tersoff and Van de Walle, 1987].

The effect of strain on the position of the core levels relative to the valence-band maximum E_v is comprised of hydrostatic and uniaxial contributions. The separation between the core level and the centroid of the valence bands at Γ in the Brillouin zone is only influenced by the hydrostatic contribution. The uniaxial component of the distortion removes the valence-band degeneracy and modifies the position of the spin-split band, but does not shift the centroid of the valence bands [Schwartz et al., 1989; Yu et al., 1990; Grant et al., 1990]. Therefore although in principle one can still use Eq. (3) to derive the band offsets for strained layer systems, one should use core binding energies determined in "bulk" standards (see ΔE_b in Eq. (3)) that have the same strain configuration present in the strained-layer heterostructure. If the critical thickness is small, however, it may be difficult to obtain suitably strained "bulk" standards. This is the case for many of the strained heterojunction systems studied to date.

5.1.2. Early results

Prior to the seminal work by Tersoff and Van de Walle [Tersoff and Van de Walle, 1987], most photoemission determinations of the offsets ignored the effect of strain on the core binding energies. For example, based on the core binding energies in bulk unstrained semiconductor standards, and the observed experimental ΔE_{cl} in the lattice-mismatched CdTe–ZnTe $(\bar{1}\bar{1}\bar{1})$ and HgTe–ZnTe $(\bar{1}\bar{1}\bar{1})$ heterojunctions, linearity and commutativity of the band offsets was reported [Duc et al., 1987a]. The two heterojunctions, however, exhibit 5.8% and 5.1% in-plane lattice mismatch, respectively, so that the overlayer thicknesses employed for photoemission determinations of the offsets ($\sim$ 20–30 Å) are just above the critical thickness for strain relaxation [Matthews and Blakeslee, 1974, 1975, 1976]. Consequently a variable degree of strain is likely to remain present in the interface region, and the core binding energies determined in bulk, unstrained standards do not apply to the interface situation. Strain-induced corrections to the valence band offsets are expected to break the commutativity of the band offsets even in isovalent heterojunctions such as those considered by the authors [Duc et al., 1987a]. In a later report, only some relatively minor deviations from linearity were reported for the same interfaces with (001) orientation [Duc et al., 1987b], but based solely on variations in ΔE_{cl}.

The problem with the above analyses is that the numerical value of the strain-induced variation of the core level binding energy is quantitatively mostly affected by the uniaxial component of the distortion, that splits the valence-band degeneracy and modifies the position of the spin-split band, but does not shift the centroid of the valence bands. Conversely, the photoemission measurements tend to focus on the separation between the core level and the centroid of the valence bands, that is only influenced by the smaller hydrostatic contribution [Tersoff and Van de Walle, 1987; Van de Walle, 1989]. Since strain affects ΔE_v mostly by removing the light and heavy hole degeneracy, and this is also the main contribution to the change of the core binding energies relative to E_v, the implication is that large offset changes may occur with little change in ΔE_{cl}. In the case of Si layers pseudomorphically strained on GaAs (001), for example, strain is expected to yield a 0.45 eV change in the unstrained, zero-order valence-band offset [Van de Walle, 1989], and at the same time increase the Si 2p binding energy relative to E_v by 0.44 ± 0.03eV [Bratina et al., 1991], so that little net change is expected in ΔE_{cl} in comparing the strained and the relaxed interface configurations.

For some heterojunctions the strain-induced corrections to the band offsets might be comparable with the experimental uncertainty. For example, nonmonochromatized XPS measurements of the band offsets of AlSb/GaSb (001) and GaSb/AlSb (001) heterostructures grown by MBE and involving 30 Å thick semiconductor overlayers [Gualtieri et al., 1986] were interpreted based on the experimental core level separation ΔE_{cl} (see Eq. (3)), using the literature value of the Au/AlSb and Au/GaSb Schottky barriers fabricated on bulk, unstrained semiconductor standards, and the photoemission values of the Au–Ga and Au–Al core level separation to infer the core level binding energies relative to the valence band maxima in Eq. (3). A value of $|\Delta E_v| = 0.40 \pm 0.15$ eV was reported for the two heterojunctions, irrespective of the growth sequence. Such heterojunctions are expected to exhibit a 0.65% in-plane mismatch, so that the use of the literature Schottky barrier values and the corresponding measurements of the Au-cation core level separation, which are obtained for unstrained system, may be the source of systematic errors that obscure the expected strain-induced violation of the commutativity rule for such interfaces. The authors used a similar method for InAs–GaSb (001) and GaSb–InAs (001) heterojunctions [Gualtieri et al., 1987], with reported valence band offsets of $+0.53$ and -0.48eV, respectively, while neglecting corrections for the 0.62% in-plane lattice mismatch.

In a more recent study of InAs/AlSb (001) heterojunctions grown by MBE in different conditions to achieve different interface compositions (AlAs-like versus InSb-like) tight-binding model calculations of the effect of local strain were used to interpret the experimental data [Waldrop et al., 1992]. The authors concluded that a staggered band alignment is present at the interface, with at most a 0.06 eV variation in band alignment in going from AlAs-like interfaces ($\Delta E_v = 0.22$ eV) to InSb-like interfaces ($\Delta E_v = 0.16$ eV). The small change in band offset with interface composition is unexpected due to the isovalent character of this interface (see Section 4.1), and is, in our opinion, close to the experimental uncertainty. This, together with the close match of the experimental offset with the predictions of the transitivity rule based on the results for InAs–GaSb [Gualtieri et al., 1987], suggests that in this materials system the effect of strain is indeed only comparable with the experimental uncertainty.

Among more recent band offset measurements reported for strained heterojunction systems we mention Si–$Si_{1-x}Ge_x$, Ge–$Si_{1-x}Ge_x$, Si–GaAs, Si–AlAs, and InGaAs–GaAs heterojunctions (see below). However, only for two of these (Si–$Si_{1-x}Ge_x$ and Ge–$Si_{1-x}Ge_x$) direct measurements of the effect of strain on the core level binding energy relative to the valence-band maximum were attempted. For the others, theoretical or semiempirical corrections were introduced to take the effect of strain into account.

5.1.3. Si–Ge

Si–Ge heterojunctions exhibit a 4% in-plane mismatch, leading to substantial strain-related effects in pseudomorphic heterojunctions, and to a relatively small expected critical thickness. In early studies, nonmonochromatized XPS measurements of the Si 2p-Ge 3d ΔE_{cl} in Ge–Si (001) and Si–Ge (001) heterostructures grown by MBE at 450°C—500°C for overlayer thicknesses below the critical thickness, yielded $\Delta E_{\mathrm{cl}} = 69.90 \pm 0.10$ and 70.12 ± 0.10 eV (see Eq. (3)), respectively, for the two interfaces [Schwartz et al., 1989]. The strain configuration of the interfaces was gauged by Raman, and corrections to the literature value of E_{b} for the two core levels were introduced using selfconsistent LMTO calculations to estimate the effect of the hydrostatic component of the strain [Schwartz et al., 1990; Hybertsen, 1991]. Two different codes produced calculated values of 0.22 and 0.1 eV for the hydrostatic correction to the Si 2p binding energy, and 0.08 eV for the Ge 3d core level, respectively. To the 0.22 and 0.08 eV hydrostatic corrections selected, the combined spin orbit-uniaxial strain splitting of the valence bands was added using deformation potentials [Van de Walle, 1989]. Taking into account the effect of strain, the magnitudes of the valence band offsets were evaluated as 0.74 ± 0.13 and 0.17 ± 0.13, for Si on Ge (001) and Ge on Si (001), respectively [Schwartz et al., 1989].

The effect of strain on the bandgap of $Si_{1-x}Ge_x$ alloys, and on the $Si–Si_{1-x}Ge_x(001)$ heterojunction band offsets was determined directly in an intriguing study by means of nonmonochromatized XPS [Ni et al., 1987]. Alloys and heterojunctions were grown by MBE at 570°C on either Si (001) substrate layers, or on relaxed $Si_{1-x}Ge_x$ alloy layers (with $x = 0.25$ and 0.48). The bulk core binding energies were determined in especially grown 80Å-thick pseudomorphic standards with the same strain configuration as that encountered in the interface (i.e., grown on appropriate substrates). Such standards were heavily doped p^+ or n^+ with In or Sb during growth to bring the Fermi level near the valence-band maximum or conduction-band minimum, respectively, and the final surfaces were passivated with the deposition of 1–2 ML of In or Sb to remove band bending [Ni et al., 1987; Himpsel et al., 1983]. With this method the alloy bandgap could be evaluated simply comparing the core level shifts in going from p^+ to n^+ standard, and the band offsets evaluated from Eq. (3) simply using the core level positions relative to the spectrometer Fermi level, that coincide with the band extrema. Strain-induced variations in bandgaps and band offsets of the order of 0.13 eV were observed in this study, and agreement was claimed with theoretical predictions [Ni et al., 1987; People and Bean, 1986].

For the Si–Ge system, Yu et al. [Yu et al., 1990] attempted one of the very few available direct determinations of the effect of strain on the core binding energies. Measurements of the Si 2p and Ge 3d binding energy relative to E_{v} for Si and Ge strained overlayers on $Si_{1-x}Ge_x$ layers with x varying from 0.0 to 0.3 (corresponding to in-plane Si strain of 0–1.2%) and from 0.7 to 1.0 are illustrated in Fig. 24. A linear increase (decrease) in Si 2p (Ge 3d) binding energy with increasing Ge concentration x in the alloy substrate was observed in the alloy composition range explored. A linear extrapolation was used to derive a correction to E_{b} of $+0.44$ eV for the Si 2p core levels in Si layers pseudomorphically strained to bulk Ge, and $+0.28$ eV for the Ge 3d core levels in Ge layers pseudomorphically strained to bulk Si. Such corrections were used to infer valence band offsets of -0.83 ± 0.11 and $+0.22 \pm 0.13$ for Ge–Si(001) and Si–Ge (001), respectively, with the strain entirely accounting for the

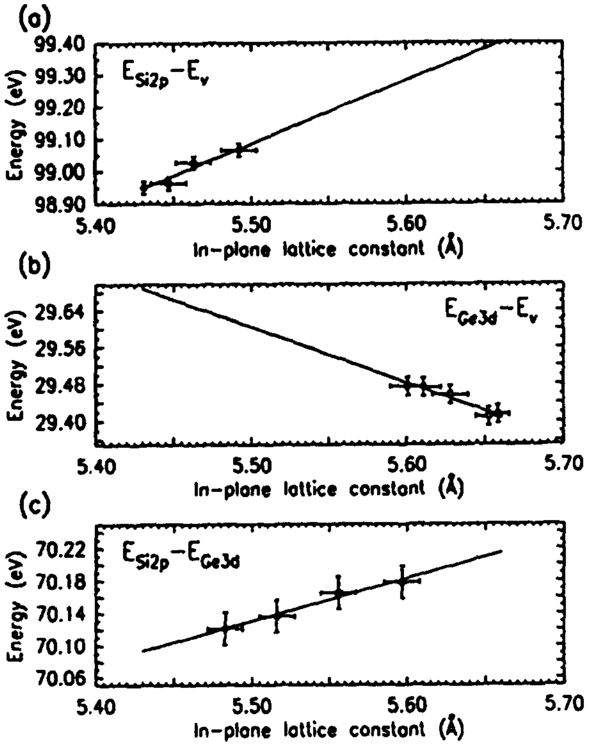

Fig. 24. Effect of strain on the Si 2p (a) and Ge 3d (b) binding energy relative to E_v for Si and Ge overlayers pseudomophically grown on $Si_{1-x}Ge_x$ alloy substrates with x varying from 0 to 0.3 or 0.7–1.0, corresponding to in-plane strains of 0–1.2%. The resulting expected Si 2p to Ge 3d core level energy separation as a function of the in-plane lattice constant in Si–Ge heterojunctions is shown in (c) [Yu et al., 1990].

deviation of the band offsets from the predictions of the commutativity rule [Yu et al., 1990]. Such values are consistent with those derived [Schwartz et al., 1989] using Hybertsen's theoretical corrections. Assuming that the offset between the weighted averages of the light-hole, heavy-hole, and spin–orbit valence bands in Si and Ge is independent of strain, the discontinuity in the average valence-band edge would be $|\Delta E_v| = 0.49 \pm 0.13$ eV [Yu et al., 1990].

Several other experiments have attempted to measure the Si–Ge band offsets in heterostructures which were partially relaxed, or in which the strain configuration was unknown. Margaritondo et al. [Margaritondo et al., 1982] obtained $\Delta E_v = -0.2 \pm 0.1$ eV upon deposition of amorphous Ge on Si (111), and Mahowald et al. [Mahowald et al., 1985] reported $\Delta E_v = +0.4 \pm 0.1$ eV for Si on Ge (111). Capacitance measurements of Ge overlayers on Si (001) by Kuech et al. [Kuech et al., 1981] were interpreted as indicating a valence-band offset $\Delta E_v = -0.39 \pm 0.04$ eV.

A new twist to the Si–Ge saga was provided by an intriguing analysis of the band offsets in the absence of strain based on measurements of core-to-conduction band transition energies in $Si_{1-x}Ge_x$ alloys by means of transmission electron energy loss spectroscopy [Morar et al., 1993]. The authors used and extended an idea originally applied by Shih and Spicer to HgTe–CdTe [Shih and Spicer, 1987], namely that the core level positions relative to the vacuum level are approximately independent of composition in bulk alloys involving lattice-matched, common anion systems. Shih and Spicer proposed that measurements of the core level separation relative to E_v in bulk alloys could be used to map the position of E_v with composition and infer the relative positions of the band extrema (i.e., the band offset) in the corresponding heterojunctions. The same approach was also used in a theoretical analysis by Wei and Zunger [Wei and Zunger, 1987].

Morar and co-workers performed linear response theory calculations to show that the core level binding energies varies indeed very little with x in $Si_{1-x}Ge_x$ alloys, while the change might be more substantial for III–V and II–VI alloys [Morar et al., 1993]. They then used electron energy loss spectroscopy measurements in a scanning transmission electron microscope to determine the transition energies from the Si $2p_{3/2}$ core level to the Δ_1 and L_1 conduction band minima and the L_3 saddle point in relaxed $Si_{1-x}Ge_x$ alloys ($x = 0.0$–0.95) [Batson and Morar, 1991; Morar and Batson, 1992]. Having determined the position of the conduction band versus x, the position of E_v was obtained by subtracting the bulk alloy bandgap [Weber and Alonso, 1989]. The results of the analysis are summarized in Fig. 25 [Morar et al., 1993]. Results for band line-ups between hypothetical unstrained Si–Ge alloys of any two compositions can be read directly from Fig. 25. For any actual heterojunction, splitting and shifting of the band edges due to strain must be evaluated as described in Section 3.6, and added to the values obtained from Fig. 25.

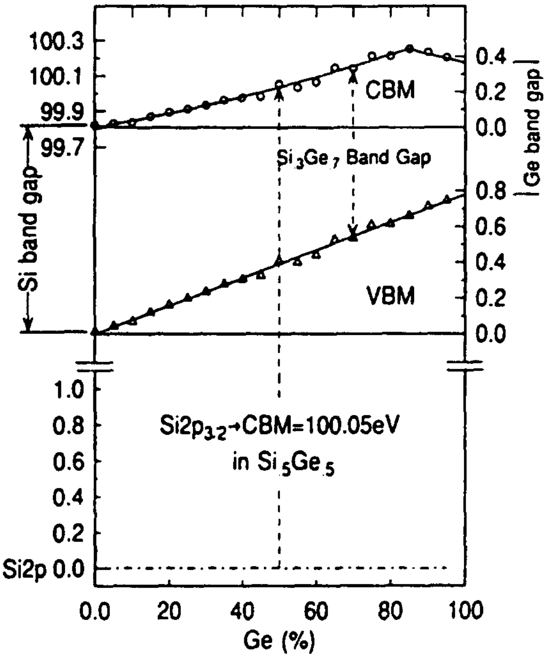

Fig. 25. Position of the conduction-band mimimum (CBM, open circles) and valence-band maximum (VBM, open triangles) as a function of x in $Si_{1-x}Ge_x$ unstrained alloys, from transmission electron energy loss measurements of the Si $2p_{3/2} \rightarrow$ CBM transition energies. The reference level is the core binding energy, which has been calculated to be independent of x in the alloys series. Band lineups between hypothetical unstrained Si–Ge alloys of any two compositions can be read directly from the position of the band extrema in the plot [Morar et al., 1993]. For any actual heterojunction, splitting and shifting of the band edges due to strain must be evaluated as described in Section 3.6, and added to the values obtained here.

5.1.4. Si–GaAs and Si–AlAs

The Si–GaAs system is of special interest to us in view of its heterovalent character, and the large amount of information available from the technological literature. In addition to the extensive materials science literature about the growth of GaAs on Si for optoelectronic applications [Stoltz et al., 1988; Freundlich et al., 1988; Lee et al., 1988; van der Ziel et al., 1989; Chen et al., 1989; Huang et al., 1987; Landa et al., 1989; Lucas et al., 1988; Sharan and Narayan, 1989; Sobiesierski et al., 1991], recently growth of Si pseudomorphic layers on GaAs has been used as a preliminary step to the formation of SiO_2–GaAs junctions, and correspondingly, reduced interface state densities [Tiwari et al., 1988; Hasegawa et al., 1989] and reduced Fermi level pinning [Tiwari et al., 1988; Fountain et al., 1988; Hasegawa et al., 1989] have been reported. Although recent studies suggest [Freeouf et al., 1990a,b] that the improvement in the electrical properties may result not from a large reduction in the interface state density but rather from a shift of the density toward the conduction band edge, this process remains a promising tool in the current search for a viable GaAs-based MOSFET technology.

Thin Si interface layers grown on GaAs have also recently been used to "unpin" the GaAs Fermi level and modulate the Schottky barrier at Au–GaAs, Cr–GaAs, Ti–GaAs [Waldrop and Grant, 1988] and Al–GaAs [Costa et al., 1991; Cantile et al., 1994a, b] contacts, although the theoretical explanation of this effect remains somewhat controversial [Sambell and Wood, 1990; Costa et al., 1991; Cantile et al., 1944b]. Also, thin pseudo- morphic Si layers fabricated in the interface region by MBE have been used to tune the band offsets in III–V/III–V heterojunctions [Sorba et al., 1991; Sorba et al., 1992a; Franciosi et al., 1993] and homojunctions [Marsi et al., 1993].

Recently pseudomorphic Si layers were fabricated by MBE at 500°C on As-stabilized GaAs(001) 2 × 4 and AlAs(001) 3 × 1 surfaces [Bratina et al., 1991]. Monochromatic XPS measurements of the Ga 3d–Si 2p core level separation ΔE_{cl} for the resulting Si–GaAs(001) and Si–AlAs(001) interfaces with Si layers of 8, 12 and 14 ML would be consistent with valence-band offsets of $+0.05 \pm 0.08$ eV and -0.57 ± 0.08 eV, respectively, for the two interfaces in the absence of strain-related corrections to the core binding energies. However, the above values have to be modified if the Si overlayer is strained to take into account the effect of strain on the position of the Si 2p core levels [Tersoff and Van de Walle, 1987]. For Si–GaAs(001) and Si–AlAs(001) the expected in-plane strain for ideal pseudomorphic growth is 4.1% and 4.2%, respectively, at room temperature.

Corrections for the strain induced change in E_{b} by Schwartz et al. [Schwartz et al., 1989] and Yu et al. [Yu et al., 1990] for Si–Ge can be directly applied to Si–GaAs and Si–AlAs interfaces [Bratina et al., 1991] because of the good lattice match between Ge and GaAs or AlAs (0.1–0.2% mismatch). For ideal Si–GaAs and Si–AlAs pseudomorphic overlayers, a $+0.44 \pm 0.03$ eV strain-induced correction to the Si 2p binding energy is required for a 4.1% in plane strain, and a $+0.45 \pm 0.03$ eV for a 4.2% in plane strain [Bratina et al., 1991]. A strain induced increase of the Si 2p binding energy would yield Si 2p binding energies of 99.33 and 99.34 eV, respectively, and therefore strain-corrected values of ΔE_{v} of -0.39 ± 0.10 eV and -1.02 ± 0.10 eV for Si–GaAs(001) and Si–AlAs(001), respectively, with the minus sign putting the valence-band maximum of Si above that of the III–V semiconductors [Bratina et al., 1991].

There are, however, several points that remain unclear. First, Bratina et al. (1991) observed no change in ΔE_{cl} for Si layers 8–14 ML thick, while gradual lattice relaxation is expected in this Si coverage range (see Section 2.4). Also, during growth of Si at lower temperatures (378°C) on nonpolar cleaved GaAs (110) surfaces, surface extended X-ray absorption fine structure (SEXAFS) results have been interpreted as evidence of a strain of only about 1.35% at a Si coverage of 10 ML, and 0.2% at 16 ML, and a large density of dislocation has been inferred [List et al., 1987]. Finally, attempts to measure directly by XPS the variation in the Si 2p binding energy and the strain-induced splitting of the valence-band maximum during progressive Si lattice relaxation on GaAs [Chambers and Loebs, 1993], revealed no consistent decrease in core binding energy or evidence of a change in the lineshape of the leading valence band edge with decreasing strain . Some authors therefore questioned the applicability of the strain-induced correction to the Si 2p binding energy for Si–GaAs and Si–AlAs interfaces [Chambers and Loebs, 1993]. Our view is that the effect of strain on semiconductor bandgaps and heterojunction band offsets is well demonstrated by a wide variety of optical studies [Pollak and Cardona, 1968; Aspnes and Cardona, 1978], including photoluminescence spectroscopy studies of pseudomorphic GaAs–Si heterostructures [Sobiesierski et al., 1991] and Raman studies of strained-layer Si–GaAs superlattices [Sorba et al., 1992b; Scamarcio et al., 1992a,b] and cannot be ignored, even if sometime the limited resolution available in XPS studies may hinder a direct determination of the magnitude of these effects in the photoemission spectra.

We mention that there have also been a number of band offset determinations for samples in which the exact strain configurations was unknown, especially as far as Si–GaAs (011) interfaces are concerned. In two studies using synchrotron radiation photoemission [Katnani and Margaritondo, 1983; List et al., 1986] Si was deposited at room temperature on substrates cleaved in situ, a procedure reportedly yielding an amorphous Si layer, and valence-band offsets of -0.05 ± 0.10 eV and -0.6 ± 0.1 eV, respectively, were deduced. The first value, obtained with higher resolution, is close to the XPS result for pseudomorphic interfaces [Bratina et al., 1991] prior to correction for the strain, as expected. In a later paper [List et al., 1987], a -0.23 ± 0.01 eV valence-band offset was reported for partially strained and relaxed crystalline Si grown at 375°C on GaAs (011). This value is apparently consistent with the XPS results for pseudomorphic interfaces [Bratina et al., 1991], but we have to emphasize that a strain-independent band offset was reportedly observed by List et al. [List et al., 1987] for Si-thickness larger than 2 ML, when SEXAFS results indicated a strain variation of 2% in the coverage range explored [List et al., 1987]. The very existence of a strain-independent band offset is inconsistent with the theoretical results described in Section 3.6 and with the experimental studies [Schwartz et al., 1989; Yu et al., 1990] which form the basis of the discussion of the pseudomorphic interfaces [Bratina et al., 1991].

Comparison of the photoemission results with transport-derived determinations of the offsets in complicated by the issue of strain and its effect on the Si bandgap. Calculations of the effect of strain on the fundamental bandgap by means of deformation potential theory for coherently strained Si_xGe_{1-x} bulk alloys on Ge (001) substrates are available [People, 1986]. For pure Si coherently strained on Ge, the strain induced splitting of the conduction band minima and valence-band maximum reduces the fundamental bandgap by 55%. The expected bandgap difference for Si–GaAs therefore goes from 0.31 eV (unstrained case) to 0.81 eV (pseudomorphic case) at room temperature. For a valence-band offset of -0.39 ± 0.10 eV [Bratina et al., 1991], one expects a conduction-band offset of -0.42 ± 0.10 eV (neglecting the unknown error on the predicted bandgap) in the pseudomorphic case, with the conduction-band minimum E_c in Si lying below that of GaAs.

An experimental Si–GaAs conduction-band offset of $+0.30 \pm 0.05$ eV has been proposed based on I–V and C–V measurements of Al–Si–GaAs diodes with Si thicknesses of 6, 30 and 60 Å [Costa et al., 1991]. Since the Si thicknesses employed vary from the pseudomorphic to the fully relaxed range, it is not clear at this time why the conduction-band offset would remain constant at 0.3 eV in the series. A lower value of the conduction-band offset (0.11 eV) has been reported by other authors [Aria and Mizutani, 1989] based on C–V measurements of in situ fabricated n^+ Si–GaAs interfaces with Si thicknesses of 500 Å. The lower value of the offset cannot be compared to that derived from photoemission spectroscopy [Bratina et al., 1991] since it is clearly representative of the relaxed overlayer case, but is certainly inconsistent with the transport-derived value proposed for 60 Å Si overlayers [Costa et al., 1991].

Finally, C–V measurements of metal/insulator/GaAs capacitors incorporating Si layers 10–15 Å thick grown at 500°C on GaAs (001), were interpreted as providing evidence of Si derived extended states 0.33 eV below the conduction-band minimum of GaAs [Hasegawa et al., 1989]. The authors of this study claimed good agreement between this experimental value and the prediction of their own hybrid orbital energy scheme for the Si–GaAs conduction-band offset (0.24 eV). However, since the model does not take into consideration the effect of strain and uses the unstrained bandgap difference for Si–GaAs, it is not likely to be relevant to the experimental situation.

5.1.5. *InGaAs/GaAs*

The lack of visible strain effect in XPS spectra from highly strained overlayers reported by some authors [List et al., 1987; Waldrop et al., 1989, 1990; Grant et al., 1990; Chambers and Loebs, 1993] is in contrast with the results produced by others. In addition to the results for Si–Ge already mentioned [Yu et al., 1990] several authors have reported important effects of strain on photoemission spectra from III–V epilayers [Hwang et al., 1988; Williams and Chu, 1990; Stampfl et al., 1992]. For example, angular resolved photoemission has been used to directly determine the strain-induced shift of the valence bands in CdS–GaAs (001) [Niles and Höchst, 1991], $In_xGa_{1-x}As$/GaAs (001) [Stampfl et al., 1992], and Ge–InP (001) [Rioux and Höchst, 1993] pseudomorphic heterostructures, and the results have been generally found in good agreement with theoretical predictions. The difference is probably due to the variable energy and angular resolution of the photoemission measurements, as well as the difficulty of clearly characterizing the strain configuration of the thin overlayers that one can examine by photoemission spectroscopy. Normal emission spectra with synchrotron radiation and soft-X-ray photons probably have the maximum potential to directly monitor strain-induced changes in the band structure. For investigations with lower experimental resolution, perhaps the best approach is still to assume that the experimental spectra will reflect mostly the core level separation from the center of mass of the valence bands, as suggested by Grant et al. [Grant et al., 1990] and combine the experimental results with the calculated value of the strain-induced split of the valence-band maximum.

This type of approach was used in studies of InAs/GaAs (001) and GaAs/InAs (001) heterojunctions [Hashimoto et al., 1991; Hirakawa et al., 1991]. To circumvent the problem of the very short critical thickness expected from the 7% in-plane mismatch, the authors grew by MBE GaAs/InAs/GaAs (001) and InAs/GaAs/InAs (001) double heterostructures on relaxed substrates. In each heterostructure the central layer was only 2 ML thick, while the cap layer was 5 ML thick, so that all layers could be probed at the same time by photoemission spectroscopy. The authors found that the interface core level separation ΔE_{cl} (see Eq. (3)) between the In 4d and Ga 3d core levels varied only slightly (by 0.04 eV) with the in-plane lattice constants. The data were combined with calculations of the effect of strain on the core level position relative to E_{v}, performed using a tight-binding theory and the $Z+1$ approximation [Enderlein and Harrison, 1984; Harrison and Kraut, 1988], to derive

$\Delta E_v = -0.53$ eV for InAs on GaAs (001) and -0.16 eV for GaAs on InAs (001). The variation of the band offset from the predictions of the commutativity rule is therefore purely strain-induced, and amounts to 0.7 eV [Hashimoto et al., 1991; Hirakawa et al., 1991]. We mention that earlier estimates of the band offset for InAs–GaAs ranged from -0.17 ± 0.07 eV (from XPS measurements) to -0.11 ± 0.05 eV (using the natural valence-band offset method) [Hwang et al., 1987].

Although the above results are very intriguing, they remain open to the criticism that a 2 ML thick interlayer can hardly be assimilated to a bulk semiconductor, in the sense that its band structure and dielectric constant are unlikely to be fully developed. Therefore it seems important to verify these results for related systems with a higher critical thickness. We suggest, for example, that InGaAs alloys of variable compositions could be used as substrates for MBE fabrication of InAs and GaAs epilayers of well characterized strain configuration.

5.2. *Growth paramenters and band offset modification*

5.2.1. *Heterovalent versus isovalent interfaces*

From an empirical point of view it has always been relatively clear that heterovalent heterojunctions tend to exhibit larger variations in band offsets with interface orientation and growth protocol as compared to isovalent heterojunctions. For example, while, AlAs–GaAs heterojunctions have shown relatively constant and commutative band offsets for (001) and (110) orientations in a variety of experimental studies [Margaritondo and Perfetti, 1987], reported band offsets for Ge–GaAs show a wide spread of values, and those for ZnTe–GaSb vary by as much as 0.3 eV in going from the (110) to the (001) interface orientation [Wilke and Horn, 1988; Yu et al., 1992b].

New theoretical and experimental developments are now clarifying *why* the growth conditions have an especially important role in determining the band discontinuities achieved in heterovalent heterojunctions. Linear response theory results treating the heterojunction as a perturbation relative to a virtual crystal solid (see Section 3.3), indicate that the lineup between the average electrostatic potentials on the two sides of the interface in tetrahedral semiconductors can be split into two contributions. A first contribution is independent of the details of the interface and accounts for the dependence of the band offsets on the bulk properties of the two semiconductors. The second term is formally equivalent to the lineup generated by an assembly of point charges. Each charge in the assembly corresponds to the total charge induced at a given atomic site by the perturbation, i.e., by the operator that transforms the virtual crystal into the actual heterostructure. The second term depends on the atomic structure of the interface, and therefore in principle on orientation, abruptness, and atomic reconstruction if the perturbation carries a nonzero net charge.

The LRT discussion supports the theoretical alchemy approach proposed earlier by Harrison (see Section 4.2), and easily explains why in isovalent semiconductor heterojunctions, such as AlAs–GaAs, the band offsets obtained from most first principles calculations are independent of interface orientation. Since for such systems the perturbation is neutral, and does not generate a dipole, the interface-specific term in the band alignment is expected to vanish. Conversely, in heterovalent heterojunctions, such as ZnSe–GaAs, the perturbation is in general nonneutral, and produces a dipole, so that the band offsets will depend in general on the detail of the atomic configuration of the interface.

The interface configuration achieved in practice is likely to be determined by the interplay between growth kinetics and thermodynamic stability. Therefore in heterovalent heterojunctions the band discontinuities may depend crucially on the growth protocol employed. As explained in

Section 4.2, for heterovalent heterojunctions with polar orientation, ideally abrupt interfaces would actually be charged, and therefore thermodynamically unstable. Neutral interfaces with lower free energy may be established as a result of atomic mixing. The resulting different types of interface configurations may correspond to widely different band discontinuities. Several possible types of configurations have been described in Section 4.2.

Such interfaces are therefore the best candidates for any attempt to tune the band offsets through modification of the growth conditions. Unprecedented changes in the band discontinuities have been recently achieved by MBE in Ge–GeAs, Ge–AlAs, and ZnSe–GaAs interfaces with (001) orientation, and will be discussed in Section 5.2.3. Even the band offsets in isovalent heterojunctions such as AlAs–GaAs(001) and InAs–GaAs(001) as well as GaAs–GaAs(001) homojunctions have been tuned through the fabrication of heterovalent Si or Ge interface layers, that effectively convert the isovalent interfaces in a system of two nonequivalent heterovalent IV/III–V and III–V/IV interfaces. Such techniques will be the subject of Section 5.5.

The situation is less clear for the nonpolar orientations of heterovalent heterojunctions. Since an equal number of cations and anions is present along the interface, ideally abrupt interfaces would be neutral, so that there would be no enthalpic driving force toward the formation of more complex interface configurations. Also, LRT would predict that the band offsets at ideal, unreconstructed interfaces would be a bulk property of the two semiconductors comprising the junction, since the perturbation leading from the virtual crystal to the actual heterojunction is neutral in each plane parallel to the interface (see Section 4.2.1). However, variations in the band offsets for different interface orientations or growth and processing protocols have also been reported for some (110)-oriented heterovalent heterojunctions, as described in the next section. Such variations can be reconciled with LRTor theoretical alchemy predictions if cation–anion swaps occur at the interface, perhaps as a result of interdiffusion [Baldereschi et al., 1993a], as it will be discussed in more detail in Section 5.2.2.

In the next two sections we will examine our current understanding of a few prototypical heterovalent heterojunctions with nonpolar and polar orientations. We elected to emphasize lattice-matched, or nearly lattice-matched systems to avoid the complications described in Section 2.4 and concentrate on the dependence of the band offset on the growth parameters and sequence. When possible, we will emphasize recent results for epitaxial heterostructures, and we will make no attempt to present a truly comprehensive survey. A more complete list of offset determinations can be found in recent reviews by Brillson [Brillson, 1992], and by Margaritondo and Perfetti [Margaritondo and Perfetti, 1987].

5.2.2. *Nonpolar heterovalent interface orientations*

Heterovalent heterojunctions that are nearly lattice-matched, such as those involving Ge, GaAs or AlAs, and ZnSe, are ideal model systems to study the effect of different interface terminations or orientations on the band offsets, since the complication of determining the effect of strain is removed. Such systems have therefore attracted much attention.

The in-plane lattic mismatch for Ge–GaAs and Ge–AlAs heterostructures is only 0.13% and 0.25%, respectively. The number of band-offset studies available for such heterostructures is quite substantial, and we have summarized in Table 3 some of the most recent determinations for interfaces with (110) and (001) orientation. A few results for other interface orientations show similar trends, or lack thereof [Waldrop et al., 1982].

Table 3
Experimental valence band offsets for Ge–GaAs and Ge–AlAs heterojunctions, Column 1: literature reference. Column 2: type of heterojunction. Note that with the convention used, an A–B heterojunction is obtained by deposition of an overlayer of semiconductor A onto a substrate B. The prefix α indicates an amorphous or highly disordered overlayer. Column 3: overlayer–substrate doping, if reported by the authors. Column 4: growth temperature. Column 5: method used to determine the band offset. I–V: current–voltage characteristics; XPS: X-ray photoemission spectroscopy; SRPES: synchrotron radiation photoemission spectroscopy; C–V: capacitance–voltage characteristics; IPE: internal photoemission; ARUPS: angle-resolved ultraviolet photoemission spectroscopy; PLP: picosecond laser photoemission. Column 6: magnitude of the valence-band offset

Ref.	Interface	Doping	T_g (°C)	Method	$\lvert\Delta E_v\rvert$ (eV)
a	Ge–GaAs(001)	n–n	300	I–V	0.68 ± 0.01
b	Ge–GaAs(001)Ga	i–p	340	XPS	0.55 ± 0.04
b	Ge–GaAs(001)As	i–p	340	XPS	0.60 ± 0.04
c	Ge–GaAs(001)	i–n	340	SRPES	0.46 ± 0.05
c	Ge–GaAs(001)	n–n	340	SRPES	(0.44 – 0.48) ± 0.05*
d	Ge–GaAs(001)	i–n, n–n	320	SRPES	0.47 ± 0.05
e	Ge–GaAs(001)	?–n	320	XPS	0.44 ± 0.07
f	Ge–GaAs(001)	i–i, n–i	320	XPS	0.60 ± 0.05
g	Ge–GaAs(001)	n–i	210	XPS	0.71 ± 0.07
h	Ge–GaAs(001)	p–n	500	I–V	0.72 ± 0.01
i	Ge–GaAs(001)	p–n	300	C–V	0.49 ± 0.05
j	Ge–GaAs(001)	n–i, n–n	360	XPS	0.54 ± 0.05
j	Ge–GaAs(001)	n–i, n–n	480	XPS	0.57 ± 0.05
k	Ge–GaAs(001)	p–n	300	C–V	0.80 ± 0.07
k	Ge–GaAs(001)	p–n	500	IPE	0.45 ± 0.04
k	Ge–GaAs(001)	p–n	500	C–V	0.30 ± 0.07
k	Ge–GaAs(001)	p–n	500	I–V	0.50 ± 0.1
j	GaAs–Ge(001)	i–n	360	XPS	0.17 ± 0.05
j	GaAs–Ge(001)	i–n	580	XPS	0.31 ± 0.05
l	Ge–GaAs(110)	i–n	350	SRPES	$0.7^{+0.05}_{-0.3}$
m	αGe–GaAs(110)	i–n	420	ARUPS	0.25
n	Ge–GaAs(110)	Unspecified	425	XPS	0.53 ± 0.03
o	Ge–GaAs(110)	i–n	320	SRPES	0.42 ± 0.1
o	αGe–GaAs(110)	i–n	RT	SRPES	0.65 ± 0.1
p	Ge–GaAs(110)	p–n	325	XPS	0.59 ± 0.05
p	Ge–GaAs(110)	p–p	325	XPS	0.54 ± 0.05
b	Ge–GaAs(110)	i–p	340	XPS	0.56 ± 0.04
q	αGe–GaAs(110)	i–n	RT	SRPES	0.35 ± 0.01
c	Ge–GaAs(110)	i–n	340	SRPES	0.43 ± 0.05
r	αGe–GaAs(110)	i–n	RT	SRPES	0.73 ± 0.08
s	Ge–GaAs(110)	i–p	350–450	PLP	0.38 ± 0.03
t	αGe–GaAs(110)	i–n	Unspecified	IPE	0.42 ± 0.05**
u	GaAs–Ge(110)	i–i	325	SRPES	0.23 ± 0.07
v	GaAs–GeAs(110)	i–i	350	XPS	~ 0.3
e	Ge–AlAs(001)	Unspecified	320	XPS	0.78 ± 0.07
j	Ge–AlAs(001)	n–i, n–n	360	XPS	0.94 ± 0.05
j	Ge–AlAs(001)	n–i, n–n	480	XPS	1.07 ± 0.05
j	AlAs–Ge(001)	i–n	360	XPS	0.69 ± 0.05
j	AlAs–Ge(001)	i–n	580	XPS	0.96 ± 0.05

Table 3 (continued)

Ref.	Interface	Doping	T_g(°C)	Method	$\lvert\Delta E_v\rvert$(eV)
w	αGe–AlAs(110)	Unspecified	RT	SRPES	0.95 ± 0.2
x	Ge–AlAs(110)	Unspecified	Unspecified	XPS	0.9

* Range of values for different initial surface reconstructions. ** Measured at 77 K.
[a] Ballingall et al., 1983; [b] Waldrop et al., 1983; [c] Katnani et al., 1984; [d] Katnani et al., 1985; [e] Katnani and Bauer, 1986; [f] Chambers and Irwin, 1988; [g] Chambers and Loebs, 1990; [h] Kawanaka and Sone, 1990; [i] Ünlü et al., 1990; [j] Biasiol et al., 1992; Sorba et al., 1993b; [k] Dahmen et al., 1993; [l] Bauer and McMenamin, 1978; [m] Perfetti et al., 1978; [n] Kraut et al., 1980; [o] Mönch et al., 1982; [p] Kowalczyk et al., 1983; [q] Katnani and Margaritondo, 1983; [r] Aldao et al., 1989; [s] Haight and Silberman, 1990; [t] Coluzza et al., 1992b; [u] Zurcher and Bauer, 1983; [v] Grant et al., 1985; [w] Kelly et al., 1985; [x] Waldrop et al., 1985.

The reported values of the valence-band offset magnitude for Ge–GaAs (110) interfaces show a substantial spread, with most values in the 0.35–0.73 eV range. If one excludes the interfaces in which the overlayer was disordered, or amorphous, and the very earliest couple of results, the spread diminishes substantially, with an average $\Delta E_v = -0.49 \pm 0.08$ eV, where the quoted uncertainty is the standard deviation on the set of seven experiments considered. As explained in Section 2.3, *variations* in band offsets, as obtained from changes in ΔE_{cl}, are less affected by systematic errors in band offset determination, and several authors have focused on offset changes as a function of interface growth sequence, interface orientation, or fabrication temperature.

As early as 1985, epitaxial growth of Ge–GaAs (110) and GaAs–Ge (110) heterostructures was successfully performed by MBE in an attempt to search for variations of the band offsets from the predictions of the commutativity rule [Grant et al., 1985]. XPS results yielded $\Delta E_v = -0.56 \pm 0.04$ eV for Ge overlayers on GaAs (110) substrates, and $\Delta E_v \sim 0.3$ eV for GaAs overlayers on Ge (110) substrates. Zurcher and Bauer had earlier obtained a value of $0.23 - 0.26 \pm 0.08$ eV for the valence-band offset in GaAs–Ge (110) heterojunctions fabricated by MBE [Zurcher and Bauer, 1983].

In an attempt to explain the unexpected, substantial (0.2–0.3 eV) deviation from commutativity, and the distribution of experimental offset values in the GaAs–Ge (110) samples, Grant et al. tentatively associated the differences with the presence of a variable concentration of antisite defects at the interface [Grant et al., 1985]. Recent LRT arguments confirm that in principle antisite defects could change the band offsets for nonpolar interface orientations, since the perturbation (Section 3.3) that transforms the virtual crystal into the actual heterojunction is not neutral in the presence of such defects [Baldereschi et al; 1993a].

For Ge–AlAs (110) interfaces, the two available results suggest a valence-band offset $\Delta E_v \sim -0.9$ eV [Kelly et al., 1985; Waldrop et al., 1985], and no large variations in going from amorphous to epitaxial overlayers. No studies of the commutativity of the offset have been reported, to our knowledge, for Ge–AlAs interfaces with (110) orientation. We note, however, that valence band offsets $\Delta E_v = -0.49 \pm 0.08$ eV for Ge–GaAs (110) and -0.9 eV for Ge–AlAs (110) would imply that the offsets follow the predictions of the transitivity rule within 0.03 eV, assuming an average AlAs–GaAs valence-band offset of $+0.44 \pm 0.02$ eV (see Section 2.3). Commutativity and transitivity of the band offsets would be expected from LRT for heterovalent heterojunctions with nonpolar interface orientation (see Section 4.2).

ZnSe–GaAs heterostructures also exhibit a relatively low (0.27%) in-plane lattice mismatch. Determinations of ΔE_v for ZnSe–GaAs (1 1 0) by XPS yielded $\Delta E_v = +0.94 \pm 0.03$ eV for ZnSe epitaxial layers grown at 300°C, while for ZnSe films deposited at room temperature and post-annealed at 300°C to produce an observable LEED pattern, an offset $\Delta E_v = +1.08 \pm 0.03$ eV was reported [Kowalczyk et al., 1982; Waldrop et al., 1987]. In both cases the ZnSe source was a compound solid source, and the Zn to Se beam pressure ratio (BPR) was not monitored during deposition. The variation in band offsets with fabrication procedure was tentatively associated with different interface atomic structures.

To further explore the effect of the entropically-driven interface disruption on the ZnSe–GaAs (1 1 0) band offset, recent studies attempted to minimize the growth temperature and used high resolution synchrotron radiation photoemission spectroscopy to determine the band offset [Vanzetti et al., 1992; Bratina et al., 1993a,b]. Fig. 26 shows RHEED patterns from ZnSe–GaAs (1 1 0) at different stages of growth, for substrates kept at RT and ZnSe deposition from a single compound solid source. All patterns displayed are for a $[1\bar{1}0]$ azimuth. Fig. 26(a) shows a representative pattern for the as-cleaved GaAs (1 1 0) surface. The sharp and well defined 1 × 1 pattern co-exists with some evidence of cleavage steps. Upon deposition of 30 Å (b) and 100 Å (c) of ZnSe at RT onto the GaAs (1 1 0) surface, the pattern remains 1 × 1, while becoming increasingly sharp and well defined. ZnSe films as thick as 200 Å were grown at RT without visible degradation of the RHEED pattern.

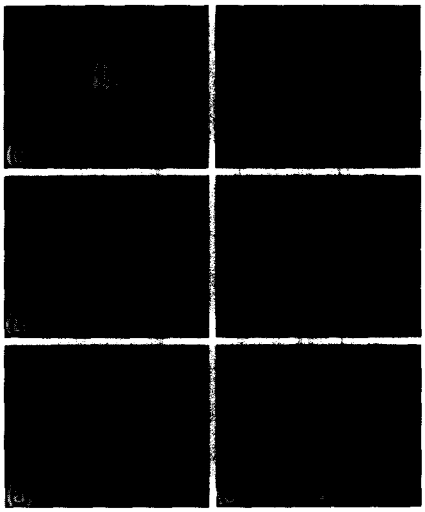

Fig. 26. Reflection high energy electron diffraction (RHEED) patterns at 10 keV and a $[1\bar{1}0]$ azimuth from ZnSe–GaAs (1 1 0) and ZnSe–Ge–GaAs(1 1 0) heterostructures at different stages of growth. (a) 1 × 1 RHEED pattern of the initial GaAs (1 1 0) surface cleaved in situ. (b) 1 × 1 RHEED pattern from a ZnSe–GaAs (1 1 0) heterostructure for a ZnSe thickness of 30 Å, obtained by molecular beam epitaxy (MBE) at room temperature (RT). (c) 1 × 1 RHEED pattern from a ZnSe–GaAs (1 1 0) heterostructure with ZnSe thickness of 100 Å. (d) Deposition of two monolayers (ML) of Ge at RT on GaAs(1 1 0) yields a disordered overlayer with no detectable RHEED pattern. (e) RHEED pattern observed following deposition of 30 Å of ZnSe at RT on the Ge–GaAs (1 1 0) interface examined in (d). A 1 × 1 pattern coexists with clear evidence of three-dimensional ZnSe island growth (spots). (f) RHEED pattern observed following deposition of a total of 100 Å of ZnSe at RT on the Ge–GaAs (1 1 0) interface examined in (d) [Vanzetti et al., 1992; Bratina et al., 1993a,b].

The results in Fig. 26 provide clear evidence that epitaxy at RT is possible for ZnSe–GaAs (110), possibly assisted by the presence of cleavage steps on the starting surface [Vanzetti et al., 1992; Bratina et al., 1993a,b]. The situation was quite different for deposition of Ge at RT on GaAs (110), despite the good lattice matching. Fig. 26(d) shows the RHEED pattern observed in the [$1\bar{1}0$] azimuth following deposition of 2 ML of Ge at RT on a GaAs (110) 1 × 1 surface. The RHEED pattern disappears gradually at submonolayer coverages (not shown), and at 2 ML coverage (d) there is no detectable surface long-range order. Deposition of ZnSe at RT on top of the disordered surface yielded a surprisingly prompt recovery of the long-range order (Fig. 26(e) and (f)). Studies of the band offsets for ZnSe – Ge–GaAs structures will be presented in Section 5.5.

ZnSe epitaxy at RT with 1 × 1 symmetry on GaAs (110) was previously reported by Meng et al. [Meng et al., 1990], although these authors did not present any structural data. Kowalczyk et al. [Kowalczyk et al., 1982], could not detect long-range order by LEED in ZnSe overlayers deposited at RT on GaAs (110) substrates. Annealing of the interface at 300°C after deposition, reportedly yielded a LEED pattern of undisclosed type. The same authors observed long-range order (with undisclosed periodicity) immediately after deposition if ZnSe was deposited on GaAs (110) substrates kept at 300°C. The discrepancies may stem from the dependence of overlayer morphology on substrate preparation and deposition conditions, that should be especially critical in RT experiments. Low temperature epitaxy is bound to be influenced by the average separation of cleavage steps, and by ZnSe deposition conditions such as rate, evaporator to sample distance, etc. In particular, steps due to intentional substrate misorientation are known to play an important role in promoting compound semiconductor epitaxy on GaAs (001) surfaces, and the deposition rate and radiated power may affect the nucleation rate away from the steps [Herman and Sitter, 1989]. All of these factors may contribute in general to determine the type and location of the ZnSe nucleation sites, and their role should be even more important when surfaces are prepared by cleavage, and the low growth temperature corresponds to comparatively low surface diffusion lengths.

Synchrotron radiation photoemission studies of epitaxial ZnSe–GaAs (110) heterostructures grown at RT yielded a valence-band offset $\Delta E_v = +1.10 \pm 0.09$ eV. For such a valence-band offset we expect a conduction-band offset of $\Delta E_c = +0.18 \pm 0.09$ eV (neglecting the uncertainty in the semiconductor bandgap difference ΔE_g), with the conduction-band minimum of ZnSe lying above that of GaAs [Vanzetti et al., 1992; Bratina et al., 1993a,b]. This is quantitatively consistent with some of the latest theoretical predictions [Christensen, 1988; Baldereschi et al., 1993a] for the offsets of ideally abrupt, (110)-oriented interfaces ($\Delta E_v = +1.07 - 1.11$ eV). More importantly, the above result is quantitatively consistent with that ($\Delta E_v = 1.08 \pm 0.03$ eV) reported by Kowalczyk et al. [Kowalczyk et al., 1982] for ZnSe films deposited at room temperature and post-annealed at 300°C to produce an observable LEED pattern, and at variance with that ($\Delta E_v = +0.94 \pm 0.03$ eV) reported by the same authors for ZnSe epitaxial layers grown at 300°C. This suggests that the value of the offset depends on the sample temperature during interface formation, rather than on the post-annealing treatment or film microstructure.

The relatively small lattice mismatch (0.47%) of ZnSe and Ge should make strain-related corrections to the band offsets comparable with the experimental uncertainty for this prototype IV/II–VI heterojunction. Ge–ZnSe (110) epitaxial structures obtained on substrates cleaved in situ yielded $\Delta E_v = -1.40$ eV when studied by means of synchrotron radiation photoemission [Margaritondo et al., 1984; Margaritondo and Perfetti, 1987]. Earlier comparative XPS studies of epitaxial Ge–ZnSe(110) and ZnSe–Ge(110) heterostructures yielded band offsets $\Delta E_v = -1.52$

and + 1.29 ± 0.03 eV, respectively, for the two interfaces, with a substantial deviation (0.23 eV) from commutativity [Kowalczyk et al., 1982; Waldrop et al., 1987]. ZnSe deposition in these experiments was also performed using a single compound effusion cell.

The dependence of the band offsets on the growth sequence for Ge–GaAs and ZnSe–Ge interfaces with (110) orientation, the dependence of the offsets on the growth temperature for ZnSe–GaAs (110) heterojunctions, as well as the deviation of the offsets from the prediction of the transitivity rule in ZnSe–Ge–GaAs (110), that will be discussed in Section 5.4, are quite puzzling, based on the theoretical results discussed in Sections 4.2.1 and 5.2.1. From a LRT standpoint, they may indicate that at these interfaces local configurations are established that cannot be obtained from the virtual crystal through a *neutral* perturbation (see Section 3.3).

For Ge–GaAs and Ge–ZnSe interfaces with (110)-orientation, Baldereschi et al., recently suggested that changes in band offsets may derive from atomic swaps between Ge and anion (or Ge and cation) atoms of two adjacent planes parallel to the interface [Baldereschi et al., 1993a]. A series of Ge-anion swaps would give rise to a local dipole oriented as a n^+– p^+ double layer, and lower the bands of Ge relative to those of the compound semiconductor. A series of Ge-cation swaps would give rise to a local dipole oriented as a p^+– n^+ double layer, and raise the bands of Ge relative to those of the compound semiconductor.

Although this type of defect formation mechanism is conceptually simple, and given a variable number of swaps, it can account for any observed variation in the offsets, we suggest that it should be taken in the spirit of a didactical example. This is primarily because the model tends to describe the real interface as originating from an ideal abrupt (110) interface through atomic swaps. Real interfaces, however, form through kinetic processes that are dramatically temperature-dependent, from atomic or molecular beams of variable intensity. In a sense, interfaces are open systems during the growth process, and there is no basis to assume that the overall interface stoichiometry is related in any obvious way to the stoichiometry of the ideal abrupt interface.

Furthermore, the driving force toward the formation of such defects remains unclear, since (as explained in Section 4.2) (110)-oriented interfaces are electrically stable, so that there should be little enthalpic driving force toward the formation of intermixed interfaces. One is therefore forced to call upon the entropic driving force toward atomic intermixing to explain the reported variations in band offsets at (110)-oriented interface. It could also be argued that the starting abrupt (110) interface has no net ionic dipole, while any interface reconstruction that follows from defect formation and is effective in modifying the band offset would have to add at the very least a local interface dipole to the electric field profile of the ideal, abrupt interface. This would increase the enthalpy of the system and partially offset any entropy-related gain in the free energy of the system.

Finally, we caution the reader that a purely enthalpic driving force should be dramatically temperature dependent, so that even relatively small changes in growth temperature should induce comparatively large differences in defect concentrations and therefore band offsets. The available experimental systematics does not support this contention.

5.2.3. Heterovalent interfaces with polar orientation

5.2.3.1. Ge–GaAs and Ge–AlAs In Table 3 we list a substantial number of recent band offset determinations for Ge–GaAs (001) interfaces, all of them relating to epitaxial heterostructures. Unless noted otherwise, the epilayers were fabricated on the As-stabilized GaAs (001) 2 × 4 surface. Most experimental data are in the − 0.4–0.7 eV range, but the spread of the experimental values is quite substantial, especially in view of the fact that all data were obtained for a well characterized epitaxial system. This suggests that variations in the growth protocol from experiment to experiment may have affected the band offset. The average offset is $\Delta E_v = -0.55 \pm 0.13$ eV, where the quoted error is the standard deviation.

As explained in the previous sections, *variations* in band offsets as determined by the same technique are less affected by systematic errors in band offset determination, and will be emphasized here. For example, in photoemission determinations of the offset, variations of the band discontinuity as a result of changes in growth sequence, interface orientation, or fabrication temperature, can be obtained directly from changes in ΔE_{cl}, and several authors have exploited such a simplification.

Waldrop et al. [Waldrop et al., 1983] fabricated by MBE Ge–GaAs interfaces at 340°C on (001)Ga and (001)As surfaces, and by XPS found corresponding valence band offsets $\Delta E_v = -0.55 \pm 0.04$ and -0.60 ± 0.04 eV, respectively. Similar results were obtained on (111)Ga and (111)As surfaces, with offsets of -0.48 ± 0.04 and -0.60 ± 0.04 eV, respectively. As usual, we take the minus sign to signify that the valence-band maximum in the overlayer is above that of the substrate. Katnani et al. [Katnani et al., 1984] examined the influence of the initial reconstruction of the GaAs(001) surface on the band offset for Ge–GaAs interfaces fabricated by MBE at 340°C, and found $\Delta E_v = -0.44$ to -0.48 ± 0.05 eV for all interfaces examined. More recently Sorba et al. [Sorba et al., 1993] fabricated Ge–GaAs interfaces on GaAs(001) 2×4 at growth temperatures of 360° and 480°C, and found by XPS valence-band offsets of -0.54 ± 0.05 and -0.57 ± 0.05 eV, respectively.

The above results imply that there is only limited evidence that changes in the growth temperature and substrate orientation for Ge–GaAs interfaces lead to changes in the band offsets. We mention, however, a surprising result already quoted in Section 2.2.3. From internal photoemission studies of p-Ge/n-GaAs(001) heterojunctions grown by MBE at 500°C and 300°C, a conduction-band discontinuity $\Delta E_c = -0.33 \pm 0.04$ eV was obtained for heterostructures in which the Ge overlayer was grown at 500°C, while a conduction-band offset ~0.3 eV lower was found for Ge growth at 300°C. Transport (C–V) measurements reportedly confirmed the trend ($\Delta E_c = -0.48 \pm 0.07$ eV and $+0.025 \pm 0.07$ eV for the two samples) [Dahmen et al., 1993]. Dahmen et al. attributed the large variation in the offset to the establishment of different microscopic configurations at the two interfaces. These internal photoemission results are difficult to reconcile at present with the XPS systematics.

For Ge–AlAs(001) heterojunctions the available systematics is more limited, but perhaps more intriguing (see Table 3). Katnani and Bauer found by XPS a valence-band offset $\Delta E_v = -0.78 \pm 0.07$ eV for heterojunctions grown by MBE at 320°C. Sorba et al. grew similar interfaces at 360° and 480°C, and measured offsets of -0.94 ± 0.05 and -1.07 ± 0.05 eV, respectively, with the increased growth temperature leading to increasing interdiffusion across the interfaces, as determined from the coverage dependence of the core intensity ratios [Sorba et al., 1993]. The implication of this – admittedly limited – set of results is that for Ge–AlAs(001) interfaces, an increase in growth temperature may result in increased disruption and larger valence-band offsets.

The symmetric III–V/IV systems contribute a set of even more intriguing, and temperature-dependent results. In Figs. 27(a)–(d) we show monochromatic XPS spectra for the core level emission from Ge–GaAs(001), GaAs–Ge(001), Ge–AlAs(001) and AlAs–Ge(001) individual isolated heterojunctions grown at 360°C [Biasiol et al., 1992; Sorba et al., 1993b]. The zero of the energy scale is taken at the position of the Ge 3d centroid. The vertical solid line for each core level marks the position of the core level relative to E_v in the bulk standards, so that the separation of the vertical

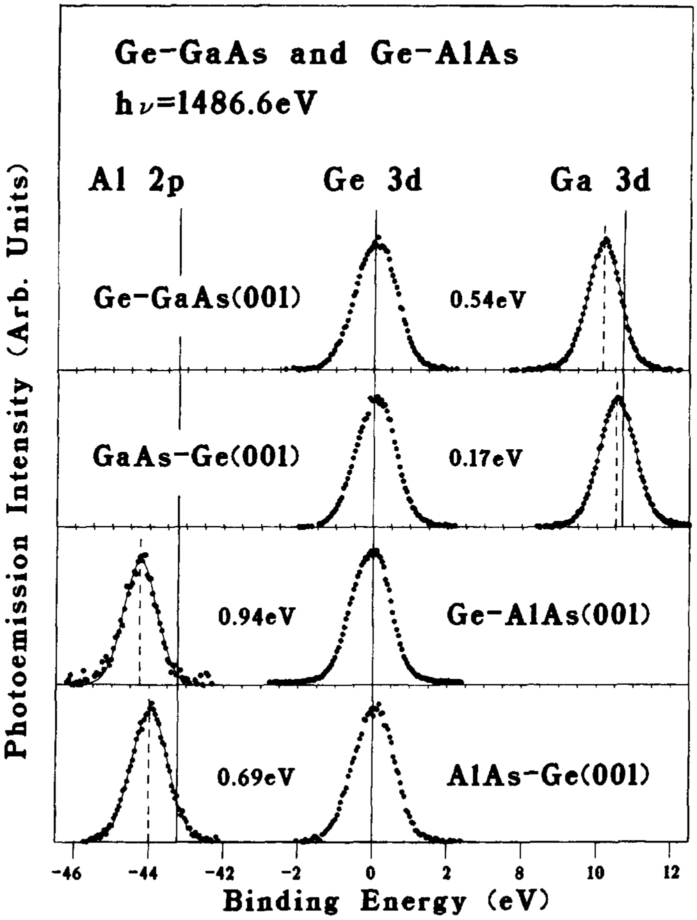

Fig. 27. Band-offset measurements in individual isolated heterojunctions grown at 360°C. (a) Ge 3d and Ga 3d core emission from a Ge–GaAs(001) heterojunction. The zero of the energy scale was taken at the position of the Ge 3d centroid, and the solid lines give the core binding energy in bulk standard. The variation in core separation (see dashed versus solid vertical lines) gives directly the valence-band offset. (b) Ge 3d and Ga 3d core emission from a GaAs–Ge(001) heterojunction (c) Al 2p and Ge 3d core emission from a Ge–AlAls (001) heterojunction. (d) Al 2p and Ge 3d core emission from an AlAs–Ge(001) heterojunction [Biasiol et al., 1992; Sorba et al., 1993b].

solid lines is that expected from an hypothetical heterojunction with zero valence-band offset [Sorba et al., 1992a]. In the absence of artefacts (see Section 2.3), the variation in core separation for each heterojunction relative to the bulk standards gives directly the valence-band offset. It was found that $\Delta E_v = -0.54 \pm 0.05$ eV for Ge–GaAs(001), $\Delta E_v = 0.17 \pm 0.07$ eV for GaAs–Ge(001), $\Delta E_v = -0.94 \pm 0.07$ eV for Ge–AlAs(001), and $\Delta E_v = 0.69 \pm 0.07$ eV for AlAs–Ge(001) [Sorba et al., 1993b]. Similar numerical results were also obtained from thin Ge quantum wells in III–V heterostructures [Biasiol et al., 1992], to be discussed in Section 5.5.

Some insight on the possible origin of such substantial deviations from commutativity (0.37 eV for Ge–GaAs and 0.25 eV for Ge–AlAs) can be derived from comparison with the predictions of first principles self-consistent field (SCF) calculations incorporating different types of atomic reconstruction at the interface [Biasiol et al., 1992]. As explained in Section 4.2.3, a number of atomic reconstructions would give rise to neutral interfaces. An example of some of the simplest possible resulting environments – in which atomic rearrangement involves only one or two atomic planes – are shown in the midsection and bottom-most section of Fig. 28, viewed in the $(\bar{1}10)$ plane. Configurations A and B correspond to a mixed Ge-As or Ge-cation plane with 50-50 composition at the interface, respectively. Configuration C includes two mixed planes in sequence with Ge-cation 25-75 and Ge-As 75-25 composition, and configuration D is the complementary configuration, in which the cation and anion sublattices are interchanged.

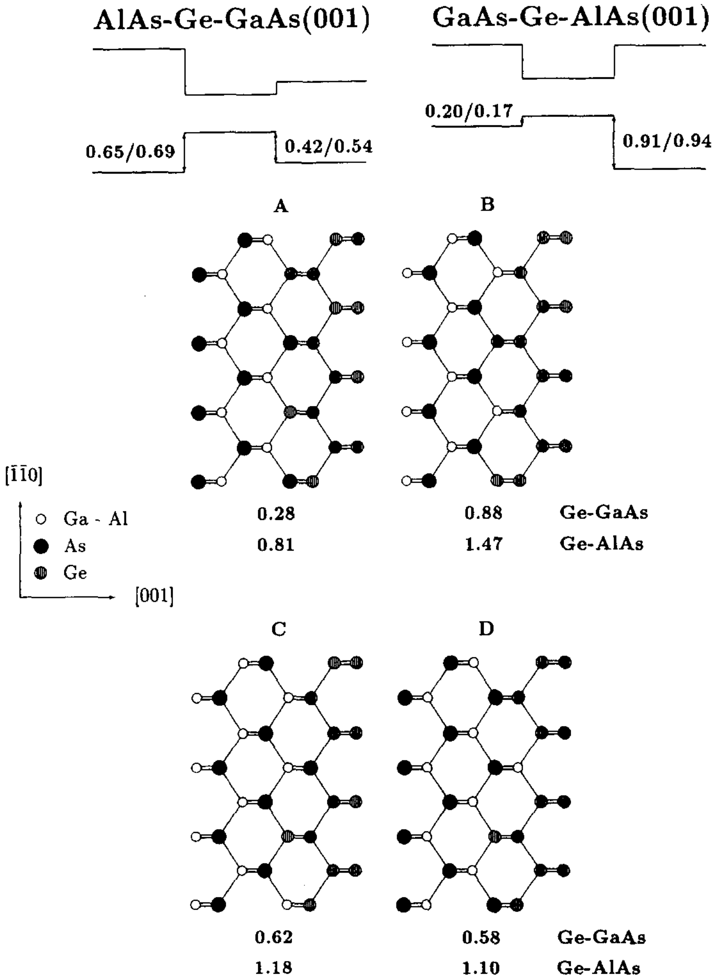

Fig. 28. Top: Experimental band offsets for AlAs–Ge and Ge–GaAs interfaces (left) and GaAs–Ge and Ge–AlAs interfaces (right) with (001) orientation. For each interface, the first numerical value was measured in single quantum wells, the second value in individual isolated interfaces. Bottom: Examples of simple interface structures that would lead to neutral interfaces. (A) Ge–As mixed termination. (B) Ge-cation mixed termination. (C) Mixed two-plane termination, 25-75 Ge-cation and 75-25 Ge-As. (D) Mixed two-plane termination, 25-75 Ge-As and 75-25 Ge-cation. Theoretical predictions for the magnitude of the valence-band offsets from self-consistent field calculations are shown directly below the corresponding interface structure [Biasiol et al., 1992].

The predicted valence-band offsets are shown directly below each interface configuration [Baroni et al., 1989; Biasol., 1992]. Configurations A and B would correspond to offsets of sensibly different magnitude. Configurations C and D have no ionic dipole, as would be the case for the nonpolar (110) orientation. Within linear response theory the corresponding band offsets are equal to one another and to the offsets for (110)-oriented interfaces. Formation of antisite defects leading to neutral interfaces is also expected to yield offset values similar to those obtained for (110)-oriented interfaces. Both for GaAs–Ge(001) and AlAs–Ge(001), agreement between theory and experiment (see topmost section of Fig. 28) is found for a type A interface configuration (mixed Ge–As interface). For Ge–GaAs(001) and Ge–AlAs(001) interfaces, good agreement between theory and experiment is found for a type C or D interface.

While Biasiol et al. [Biasiol et al., 1992] emphasized that the interface structures considered in Fig. 28 are only some of simplest structures which would lead to agreement between theory and experiment, the same authors noted [Franciosi et al., 1993] that the formation of a single mixed As–Ge interface plane during III–V growth on Ge may be consistent with the reported As segregation at the surface of group-IV epitaxial layers on III–V substrates [Bauer and Mikkelsen, 1982; Katnani et al., 1985; Copel et al., 1989] under comparable growth conditions. Also, Ge indiffusion at submonolayer coverage on the scale of 2 atomic layers or the formation of antisite defects during group-IV epitaxial growth on III–V substrates are both possible consequences of the release of the Ge chemisorption energy [Katnani and Bauer, 1986; Brillson, 1992].

On a purely phenomenological basis, the fact that kinetically determined modifications in the local interface environments may be responsible for the observed asymmetries is supported by the fact that the substantial deviations from commutativity are found to depend on the growth temperature employed. For example, in studies of GaAs–Ge(001) interfaces grown at 480°C rather than at 360°C, the valence-band offset was found to increase to 0.31 ± 0.05 eV, reducing the deviation from commutativity by 38% to 0.23 eV. For AlAs–Ge(001) interfaces grown at 480°C rather than at 360°C, the measured offset was -0.96 ± 0.05 eV, reducing the deviation from commutativity to zero within experimental uncertainty. Correspondingly, XPS core intensity profiles as a function of overlayer thickness indicated enhanced atomic interdiffusion [Sorba et al., 1993b]. The implication of these results is that enhanced interdiffusion in III–V/IV heterojunctions leads to more symmetric interfaces with band offsets converging toward the value calculated for (110)-oriented heterojunctions [Franciosi et al., 1993].

Comparisons between experiment and theory such as those illustrated in Fig. 28 are undoubtedly stimulating, but we caution the reader that: (1) only a few of the infinite possible reconstructions have been examined by theory (see Sections 4.2); (2) calculations of the corresponding formation enthalpies – let alone free energies – are unavailable (see Section 4.2); (3) the predictions apply to interfaces with polar orientation only, and deviations from commutativity have also been reported for selected interfaces with nonpolar orientations (see Section 5.2.2).

5.2.3.2. ZnSe–GaAs To our knowledge, the largest change in band offset as a result of a change in the growth protocol was reported quite recently for ZnSe–GaAs(001) interfaces. Nicolini et al. [Nicolini et al., 1994] explored the effect of variable Zn/Se beam pressure ratio during ZnSe MBE at 290°C on GaAs (001) 2 × 4 surfaces, and found an intriguing correlation between local interface composition and band offsets. This required ZnSe growth with independent Zn and Se solid sources, in an MBE system with separate but interconnected chambers for GaAs and ZnSe growth. In situ studies of the interface composition were conducted by means of monochromatic XPS. Fig. 29 shows the local Zn/Se ratio R, as a function of ZnSe overlayer thickness. Different symbols denote the effect of different BPRs in the 0.1–10 range. R was determined from the XPS ratio of the intergrated emission of the Zn 3d and Se 3d doublets, normalized to the value observed in all ZnSe bulk standards, irrespective of the BPR. The values of R in the first few monolayers exhibit large variations from the nominal 1:1 stoichiometry. Large relative fluxes of Zn (high BPRs) during growth correspond to Zn-rich interface compositions, while large relative fluxes of Se correspond to Se-rich interface compositions [Nicolini et al., 1994; Franciosi et al., 1994].

The band offsets coresponding to the different interface compositions were determined in situ by XPS. In view of the reported atomic interdiffusion and doping near the interface [Kassel et al., 1991a,b], three independent tests were performed to ensure that possible changes in band bending near the interface would not affect the measured core separation (see Section 2.3). No change in core separation was found upon varying the photoemission sampling depth (by changing the photoelectron collection angle), and consistent results were obtained using the Zn–Ga and Se–As core levels, and for samples with different amount of band bending [Nicolini et al., 1994].

Results for a number of ZnSe interfaces fabricated on GaAs(001) substrates with different types of doping are summarized in Fig. 30. The valence-band offsets were determined for overlayer coverages at which the ZnSe film appeared stoichiometric (25–40 Å), but are plotted in Fig. 30 versus the experimental value of the Zn/Se ratio R observed for each interface in the early growth stage, i.e., at an arbitrary ZnSe coverage of 3 Å. Maximum valence-band offsets of 1.20 eV are observed for interfaces grown with the highest BPRs explored (Zn-rich case), while offsets as low as 0.58 eV are observed for the Se-rich case. The large reduction in the offset achievable as compared to published values has the potential of substantially improving hole injection efficiency in blue lasers [Franciosi et al., 1994].

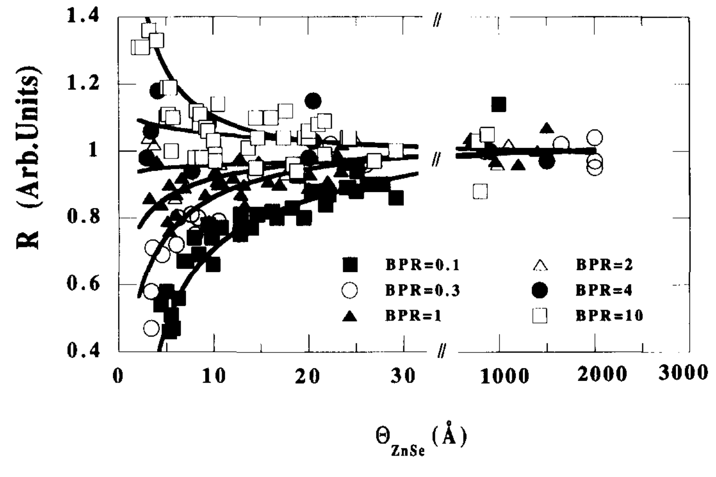

Fig. 29. Experimental Zn/Se photoemission intensity ratio R in ZnSe–GaAs(001) heterojunctions grown by MBE with different Zn/Se beam pressure ratios (BPRs), as a function of ZnSe thickness. Values of R were normalized to the value observed in all ZnSe bulk standards, irrespective of the BPR. All data were obtained in situ by monochromatic X-ray photoemission spectroscopy (XPS) [Nicolini et al., 1994].

The correlation between the interface composition in the early growth stage and the final value of the valence-band offset depicted in Fig.30 is remarkable, in view of the simplistic use of the parameter R to gauge interface composition. Such parameter provides no information on the Ga/As ratio at the interface, which may be in principle as important as the Zn/Se ratio in determining the overall interface composition. At XPS energies, however, only relatively small variations in the Ga/As ratio could be detected between the different interfaces, since the small interface contribution to the Ga and As core emission is superimposed in all cases on the much larger signal from the GaAs bulk [Nicolini et al., 1994].

The authors attempted to correlate the observed changes in interface composition and band offsets using SCF calculations for simple interface model reconstructions. Fig. 31 shows theoretical predictions for ZnSe–GaAs and ZnSe–Ge interfaces with (001) orientation. The neutral configurations depicted in Fig. 31 are totally analogous to those in Fig. 28, and involve atomic intermixing on one (configurations A and B) or two (C and D) atomic planes at the interface.

The four configurations are neutral, in the sense that the atomic arrangement produces no long range electrostatic field. However, a dipole field localized at the interface may exist, and may be quite substantial. This may affect the band alignment across the heterojunction, and the total formation energy of the interface. For example, configuration A includes a mixed Se–As (or Ge–Se) plane with 50-50 composition at the interface, and configuration B, which includes a mixed Zn–Ga (or Ge–Zn) plane with 50-50 composition at the interface, are characterized by a local interface dipole of equal magnitude and opposite orientation. Consequently, they correspond to widely different band offsets. Theoretical predictions for the valence-band offset ΔE_v from self-consistent field calculations are indicated below each atomic configuration in Fig. 31. We see that the band alignment corresponding

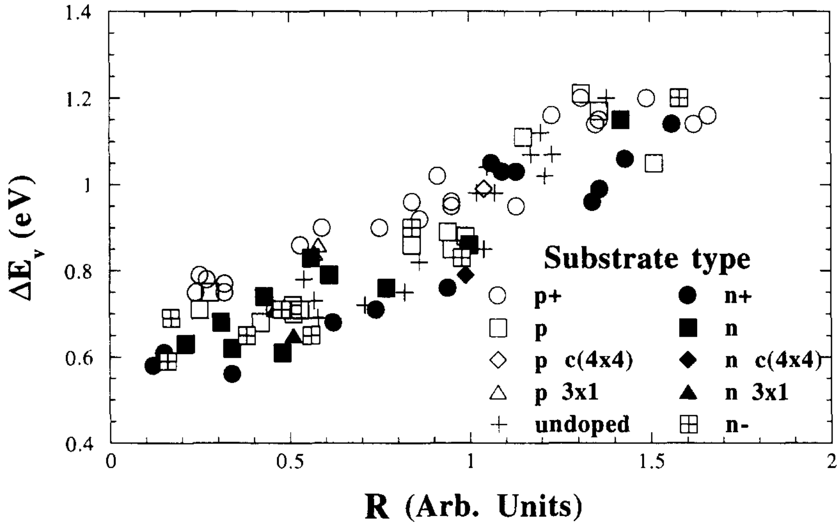

Fig. 30. Experimental valence-band offset for ZnSe interfaces fabricated on GaAs(001) substrates with different type of doping. Unless noted otherwise, the substrate reconstruction was the As-stabilized 2 × 4 reconstruction. The offsets are plotted versus the Zn/Se ratio R observed for each interface in the early growth stage (at a ZnSe coverage of 3 Å) [Nicolini et al., 1994].

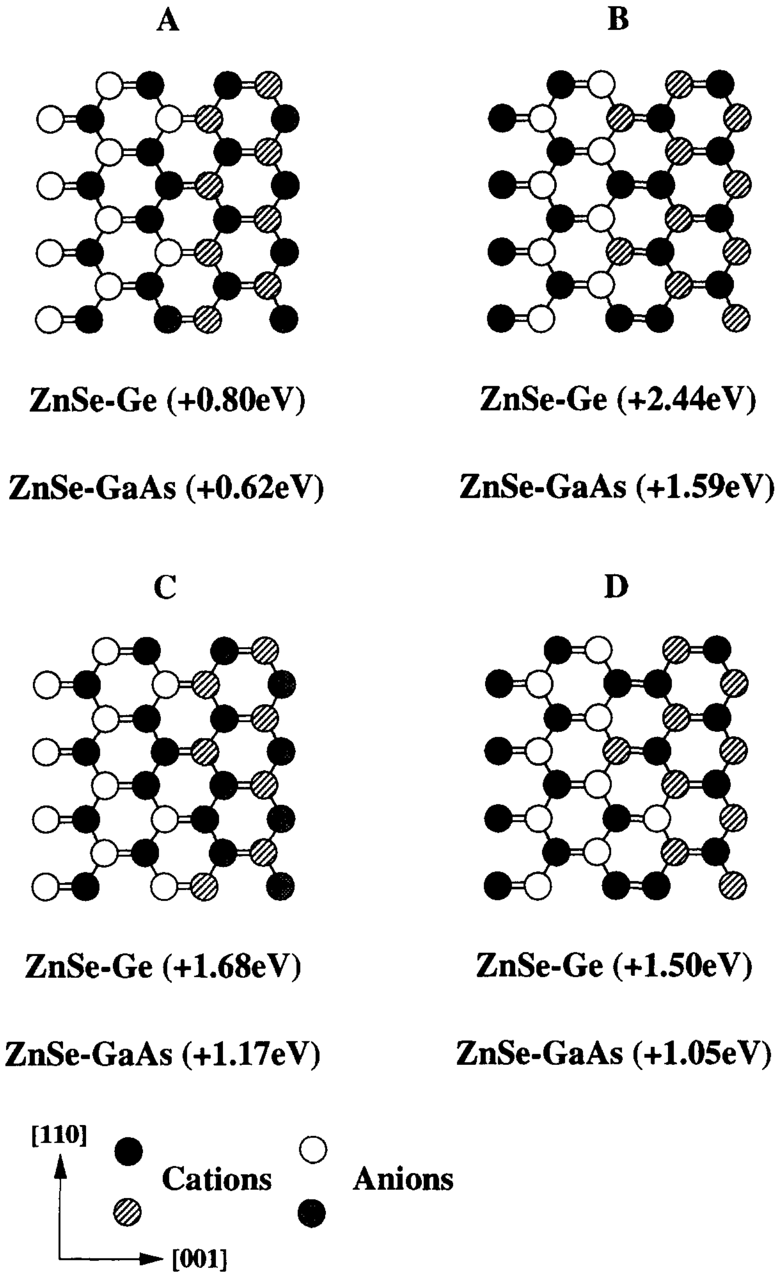

Fig. 31. Theoretical predictions for ΔE_v for ZnSe–GaAs and ZnSe–Ge interfaces with (001) orientation, from self-consistent field calculations for simple neutral interface configurations including substitutional defects on one or two atomic planes at the interface (configurations A–D, viewed in the $(\bar{1}10)$ plane). Configuration A includes a mixed Se–As (or Se–Ge) plane with 50-50 composition at the interface. Configuration B includes a mixed Zn–Ga (or Zn–Ge) plane with 50-50 composition at the interface. Configuration C includes two mixed planes in sequence with Se–As (or Se–Ge) 25-75 and Zn–Ga (or Zn–Ge) 75-25 composition. Configuration D is the complementary configuration, in which the cation and anion sublattices are interchanged. Configurations C and D have no ionic dipole, as would be the case for the nonpolar (110) orientation. The calculated valence-band offset ΔE_v is indicated below the corresponding atomic configuration for ZnSe–GaAs and ZnSe–Ge (adapted from [Bratina et al., 1994]).

to configurations A and B differs by as much as 0.97 eV for ZnSe–GaAs [Nicolini et al., 1994; Bratina et al., 1994].

Conversely, configuration C, which includes two mixed planes in sequence with Se–As (or Ge–anion) 25-75 and Zn–Ga (or Ge–cation) 75-25 composition, and configuration D, which is the complementary configuration, in which the cation and anion sublattices are interchanged, have no ionic dipole, as would be the case for the nonpolar (110) orientation, and correspond to more similar band alignments.

The experimental range of tunability of the band alignment depicted in Fig. 30 is very similar to the difference in band alignment predicted by theory for the A and B interface configurations of ZnSe–GaAs (see Fig. 31). Valence band offsets as low as 0.62 eV (configuration A) and as high as 1.59 eV (configuration B) may in principle derive from atomic intermixing leading to different interface configurations. Although it would be tempting to associate the low valence-band offset observed for Se-rich growth conditions (~ 0.6 eV) with a Se–As intermixed interface (predicted offset 0.62 eV), and the high offset observed for Zn-rich conditions (~ 1.2 eV) with configurations B or C (predicted offsets 1.59 and 1.17 eV, respectively), the usual words of caution are required.

First, the calculations examined only a few of the simplest of the infinite number of possible interface reconstruction that would lead to neutral interfaces. Second, the value of R in Figs. 29 and 30 provides no information on the local Ga/As concentration at the interface. Third, the data obtained for ZnSe growth on As-rich GaAs (001)c(4 × 4) surfaces, and Ga-stabilized GaAs(001)3 × 1 surfaces do not show conclusively a dependence of the band offsets on the initial Ga/As surface ratio. One might have thought that Se–As (Zn–Ga) intermixed phases would be more difficult (easier) to form on the 3 × 1 surface, and easier (more difficult) to form on the c(4 × 4) relative to the 2 × 4 surface, but this is not evident in the available data [Nicolini et al., 1994; Franciosi et al., 1994].

5.2.3.3. Other II–VI/III–V interfaces In general, lattice-matched II–VI/III–V heterovalent heterojunctions seem a promising test case to correlate local composition and band offsets. In addition to ZnSe–GaAs, we also mention the lattice-matched heterojunction (in-plane mismatch <0.5%) between InP and the metastable zincblende form of CdS. Epitaxial growth of cubic CdS on InP has been reported in the 145–225°C range with 1 × 1 symmetry [Wilke et al., 1989; Zahn et al., 1991]. Measurements of ΔE_c by the $C-V$ techniques for (111)-oriented heterostructures grown on P-stabilized surfaces under high sulphur overpressure yielded $\Delta E_v = +1.63$ eV [Wagner et al., 1975; Shay et al., 1976], while recent photoemission determinations of the offset for (110)-oriented interfaces grown by MBE using a single compound source yielded $\Delta E_v = +0.77$ eV, with a type -I rather than type-II band alignment [Wilke et al., 1989; Wilke et al., 1990a].

Yu et al. fabricated lattice matched ZnTe–GaSb (001) (0.1% in-plane mismatch) and ZnTe–AlSb (001) (0.6% in-plane mismatch) heterojunctions by MBE (see Section 5.4.5 for detail), and attempted to modify the offsets by exposing the III–V surface to an elemental Zn flux prior to ZnTe growth. They measured a decrease of 0.05 and 0.1 eV in the valence-band offset for the two interfaces [Yu et al., 1992b], despite the fact that little Zn is known to condense on the substrate surface at the growth temperature employed. By analogy with the results for ZnSe–GaAs (001) [Nicolini et al., 1994], it is likely that the effect observed by Yu et al. [Yu et al., 1992b] will be magnified by the use of a high Zn overpressure during growth.

5.2.3.4. Practical offset engineering Although interfacial engineering attempts to bring about desired changes in interface properties through suitable modifications of the local interface environment during growth, if a given interface configuration is achieved in practice or not will depend on the free energy of the configuration, and on the kinetics of the growth process, and these are hard to evaluate theoretically. One encouraging piece of news is that recently the formation energy of some of the different neutral ZnSe–GaAs interface configurations with (001) orientation were calculated from first principles [Kley and Neugebauer, 1994]. It was found that the formation energies of configurations A and B are the same, and 30–60% lower than those of configurations C or D, and Kley and Neugebauer suggested that the results in Fig. 30 might reflect a dominant type-A interface configuration for Se-rich interfaces, and a mixture of the two degenerate A and B configurations in the Zn-rich case.

The possibility of engineering heterojunction parameters properties in such a wide range of values would have obvious implications in device technology, provided that engineered interfaces can be incorporated in device structures without degrading the other relevant device properties. An example of this is the ZnSe–GaAs(001) case just described, where for better hole injection in blue-green lasers a low valence-band offset (and therefore BPR) should be used [Franciosi et al., 1994], but a major concern is that minimization of unintentional doping and dislocation density during ZnSe growth requires BPR ~ 1 [Cheng et al., 1987].

A second problem has to do with the *stability* and *deep level* concentration in engineered heterojunctions. This is exemplified in recent studies of deep level formation in ZnSe–GaAs(001) heterostructures as a function of annealing temperature and BPR employed during growth [Raisanen et al., 1995a,b,c,]. Fig. 32(a) shows HeCd photoluminescence spectra recorded from a 500nm ZnSe epilayer grown by MBE on GaAs(001) with BPR = 1. The spectra were recorded at

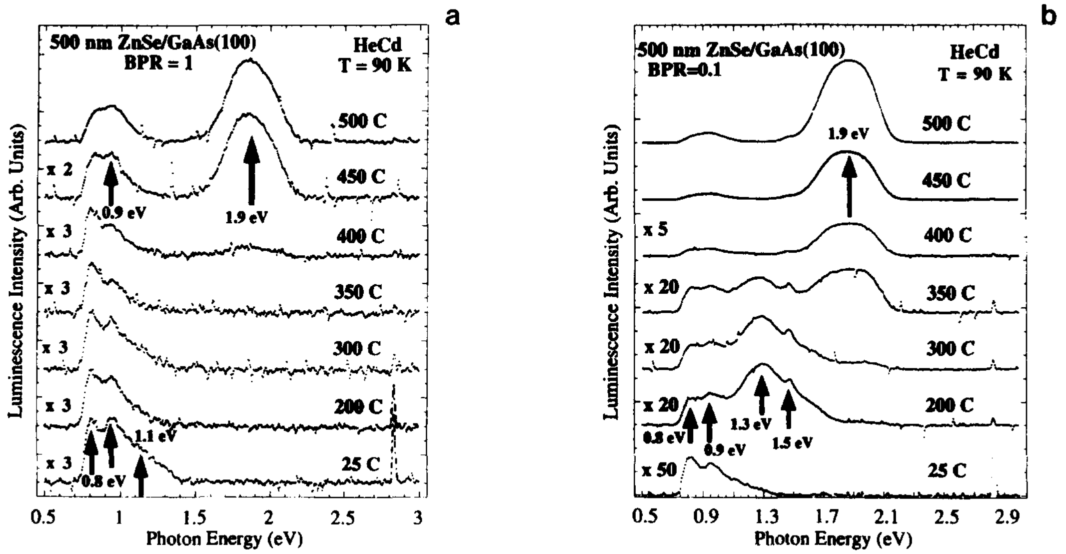

Fig. 32. (a) Deep level emission spectra as a function of annealing temperature for ZnSe–GaAs(001) heterostructures grown by MBE with Zn/Se BPR = 1. Annealing at increasing temperature above 400 °C gives rise to a new 1.9–2.0 eV feature. (b) Same as (a), for ZnSe–GaAs(001) heterostructures grown with Zn/Se BPR = 0.1 (Se-rich). Annealing gives rise to a new 1.9–2.0 eV feature at temperatures above 300°C [Raisanen et al., 1995c].

90K after 5min annealing cycles at increasing temperature [Raisanen et al., 1995c]. The spectral region below 1.3eV contains multiple spectral features involving native deep level features [Raisanen et al., 1995a,b], but there is no evidence for emission in the 1.9eV range for temperatures up to 350°C. With annealing above 350°C a new 1.9eV deep level feature related to complex defect centers involving Zn vacancies and substitutional Ga atoms on Zn sites emerges, which dominates the deep level spectrum at temperatures above 450°C [Raisanen et al., 1995c]. Fig. 32(b) shows the corresponding results from a sample grown in Se-rich growth conditions (BPR = 0.1). Here the 1.9eV deep level feature appears at lower temperature, and dominates all other deep level features at 350°C [Raisanen et al., 1995c]. The implication of these results is that interdiffusion, possibly related to Zn vacancies, and the related deep level density, are a more serious problem for heterostructures grown in Se-rich conditions.

We emphasize that the incorporation of engineered interfaces in device structures is still possible, if one realizes that the changes in interface parameters depicted in Figs. 30 and 31 are all determined by the *local* interface environment, as opposed to the bulk properties of the two semiconductor materials comprising the junction [Franciosi et al., 1994]. It may therefore be sufficient to limit the non-stoichiometric growth conditions to the early stages of interface formation to achieve a desired interface configuration. Provided that no extensive atomic redistribution occurs during the following stages of device fabrication, the configuration achieved during the early stages of interface formation will determine the properties of the final junction [Franciosi et al., 1994].

This was unambiguously demonstrated by a recent experiment in which the band alignment was examined together with the optical adsorption and photoluminescence in ZnSe–GaAs(001) heterostructures where the nonstoichiometric growth conditions were employed only during deposition of the first 2nm of ZnSe, while the rest of the II–VI overlayer was grown with BPR = 1 [Bonanni et al., 1995]. The 2nm-thick layer largely determines the final band offset, as shown in Fig. 33, in which the XPS-determined value of the valence-band offset is plotted versus the thickness of the overall ZnSe overlayer (including the 2nm-thick interface layer). The results indicate that all samples with Se-rich interfaces have valence-band offsets within 0.05eV of an average value of 0.58eV (bottom-most section, solid horizontal line), while all samples with Zn-rich interfaces yield valence-band offsets within 0.05eV of an average value of 1.05eV. It is evident from the results of Fig. 33 that the interface composition mostly determines the band alignment across the overall heterostructure [Bonanni et al., 1995]. The technique of growing only a thin interface layer in Se-rich or Zn-rich conditions, also remarkable improvement in the optical absorption and photoluminescence spectra [Bonanni et al., 1995; Vanzetti et al., 1995]. For example, the photoluminescence spectra from samples incorporating the nonstoichiometric interface layers show dramatically lower linewidth (by almost a factor of two), and better defined intrinsic features (at 2.802eV) relative to the control samples grown with BPR = 10 and 0.1 [Vanzetti et al., 1995].

In addition, the XRD investigations indicate that the nature of the interface layer has a profound effect on the concentration and preferential orientation of extended defects throughout the II–VI epilayers. This is not surprising, in view of the direct connection between interface structure and the nucleation of defects. Recently, improvement in the structural quality of $Zn_{1-x}Mg_xS_ySe_{1-y}$/ZnSe/GaAs structures grown by MBE has been associated with exposure of the As-stabilized GaAs surface to Zn for some time prior to growth of the II–VI epilayers [Kuo et al., 1994]. The most obvious explanation of this effect is that fabrication of a Zn-rich interface negatively affects the nucleation of dislocations in the II–VI epilayers [Kuo et al., 1994].

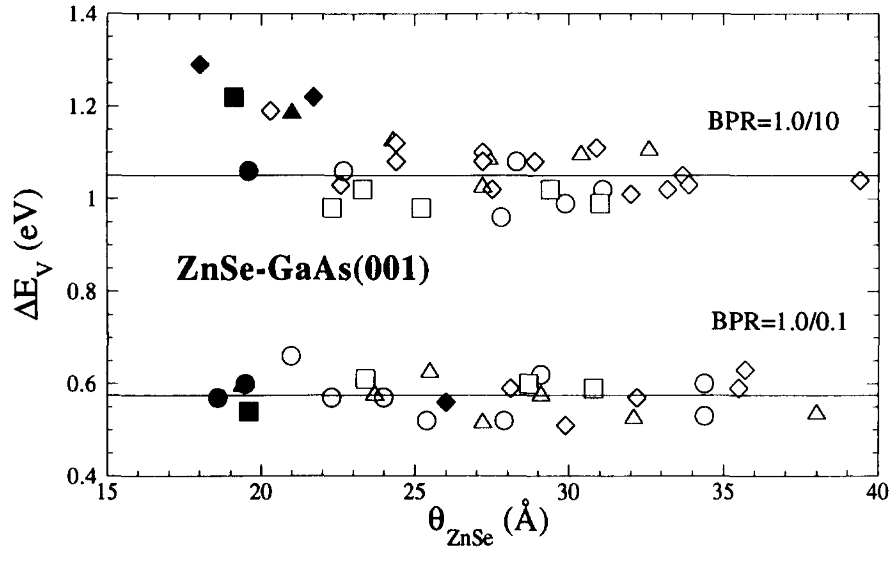

Fig. 33. XPS-derived values of ΔE_v for ZnSe–GaAs(001) heterostructures versus thickness of the overall ZnSe layer. A 2nm thick ZnSe composition control interface layer (CIL) was grown at the interface in Se-rich or Zn-rich conditions. Solid symbols denote data obtained from the CIL layers. Open symbols denote data obtained after deposition of a ZnSe overlayer with BPR = 1 on top of the CIL. Similar symbols (diamonds, squares, circles and triangles) denote data obtained in the same experimental run with a Zn-rich CIL (topmost section), or Se-rich CIL (bottom-most section). Average values of $\Delta E_v = 1.05 \pm 0.05$ eV for samples with Zn-rich CIL's, and $\Delta E_v = 0.58 \pm 0.05$ eV for Se-rich CIL'S are indicated by horizontal lines [Bonanni et al., 1995].

It remains to be ascertained what effect, if any, the above interfacial engineering methods will have on the interfacial state density, and therefore on the carrier lifetime and internal quantum efficiency. For example, C–V measurements have shown that different initial GaAs surface stoichiometries and reconstructions may have a substantial effect on the interface state density at ZnSe–GaAs(001) heterojunctions. In particular, a significant reduction in the interface state density was observed when the GaAs surface was As-deficient, with a final as-grown interface state density comparable to values obtained at AlGaAs–GaAs interfaces [Qian et al., 1989, 1990, 1991a]. The local composition, and the resulting quality of the interface between the different compound semiconductors may determine the ultimate quality of the device itself [Farrel et al., 1991].

5.2.3.5. Ge–ZnSe and Si–ZnS We conclude this section by briefly examining the promising but incomplete picture which exists for two prototypical IV/III–V heterojunctions with polar orientation which are relatively well lattice-matched. An interesting point raised by the LRT and SCF calculations for heterovalent interfaces with polar orientation (see Sections 3.2 and 3.3) is that since the dipole difference between different interface configurations (such as A and B in Figs. 28 and 31) is a function of the difference in chemical valence between the semiconductor constituents, in principle larger offset variations might be expected for IV/II–VI interfaces as compared to IV/III–V or III–V/II–VI interfaces. This is illustrated in Fig. 31 (adapted from [Bratina et al., 1994]), in which predictions for ZnSe–GaAs and ZnSe–Ge are directly compared. At the ZnSe–Ge interface the difference in the chemical valence between the constituent atoms is twice as large as in the other case, so that the maximum variation in the offset corresponding to the different composition profiles increases accordingly.

For configurations A and B that correspond to the extreme values for the band offsets, since the ionic dipoles have the maximum possible value for the type of intermixing examined, and have opposite orientation, the calculated difference in offset is 1.64 eV for Ge–ZnSe, to be compared with 0.97 eV for ZnSe–GaAs. As in the case of Ge/III–V and III–V/II–VI interfaces, configurations C and D that make the ionic dipole vanish, yield offsets similar to those calculated for (1 1 0)-oriented interfaces [Bratina et al., 1994].

Unfortunately, to our knowledge, no systematic study of the effect of different growth parameters (such as the Zn/Se BPR) on the band offsets has been yet conducted for ZnSe–Ge interfaces, to test the tunability range of the offset. To date, this heterojunction remains a largely unexplored ideal test case. There is, however, substantial evidence for a noncommutativity of the band offsets for ZnSe–Ge and Ge–ZnSe interfaces with (001) orientation. Xu et al. [Xu et al., 1988] reported $\Delta E_v = -1.65 \pm 0.1$ eV for Ge–ZnSe (001) interfaces fabricated by depositing Ge on ZnSe(001) surfaces prepared through sputter–annealing cycles and studies by XPS with a method analogous to that employed by Kowalczyk et al. [Kowalczyk et al., 1982] for Ge–ZnSe(110). The same interface reportedly yielded $\Delta E_v = -1.20 \pm 0.1$ eV when studied by ultraviolet photoemission spectroscopy along the lines used by Katnani and Margaritondo [Katnani and Margaritondo, 1983]. For the reverse case, Bratina et al. deposited ZnSe at 290–320°C on Ge(001) using a single compound source, and measured by synchrotron radiation photoemission $\Delta E_v = +0.95 \pm 0.05$ eV [Bratina et al., 1994].

Comparison of these results therefore suggests a 0.70 eV deviation from commutativity for this interface. Comparison of experiment with the theoretical results in Fig. 31 would suggest that deposition of Ge on ZnSe(001) results in the formation of interface configurations with no net ionic dipole, and lead to band offsets similar to those expected for (1 1 0)-oriented interfaces. Conversely, deposition of ZnSe on Ge(001) in the growth conditions examined by Bratina et al. [Bratina et al., 1994] may yield a mixed Ge–Se interface configuration and a substantial dipole. As usual, we hasten to add that to date there is no direct evidence that configurations A–D are achieved in practice, and that this type of considerations applies to interfaces with polar orientation only, while a deviation from commutativity has been reported also for (1 1 0)-oriented Ge–ZnSe interfaces (see Section 5.2.2).

We mention that for the related case of the ZnS–Si heterojunction, which is also lattice-matched (in-plane mismatch $< 0.4\%$), recent high resolution synchrotron radiation photoemission studies of the band offsets were performed on (1 1 1)-oriented interfaces, grown by MBE with 1 × 1 symmetry on Si (1 1 1) 2 × 1 substrates cleaved in situ [Maierhofer et al., 1991]. The authors measured a relatively wide (0.4 eV) range of valence-band offsets about an average value $\Delta E_v = +0.70$ eV, and tentatively associated the larger data scatter with a varying interface dipole due to variations in the growth conditions and interface reactions [Maierhofer et al., 1991]. In the light of the results describe above, such an interpretation seems fully justified, and remarkably far-sighted.

5.3. *Doping dipole methods*

A conceptually simple but potentially far reaching method to change the band offset in a heterojunction was proposed by Capasso and co-workers [Capasso et al., 1985a,b]. The approach

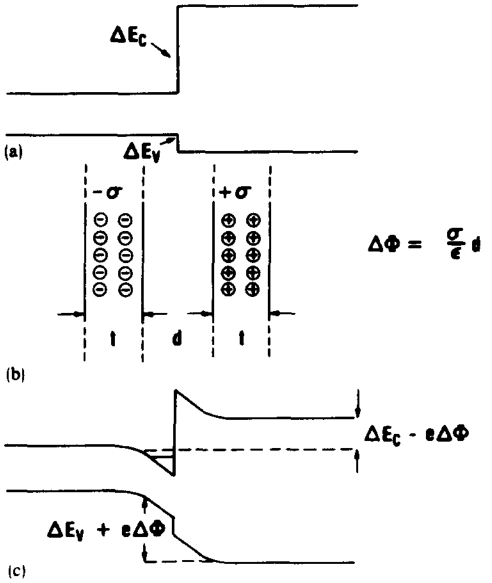

Fig. 34. (a) Band diagram of an intrinsic heterojunction. (b) Schematics of doping interface dipole. s is the sheet charge density and DF is the dipole potential difference. (c) Band diagram of the heterojunction with doping interface dipole, assuming $t \ll d$ [Capasso et al., 1985a].

is schematically shown in Fig. 34, and is often referred to as the doping interface dipole (DID) method. In (a) the band diagram of an abrupt heterojunction is sketched assuming the material to be undoped, so that one can neglect band-bending effects over a few hundred ångström. In (b), one sheet of acceptors and one sheet of donors of identical doping concentrations are fabricated during growth at a distance $d/2$ from the interface. The doping density N and the sheet thickness t are such that both are depleted of carriers. As in a parallel plate capacitor, a constant electric field and a linear potential profile is generated between the two parallel plates as a result of the charge density σ present on the two plates. The electric field between the two plates will be σ/ε, where $\sigma = eNt$, and ε is the dielectric constant of the material. The potential difference between the two plates of the capacitor will be $\Delta\Phi = (\sigma/\varepsilon)d$. The overall potential profile across the junction will be the superposition of the abrupt heterojunction profile in (a) and the capacitor-induced profile in (b). This is schematically illustrated in Fig. 35 for a donor–acceptor (top) and acceptor–donor (bottom) growth sequence. The DID shifts the relative potential of the valence and conduction bands in the two semiconductors outside the dipole region, without changing the electric field outside the DID [Capasso et al., 1985a,b].

The acceptor–donor sequence (Figs. 34(b) and 35 (bottom)) increases the valence-band offset to a value $\Delta E_v + e\Delta\Phi + (\sigma/\varepsilon)t$, where the last term takes into account the potential drop across the charge sheets. For $d \gg t$, the valence-band discontinuity has been increased by $e\Delta\Phi$. This is typically 0.1–0.2 eV for conventional doping techniques, but can in principle be increased somewhat using δ-doping techniques [Herman and Sitter, 1989; Capasso et al., 1991]. For the conduction band, the DID in Fig. 34(b) reduces the band offset, but gives also rise to a triangular quantum well on the low band gap side of the hetreojunction. Because of the high electric fields typically present in this region, the bottom of the first quantum well subband lies near the top of the well, and electrons can also

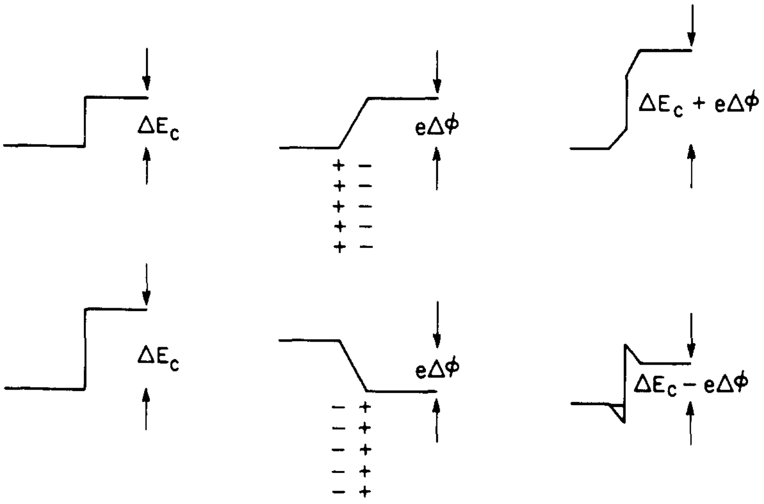

Fig. 35. Effect of a donor–acceptor (top) and acceptor–donor (bottom) doping interface dipole on the conduction-band discontinuity depicted in Fig. 34(a) [Capasso, 1987].

tunnel through the thin triangular barrier on the high band gap side of the junction. In the limit of a completely transparent barrier, the conduction-band offset is effectively lowered to $\Delta E_c - e\Delta\Phi$ [Capasso et al., 1985a,b].

The situation is reversed for the donor–acceptor sequence (Fig. 35, top), with a conduction-band offset increased by $e\Delta\Phi$, a triangular well in the valence band on the low band gap side, a thin triangular barrier in the valence band on the high band gap side, and a valence-band offset lowered to $\Delta E_v - e\Delta\Phi$ in the limit of a completely transparent barrier.

In view of the potential of the DID method, it is somewhat surprising that so few applications have appeared in the literature to date. In their original work, Capasso et al. demonstrated a reduction of the barrier height of the order of 0.1 eV in an $Al_{0.26}Ga_{0.74}As/GaAs$ heterojunction, which resulted in an enhancement by one order of magnitude of the collection efficiency of photocarriers across the heterojunction in a suitably designed p-i-n photodiode [Capasso et al., 1985a,b]. More recently, DIDs were implemented through δ-doping technology in a staircase avalanche photodiode to increase the $Al_{0.54}Ga_{0.46}As/GaAs$ conduction-band offset and therefore further enhance electron impact ionization at the interfaces and eliminate hole trapping [Capasso et al., 1988; Ripamonti et al., 1990].

The DID method can also be used to fabricate a nonzero band offset in a homojunction [Shen et al., 1992a], and doping dipole layers have recently been fabricated within the AlGaAs charge control layer of heterostructure field effect transistors (HFETs) to increase the conduction band barrier between the channel and the gate, and reduce the gate leakage current [Akinwande et al., 1990; Zou et al., 1991]. In our opinion the connection to the DID method by Capasso et al. is quite obvious, although it was not always explicitly recognized.

The relatively small number of implementations of the DID method owes probably to the difficulty of exactly balancing the charge in the two doping sheets [Wilks and Williams, 1995], the limited tunability range of the offsets that follows from the current doping technology, and the nonabrupt nature of the offset modification, which limits its applicability in some photonic devices such as lasers. It still remains a potentially useful tool in combination with bandgap engineering for a variety of device applications [Capasso, 1987, 1994].

A second class of methods to create doping induced dipoles exploits the spatial separation of carriers and ionized impurities of a single type that may derive from a tailored dopant distribution within a specific heterostructure. The well known technique of modulation doping [Störmer et al., 1979; Herman and Sitter, 1989], in which donors are selectively located in a large gap material close enough to the interface with a lower gap material, so that the corresponding electrons are transferred across the interface, also creates a dipole and modifies the electrostatic potential profile [Störmer et al., 1979].

Another interesting method specifically implemented to fabricate a doping dipole using a single dopant sheet was demonstrated by Müller et al. in $Al_{0.26}Ga_{0.74}As$–GaAs(001) heterojunctions [Müller et al., 1989]. In such heterojunctions the conduction-band discontinuity of 0.223 eV normally gives rise to a triangular well in GaAs and two-dimensional quantum confined subbands in the well. Müller et al. fabricated a Si δ-doped layer in the otherwise undoped heterojunction, 40 Å away from the interface and on the GaAs side of the junction. Electron transfer from the ionized impurities to the two-dimensional subbands which exist in the triangular well reportedly gave rise to a dipole which lowered the barrier for perpendicular electron transfer across the junction. Thermionic emission measurements as a function of temperature under an applied bias (to achieve flatband conditions) were used to determine the difference between the conduction-band minimum in the $Al_{0.26}Ga_{0.74}As$ layer and the quasi-Fermi level, i.e., the barrier. Shubnikov–de Haas measurements were used to determine the subband occupation. The barrier height, which depends on the electron charge densities in the individual subbands and their displacement from the centroid of the ionized donor sheet, was calculated self-consistently from the subband structure, using the measured total electron density. The authors found good agreement between the model and experiment, with a reduction of the barrier by 0.145, 0.085 and 0.054 eV with increasing Si coverage (from 0.2 to 0.6% of a monolayer) within the δ-layer [Müller et al., 1989].

A method only apparently similar to the DID method has been recently used to change the effective conduction band discontinuities at relaxed, isotype InAs/GaAs(001) heterojunctions [Shen et al., 1991a,b, 1992b]. Shen et al. fabricated relaxed isotype n^+-InAs/n-GaAs heterostructures by MBE and used Be to fabricate a p^+ δ-doped layer within GaAs, about 50 Å away from the interface. Au metallizations were implemented to fabricate contacts, and the effective conduction band barrier was determined through I–V measurements [Shen et al., 1991a,b], coupled with appropriate numerical modeling of the interface [Shen et al., 1991a; Morris et al., 1993], or by ballistic electron emission microscopy (BEEM) [Shen et al., 1991b]. The long-range electrostatic field of the Be δ-doped layer raises substantially the conduction band relative to the Fermi level on the GaAs side of the junction, while having relatively little effect on the bands of the degenerate InAs epilayer. In practice the long-range electrostatic field associated with the δ-doped layer is rapidly screened within n^+-InAs, while it gives rise to an additional triangular barrier on the GaAs side of the junction, with a spatial extent that depends on the Debye length. The overall effective barrier $\Phi - \Phi_{bi}$ for electron transport across the heterojunction is therefore augmented by this additional barrier, and Shen et al. reported an increase by nearly a factor of two – from $\Phi = 0.64$ eV to $\Phi = 1.2$ eV ($\Delta E_c = 0.72$ eV) – in the effective barrier [Shen et al., 1991a,b].

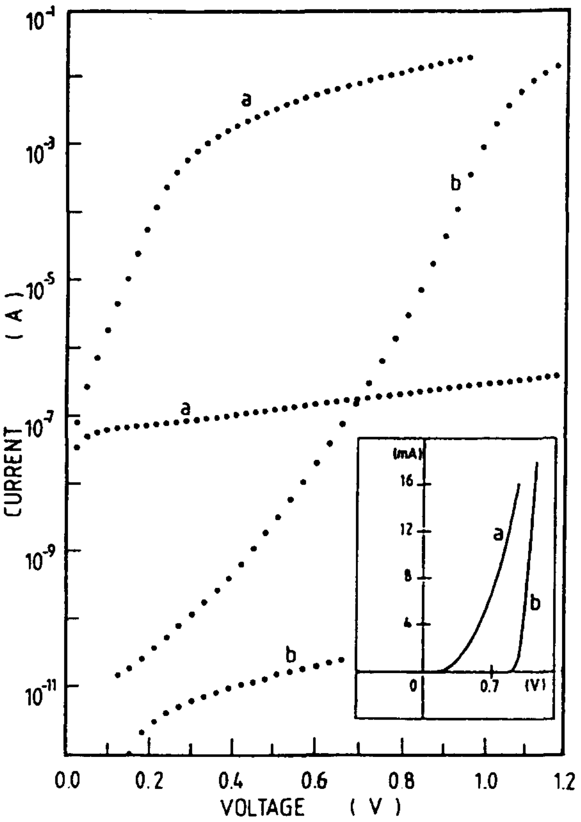

Fig. 36. Current–voltage ($I-V$) curves for relaxed n^+-InAs/n-GaAs (001) heterojunctions in the absence (a) and in the presence (b) of a p-type Be δ-doped layer fabricated by MBE in GaAs 50 Å away from the junction. The inset shows the same data on a linear plot [Shen et al., 1991a].

Fig. 36 shows the $I-V$ curves for relaxed n^+-InAs/n-GaAs heterojunctions without (a) and with (b) p-type δ-doping on the GaAs side 50 Å away from the interface [Shen et al., 1991a]. The inset shows the same data on a linear plot [Shen et al., 1991a]. The substantial increase in the barrier gives rise to a decrease of four orders of magnitude in the reverse (leakage) current, and corresponding dramatic changes in the forward characteristic. The same technique has also been applied to Al/n-GaAs interfaces grown by MBE, with a resulting substantial increase in the Schottky barrier height [Shen et al., 1992b]. In fact, the concept of Schottky barrier modification using highly doped or δ-doped surface layers is a well established technique in device technology, which has been proposed by several authors [Shannon, 1976; Eglash et al., 1984], and implemented in a number of modulation-doped GaAs/AlGaAs FET structures to reduce the gate leakage current and increase the forward biased gate turn-on voltage [Thorne et al., 1983; Ohata et al., 1984; Priddy et al., 1987].

We emphasize that the method described above is fundamentally different from the DID method. In the DID case, careful balance of the charge distribution σ of the n^+ and p^+ dipole layers is required to eliminate the long range component of the potential, and restrict the artificial band offset to the region between the plates. In the former, it is the long range component of the potential which is asymmetrically screened to create the additional triangular barrier on one side of the junction.

5.4. Nonsemiconductor interlayers

5.4.1. Early experiments

Since the mid-1980s, an increasing number of investigations have addressed the possibility of modifying the heterojunction band offset by fabricating an interface layer of some sort to vary the local interface environment. Metal interlayers were an obvious choice for three main reasons. First, there is a relatively extensive amount of information available on how metals interact with semiconductor surfaces, and modify the interface state spectrum [Margaritondo and Franciosi, 1984; Brillson, 1992]. Second, the use of different metals on the same semiconductor allows one to induce different amounts of disruption and intermixing [Brillson, 1982], and change the local work function in a relatively controlled fashion. Third, several authors have pointed out the direct phenomenological connection between the value of the Schottky barrier observed for the same metal on different semiconductors, and the band offset observed at heterojunctions between the same semiconductors [McCaldin et al., 1976; Batey and Wright, 1986; Freeouf and Woodall, 1986; Niles et al., 1986; Miles et al., 1987; Schuemayer et al., 1989; Tiwari and Frank, 1992a,b; McCaldin and McGill, 1992; Wang et al., 1995]. The transitivity of such alignments has been used to predict and consolidate the band offsets for a wide range of semiconductor heterojunctions. To attempt using metals to modify the band offset implies testing at the same time this transitivity.

To our knowledge, the first attempt to modify a heterojunction band alignment by changing the local interface chemical environment by metal deposition was performed by Katnani et al. [Katnani et al., 1985]. Katnani et al. deposited Al layers one to two monolayer thick at RT or at 340°C on GaAs (001)c(4 × 4) surfaces, prior to growing a Ge epilayer at 340°C. The structure of the metallic interlayer was unknown, as is the case for most metallic interlayer experiments. Synchrotron radiation photoemission spectroscopy was used to investigate atomic interdiffusion, the position of the Fermi level at the interface, and the band offsets of the resulting Ge/Al/GaAs (001) heterojunction. Although large changes in interdiffusion and Fermi level position were reported, the authors observed no change in the Ge 3d–Ga 3d core level separation ΔE_{cl} (see Eq. (3)) as a result of the presence of the Al interlayer, and concluded that the band offsets were unchanged within experimental uncertainty (± 0.05 eV). This was taken to support the conclusion that the band offsets would be primarily an intrinsic (bulk) property of the semiconductor constituents, which is insensitive to interfacial charge distribution or chemistry [Katnani et al., 1985].

Niles et al. examined aSi–CdS $(10\bar{1}0)$ and aGe–CdS $(10\bar{1}0)$ heterojunctions in the presence of Al interlayers 0.5 and 1.0 Å thick. Based on a fit of the overall valence band emission from the heterojunction (conceptually similar to the method described in Fig. 4), for a 1 Å Al interlayer the authors derived a $0.2-0.3 \pm 0.04$ eV increase in the magnitude of the valence-band offset $|\Delta E_{\mathrm{v}}|$ for aGe/Al/CdS $(10\bar{1}0)$ relative to aGe/CdS $(10\bar{1}0)$, and an increase of 0.15 ± 0.04 eV for aSi/Al/CdS $(10\bar{1}0)$ relative to aSi/CdS $(10\bar{1}0)$. Niles et al. attempted to explain the effect of Al in terms of two kinds of interface dipoles [Kroemer et al., 1985] that can be affected by the presence of Al, the first kind corresponding to the charge distribution of interface chemical bonds, the second to the charge distribution arising from the migration of atomic species across the junction. They consequently indicated that the charge transfer associated to the formation of Al–S bonds would not be consistent with the sign of the Al-induced change in offset, and tentatively suggested that charge transfer due to the formation of Ge–Al bonds, and/or atom migration across the junction might explain the observed behavior.

Even larger offset changes were reported by Perfetti et al. for hydrogen and cesium adsorption within the interface region of aSi/aSiO_2 interfaces [Perfetti et al., 1986]. These authors evaporated Si by electron bombardment under an oxygen partial pressure on Si(111) substrates cleaved in situ. Substrate temperatures of 250°C and bombardment with 200 eV oxygen ions were used during deposition to produce what the authors identified as an aSiO_2 substrate layer based solely on valence band photoemission spectra. Exposure to activated hydrogen (in the presence of a hot filament, or an ion gun), or deposition of a nominal 0.5 Å coverage of Cs prior to deposition of aSi at room temperature reportedly gave rise to an interfacial layer of unknown structure. Using an analysis of the valence band edge similar to that described in Fig. 3, Perfetti et al. reported $\Delta E_v = +5.15$ eV for aSi/Cs/aSiO_2 and 4.4 eV for aSi/H/aSiO_2, to be compared with the value $\Delta E_v = 4.9$ eV measured in the absence of any interlayer [Perfetti et al., 1986]. Indications also exist that in bulk SiO_2–Si(001) junctions the presence of Na contamination *decreases* the magnitude of the conduction band barrier height [Williams and Wood, 1972; Bouthillier et al., 1983]. In particular, Bouthillier et al. used internal photoemission to show that the conduction band barrier height could be continuously changed by more than 0.5 eV by varying the Na concentration in the oxide over a range of 10^{10}–10^{14} atoms/cm^2 [Bouthillier et al., 1983].

The same type of photoemission experiments using H and Cs interlayers were also conducted on aSi/GaP(110) junctions [Perfetti, 1987; Russo et al., 1988], for which hydrogen adsorption at the GaP surface prior to aSi deposition reportedly yielded a reduction (by 0.4 eV) in the magnitude of the valence-band offset, while Cs interlayers (0.5 Å nominal coverage) yielded instead an increase of 0.1–0.2 eV in the magnitude of the offset [Perfetti, 1987; Russo et al., 1988], and for aSi/CdS $(10\bar{1}0)$ junctions [Perfetti, 1987], for which H adsorption reportedly yielded a 0.5 eV decrease in $|\Delta E_v|$.

We caution the reader that other authors who studied interfaces prepared and processed with different method, produced results in contrast with some of those listed above. For example, in conducting XPS studies of SiO_2–Si(111) interfaces with thicker (50 Å) oxide layers, Grunthaner and Grunthaner reported a valence-band offset $\Delta E_v = 4.5$ eV, which *increased* to 4.9 eV upon annealing in atomic deuterium [Grunthaner and Grunthaner, 1986]. Other authors used photon assisted tunneling measurements to examine the conduction band barrier height for SiO_2–Si(111), and observed a barrier height of 3.86 eV before anneal, which was *reduced* by 0.48 eV after annealing in hydrogen [Weinberg and Harstein, 1983]. The reduction of the conduction band barrier would be consistent with the deuterium- or hydrogen-induced increase in the valence-band offset proposed by Grunthaner and Grunthaner for SiO_2/H/Si(111), but in contrast with that proposed by Perfetti et al. for the aSi/H/SiO_2 interface [Grunthaner and Grunthaner, 1986].

5.4.2. *Electronegativity considerations*

Perfetti et al. attempted to estimate the effect of the interlayer on the charge transfer upon formation of interface bonds using electronegativity arguments [Perfetti et al., 1986]. The basic idea is to estimate the charge transfer between the interlayer atoms and the semiconductor atoms on each side of the junction, and use any calculated difference between the transferred charge to the left and to the right to calculate an interface dipole. It is assumed, following Sanderson [Sanderson, 1967, 1971; Carver et al., 1984], that the electronegativity of a molecule of a stable compound can be obtained from the electronegativity of each of the atomic constituents. The charge transfer (in electron charges) affecting the *i*th atom is given by

$$\rho_i = \frac{(S_m - S_i)}{2.08 S_i^{1/2}}, \tag{9}$$

where S_i is the electronegativity of the *i*th atom of the molecule, and S_m is the molecular electronegativity. Using Eq. (9) it is possible to estimate the charge transfer between the SiO_2 molecule and the interlayer atom, and between Si and the interlayer atom. In the picture by Perfetti et al. the transferred charge for isolated overlayer/interlayer/substrate planes is assumed to be decaying exponentially on each *n*th plane further away from the junction. The calculated values of the charge transfer on each plane, together with the atomic or molecular density on each plane, the interplanar spacing, and an average dielectric constant allows one to obtain a rough estimate of the total voltage drop across the junction [Perfetti et al., 1986]. Assuming the density of hydrogen atoms to be of the order of the dangling bond density, Perfetti et al. estimated that the presence of an hydrogen interlayer should decrease the valence-band offset by 0.3 eV, while the presence of a 0.5 Å Cs interlayer should reduce the offset by 0.2 eV. Such estimates are remarkably close to the experimental modification of the offset.

Admittedly, the agreement could be fortuitous, and should have been tested at least by varying the the interlayer coverage. Surprisingly, neither data of this type, nor data for other semiconductor constituents and interface orientation have been obtained to date, with the exception of the results for aSi/GaP(110) and aSi/CdS(10$\bar{1}$0) nonpolar interfaces mentioned above, for which the model reportedly yields predictions in good agreement with experiment [Perfetti, 1987]. The same model was also used to show that a 0.2 eV change in valence-band offset observed for aSi–InP(110) heterojunctions prepared at RT versus 120 K could be consistent with the presence of a P interface layer left behind by In outdiffusion at the higher temperature [Dell'Orto et al., 1993a]. In view of the larger lattice mismatch between Si and InP (8%), and the possibility of temperature dependent changes in overlayer morphology [List and Spicer, 1988] and strain, this interpretation seems not unequivocal.

Shihong et al. recently examined the effect of Na interlayers on the valence-band offset of aGe–GaAs(001) interfaces [Shihong et al., 1993]. The substrate was cleaned by sputter–anneal cycles to obtain a clean surface with unknown periodicity, and Na and Ge overlayers were deposited on surfaces kept at room temperature. The valence-band offset was probed by means of photoemission spectroscopy using the two methods described in Figs. 3 and 5 with consistent results. Increasing coverages of Na at the interface yielded a gradual decrease in the magnitude of the valence-band offset [Shihong et al., 1993], as opposed to the increase observed for aSi/GaP (110) [Perfetti, 1987; Russo et al., 1988]. The effect reportedly saturated near the Na saturation coverage (estimated to be ~ 1 monolayer), with a decrease in the magnitude of the offset by 0.2 eV [Shihong et al., 1993]. The authors drew no comparison with the predictions of the electronegativity model.

In any case, we emphasize that electronegativity arguments are not likely to explain the behavior of many interlayer atoms in semiconductor heterojunctions. We note, for example, that alkali metals such as Cs, Na or Li within the interface region of II–VI/II–VI heterojunctions would be expected to be net charge donors based on electronegativity arguments, while they act instead as acceptors. Analogous arguments could be made for many other nonisoelectronic impurities. For example, Bass and Matthai used pseudopotential calculations to study the effect of In atoms in substitutional lattice positions on the charge distribution in Si/Ge(001) superlattices, and found substantial charge transfer from Si and Ge to In, which has a lower electronegativity than both Si and Ge in its atomic form [Bass and Matthai, 1991]. It is unlikely that P atoms on Si lattice sites will ever give rise to the charge transfer from Si to P calculated by Dell'Orto et al. based on Sanderson's electronegativity for P (3.43) and Si (2.84) [Dell'Orto et al., 1993a,b].

In view of the considerations presented in Section 4.2, and the requirement that isolated polar interfaces between heterovalent materials form suitable defects to suppress the long-range electrostatic field, the above model seems insufficient to capture the essential physics of such interfaces. However, it represents the first empirical attempt to gauge the effect of interfacial bond formation on the band offset, and may still be of interest to estimate the charge transfer in disordered interfacial system with nonpolar orientation, for which no structural parameters are available to guide the implementation of quantum mechanical calculations.

5.4.3. *Metallic interlayers and Schottky barriers*

Niles et al. performed the first exploration of the effect of the *thickness* of Al interlayers on ΔE_v for aGe/ZnSe(110), aGe/CdS(10$\bar{1}$0), and aSi/GaP(110) heterojunctions. [Niles et al., 1988, 1989]. The results were obtained by synchrotron radiation photoemission investigations, and are shown in Figs. 37–39. The results for the first two heterojunctions are compellingly similar, with a monotonic increase in the magnitude of the offset with increasing Al coverage that saturates at a coverage of

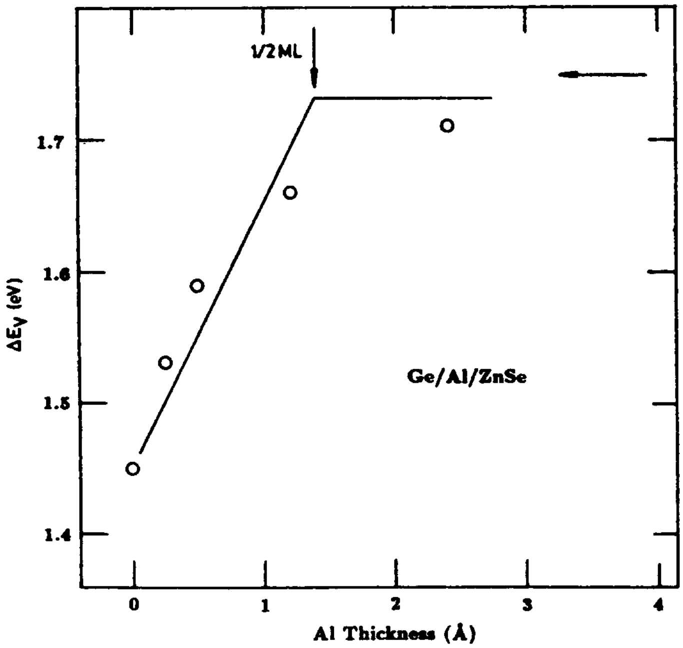

Fig. 37. Photoemission-derived magnitude of the valence-band offset for a Ge/Al/ZnSe(110) heterojunctions as a function of the thickness of the Al interlayer. Following the convention used throughout this report, the sign of the valence-band offset would be negative. The vertical arrow marks the 0.5 ML coverage. The horizontal arrow marks the value expected in the thick interlayer limit, calculated assuming a back-to-back Schottky barrier configuration, and the photoemission-determined value of the Schottky barrier for Al/aGe and Al/ZnSe(110) junctions [Niles et al., 1988].

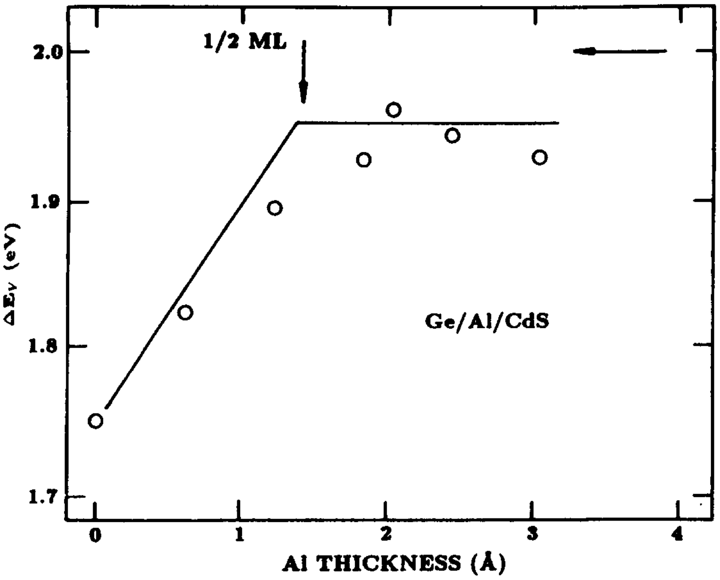

Fig. 38. Photoemission-derived magnitude of the valence-band offset for aGe/Al/CdS(10$\bar{1}$0) heterojunctions as a function of the thickness of the Al interlayer. Following the convention used throughout this report, the sign of the valence-band offset would be negative. The vertical arrow marks the 0.5 ML coverage. The horizontal arrow marks the value expected in the thick interlayer limit, calculated assuming a back-to-back Schottky barrier configuration, and the photoemission-determined value of the Schottky barrier for Al/aGe and Al/CdS(10$\bar{1}$0) junctions [Niles et al., 1988].

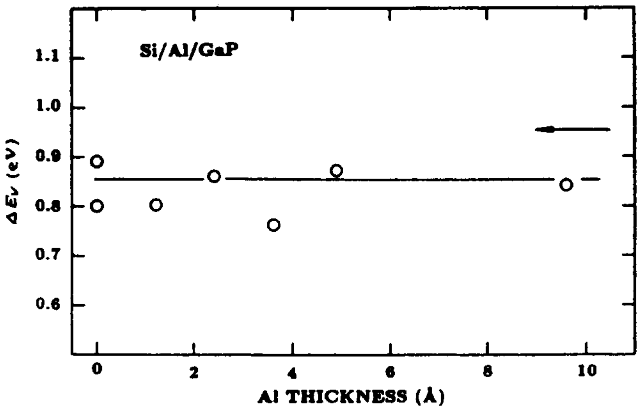

Fig. 39. Photoemission-derived magnitude of the valence-band offset for aGe/Al/GaP(1 1 0) heterojunctions as a function of the thickness of the Al interlayer. Following the convention used throughout this report, the sign of the valence-band offset would be negative. The horizontal arrow marks the value expected in the thick interlayer limit, calculated from a back-to-back Schottky barrier configuration, and the photoemission-determined value of the Schottky barrier for Al/aGe and Al/GaP(1 1 0) junctions [Niles et al., 1988].

about 0.5 ML (vertical arrow in Figs. 37 and 38). This was phenomenologically related by the authors to the presence of a surface concentration of Al atoms sufficient to engage all of the surface anion atoms in Al–Se or Al–S bonds. The maximum offset change was 0.2–0.3 eV. For the third interface the Al interlayer failed to yield a modification of the offset, as shown in Fig. 39. The horizontal arrows in Figs. 37–39 mark the value of the offset expected for a very thick Al interlayer, i.e., the difference of the photoemission-determined Schottky barrier heights between Al and each of the two semiconductor constituents.

An interesting attempt to consolidate the available information was performed by Niles et al. [Niles et al., 1988, 1989] using a point of view quite unlike that of Perfetti et al. [Perfetti et al., 1986], and focusing on the back-to-back Schottky barrier configurations. Following Tersoff [Tersoff, 1984, 1989] and Cardona and Christensen [Cardona and Christensen, 1987], Niles et al. wrote the p-type Schottky barriers for the two Al/semiconductor junctions in terms of Tersoff's midgap energy level position relative to the valence-band maximum in the ith semiconductor E_M^i, the Al work function ψ^{Al}, and the so-called pinning strength parameter S^i. In first approximation S^i is proportional to $1/\varepsilon_\infty$, the reciprocal of the optical dielectric constant, and was taken to increase linearly with E_M^i [Niles et al., 1988]. The basic idea behind this approximation was to include a Schottky-like correction to explain the discrepancy between the theoretical midgap-energy predictions and the observed correlations between heterojunction band lineups and Au/semiconductor Schottky barriers [Niles et al., 1988; Tersoff, 1989].

When comparing the case of back-to-back Schottky barriers (thick interlayer limit), to the no-interlayer case, a difference in the valence-band offset derives from the fact that in the thick interlayer limit, Niles et al. consider the two Schottky barriers separately, each with its own pinning strength parameter, while in the absence of any interlayer they use an average value. This is an attempt to recognize that screening can be considered separately for the two interfaces in the presence of a thick enough interlayer, while it needs to be uniquely defined in the absence of the interlayer. The change in band offset in the thick interlayer limit can then be expressed as

$$\Delta E_v(\infty) = \Delta E_v(0)(1 + k), \tag{10}$$

where

$$k = \frac{a}{2}[(\chi^1 - E_G^1 - \psi^{Al}) - E_M^1 + (\chi^2 + E_G^2 - \psi^{Al}) - E_M^2] \tag{11}$$

and the parameter a relates the pinning strength parameter to Tersoff's midgap-energy level. The relative change in band offset k was calculated using Eq. (11) and the parameters listed by Cardona and Christensen [Cardona and Christensen, 1987], and found to have the correct sign and order of magnitude as compared to the experimental trend in Figs. 37–39.

Although the above model is an intriguing attempt to bring metal induced local screening into the heterojunction interlayer picture, it should be considered as a stimulating suggestion rather than as an approach with truly predictive capabilities. First, the numerical agreement with the experimental values in Figs. 37 and 38, remains rather poor. Secondly, evidence of an interlayer saturation coverage of 0.5 ML in Figs. 37 and 38 remains unexplained. The connection with the Al-anion reactions made to explain the saturation, and the role of interface metallization remains unclear. Third, although the parameters in the calculations were taken from a comparative study of

Au-semiconductors Schottky barriers and heterojunction band offsets, the model seems to be at its worst when called upon to explain the effect of Au interlayers in heterojunctions. McKinley et al. found that in aSi/Au/GaP (110) junctions the Au interlayer yields a 0.6 eV increase in the magnitude of the valence-band offset relative to the no-interlayer case, while the back-to-back Schottky barrier limit would predict a 0.5 eV *decrease* in the magnitude of the offset [McKinley et al., 1990]. For aGe/Au/ZnSe (110) the same authors reported first a decrease and then an increase in the magnitude of the valence-band offset with increasing Au thickness.

5.4.4. *First-principles calculations of Schottky barriers*

The interpretation of the band-offset modification due to metal interlayers unfortunately could not take into account the recent theoretical developments described in Section 4.2. Such developments have been extended to metal–semiconductor interfaces. Dandrea and Duke have recently studied by means of first-principles local density functional calculations the influence of different interfacial chemical compositions on the Schottky barrier height across the Al/GaAs(001) interface [Dandrea and Duke, 1993a,b]. They considered seven different interfacial configurations, including the ideally abrupt As-terminated and Ga-terminated interfaces, and others related to Al–Ga cation swaps or containing As antisites, and found variations in the p-type Schottky barrier heights of 0.4 eV. As for heterovalent heterojunctions with polar orientation, also in Schottky barriers the band offset is dramatically affected by the local interface configuration achieved at the interface. The implication is that several of the metal-induced deviations from transitivity described in the previous sections may well originate from the establishment of inequivalent atomic configurations at the individual metal–semiconductor interfaces, and that, in general, there is no guarantee that the back-to-back Schottky barrier limit is the true limit at which the metal interlayer induced change in offset should tend, since metal-on-semiconductor and semiconductor-on-metal interfaces may correspond to different configurations [Dandrea and Duke, 1993a,b].

The results by Dandrea and Duke [Dandrea and Duke, 1993a,b] suggest that metal interlayers may also induce artificial offsets in homojunctions if suitably different configurations are achieved at the metal-on-semiconductor and semiconductor-on-metal interfaces. Neither the model by Niles et al. [Niles et al., 1988], nor the model by Perfetti et al. [Perfetti et al., 1986] can be easily extended to yield predictions for such systems. Experiments on homojunctions, such as those described in Section 5.5.3, should therefore be extended to consider metallic interlayers.

5.4.5. *The future of metallic interlayers*

The stimulating experimental investigations described above have had a limited impact on heterojunction technology. In our view this is mainly due to the fact that most of them have involved disordered or amorphous and often very thin (4–20 Å) overlayers. There has been little attempt to extend these results to device-grade heterostructures, and confirm them by means of transport and optical techniques for the corresponding buried interfaces. In addition, the lack of any information about the atomic positions of the interlayer atoms has reduced our ability to perform true quantum mechanical modeling of such interfaces. As described in Section 4.2, most theoretical attempts have had to postulate a substitutional or interstitial positions for the interlayer atoms which may or may not have anything to do with the interface structure achieved in practice [Duran et al., 1986; Muñoz et al., 1989; Perez et al., 1990; Bass and Matthai, 1991]. This has severely hindered our ability to develop predictive capabilities for band-offset engineering by means of such interlayers. The scarce information obtained for device-grade heterostructures and the unavailability of truly predictive models account for the lack of progress in the exploitation of these results.

Studies involving epitaxial heterostructures and well characterized metallic interlayer may help bridging the gap. One such study was the original work by Katnani et al. on the Ge/Al/GaAs (001)c(4 × 4) heterojunction, which, however, reported no offset change as a result of the presence of the interlayer [Katnani et al., 1985]. More recently, Maierhofer et al. studied the influence of Sb, Bi, and Al interlayers in epitaxial CdS–InP heterojunctions with (110) orientation [Maierhofer et al., 1992, 1993]. The heterojunction system was carefully selected, since the metastable form of cubic CdS is lattice matched to InP (see Section 5.2.2), and good epitaxy with 1 × 1 periodicity has been observed at 200°C on surface cleaved in situ, with $\Delta E_v = +0.77\,\text{eV}$ in the absence of interlayers [Wilke et al., 1989, 1990a; Maierhofer, 1991]. Furthermore, it is well known that Sb and Bi on InP(110) form ordered unreactive monolayers [Kendelewicz et al., 1989; Zahn et al., 1989; Spindt et al., 1990; Stephens et al., 1990], while Al deposition leads to a relatively well characterized Al–In exchange reaction [Kahn et al., 1983; Kendelewicz et al., 1985; McLean et al., 1988].

For ordered monolayers of Sb, it was found that the interlayer passivates the surface suppressing In–S interface reaction, while Bi monolayers do not, and segregate at least in part at the surface. In spite of such a different effect of Sb and In on interface reactions, photoemission studies showed a similar decrease of the valence-band offset for both interlayers, with $\Delta E_v = +0.55 \pm 0.05\,\text{eV}$ for CdS/Sb/InP(110), and $\Delta E_v = +0.54 \pm 0.05\,\text{eV}$ for CdS/Bi/InP(110). Due to the In–Al exchange reaction, Al interlayers were found to promote In–S reaction, and lead to an increased $\Delta E_v = +0.87 \pm 0.05\,\text{eV}$. In our opinion such promising initial studies should be extended to consider interfaces with polar orientation, which offer higher promise of yielding widely tunable band offsets.

A different approach which has been unexplored to date would be to exploit the few metallic systems that can grow epitaxially on semiconductors, and which are compatible with semiconductor regrowth. Elemental metals are unlikely to offer sufficient lattice match and thermodynamic stability [Palmstrøm, 1995], but a number of transition metal/III intermetallic compounds offer a promising alternative. For example, MBE growth of AlAs/NiAl/AlAs(001) epitaxial structures has been successfully achieved [Sands et al., 1990] and although the relatively high twin density in the III–V epilayer might complicate transport measurements [Palmstrøm, 1995], photoemission spectroscopy should allow one to probe the overall band offsets in epitaxial GaAs/NiAl/AlAs(001) heterostructures and related systems.

5.5. Semiconductor interlayers

5.5.1. Heterovalent versus isovalent interlayers

As described in the previous section, experiments involving metallic interlayers have been hindered for the most part by the difficulty of obtaining information on the atomic structure of the interlayer, and by the impossibility of achieving epitaxial regrowth on top of the metallic interlayer to obtain device-grade heterostructures. Such limitations could be overcome if one were to employ as interfacial layers semiconductors which are lattice-matched or pseudomorphic to the two semiinfinite materials comprising the heterojunction. A change in the overall band alignment would then imply a deviation of the band offsets from the predictions of the transitivity rule (see Eq. (2)).

In general, the offsets in lattice-matched, isovalent heterojunctions tend to follow the predictions of the commutativity and transitivity rules (see Eqs. (1) and (2)). For example, the commutativity of the band offsets has been verified within 0.03 eV for AlAs–GaAs (see Section 2.3) and for AlSb–GaSb [Yu et al., 1992b], while deviations of less than 0.09 eV have been reported for ZnTe–CdS [Wilke et al., 1990b] and InAs–GaSb [Wang et al., 1995]. It is therefore unlikely that isovalent interlayers may be used to induce large changes in the band offsets, i.e., show large deviations from transitivity.

Since the late 1980s the theoretical developments summarized in Section 4.2 have clearly indicated a number of conditions under which semiconductor heterojunctions might be charged, and/or exhibit band offsets that deviate from the predictions of the commutativity and transitivity rules. Most calculations point toward heterovalent heterojunctions. On the one hand, ideally abrupt polar interfaces between heterovalent semiconductors should be charged. On the other hand, since long range electrostatic fields are incompatible with thermodynamic stability, charged interfaces might be observable only in short enough period superlattices. In general, the formation of different point defects may lower the free energy of the system with the formation of neutral interfaces. Different defects may result in widely different band offsets (see Section 4.2).

This suggests two possible avenues by which changes in band offsets might be obtained. If charged interfaces of opposite polarity are formed across a thin enough interface layer, the increase in free energy of the system can be relatively small, and the two interfaces would act as the parallel plates of a microscopic capacitor. In this picture, III–V/IV/III–V single quantum well structures involving abrupt group IV bilayers, for example, should exhibit a positively charged interface where the III–V material is anion terminated, and a negatively charged interface where the III–V semiconductor is cation terminated [Muñoz et al., 1990; Peressi et al., 1991].

Alternatively, deviations from transitivity could be obtained through the establishment of inequivalent neutral heterovalent interfaces in the structure. For example, neutral inequivalent interfaces in III–V/IV/III–V heterostructures might be induced by the formation of a single mixed III/IV versus V/IV plane at the interface, or antisite defects formation in the III–V region near the interface, or through III/IV (cation) or V/IV (anion) swaps across the (001) interface, leading to an intermixed interface region (see Section 4.2).

When band offset changes are observed in the presence of heterovalent semiconductor interfaces with polar orientation, to identify which of the two avenues has been achieved in practice should require a simple enough analysis of the offset change versus interlayer thickness. In view of the considerations listed above, charged polar interfaces should be observable only in short period superlattices or thin quantum wells, and correspond to a deviation from transitivity that increases monotonically with interlayer thickness. Individual, isolated interfaces should always be neutral.

In what follows we will focus on recent experiments involving the fabrication of heterovalent semiconductor interlayer in heterojunctions and homojunctions. The results are classified in terms of the valence of the two semiinfinite semiconductors comprising the junctions. The corresponding theoretical predictions have been described in detail in Section 4.2, and will be summarized here only briefly.

5.5.2. *Heterovalent interlayers in III–V/III–V heterojunctions*

5.5.2.1. Si interlayers A number of recent studies have examined III–V/IV heterojunctions (with IV = Si, Ge, and III–V = GaAs, AlAs) [Bratina et al., 1991; Biasiol et al., 1992; Sorba et al., 1993b] as well as III–V/IV/III–V single [Ceccone et al., 1991; Sorba et al., 1991, 1992a, 1993b; Bratina et al., 1992] and multiple [Sorba et al., 1992b, 1993a; Scamarcio et al., 1992a, 1993b] quantum well structures. Such structures have the advantage that they are lattice matched in the case of Ge, and pseudomorphic in the Si case for interlayer thicknesses below 6–8 ML. All heterostructures were synthesized by MBE and examined in situ by RHEED and monochromatic XPS. In view of the potential of III–V/III–V systems for interdiffusion [Herman and Sitter, 1989], segregation [Brandt et al., 1991], antiphase domain formation [Neave et al., 1983; Strite et al., 1990a,b,c], and – in the case of III–V/Si/III–V heterostructures – strain-induced defect formation (see Sections 3.6 and 5.1), substantial effort was devoted to the structural characterization of model structures by means of TEM and XRD. Some of these results are shown in Figs. 7–10. In particular, TEM and XRD studies indicated that spatially localized, pseudomorphic Si and Ge interface layers could be fabricated in AlAs–GaAs(001) and GaAs–AlAs(001) heterojunctions as well as GaAs–GaAs homojunctions with a combination of relatively high rate and low temperature deposition conditions (under As flux) to reduce interdiffusion.

It should be emphasized that TEM and XRD studies only indicated that *most* of the group-IV atoms could be localized in well defined pseudomorphic layers with relatively abrupt interfaces by an appropriate growth protocol [Sorba et al., 1992a; Franciosi et al., 1993]. It is certainly likely that a minority fraction of the deposited group-IV atoms diffuse in the III–V layers [Brandt et al., 1991]. Comparison of the numerical values of Si-layer thicknesses derived from XRD and flux calibrations suggest, for example, actual layer thicknesses ranging from 70% to 90% of the nominal values [Sorba et al., 1992a]. In addition, features associated with Si_{Ga} and Si_{As} local vibrational modes, i.e., substitutional defects, are observed in Raman spectra together with the dominant Si-like optical modes (see Fig. 10) [Sorba et al., 1992b, 1993a; Scamarcio et al., 1992a,b].

The determination of the offset, together with selected results illustrating the effect of a Si interface layer, is exemplified in Fig. 40 [Sorba et al., 1992a; Franciosi et al., 1993]. The rightmost inset shows valence band spectra for a GaAs (top) and an AlAs (bottom) epitaxial substrate. The binding energy scale is referenced to the valence-band maximum E_v as derived from a least squares linear fit of the leading valence band edge. Photoemission spectra for the Al 2p and Ga 3d core emission from these two samples are shown below the inset in Fig. 40a. The corresponding core binding energy difference is that expected from a hypothetical heterojunction with zero valence-band offset. In Fig. 40b we show spectra from an AlAs–GaAs(001) heterostructure fabricated by growing a 15 Å-thick AlAs epilayer on top of a GaAs (001) substrate. The core separation is independent of overlayer thickness in the coverage range 10–25 Å, as illustrated in the leftmost inset, and the variation in core separation relative to Fig. 40a gives directly the valence-band offset $\Delta E_v = +0.42 \pm 0.07$ eV [Sorba et al., 1992a].

Figs. 40(c) and (d) show the Ga 3d and Al 2p core levels for AlAs–GaAs(001) and GaAs–AlAs(001) heterostructures in the presence of 0.5 ML of Si at the interface. The interlayer causes a 0.4 eV decrease or an increase in the apparent magnitude of the offset depending on the growth sequence. The leftmost inset of Fig. 40 shows for AlAs–Si–GaAs(001) that the core separation (open circles) is independent of AlAs overlayer thickness in the coverage range of 15–30 Å. This result, together with the relatively short photoemission sampling depth employed, argues for an actual variation in band offset rather than a doping-induced band bending variation or an interface reaction [Sorba et al., 1992a; Franciosi et al., 1993]. This is because the core separation reaches its final value at overlayer thicknesses relatively small compared to the typical Debye lengths, and remains the same for overlayer thicknesses at which the contribution of interface-related chemical shifted components should be negligible [Franciosi et al., 1993].

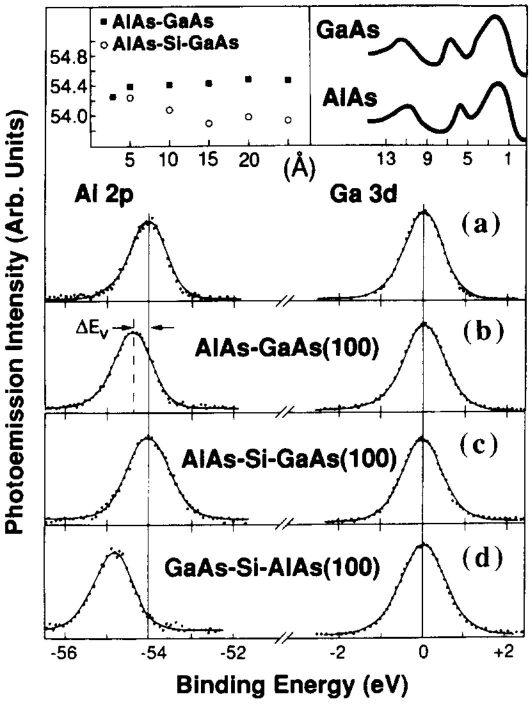

Fig. 40. XPS determination of ΔE_v in III-V/Si/III-V pseudomorphic heterostructures with (001) orientation. Leftmost inset: Al 2p-Ga 3d core level separation at the interface as a function of AlAs overlayer thickness for AlAs-GaAs(001) (squares) and AlAs-Si-GaAs(001) (circles). Rightmost inset: valence band emission from thick AlAs(001) and GaAs(001) epitaxial layers. (a) Al 2p and Ga 3d core level emission from bulk AlAs(001) and GaAs(001) samples. The zero of the energy scale was taken at the position of the Ga 3d cores in GaAs and the apparent core separation is that expected for a hypothetical heterojunction with zero valence-band offset. (b) Core emission from an actual AlAs-GaAs(001) heterostructure. (c) Same as (b) for an AlAs-Si-GaAs(001) heterostructure with a Si layer 0.5 ML thick. (d) Same as (b) for a GaAs-Si-AlAs(001) heterostructure with a Si layer 0.5 ML thick [Sorba et al., 1992a].

The average values of $|\Delta E_v|$ measured in 50 AlAs-Si-GaAs(001) heterostructures and 30 GaAs-Si-AlAs(001) heterostructures as a function of Si interface layer thickness in the 0-4 ML range are summarized in Fig. 41 [Sorba et al., 1992a; Franciosi et al., 1993], with error bars reflecting the standard deviation of the distribution (thick vertical bars) or the uncertainty on a single measurement (thin vertical bars). The effect of the Si interface layer is to increase the magnitude of the valence-band offset for GaAs-Si-AlAs(001) heterostructure and decrease the offset in AlAs-Si-GaAs(001) structures. The Si-induced change in offset increases monotonically with layer thickness up to 0.5 ML, the coverage at which it accounts for a ~0.4 eV decrease or increase in the offset [Sorba et al., 1992a; Franciosi et al., 1993]. In the highest Si coverage range explored (2-4 ML), the Si layer still accounts for a 0.12 eV deviation from the transitivity rule in AlAs-Si-GaAs(001) structures and a 0.31 eV deviation in GaAs-Si-AlAs structures.

The existence of a saturation of the effect of the Si interface layer on the band offsets for high interface layer thicknesses cannot be easily ascertained at coverages above 4 ML, because of the onset of strain relaxation. The observed deviations from the transitivity rule could be quantitatively

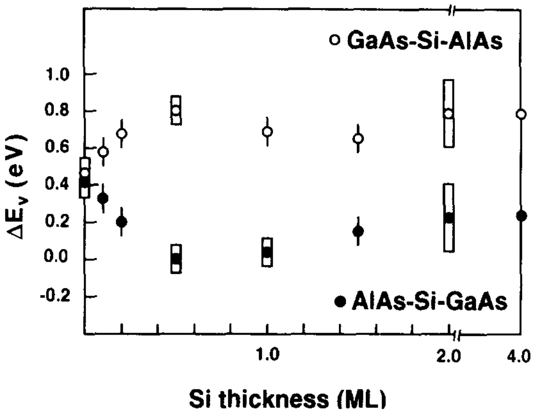

Fig. 41. Magnitude of the valence-band offset for AlAs–Si–GaAs(001) (solid circles) and GaAs–Si–AlAs(001) heterostructures (open circles) as a function of the thickness of the pseudomorphic Si layer at the interface. Following the convention used throughout this report, the sign of the valence-band offset would be negative for GaAs–Si–AlAs(001) and positive for AlAs–Si–GaAs(001). Thick vertical bars show the standard deviation of the data from a series of samples. Thin vertical bars show the uncertainty on a single measurement [Franciosi et al., 1993].

correlated to violations of the commutativity rule for individual Si–GaAs, GaAs–Si, Si–AlAs and AlAs–Si interfaces if the corresponding band offsets were to be measured separately, but this is, again, complicated by the highly strained nature that such interfaces would have (see Sections 4.2.5 and 5.1).

Analogous results were obtained by Moison et al. in studies of InAs–Si–GaAs(001) relaxed epitaxial heterostructures fabricated by MBE [Moison et al., 1992]. These authors grew pseudomorphic Si interlayers on GaAs with a protocol similar to that used by Sorba et al. and measured by XPS a gradual variation in the In $4d_{5/2}$–Ga $3d_{5/2}$ core separation consistent with a gradual increase in the magnitude of the valence-band offsets. The change saturated at a Si interlayer coverage of about 0.7–0.8 ML, giving rise to a maximum offset change of about 0.2 eV. For GaAs/Si/InAs(001) heterostructures the same authors observed a diffuse interface with In surface segregation during growth. This prevented an accurate photoemission determination of the band offset. Preliminary indications though are that the effect of Si on the diffuse interface may cause an increase in the magnitude of the offset of the order of 0.1 eV [Moison et al., 1992].

Similar variations in core level separation as a function of Si interlayer thickness were also observed by Hashimoto et al. for AlAs/Si/GaAs heterostructures fabricated by MBE on Ga-stabilized GaAs(001)4 × 2 surfaces, GaAs(311) A surfaces, and GaAs(110) surfaces [Hashimoto et al., 1994]. These authors, however, propose a different interpretation of the change in core level separation, that will be discussed in Section 5.5.4.

5.5.2.2. Ge interlayers Ge interface layers, while isovalent with Si, offer the advantage of being lattice matched to GaAs and AlAs, so that pseudomorphic layers can be fabricated in a wide range of layer thicknesses. The effect of Ge interface layers on the overall band alignment in III–V/Ge/III–V heterostructures was investigated with the same protocol employed earlier for Si interlayers [Bratina et al., 1992; Franciosi et al., 1993]. Measured valence-band offsets as a function of Ge

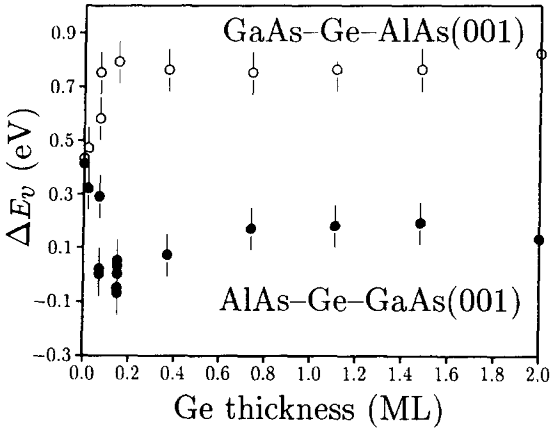

Fig. 42. Magnitude of the valence-band offset for AlAs-GaAs (001) (solid circles) and GaAs-AlAs (001) heterostructures (open circles) as a function of the thickness of an ordered Ge layer at the interface. The layer is grown in both cases on an As-stabilized substrate surface. The presence of the group-IV layer yields a local interface dipole that is subtracted from, or added to the natural (i.e., unmodified) valence-band offset [Bratina et al., 1992].

interface layer thickness are summarized in Fig. 42 for a number of AlAs-Ge-GaAs(001) (solid circles) and GaAs-Ge-AlAs (001) (open circles) heterostructures. The relatively symmetric behavior of the data suggest that a Ge-induced dipole is subtracted from the natural valence-band offset in AlAs-GaAs(001) heterostructures, and added to the offset in GaAs-AlAs(001) heterostructures [Bratina et al., 1992; Franciosi et al., 1993]. The magnitude of the dipole increases linearly with nominal interlayer thickness up to a maximum value of about 0.4 eV at ~ 0.2 ML, and decreases slowly for higher Ge coverages.

The results of Fig. 42 exhibit compelling qualitative similarities together with important quantitative differences relative to those shown in Fig. 41 for Si interface layers in analogous structures. For both, the microscopic capacitor model predicts the correct direction and order of magnitude of the dipole if one assumes that the group IV interlayer is always grown on an As-terminated substrate and that the III-V overlayer growth is cation-initiated in all cases [Sorba et al., 1991]. Peressi et al. performed self-consistent calculations of the band-lineups for AlAs-Si-GaAs(001) and GaAs-Si-AlAs (001) assuming that Si atoms are uniformly distributed over two consecutive atomic layers to ensure local charge neutrality, on top of an As-terminated III-V substrate and below a cation-initiated III-V overlayer [Peressi et al., 1991]. In what is probably the most notable success of the microscopic capacitor picture to date, they found remarkable quantitative agreement with the results in Fig. 41 up to Si coverages of 0.5 ML (see Section 4.2.4 and Fig. 23). At higher coverages any microscopic capacitor picture would predict a dipole increasing monotonically with interlayer thickness, in contrast with experiment (see also Section 4.2.5).

Another attractive point of the charged interface picture is that it may offer an admittedly speculative argument to explain the absence of antiphase domains in the III-V overlayers (see Fig. 7). Since the group-IV atoms are likely to arrange themselves over two consecutive atomic layers to ensure charge neutrality, monoatomic steps are unlikely, and so will be the formation of antiphase domains during III-V overlayer growth on top of the group-IV interlayers [Franciosi et al., 1993].

In contrast, during III–V semiconductor growth on bulk group-IV substrates, the resulting isolated interfaces cannot be charged, and steps with odd number of layers are possible, leading to antiphase domain formation [Bringans et al., 1986, 1988].

Major shortcomings of the charged interface picture are that it cannot explain dipole saturation with increasing interlayer thickness, nor the differences between the effect of Si and Ge on the band offset for low interlayer thicknesses. If one defines here for simplicity the total dipole as the modification of the valence-band offset resulting from the presence of the group-IV layer, and the specific dipole as the offset modification per group-IV atom, then Ge exhibits a maximum total dipole identical, within experimental uncertainty, to that of Si (0.4 eV), but a specific dipole about three times as large (Fig. 42) as that of Si (Fig. 41) at low coverages. The microscopic capacitor picture would predict [Muñoz et al., 1990; Baroni et al., 1991; Peressi et al., 1991] an initial specific dipole for Ge essentially identical to that of Si, and a total dipole increasing monotonically to 1.3 eV for Ge and 1.4 eV for Si, at a coverage of 2 ML [Baroni et al., 1991; Peressi et al., 1991].

The experimental value of the maximum dipole (0.4 eV) is compellingly similar to that observed by a number of authors during studies of IV/III–V/IV homojunctions, to be discussed in the next section). The existence of a maximum interface dipole of identical magnitude for AlAs–Ge–GaAs, GaAs–Ge–AlAs, Ge–GaAs–Ge, Ge–AsGa–Ge, AlAs–Si–GaAs and GaAs–Si–AlAs, with quite different interface layer thicknesses, will represent an important challenge to all theoretical models of interface dipole formation [Bratina et al., 1992; Franciosi et al., 1993].

To investigate the high interlayer thickness limit of the group-IV-induced dipole, Biasol et al. and Sorba et al. fabricated Ge layers 4, 8 and 16 ML thick in III–V/Ge/III–V quantum well structures [Biasiol et al., 1992; Sorba et al., 1993b]. Deviations from transitivity for AlAs–Ge–GaAs (001) and GaAs–Ge–AlAs (001) structures of 0.2–0.3 eV, independent of Ge thickness in the range explored, and consistent with those observed for Ge layer thicknesses in the 1–2 ML range were observed [Bratina et al., 1992; Franciosi et al., 1993]. Since for interlayer thicknesses of 8–14 ML the band structure of Ge is likely to be fully developed, it is meaningful to determine the contribution of each III–V/IV and IV/III–V interface to the overall band offset. The authors found $\Delta E_v = 0.23 \pm 0.05$ eV across the overall AlAs–Ge–GaAs (0 0 1) heterostructure, with $\Delta E_v = 0.65 \pm 0.05$ eV for the AlAs–Ge interface and $\Delta E_v = -0.42 \pm 0.05$ eV for the Ge–GaAs interface [Biasiol et al., 1992; Bratina et al., 1992; Franciosi et al., 1993]. For GaAs–Ge–AlAs (001), i.e., the reverse growth sequence, the same authors found $\Delta E_v = -0.71 \pm 0.05$ eV across the overall heterostructure, with $\Delta E_v = -0.91 \pm 0.05$ eV for the Ge–AlAs interface and $\Delta E_v = 0.20 \pm 0.05$ eV for the GaAs–Ge interface.

Such results can be compared with those obtained for individual, isolated interfaces grown in identical conditions [Biasiol et al., 1992], and summarized in Section 5.2.3. It was found that the offsets for isolated interfaces are compellingly similar to those obtained in III–V/Ge/III–V quantum well structures, as shown in the uppermost section of Fig. 28. Since individual isolated IV/III–V interfaces, that cannot be charged, exhibit deviations from the commutativity rule (see Section 5.2), such deviations must be associated with the establishment of inequivalent local environments leading to neutral interfaces. It was therefore proposed that, at least for Ge layer thicknesses larger than 1–2 ML, the observed deviations from the transitivity rule may be due to the establishment of *inequivalent neutral* IV/III–V interfaces rather than to the presence of *charged* interfaces, i.e., a microscopic capacitor [Biasiol et al., 1992; Franciosi et al., 1993; Sorba et al., 1993b].

As far as the nature of the inequivalent local interface configurations that lead to the observed deviation of the offsets from transitivity, little direct experimental information is available at this stage. A number of speculations are possible based on comparison of the experimental results with theoretical predictions for the band offsets of neutral IV/III–V interfaces involving atomic mixing on one or two atomic planes (see Section 4.2.5). Such speculations should be taken with great caution. Only a few simple interface reconstructions have been examined by theory, and often with no attempt to calculate the corresponding formation free energy. Also, if similar phenomena are observed on As-stabilized GaAs(001)2 × 4 surfaces, as well as Ga-stabilized GaAs(4 × 2), GaAs(311)A, and nonpolar GaAs(110) surfaces, this may point to a more general phenomenon than envisioned to date in the formation of the simple interface reconstructions considered by theory. In this respect, we feel that two different avenues of investigation might be essential to further clarify the origin of the phenomena described in this section.

First, the connection between the effect of group-IV interlayers and self-compensation during δ-doping should be clarified. Even a cursory comparison of Fig. 41 with Fig. 11 suggests that the onset of the effect of the group-IV interlayer on the III–V/III–V band offsets mirrors the onset of self-compensation during δ-doping experiments. Since self-compensation should derive from the formation of acceptor-like defects that compensate $\mathrm{Si_{Ga}}$ centers, a direct connection with the establishment of a Si-related local interface dipole with well defined orientation might exist.

Second, the connection between the effect of group-IV interlayers on III–V/III–V heterojunction band offsets and the effect of Si interlayers on Schottky barriers should be clarified. Recently, transport and photoemission measurements have shown that Si interlayers one to two monolayers thick can be used to tune the Schottky barrier in the 0.2–1.1 eV range in Al/n–GaAs(001) diodes [Cantile, 1994a,b]. A relatively large excess flux of anions (As) or cations (Al) was used during Si deposition. It was clearly demonstrated that the presence of a Si interlayer grown under As flux yielded a substantial decrease of the n-type Schottky barrier (to about 0.2–0.3 eV), while the presence of a Si interlayer grown under an excess cation flux had an opposite effect. The control samples without the Si interlayers, or with Si interlayers grown without an excess cation or anion flux showed an unperturbed barrier of 0.7–0.8 eV. The implication is that the Si interlayer caused a ±0.4 eV variation in the Schottky barrier, and that the direction of the change was controlled by the excess flux (anion versus cation) used during Si deposition. The fact that the magnitude of the barrier variation is compellingly similar to the changes in band offsets described in this section, and the conceptual connection between Schottky barriers and heterojunction band alignment (see Section 5.4) should be motivation enough to extend this type of study to heterojunctions.

5.5.3. Heterovalent interlayers in III–V and IV homojunctions

The possibility of using heterovalent interface layers to change the band alignment in semiconductor homojunctions stems from the same theoretical developments that motivated the heterojunction experiments described in Section 5.5.2. From an experimental point of view, verification of interlayer-related effects is simpler in homojunctions when transport techniques are employed, since contact fabrication is identical for the substrate semiconductor and the topmost epilayer, eliminating possible artifacts. On the other hand, photoemission investigations of the offset in homojunctions are more difficult, since the same core levels have to be used as markers of the overlayer and substrate potential, so that a deconvolution of substrate and overlayer features is required, and a sufficient energy resolution is indispensable. The limitations on the detectable band offset become quite similar to those encountered when applying the direct methods to extract the band offset illustrated in Figs. 3 and 4.

To our knowledge, the first experiment of this type was reported by McKinley et al. for aGe–Ge(1 1 1) homojunctions in which As–Ga and Ga–As bilayers were fabricated at room temperature at the interface [McKinley et al., 1991, 1992], and the resulting band alignment was probed by synchrotron radiation photoemission spectroscopy. Adsorption of As at room temperature on Ge(1 1 1) substrates cleaved in situ gave rise to an As adsorbed layer of unknown symmetry, on which a Ga monolayer was also deposited at room temperature. Deposition of aGe at room temperature resulted in a broad Ge 3d core lineshape that could be decomposed in two 3d doublets shifted by 0.38–0.41 eV. Having associated the low binding energy doublet with the overlayer emission, and the high binding energy doublet with the substrate emission based on the coverage dependence of their intensity, McKinley et al. reported a valence-band offset $\Delta E_v = -0.38$–0.41 eV for the resulting aGe/Ga/As/Ge(1 1 1) junctions [McKinley et al., 1991, 1992].

The situation was more complicated when Ga adsorption was performed before As adsorption, since three Ge 3d doublets were detected. McKinley et al. associated two doublets with overlayer and substrate emission, corresponding to $\Delta E_v = +0.33$–0.46 eV, and the third doublet with regions of the surface in which As-substrate bonds (deemed more energetic) exist despite the initial Ga adsorption, possibly due to clustering of the initial Ga monolayer. Enhanced Ga outdiffusion within the aGe film was also observed for the second growth sequence.

An analogous behavior was reported by Marsi et al. [Marsi et al., 1992a, b] for aGe/Al/As/Ge(1 1 1), i.e., initial adsorption of the anion followed by deposition of one monolayer of cations at the interface reportedly gave rise to two Ge 3d doublets, with energy separation consistent with $\Delta E_v = -0.4$ eV. However, when Al deposition was performed first, followed by As adsorption, only two Ge 3d features were observed, with energy separation and coverage dependent intensity still consistent with $\Delta E_v = -0.4$ eV even for the aGe/As/Al/Ge(1 1 1) heterojunction. The authors proposed that a complete exchange of the Al and As planes occurred in view of the stronger Ge–As bonds as compared to Al–Ge bonds [Marsi et al., 1992a,b].

Interpretation of the above early results most often employed the microscopic capacitor picture, with charged interfaces of opposite polarity at the Si–As and Si–Ga boundaries. As described in Sections 4.2 and 5.2, charged interfaces with opposite polarity would be consistent with a change in the offset in the same direction and of the same order of magnitude as that observed experimentally in III–V/III–V homojunctions and heterojunctions in the presence of group-IV interlayers.

Experiments on aSi/Si(1 1 1) junctions in the presence of AlP and GaP layers at the interface reportedly produced a more symmetric behavior than the early homojunction experiments. Also for these interfaces, as for Ge–GaAs and Ge–AlAs, there is good lattice match between III–V and IV materials, and it is unfortunate that room temperature deposition did not allow epitaxial structures to be formed. Nevertheless Marsi et al. reported that P adsorption at room temperature on Si(1 1 1) surfaces cleaved in situ, followed by deposition of Ga or Al monolayers, and aSi growth, gave rise to two Si 2p doublets, with core separation consistent with $\Delta E_v = -0.5$ eV for aSi/Ga/P/Si(1 1 1), and $\Delta E_v = -0.4$ eV for aSi/Al/P/Si(1 1 1) heterojunctions [Marsi et al., 1992a]. The reverse deposition sequence gave rise to reversed offsets, $\Delta E_v = +0.5$ eV for aSi/P/Al/Si(1 1 1), and $\Delta E_v = +0.4$ eV for aSi/P/Ga/Si(1 1 1) heterojunctions, with only two Si 2p components visible in the spectrum and therefore no evidence of the partial or total anion/cation exchange observed for GaAs and AlAs interface layers in aGe/Ge(1 1 1) homojunctions. The analysis was refined and extended in a second series on experiments considering aSi/Si(1 1 1) junctions and a stack of one, two, or three Al–P layers at the interface [Marsi et al., 1992a]. The authors reported the presence of three Si 2p contribution to the overall lineshape, the third being a small "reacted" component observed only for aSi coverages below 5 ML. The presence of two or three stacked Al–P interface layer, as opposed to a single layer, did not change the measured offset, which was reportedly $\Delta E_v = -0.5$ eV for aSi/Al/P/Si(1 1 1) and $+0.5$ eV for aSi/P/Al/Si(1 1 1).

As described in Sections 4.2, 5.5.1 and 5.5.2, evidence of a band offset change independent of the interlayer thickness is difficult to reconcile with the microscopic capacitor picture, in which the band offset modification originates from the field established between two charged interfaces. A first suggestion by Marsi et al. [Marsi et al., 1992a] was that the saturation value of the offset modification is set by the distance between the band edges and the extrinsic charge neutrality level [Gozzo et al., 1992]. However, the very concept of an *extrinsic* charge neutrality level, as opposed to Tersoff's intrinsic charge neutrality level, is open to a number of criticisms (see Section 3.5).

A far more ionic interlayer was used by Dell'Orto et al. to fabricate artificial band offsets in aSi–Si(1 1 1) homojunctions [Dell'Orto et al., 1993b]. The authors deposited CaF monolayers at 500–600°C on Si(1 1 1) substrates cleaved in situ, prior to deposition of aSi at room temperature. Synchrotron radiation photoemission studies showed a complex Si 2p lineshape, which they decomposed in terms of no less than four 2p doublets, two of which they assigned to substrate and overlayer emission, based on the dependence of their intensity on aSi coverage, while the other two they assigned to Si–Ca (majority) and Si–F (minority) bond formation on Si(1 1 1). From this it was deduced $\Delta E_v = -0.35$ eV, with an artificial offset consistent in sign with that expected from the charge transfer from Ca atoms (mostly bonded to the substrate) to F atoms (mostly bonded to the overlayer). They compared this value with the potential difference expected from the electronegativity model outlined in Section 5.4.2, which allowed them to obtain an estimate of the charge transfer from Ca to F within the interlayer, and (using a dielectric constant appropriate for CaF_2) yielded a predicted offset magnitude of 1 eV [Dell'Orto et al., 1993b]. We emphasize that the offset modification obtained by Dell'Orto et al. using CaF interlayers is actually smaller than that obtained by Marsi et al. using an AlP interlayer. The implication seems to be, in our opinion, that the electronegativity-induced charge transfer within the binary interlayer is unlikely to explain the essential physics of the situation, as already illustrated in Section 5.4.2.

A first attempt to study artificial band offset formation in epitaxial homojunction systems was performed by growing by MBE As-capped GaAs/Si/GaAs (001) homojunctions incorporating Si interlayers with 1 and 1.5 ML coverage, and thermally desorbing the As-cap in situ to expose the heterostructure for synchrotron radiation photoemission investigation of the band offsets [Margaritondo, 1993; Marsi et al., 1993] With this type of experiment, it is not possible to vary the epilayer thickness to distinguish substrate and epilayer features, and the authors ingeniously used the tunability of synchrotron radiation to probe the interface with different photon energies and therefore sampling depths. The results are shown in Fig. 43. With increasing photon energy in Fig. 43 the photoelectron escape depth decreases from 20 to 6 Å for the Ga 3d emission, and from 25 to 6 Å for the As 3d emission [Marsi et al., 1993], allowing the authors to emphasize the overlayer contribution to the core level lineshape, shifted by 0.30 ± 0.05 eV (for the monolayer interlayer) and 0.25 ± 0.05 eV (for the 1.5 ML Si coverage) to higher binding energy relative to the substrate contribution. This implies $\Delta E_v = -0.30 \pm 0.05$ and $\Delta E_v = -0.25 \pm 0.05$ eV in the two cases. The observed Si-induced change in the offset is consistent in sign and magnitude with that observed by Sorba et al. in AlAs–GaAs(001) and GaAs–AlAs(001) heterostructures (see Section 5.5.2 and Fig. 41), and points to a similar physical origin of the band offset variation.

A confirmation of the above results for homojunctions was recently obtained by measuring by internal photoemission at 77 K the conduction-band offset in p–GaAs/Si/n–GaAs(001) diodes

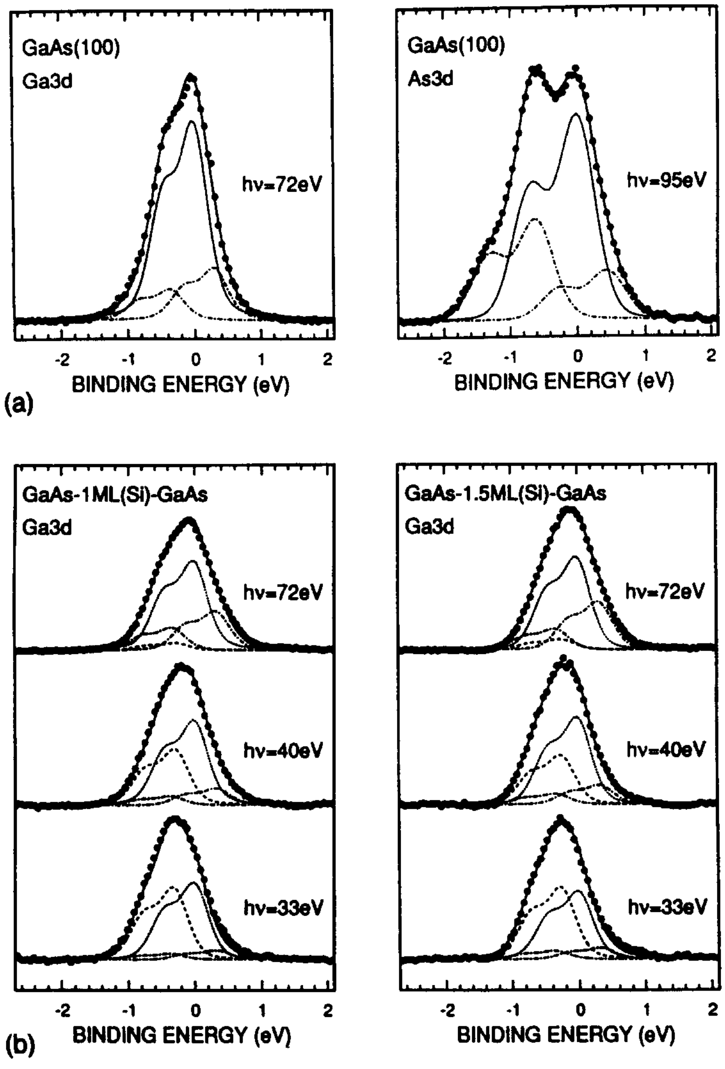

Fig. 43. Photoemission determination of the valence-band offset in epitaxial GaAs–Si–GaAs(001) heterostructures incorporating a Si coverage of 1 or 1.5 ML at the interface. (a) As 3d and Ga 3d core level emission (solid circles) for the As-rich GaAs(001)c(4 × 4) surface. Also shown are the different contributions to the overall detected signal, from a least squares fit of the data (solid line) in terms of a bulk (dotted line), and surface shifted (dash-dotted line) contribution. (b) Ga 3d emission from heterojunctions incorporating 1 (left) and 1.5 ML (right) of Si for different sampling depths (photon energies). The dotted, dashed, and dash-dotted components denote the overlayer, substrate and surface contributions. (c) Same as in (b), for the As 3d emission [Margaritondo, 1993].

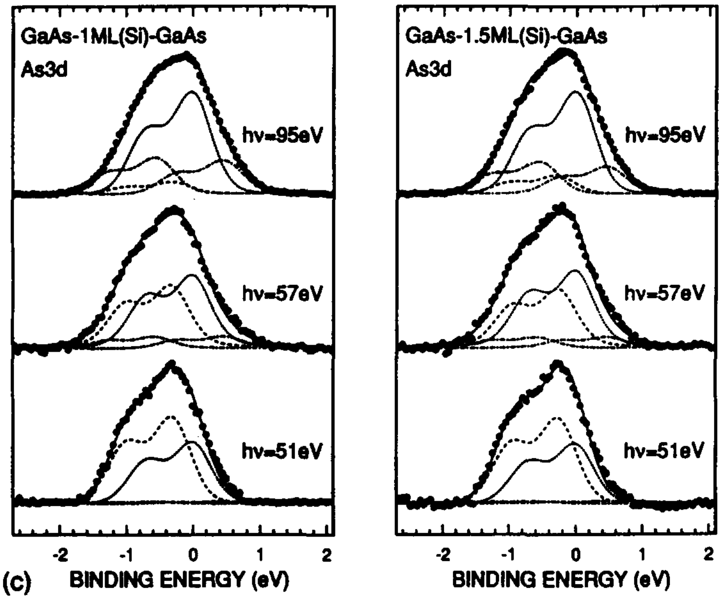

Fig. 43 (continued).

grown by MBE and incorporating a Si coverage of 0.5 ML [Dell'Orto et al., 1994]. The authors measured $\Delta E_c = 0.27 \pm 0.04$ eV, in remarkable agreement with the photoemission results, since for artificial band offsets in homojunctions $|\Delta E_v| = |\Delta E_c|$. In a very recent paper, Dell'Orto et al. measured by internal photoemission $|\Delta E_c|$ in a n-GaAs/Si/p-GaAs(001) heterostructure fabricated in identical conditions, and reported a slightly larger value $\Delta E_c = 0.37 \pm 0.04$ eV [Dell'Orto et al., 1995]. It is worth mentioning that in the latter experiment the authors have reported direct evidence of resonant states induced by the artificial triangular conduction band well.

The agreement between internal photoemission and XPS results is especially comforting for two reasons. First, it shows that the same band offset changes observed for thin overlayers are also found in heterojunctions buried well below the photoemission sampling depth, and incorporated within a device-grade heterostructure. Second, the Si-induced band offset change was observed both in n–p and p–n junctions. As it will be discussed in Section 5.5.4, outdiffusion of interlayer atoms to selectively dope the overlayer n^+ has been proposed as an alternative mechanism to change the apparent band offset during photoemission measurements. Such a mechanism would be unlikely to yield the same effect in bulk n–p and p–n diodes.

We conclude this section pointing out the remarkable symmetry of the offset modifications observed in heterojunctions, and homojunctions. It seems quite clear that the maximum band alignment modification achievable in practice is of the order of 0.4–0.5 eV, and that the offset modification saturates for interlayer coverages at or below the monolayer level. This makes any explanation of the offset change in terms of charged interfaces problematic. It is therefore not likely that the microscopic capacitor picture reflects the actual interfacial situation.

The possible formation of inequivalent neutral interfaces, as discussed in Sections 4.2, 5.5.1 and 5.5.2 seems a more likely explanation for the observed deviations from the transitivity and commutativity rules. As illustrated in Sections 4.2 and 5.2.3, an increasing number of quantum mechanical calculations now exist for band offsets deriving from specific interface configurations. Unfortunately, the wide range of possible interface reconstructions that may lead to neutral interfaces while giving rise to different offsets negates to us for the time being truly predictive capabilities. Molecular dynamics studies of defect formation at interfaces may address this problem, but may still take years to implement for realistic interface configurations.

5.5.4. *Interdiffusion and anomalous Debye length*

Recently two different research groups have proposed identical interpretations of the effect of Si interlayers on the band offsets in AlAs/GaAs junctions [Akazawa et al., 1992; Hashimoto et al., 1994]. The authors proposed that Si-induced changes in core separation such as those depicted in Fig. 40 would be due to interdiffusion and doping-related phenomena, rather than to a localized interface dipole. Their argument can be summarized as follows. Preferential Si outdiffusion toward the surface produces a highly degenerate n-type III–V overlayer with an anomalously short Debye length. This, together with Fermi level pinning near mid-gap at the surface, would preferentially localize band bending in the overlayer. For unprecedentedly high doping within the overlayer, a large potential difference could be created across the thin (15–20 Å thick) overlayers used in photoemission determinations of the band offsets, giving rise to a change in ΔE_{cl} (see Eq. (3)), as illustrated in Fig. 44. The Debye length required to sustain such a band bending within relatively thin overlayers would require, in turn, a doping of the order of $1\text{–}5 \times 10^{20}\,\mathrm{cm}^{-3}$ within the III–V overlayer [Akazawa et al., 1992], which exceeds by several orders of magnitude the highest doping levels ever achieved in AlAs [Herman and Sitter, 1989].

We will discuss the model in some detail, for three reasons. First, doping effects and band bending in heterovalent heterojunctions are potentially important issues, which have been insufficiently addressed in the literature. They have also far-reaching implications, since they would affect not only the heterojunction results summarized in Section 5.5.2, but also those in Section 5.4, as well as the homojunction results in Section 5.5.3. For example, in Ge/Al/ZnSe, Ge/Al/CdS, Si/AlP/Si, Ge/GaAs/Ge, etc., one could envision preferential diffusion of cations or anions to selectively dope at an unprecedented level the overlayer or the substrate, and obtain a wide range of diffusion-related effects. Second, if the proposed picture is correct, interface δ-doping would represent a simple method of achieving and studying doping concentrations that cannot be realized with any other method known to us. Third, the situation envisioned in Fig. 44 gives rise to a charge transfer from the ionized impurities in the overlayer to the quantum well states in GaAs, and therefore still changes the band alignment. The model effectively replaces a localized interface dipole (independent of doping) with a doping-induced dipole (see Section 5.3) analogous to that discussed by other authors [Störmer et al., 1979; Müller et al., 1989]. This type of dipole, however, as opposed to those described in Section 4.2, should be affected by the bulk doping of the two semiconductors comprising the heterojunction, and may be modified by further impurity redistribution in buried heterostructures of technological interest.

We also mention that Hashimoto et al. have recently performed studies of AlAs/Si/GaAs(001) heterojunctions fabricated on Ga-stabilized GaAs(001) surfaces, as well as GaAs(311)B surfaces and nonpolar (110) surfaces, and found results analogous to those observed on As-stabilized GaAs(001)2 × 4 surfaces. A summary of these results is shown in Fig. 45. The authors used the lack of a visible dependence of the offset from the initial surface termination to conclude that Fig. 44 gives a correct description of the interface, and that work to fabricate a truly local interface dipole should

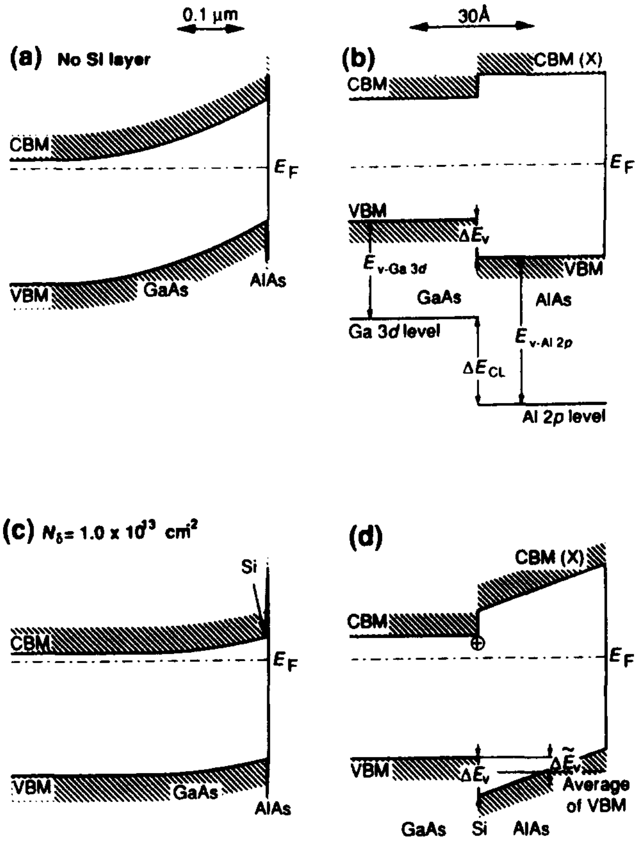

Fig. 44. Band diagram for AlAs/GaAs(001) [(a) and (b)] and AlAs/Si/GaAs(001) [(c) and (d)] heterojunctions which include a 30 Å thick AlAs overlayer. A Si coverage of $1.0 \times 10^{13}\,\mathrm{cm}^{-2}$ is assumed to have preferentially doped the AlAs overlayer. The GaAs is assumed doped at $n \sim 1 \times 10^{16}\,\mathrm{cm}^{-3}$· Enlargements of the near-surface region probed by photoemission spectroscopy are shown in (c) and (d). The Fermi level is assumed to be pinned near midgap at the AlAs surface. The band bending in the overlayer gives rise to an apparent change in the energy separation of valence band maxima and core levels [Hashimoto et al., 1994].

focus on the (311)A surface [Saito et al., 1994a,b]. The latter suggestion is motivated by the fact that Si reportedly behaves as a donor or an acceptor impurity depending on the temperature during GaAs growth on (311) A surfaces [Agawa et al., 1994], so that a true microscopic capacitor might be built at the junction by varying the growth temperature during Si deposition.

The theoretical issue of which of the possible band-structure models is more appropriate to explain changes in band alignment should not be confused with the purely experimental issue of ascertaining if Fig. 44 gives a correct description of the interface or not. Once it is decided based on the data if one is in the presence of an interface dipole localize at the interface, or of a doping dipole extending throughout overlayer (Fig. 44), then one can examine the relevance of the different theories.

The situation outlined in Fig. 44 is quite simple. The Fermi level is pinned at the surface near midgap, and most of the band bending occurs within a highly degenerate (1–$5 \times 10^{20}\,\mathrm{cm}^{-3}$) thin

III–V overlayer, yielding an apparent decrease in ΔE_{cl} for AlAs–Si–GaAs(001) structures and an apparent increase in ΔE_{cl} for GaAs–AlAs(001) structures [Akazawa et al., 1992]. Since the Si coverage dependence of ΔE_{cl} would be identical for the situation described in Fig. 44, and for a true localized interface dipole, any discrimination between the two should be sought elsewhere. Akazawa et al. and Hashimoto et al. indicated that a 0.1 eV broadening of the overlayer core levels in the presence of a Si interface layer is evidence enough that the band bending is localized within the overlayer. However, since core level broadening may also derive from other effects, including the reduced structural quality of a 15–20 Å-thick III–V overlayer grown on highly strained Si, as opposed to bulk GaAs, this seems hardly conclusive. A very simple and direct verification can be made, instead, based on the position of the individual core levels.

If Fig. 44 gives a good description of the interface, the Fermi level is pinned near the AlAs mid-gap at the top of the overlayer, and near the conduction-band minimum of GaAs in the substrate. Core binding energies relative to the Fermi level should reflect this. The Ga 3d core binding energy relative to the Fermi level should be consistently ~ 20.2 eV. If the Fermi level in the AlAs overlayer were near midgap, the Al 2p core binding energy relative to the Fermi level should vary accordingly. Changes in band bending should affect only the apparent Al 2p binding energy and lineshape, and not the Ga 3d position. However, neither the experimental position of the core levels relative to the Fermi level, nor the escape depth dependence of ΔE_{cl} support this. As far as the Fermi level position is concerned, variations of up to 0.6 eV in band bending from sample to sample result in a *rigid* shift of the core levels [Sorba et al., 1992a], with no change in ΔE_{cl}. This is exemplified in Fig. 46 where the Al 2p and Ga 3d core emission is shown for two different AlAs–Si–GaAs (001) structures involving a 0.5 ML Si interface layer. The zero of the energy scale corresponds to the spectrometer Fermi level. The reduction in band bending in Fig. 46 may originate from small differences in the growth procedure [Sorba et al., 1992a], and surface photovoltage. A variation of 0.6 eV in the position of the core levels in Fig. 46 indicates that the position of the Fermi level in the gap has varied by the same amount from

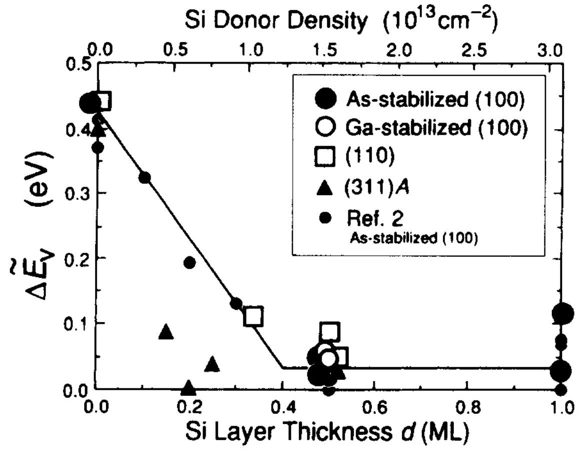

Fig. 45. Average apparent valence-band offset determined by XPS for AlAs/Si/GaAs heterojunctions fabricated on As- and Ga-stabilized GaAs surfaces with (100), (110), and (311)A orientation, as a function of the Si layer equivalent thickness *d*. The solid line shows the variation expected from the model outlined in Fig. 44 [Hashimoto et al., 1994].

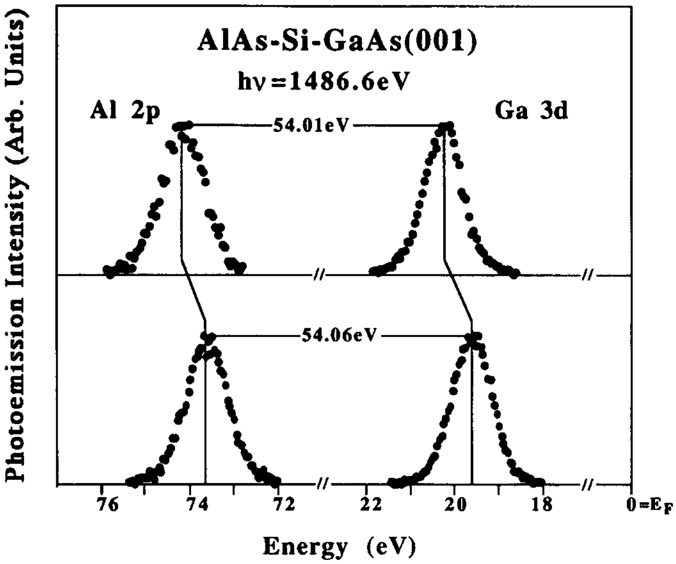

Fig. 46. Al 2p and Ga 3d core emission from two representative AlAs–Si–GaAs(001) heterostructures with a Si layer thickness of 0.5 ML. The zero of the energy scale is at the position of the Fermi level. A variation of 0.6 eV in band bending is observed as a rigid shift of the core levels that does not affect the core separation within experimental uncertainty [Franciosi et al., 1993].

one sample to the other. Correspondingly, the core level separation and width remains unchanged, indicating that Fermi level pinning near midgap at the surface and near the conduction-band minimum in the substrate is not the cause of the Si-induced low value of ΔE_{cl} (i.e., low valence-band offsets) observed in Figs. 40 and 45. Since the change in band bending in Fig. 46 does not affect ΔE_{cl}, the variation in band bending on the scale of the photoemission sampling depth is negligible, i.e., the Debye length is still longer than the escape depth.

As far as the escape depth dependence of ΔE_{cl} is concerned, Fig. 47 shows the core emission from a GaAs–Si–AlAs(001) structure as a function of the average photoelectron take-off angle θ. As expected, the Al 2p substrate emission is dramatically attenuated at grazing incidence, because of the $\cos(\theta)$ dependence of the photoelectron sampling depth. The core separation ΔE_{cl} and the width of the individual core levels in Fig. 47 are remarkably independent of θ, however, indicating that band bending is negligible over the photoemission sampling depth.

The internal photoemission results discussed in Section 5.5.3 for GaAs–Si–GaAs(001) homojunctions [Dell'Orto et al., 1994, 1995], which yielded similar band offsets for the n-on-p and p-on-n configurations of the buried heterojunctions, and consistent with those determined by photoemission spectroscopy on thin overlayers [Margaritondo, 1993; Marsi et al., 1993], also argue strongly against the presence of an extended doping dipole, as opposed to an interface local dipole (see Section 5.5.3) to explain the photoemission results.

Finally, we note that for the picture in Fig. 44 to work, all of the Si atoms deposited at the interface should outdiffuse in the overlayer and act as donors (unity activation). In fact, the Si coverages that correspond to full self-compensation of Si δ-doped layers in GaAs (see Fig. 11) are comparable to

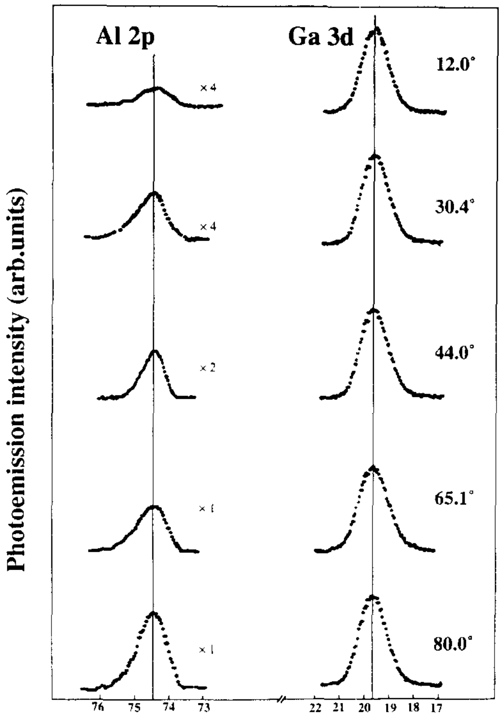

Fig. 47. Al 2p and Ga 3d core emission from a GaAs–Si–AlAs(001) heterostructure comprised of a 0.5 ML Si interface layer and a 15Å-thick GaAs overlayer. The different spectra (top to bottom) show the effect of increasing the average photoelectron collection angle from 12° to 80° relative to the sample surface. The Al 2p substrate emission is dramatically attenuated at small angles (top) due to the decrease in the effective photoemission sampling depth. Core separation and individual core widths are not affected [Franciosi et al., 1993].

those at which the Si interlayer is seen to affect the band offsets, and about two orders of magnitude higher than those employed in technology for maximum δ-doping [Ashwin et al., 1993]. The message seems clear enough. Band offset changes are observed when self-compensation sets in, i.e., when δ-doping becomes ineffective. Conversely, the conditions that maximize δ-doping (i.e., give minimum self-compensation) correspond to no band offset change. There might instead be a connection between self-compensation, i.e., the formation of acceptor-like defect that compensate $\mathrm{Si_{Ga}}$ impurities, and the establishment of a local interface dipole (see Section 5.5.2).

As far as the possibility that the situation outlined in Fig. 44 might be relevant to other heterojunction or homojunction systems, there is little direct information available, but it should be considered unlikely based on the following considerations. First, Si outdiffusion should be enhanced by temperature, which is also known to delay the onset of self-compensation [Ashwin et al., 1993]. For heterojunctions or homojunctions grown at room temperature, as are the majority of those discussed in Sections 5.4 and 5.5.3, Si outdiffusion should be suppressed, and the onset for self-compensation lowered. However, changes in band offsets of direction and magnitude consistent with the AlAs–Si–GaAs case are observed in all such systems, suggesting that the establishment of an anomalous Debye length in the overlayer is not a problem in any of these systems. Second, if one examines the systematics of AlAs–Si(Ge)–GaAs, GaAs–Si(Ge)–AlAs, Ge–GaAs–Ge, etc., heterostructures, a picture in which the Fermi level at the surface is pinned near the overlayer mid-gap at the surface, and near the conduction-band minimum in the substrate would predict apparent offset modifications of magnitude that would reflect the overlayer bandgap. This is not the case, as similar band offset changes are observed in all cases (e.g. AlAs–Ge–GaAs and Ge–GaP–Ge).

5.5.5. *Heterovalent interlayers in II–VI/III–V heterojunctions*

Prior to the theoretical developments presented in Section 4.2, few experimental studies had addressed the issue of transitivity and commutativity of the band offsets in II–VI/III–V junctions. Yu et al. conducted detailed systematic studies of ZnTe–GaSb(001), AlSb–GaSb(001), GaSb–AlSb(001), and ZnTe–AlSb(001) heterostructures fabricated by MBE. All structures were grown on GaSb(001) wafers, with III–V buffer layers grown at 475°C (GaSb) or 530°C (AlSb) with 1 × 3 RHEED pattern, and the ZnTe epilayers grown at 270–330°C with 2 × 1 RHEED pattern. Using monochromatic XPS in situ, the authors determined the band offsets without any strain-related correction, the in-plane mismatch being only 0.1% for ZnSe–GaSb, 0.6% for ZnTe–AlSb, and 0.7% for AlSb–GaSb. Yu et al. reported $\Delta E_v = +0.60 \pm 0.07$ and $+0.42 \pm 0.03$ eV for ZnTe–GaSb(001) and ZnTe–AlSb(001) heterojunctions, while for AlSb–GaSb they found commutativity to be satisfied, with $\Delta E_v = 0.39 \pm 0.07$ eV. Based on such measurements for individual, isolated interfaces, Yu et al. reported a 0.21 ± 0.05 eV deviation from transitivity of the offsets, and tentatively associated this effect with the chemistry of the II–VI/III–V interfaces.

In the last couple of years, there has been a substantial renewed interest in the properties of II–VI/III–V heterostructures, due to the fact that most blue and blue–green laser diodes demonstrated to date exploit II–VI active layers grown by MBE on III–V substrates. The remarkable progress which has been recently achieved [Gaines et al., 1993; Haase et al., 1993; Nakayama et al., 1993] toward the realization of emitters operating at room temperature has been mainly due to the reduction or the elimination of bulk material problems, such as the lattice mismatch between the II–VI epilayers and the GaAs(001) substrate, which has been eliminated with the implementation of $Zn_{1-x}Mg_xSe_{1-y}S_y$ alloys lattice-matched to the substrate [Okuyama et al., 1992; Ukita et al., 1993; Petruzzello et al., 1994], or the lack of a viable p-type doping technology for ZnSe-based materials, which has been addressed with the use of nitrogen plasma sources [Qiu et al., 1991b; Yang et al., 1992; Petruzzello et al., 1993; Mensz et al., 1993; Okuyama et al., 1994]. The remaining material issues that still hinder the development of a viable technology are predominantly interface-related [Franciosi et al., 1994].

The formation of dark-line defects during cw operation at room temperature of pseudomorphic laser structures has been associated with stacking faults at the ZnSe/GaAs or $ZnSe_{1-y}S_y$/GaAs interface. Such defects would propagate through the structure during growth, and generate dislocation sources within the strained $Zn_{1-x}Cd_xSe$ active layers [Guha et al., 1993a,b]. The existence of a large valence-band offset and a depletion region at the ZnSe/GaAs interface hinders hole injection, and lowers the efficiency of the overall device [Qiu et al., 1990; Cavenett et al., 1995]. Finally, the problem of obtaining ohmic contacts to p-type, wide-gap, II–VI materials has been solved only in part with the exploitation of perpendicular transport in modulation-doped ZnTe–ZnSe superlattices [Fan et al., 1993; Hiei et al., 1993], which involve a large lattice mismatch and high defect densities, and remains a main possible culprit of the observed high current thresholds and short device lifetime.

The possibility of tuning the properties of II–VI/III–V heterojunctions with the methods outlined in the previous sections is therefore of an obvious practical interest. In fact, we feel that this is one of the areas in which heterojunction band offset engineering may have the highest impact in the near future. In view of the good lattice match between ZnSe, Ge, and GaAs, and of the reported deviations of the Ge–GaAs band offsets from commutativity and transitivity for both (001) and (110) orientations (see Section 5.2.2 and 5.2.3), several studies have focused on the use of Ge interlayers in ZnSe–GaAs junctions.

Vanzetti et al. have fabricated epitaxial ZnSe/Ge/GaAs(110) heterostructures at room temperature on substrates cleaved in situ [Vanzetti et al., 1992]. Representative RHEED results are illustrated in Fig. 26. Upon deposition of 2 ML of Ge at RT, the sharp 1 × 1 RHEED pattern of the initial GaAs(110) surface disappeared, but further deposition of ZnSe yielded a surprisingly prompt recovery of the long-range order. Deposition of 30 Å [Fig. 26(e)] and 100 Å [Fig. 26(f)] of ZnSe at RT on the Ge(2ML)–GaAs(110) interface examined in Fig. 26(d) yields an increasingly well defined 1 × 1 RHEED pattern. Diffraction spots derive from the presence of three-dimensional ZnSe islands at the surface, and remain visible even at the largest ZnSe coverages explored (~ 200 Å) [Vanzetti et al., 1992; Bratina et al., 1993b].

The effect of Ge interface layers on the ZnSe–GaAs(110) valence-band offset was examined by Vanzetti et al. by XPS using the interface separation ΔE_{cl} of the Zn $2p_{3/2}$ and Ga $2p_{3/2}$ core levels as a function of Ge coverage, for ZnSe overlayer thicknesses in the 10–20 Å range. In Fig. 48, the interface core level separation ΔE_{cl} (rightmost vertical axis) and the corresponding values of ΔE_{v} (leftmost vertical axis) are plotted as a function of Ge interface layer thickness in ångströms (bottom-most horizontal axis) and monolayers (topmost horizontal axis). In the presence of a Ge interface layer, the valence-band offset is seen to decrease gradually with increasing Ge layer thickness in the 0.3–4.0 ML range, and saturate in the 4–6 ML range. The corresponding decrease in the valence-band offset for ZnSe–Ge–GaAs(110) relative to ZnSe–GaAs(110), is 0.17 ± 0.05 eV.

Ge interface layers in ZnSe–GaAs(001) heterostructures were obtained by Bratina et al. [Bratina et al., 1993a,b] by MBE depositing pseudomorphic Ge layers under As flux at 360°C on GaAs(001)2 × 4. The layers exhibited a 2 × 2 reconstruction at all coverages above 2 ML and grew in the layer by layer growth mode. Epitaxial ZnSe overlayers were grown at 290°C with BPR = 1 and a mixed c(2 × 2)–2 × 1 RHEED pattern. Fig. 49 summarizes the effect of the pseudomorphic Ge interlayer on the valence-band offset as determined in situ by monochromatic XPS. The valence-band offset is seen to decrease monotonically with Ge coverage in the 1–6 ML range and saturate for higher Ge thicknesses. The minimum measured value of the valence-band offset for the engineered interface was 0.43–0.48 eV, i.e., 42–45% lower than the offset of the (100) oriented heterostructure synthesized at 290–320°C with BPR = 1 without a Ge interlayer [Bratina et al., 1993a,b].

Although pseudomorphic Ge (and Si) interface layers also cause a decrease of ~ 0.4 eV in the valence-band offset of AlAs–GaAs(100) heterojunctions and GaAs–GaAs homojunctions (see Sections 5.5.2 and 5.5.3), the dependence of the magnitude of the dipole on interlayer thickness is widely different in the two cases. In III–V/III–V(100) systems, the maximum offset reduction was observed at submonolayer group IV coverage, while for ZnSe–GaAs(100) and ZnSe–GaAs(110) junctions an interlayer ~ 6 ML thick is required to achieve the minimum valence-band offset.

The observed analogies and differences between ZnSe–Ge–GaAs(110) and ZnSe–Ge–GaAs(001) interfaces will represent a major challenge to quantitative theoretical models. The effect of Ge interface layers on the ZnSe–GaAs band offsets in (110)- and (001)-oriented interfaces is similar, in

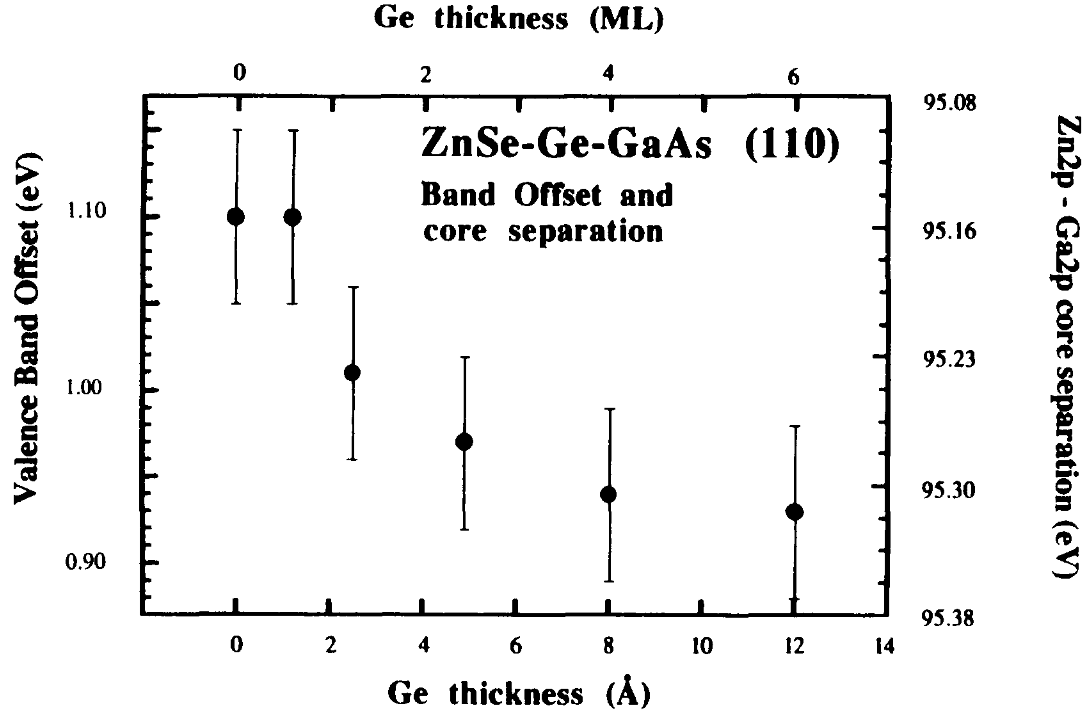

Fig. 48. XPS determined valence-band offset for ZnSe–Ge–GaAs(110) epitaxial heterojunctions grown at room temperature (RT). The energy separation of the Zn $2p_{3/2}$ and Ga $2p_{3/2}$ core levels (rightmost vertical axis) was converted in valence-band offset values for the engineered interface (leftmost vertical axis) using the value of the offset for ZnSe–GaAs (110) junctions grown by RT MBE (1.10 ± 0.05 eV). The error bars reflect the uncertainty in the numercial value of the offset (leftmost vertical axis) for each interface rather the smaller uncertainty on the variation of the offset from the no-interlayer case. Since such a variation can be gauged directly from the *variation* in core separation (rightmost vertical axis), the corresponding uncertainty is comparatively smaller (0.05 eV) [Vanzetti et al., 1992].

that a reduction in ΔE_v is observed with increasing Ge layer thickness in both cases, and the effect saturates for a Ge thickness of about 6 ML [Vanzetti et al., 1992]. However, the maximum Ge-induced change in the offset is exactly twice as large in (001)-oriented interfaces (0.34 ± 0.03 eV, [Bratina et al., 1993a,b]) as compared to (110)-oriented interfaces (0.17 ± 0.05 eV). We caution the reader that, in addition to the different interface orientations, there were also substantial differences in the growth parameters employed. First, (110)-oriented heterostructures were obtained at RT, while (001)-oriented heterostructures were fabricated at higher temperatures (360°C for the Ge interlayer and 290–320°C for the ZnSe overlayer [Vanzetti et al., 1992]). Secondly, the Ge interface layer showed no detectable RHEED pattern when grown on GaAs(110) at RT, while a clear 2 × 2 pattern was observed following Ge growth at 360°C under As flux on GaAs(001).

For the (001)-oriented interface, Bratina et al. observed that the reduction in the valence-band offset (0.34 ± 0.03 eV) that could be achieved through the fabrication of thin interface layers of pseudomorphic Ge is consistent in sign and magnitude with the deviation from the transitivity rule (0.37 ± 0.09 eV) reported for ZnSe–Ge(001), Ge–GaAs(001) and ZnSe–GaAs(001) neutral isolated

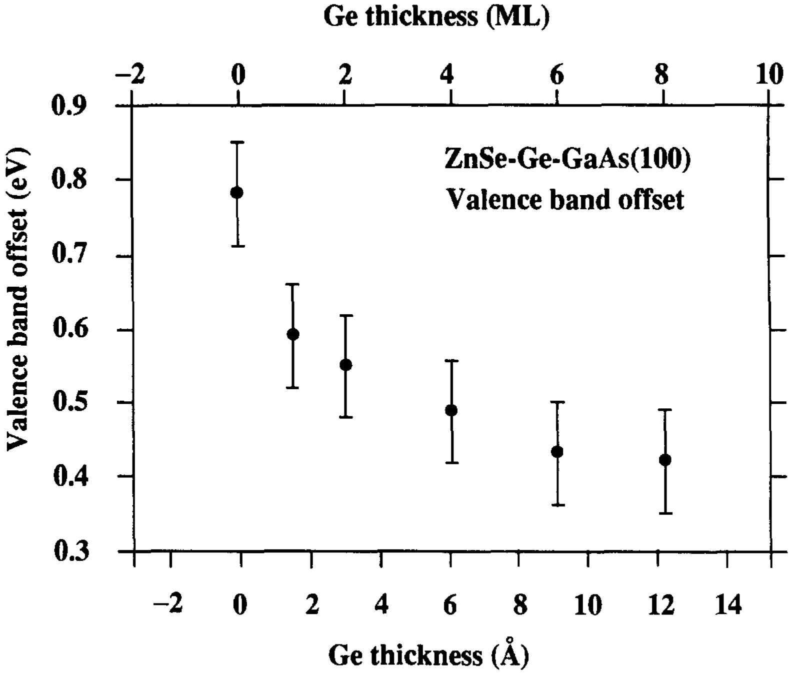

Fig. 49. Monochromatic XPS measurements of the valence-band offset for ZnSe–Ge–GaAs(100) as a function of the thickness of the Ge interface layer. The energy separation of the Ga 3d and Zn 3d core levels was converted in valence-band offset values for the engineered interface using the value of the offset for ZnSe–GaAs(001) junctions grown by MBE in identical growth conditions (0.78–0.83 eV). Analogous results were obtained measuring the Ga 3d–Se 3d and the As 3d–Zn 3d core level emission [Bratina et al., 1993b].

heterojunctions grown in analogous growth conditions [Bratina et al., 1994]. The authors proposed that this deviation may reflect the presence of Ge-induced interface dipoles of different magnitudes at the ZnSe–Ge and ZnSe–GaAs interfaces (see Sections 4.2 and 5.2.3), and cause the observed offset reduction.

In comparing ZnSe–Ge–GaAs(110) and ZnSe–Ge–GaAs(001) heterojunctions, Bratina et al. [Bratina et al., 1993b] suggested that any attempt to explain the different band offsets should focus primarily on the character of the ZnSe–Ge interface in the two structures. This is because the Ge–GaAs(001) valence-band offset observed experimentally in their growth conditions [Biasiol et al., 1992; Sorba et al., 1993b] was 0.54 ± 0.05 eV, i.e., identical to that reported for Ge–GaAs(110) interfaces in comparable growth conditions (0.55 ± 0.03 eV [Grant et al., 1985]), and close to the value predicted by LRT for an ideally abrupt (110)-oriented interface.

For ZnSe–Ge–GaAs(110) interfaces formed at RT, the presence of an equally abrupt ZnSe–Ge(110) interface would obviously not explain the Ge-induced decrease in valence-band offsets in Fig. 48, since it would give rise to offsets that follow the predictions of the transitivity rule, i.e., $\Delta E_v = 1.11$ eV. The effect of Ge could be explained in the atomic swaps picture (see Section 5.2.2, and [Baldereschi et al., 1993a]) if a series of Ge–Se swaps occur at the ZnSe–Ge interface, lowering the bands of Ge relative to those of ZnSe. The swaps would produce mixed $ZnGe_xSe_{1-x}$ and

$Ge_{2-x}Se_x$ adjacent planes across the interface. For ZnSe–Ge–GaAs(001) the Ge-induced reduction in the offset would also be consistent [Bratina et al., 1994] with the formation of a mixed Ge–Se plane at the ZnSe–Ge interface. The mixed Ge–Se interface plane would occur between the Ge-terminated interlayer and the Zn-initiated overlayer, and yield a neutral ZnSe–Ge interface with a valence-band offset of relatively small magnitude [Bratina et al., 1994].

In summary, both interface configurations could be thought as originating from a first interface formation stage involving Ge–anion swaps [Baldereschi et al., 1993a]. The similar defect formation mechanism would therefore be the common element to explain the analogy in the results of Figs. 48 and 49. However, we see no obvious reason why in the above theoretical models the number of swaps occurring at a (110)-oriented interface should saturate when a local interface dipole exactly half as large as that encountered for (001)-oriented interfaces is achieved. We imply no criticism to the available theoretical models. The problem resides with the wide variety of possible microscopic configurations that may correspond to a given offset, and the kinetic aspects of interface formation.

6. Conclusions

6.1. The present situation

There is by now a substantial experimental systematics that supports the concept of *tunable* band discontinuities in semiconductor heterojunctions. The remarkable progress achieved by theory in identifying heterovalent heterojunctions as the most promising interfaces in this area, and in providing a microscopic rationale for the observed tunability range of the offsets is being exploited to identify the most promising avenues for experimental investigation. These developments are providing a conceptual framework in which interfacial engineering can develop. However, truly predictive capabilities are still out of reach.

For example, while the prediction that isovalent heterojunctions should exhibit discontinuities which reflect the bulk properties of the two semiconductor constituents seems well verified in practice, the available experimental results show at best a blurred distinction between the properties of heterovalent heterojunctions with polar orientation, and those with nonpolar orientation. Deviations from commutativity and transitivity have been reported for not only heterovalent heterojunctions with polar orientation, but also for (110)-oriented interfaces. Heterovalent semiconductor interlayers have been shown to induce offset changes in heterojunctions and homojunctions with both types of orientation. The magnitude of the observed changes in the offsets does not appear dramatically different in (001), (111) and (110)-oriented interfaces.

Experiments on thick pseudomorphic interlayers seem to indicate quite clearly that, at least in this limit, the offset changes are due to the presence of individual neutral interfaces with inequivalent microscopic environments as opposed to charged interfaces with opposite polarities. This is indeed what is predicted based on energetics. However, one frequently observes a maximum offset change for submonolayer coverages, which saturates or even decreases with increasing interlayer thickness. Although the establishment of inequivalent neutral interfaces can explain remarkably well the observed saturation of the offset change at high interlayer thickness, it cannot explain per se the occurrence of *larger* deviations from the transitivity rule at lower interlayer thicknesses. The possibility of a gradual transition from charged to inequivalent neutral interfaces with increasing interlayer thickness, as a result of the gradual formation of an increasing number of point defects at the interface, is difficult to prove or disprove experimentally.

Finally, the existence of an infinite number of possible interface configurations that would lead to neutral interfaces, and in principle correspond to a wide range of band offsets, implies that given almost any experimental result about the band alignment, one can find a suitable configuration giving rise to a theoretical offset in agreement with experiment. This, however, is no guarantee that the selected configuration is appropriate to describe the actual interface, and, in turn, makes *true* predictions difficult or impossible.

6.2. *Outlook and future directions*

How do we predict and control the band-lineup? What is the likelihood of actually achieving the theoretical atomic structure that will produce a desired dipole at an interface? Entropy argues against the stability of many such structures [Martin, 1989], since obtaining the dipole depends on achieving a certain degree of ordering at the interface; entropy would be increased if mixed structures are formed. Also, the presence of dipoles is likely to increase the electrostatic energy, as compared to a nonpolar structure. Driving forces away from the ordered structures thus exist; however, even if the final structure would only be partially ordered, a significant dipole could remain.

On the theoretical side, the main focus should be on determining which structures can actually be achieved, given thermodynamic and/or kinetic limitations. Most first-principles calculations so far have *assumed* one or the other of a small set of specific geometries, and produced a band-lineup value for those geometries. These results are very valuable, and have already taught us a lot about the interplay between atomic and electronic structure. However, the major challenge for theory in the near future will be to *calculate* (as opposed to *assume*) the geometries and interfacial structures. This type of investigation is a lot more demanding, since total-energy calculations have to be carried out for a large number of possible configurations. Some work along these lines has already been performed: e.g., investigations of GaAs on Si(111) by Northrup et al. [Northrup et al., 1988], Ge interdiffusion at III–V homojunctions by Rodriguez-Hernandez and Muñoz [Rodriguez-Hernandez and Muñoz, 1993] (see Section 4.2.5), ZnSe/GaAs(001) energetics by Kley and Neugebauer [Kley and Neugebauer, 1994], and studies of interface stability by Laks and Zunger [Laks and Zunger, 1992] and strain-induced interdiffusion by Dandrea and Duke [Dandrea and Duke, 1992]. In studies of this kind it will be important not just to calculate total energies, but to construct a thermodynamic formalism using formation energies and chemical potentials, recognizing that the details of the microscopic structure may depend on the growth conditions [Lambrecht et al., 1992; Chetty et al., 1992].

Another issue that should receive more theoretical attention is that of interface states. We mentioned in Section 4.2.2 that interface states will occur at ideal, polar, heterovalent interfaces. It is not clear yet to what extent such states will also play a role in the case of thin interlayers (microscopic capacitors), or in the case of mixed interfaces. The theoretical studies that have been performed so far for such systems have not made any mention of the issue of interface states; the only exception is the work of Saito and Ikoma [Saito and Ikoma, 1992], who found impurity-localized states in the band gap of GaAs/AlAs(001) heterostructures with a Ge interlayer. If interface states are present, they could seriously jeopardize the usefulness of these "engineered" heterojunctions for device applications [Tersoff, 1993], since interface states can act as traps for the carriers that will flow across or along the interface in an electronic device. Particular attention should therefore be paid in future theoretical studies to the presence and behavior of such interface states.

This brings us to the issue of the gap which still exists between those who are pioneering heterojunction engineering, and the microelectronic and optoelectronic device community. Undoubtedly, promising characterization tools such as ballistic electron emission microscopy, photoemission spectomicroscopy, and high resolution TEM when applied to the study of the widest possible range of heterojunction systems, offer the highest probability of clarifying the connection between local interface structure and composition, and band offsets. However, the device community is unlikely to take notice of these results until they are verified in device-grade heterostructures, by means of conventional transport techniques, and until the pioneers shed light on the connection between interface dipoles in engineered interfaces, and crucial device parameters such as the interface state density, carrier lifetime, and internal quantum efficiency. This, and the development of truly predictive theoretical capabilities, will be among the major challenges to the coming of age of heterojunction band offset engineering.

Acknowledgements

The work at the University of Minnesota was supported by the US Army Research Office under grants No. DAAH04-93-G-0206 and DAAH04-93-G-0319, and by the Center for Interfacial Engineering at the University of Minnesota under NSF grant CDR 8721551. The work in Trieste was supported by the Istituto Nazionale per la Fisica della Materia, the Area di Ricerca di Trieste, the Consiglio Nazionale delle Ricerche, and the Commission of the European Communities. One of us (A.F.) would like to thank John Zavada for his steadfast support over the years, Carlo Calandra and Fennell Evans for their help in getting interfacial engineering started on both sides of the Atlantic, and his many co-workers over the years in Minneapolis and in Trieste. In particular Alberta Bonanni, Gvido Bratina, Alan Raisanen, Lucia Sorba, and Lia Vanzetti, and the many collaborators and students that cannot be listed here. Without them, this work would have been impossible. We acknowledge valuable discussions with Alfonso Baldereschi, Stefano Baroni, Fabio Beltram, Nadia Binggeli, Len Brillson, Federico Capasso, Roberto Cingolani, Walter Harrison, Karsten Horn, Giorgio Margaritondo, Alfonso Muñoz, Chris Palmstrøm, Maria Peressi, Raffaele Resta, and Jerry Tersoff.

Appendix: Abbreviations and acronyms

APW	augmented plane wave
ARUPS	angle-resolved ultraviolet photoemission spectroscopy
BEEM	ballistic electron emission microscopy
CNL	charge neutrality level
C–V	capacitance–voltage
DID	doping interface dipoles
DOS	density of states

EDC	photoelectron energy distribution curve
HBT	heterojunction bipolar transistor
IPE	internal photoemission
I–V	current–voltage
LCAO	linear combination of atomic orbitals
LDA	local density approximation
LED	light emitting diode
LEED	low-energy electron diffraction
LMTO	linearized muffin-tin orbital
LRT	linear response theory
MBE	molecular beam epitaxy
MESFET	metal–semiconductor field effect transistor
MIGS	metal-induced gap states
MOCVD	metal-organic chemical vapor deposition
MODFET	modulation–doped field effect transistor
MOSFET	metal-oxide–semiconductor field effect transistor
MQW	multiple quantum well
MQWS	multiple quantum well structure
PLP	picosecond laser photoemission
QW	quantum well
RHEED	reflection high-energy electron diffraction
RT	room temperature
SCF	selfconsistent field
SL	superlattice
SRPES	synchrotron radiation photoemission spectroscopy
STM	scanning tunneling microscopy
TEM	transmission electron microscopy
XC	exchange and correlation
XPS	X-ray photoemission spectroscopy
XRD	X-ray diffraction
XTEM	cross-sectional transmission electron microscopy

References

Abstreiter, G., in: Molecular Beam Epitaxy and Heterostructures, Eds. L.L. Chang and K. Ploog (Nijhoff, The Hague, 1985).

Abstreiter, G., U. Prechtel, G. Weimann and V. Schlapp, Physica B 134 (1985) 433.

Adomi, K., S. Strite, H. Morkoç, Y. Nakamura and N. Otsuka, J. Appl. Phys. 69 (1991) 220.

Agawa, K., K. Hirakawa, N. Sakamoto, Y. Hashimoto and T. Ikoma, Appl. Phys. Lett. 65 (1994) 1171.

Akazawa, M., H. Hasegawa, H. Tomozawa and H. Fujikura, Jpn. J. Appl. Phys. 31 (1992) L1012.

Akinwande, T., J. Zou, M.S. Shur and A. Gopinath, IEEE Electron Device Lett. EDL-11 (1990) 332.

Aldao, C.M., I.M. Vitomirov, F. Xu and J.H. Weaver, Phys. Rev. B 40 (1989) 3711.

Anderson, R.L., Solid-State Electron. 5 (1962) 341.

Arai, K. and T. Mizutani, J. Vac. Sci. Technol. B 7 (1989) 497.

Arch, D.K., J.P. Faurie, J.-L. Staudenmann, M. Hibbs-Brenner and P. Chow, J. Vac. Sci. Technol. A 4 (1986) 2101 (a).

Arch, D.K. J.L. Staudenmann and J.P. Faurie, Appl. Phys. Lett. 48 (1986) 1588 (b).

Ashwin, M.J., M. Fahy, J.J. Harris, R.C. Newman, D.A. Sansom, R. Addinall, D.S. McPhail and V.K.M. Sharma, J. Appl. Phys. 73 (1993) 633.

Aspnes, D.E. and M. Cardona, Phys. Rev. B 17 (1978) 726.

Bachelet, G.B., D.R. Hamann and M. Schlüter, Phys. Rev. B 26 (1982) 4199.

Baldereschi, A., S. Baroni and R. Resta, Phys. Rev. Lett. 61 (1988) 734.

Baldereschi, A., R. Resta, M. Peressi, S. Baroni and K. Mäder, in: Proc. NATO Advanced Research Workshop on Physical Properties of Semiconductor Interfaces at Sub-Nanometer Scale, Ed. H.W. Salemink (Kluwer, Dordrecht, 1993) (a).

Baldereschi, A., M. Peressi, S. Baroni and R. Resta, in: Proc. Int. School of Physics "Enrico Fermi", Course CXVII, Semiconductor Superlattices and Interfaces, Eds. L. Miglio and A. Stella (Academic Press, New York, 1993) p. 59 (b).

Ballingall, J.M., C.E.C. Wood and L.F. Eastman, J. Vac. Sci. Technol. B 1 (1983) 675.

Baraff, G.A., J.A. Appelbaum and D.R. Hamann, Phys. Rev. Lett. 38 (1977) 237 (a).

Baraff, G.A., J.A. Appelbaum and D.R. Hamann, J. Vac. Sci. Technol. 14 (1977) 999 (b).

Bardeen, J. and W. Shockley, Phys. Rev. 80 (1950) 72.

Baroni, S., R. Resta and A. Baldereschi, in: Proc. 19th Int. Conf. on the Physics of Semiconductors, Ed. W. Zawadzki (Institute of Physics, Polish Academy of Sciences, Warsaw, 1988) p. 525.

Baroni, S., R. Resta, A. Baldereschi and M. Peressi, in: Spectroscopy of Semiconductor Microstructures, Eds. G. Fasol, A. Fasolino and P. Lugli (Plenum, London, 1989) p. 251.

Baroni, S., M. Peressi, R. Resta and A. Baldereschi, in: Proc. 21th Int. Conf. on the Physics of Semiconductors, Eds. Ping Jiang and Hou-Zhi Zheng (World Scientific, Singapore, 1993) p. 689.

Bass, J.M. and C.C. Matthai, Semicond. Sci. Technol. 6 (1991) 69.

Batey, J.L. and S.L. Wright, J. Appl. Phys. 59 (1986) 200.

Batson, P.E. and J.F. Morar, Appl. Phys. Lett. 59 (1991) 3285.

Bauer, R.S. and J.C. McMenamin, J. Vac. Sci. Technol. 15 (1978) 1444.

Bauer, R.S. and J.C. Mikkelsen, Jr., J. Vac. Sci. Technol. 21 (1982) 491.

Berthold, K., A.F.J. Levi, J.F. Walker and R.J. Malik, Appl. Phys. Lett. 52 (1988) 2247.

Beltram, F., F. Capasso and S. Sen, in: Electronic Materials: A New Era of Materials Science, Eds. J.R. Chelikowsky and A. Franciosi, Topics in Applied Physics Series, Vol. 95 (Springer, Berlin, 1991) p. 233.

Berroir, J.M., Y. Guldner, J.P. Vieren, M. Voos and J.P. Faurie, Phys. Rev. B 34 (1986) 891 (a).

Berroir, J.M., Y. Guldner, and M. Voos, IEEE J. Quantum Electron. 22 (1986) 1793 (b).

Biasiol, G., L. Sorba, G. Bratina, R. Nicolini, A. Franciosi, M. Peressi, S. Baroni, R. Resta and A. Baldereschi, Phys. Rev. Lett. 69 (1992) 1283.

Blöchl, P., private communication (1993).

Bonanni, A., L. Vanzetti, L. Sorba, A. Franciosi, M. Lomascolo, P. Prete and R. Cingolani, Appl. Phys. Lett. 66 (1995) 1092.

Bouthillier, T.M., L. Young and H.Y. Tsoi, J. Appl. Phys. 54 (1983) 957.

Brandt, O., G.E. Crook, K. Ploog, J. Wagner and M. Maier, Appl. Phys. Lett. 59 (1991) 2732.

Bratina, G., L. Sorba, A. Antonini, L. Vanzetti and A. Franciosi, J. Vac. Sci. Technol. B 9 (1991) 2225.

Bratina, G., L. Sorba, A. Antonini, G. Biasiol and A. Franciosi, Phys. Rev. B 45 (1992) 4528.

Bratina, G., L. Vanzetti, R. Nicolini, L. Sorba, X. Yu, A. Franciosi, G. Mula and A. Mura, Physica B 185 (1993) 557 (a).

Bratina, G., R. Nicolini, L. Sorba, L. Vanzetti, G. Mula, X. Yu and A. Franciosi, J. Cryst. Growth 127 (1993) 387 (b), and unpublished.

Bratina, G., L. Vanzetti, L. Sorba, G. Biasiol, A. Franciosi, M. Peressi and S. Baroni, Phys. Rev. B 50 (1994) 11723.

Brillson, L.J., Surf. Sci. Rep. 2 (1982) 123.

Brillson, L.J., in: Handbook on Semiconductors, Vol. I, Ed. P.T. Landsberg (North-Holland, Amsterdam, 1992) p. 281.

Bringans, R.D., M.A. Olmstead, R.I.G. Uhrberg and R.Z. Bachrach, Phys. Rev. B 34 (1986) 191.

Bringans, R.D., M.A. Olmstead, F.A. Ponce, D.K. Biegelsen, B.S. Krusor and R.D. Yingling, J. Appl. Phys. 64 (1988) 3472.

Bringans, R.D., D.K. Biegelsen, L.-E. Swartz, F.A. Ponce and J.C. Tramontana, Phys. Rev. B 45 (1992) 13400.

Bylander, D.M. and L. Kleinman, Phys. Rev. Lett. 59 (1987) 2091.

Bylander, D.M. and L. Kleinman, Phys. Rev. B 38 (1988) 7480 (a).

Bylander, D.M. and L. Kleinman, Phys. Rev. Lett. 60 (1988) 472 (b).

Bylander, D.M. and L. Kleinman, Phys. Rev. B 39 (1989) 5116.

Bylander, D.M. and L. Kleinman, Phys. Rev. B 41 (1990) 3509.
Cantile, M., L. Sorba, S. Yildirim, P. Faraci, G. Biasiol, A. Franciosi, T.J. Miller and M.I. Nathan, Appl. Phys. Lett. 64 (1994) 988 (a), and references therein.
Cantile, M., L. Sorba, P. Faraci, S. Yildirim, G. Biasiol, G. Bratina, A. Franciosi, T.J. Miller, M.I. Nathan and L. Tapfer, J. Vac. Sci. Technol. B 12 (1994) 2653 (b).
Capasso, F., A.Y. Cho, K. Mohammed and P.W. Foy, Appl. Phys. Lett. 46 (1985) 664 (a).
Capasso, F., K. Mohammed and A.Y. Cho, J. Vac. Sci. Technol. B 3 (1985) 1245 (b).
Capasso, F. and G. Margaritondo, Eds., Heterojuction Band Discontinuities: Physics and Device Applications (North-Holland, Amsterdam, 1987).
Capasso, F., Science 235 (1987) 172.
Capasso, F., G. Ripamonti, A.L. Hutchinson, D.J. Meuhlner, J.F. Walker and R.J. Malik, IEDM Tech. Dig. (1988) 902, 491.
Capasso, F., Mater. Res. Soc. Bull. 16 (1991) 23.
Capasso, F., Appl. Surf. Sci. 75 (1994) 1.
Carey, G.P., D.J. Friedman, A.K. Wahi, C.K. Shih and W.E. Spicer, J. Vac. Sci. Technol. A 6 (1988) 2736.
Carver, J.C., R.C. Gray and D.M. Hercules, J. Am. Chem. Soc. 96 (1984) 6851.
Cavenett, B.C., Mater. Sci. Forum 182–184 (1995) 5.
Ceccone, G., G. Bratina, L. Sorba, A. Antonini and A. Franciosi, Surf. Sci. 251/252 (1991) 82.
Chambers, S.A. and T.J. Irwin, Phys. Rev. B 38 (1988) 7484.
Chambers, S.A. and V.A. Loebs, J. Vac. Sci. Technol. A 8 (1990) 2074.
Chambers, S.A. and V.A. Loebs, Phys. Rev. B 47 (1993) 9513.
Chen, A.-B., A. Sher and W.E. Spicer, J. Vac. Sci. Technol. A 1 (1983) 1675.
Chen, Y., A. Freundlich, H. Kamada and G. Neu, Appl. Phys. Lett. 54 (1989) 45.
Cheng, B., J.M. De Puydt, J.E. Potts, S.K. Mohapatra and T.L. Smith, Proc. SPIE 796 (1987) 91.
Chetty, N. and R.M. Martin, Phys. Rev. B 45 (1992) 6089.
Chow, D.H., J.O. McCaldin, A.R. Bounefoi, T.C. McGill, I.K. Sou, J.P. Faurie, F.A. Shirland and O.K. Wu, J. Vac. Sci. Technol. A 6 (1988) 2614.
Christensen, N.E., Phys. Rev. B 37 (1988) 4528, and references therein.
Christensen, N.E. and L. Brey, Phys. Rev. B 38 (1988) 8185.
Cirillo, Jr., N.C., M. Shur, P.J. Vold, J.K. Abrokwah, R.R. Daniels and O.N. Tufte, IEEE Trans. Electron Devices EDL-6 (1986) 645.
Colak, S., T. Marshall and D. Cammack, Solid State Electron. 32 (1989) 647.
Coluzza, C., E. Tuncel, J.-L. Staehli, P.A. Baudat, G. Margaritondo, J.T. McKinley, A. Ueda, A.V. Barnes, R.G. Albridge, N.H. Tolk, D. Martin, F. Morier-Genoud, C. Dupuy, A. Rudra and M. Ilegems, Phys. Rev. B 46 (1992) 12834 (a).
Coluzza, C., G. Margaritondo, A. Neglia and R. Carluccio, J. Vac. Sci. Technol. A 10 (1992) 744 (b).
Copel, M., M.C. Reuter, E. Kaxiras and R.M. Tromp, Phys. Rev. Lett. 63 (1989) 632.
Costa, J.C., F. Williamson, T.J. Miller, K. Beyzavi, M.I. Nathan, D.S.L. Mui, S. Strite and H. Morkoç, Appl. Phys. Lett. 58 (1991) 382.
Dahmen, M., U. Rau, M. Kawanaka, J. Sone and J.H. Werner, Appl. Phys. Lett. 62 (1993) 261.
Dandrea, R.G., S. Froyen and A. Zunger, Phys. Rev. B 42 (1990) 3213.
Dandrea, R.G. and C.B. Duke, Phys. Rev. B 45 (1992) 14065.
Dandrea, R.G., C.B. Duke and A. Zunger, J. Vac. Sci. Technol. B 10 (1992) 1744.
Dandrea, R.G. and C.B. Duke, J. Vac. Sci. Technol. B 11 (1993) 1553 (a).
Dandrea, R.G. and C.B. Duke, J. Vac. Sci. Technol. A 11 (1993) 848 (b).
Davis, G.D., Vuoto (Italy) 16 (1986) 127.
Dawson, P., K.J. Moore and C.T. Foxon, Proc. SPIE 792 (1987) 208.
Deleporte, E., J.M. Berroir, G. Bastard, C. Delalande, J.M. Hong and L.L. Chang, Phys. Rev. B 42 (1990) 5891.
Dell'Orto, T., G. De Stasio, M. Capozi, C. Ottaviani, C. Quaresima, P. Perfetti, Y. Hwu and G. Margaritondo, Phys. Rev. B 48 (1993) 8035 (a).
Dell'Orto, T., G. De Stasio, M. Capozi, C. Ottaviani, C. Quaresima and P. Perfetti, Phys. Rev. B 48 (1993) 8823 (b).
Dell'Orto, T., J. Almeida, C. Coluzza, A. Baldereschi, G. Margaritondo, M. Cantie, S. Yildirim, L. Sorba and A. Franciosi, Appl. Phys. Lett. 64 (1994) 2111.
Dell'Orto T., M. Di Ventra, J. Almeida, C. Coluzza and G. Margaritondo, Phys. Rev. B 52 (1995) R2265.

DePuydt, J.M., H. Cheng, J.E. Potts, T.L. Smith and S.K. Mohapatra, J. Appl. Phys. 62 (1987) 4756.

DePuydt, J.M., T.L. Smith, J.E. Potts, H. Cheng and S.K. Mohapatra, J. Cryst. Growth 86 (1988) 318.

Duc, T.M., C. Hsu and J.P. Faurie, Phys. Rev. Lett. 58 (1987) 1127 (a).

Duc, T.M., C. Hsu and J.P. Faurie, Phys. Rev. Lett. 59 (1987) 947 (b).

Duggan, G., in: Heterojunction Band Discontinuities: Physics and Device Applications, Eds. F. Capasso and G. Margaritondo (North-Holland, Amsterdam, 1987) ch. 5.

Duran, J.C., A. Muñoz and F. Flores, Phys. Rev. B 35 (1987) 7721.

Eglash, S., N. Newman, S. Pan, W. Spicer, D. Collins and M. Zurakowski, IEDM Tech. Dig. (1984) 119.

Eizenberg, M., M. Heiblum, M.I. Nathan, N. Braslau and P.M. Mooney, J. Appl. Phys. 61 (1987) 1516.

Enderlein, R. and W.A. Harrison, Phys. Rev. B 30 (1984) 1867.

Eppenga, R., Phys. Rev. B 40 (1989) 10402.

Fan, Y., J. Han, L. He, J. Saraie, R.L. Gunshor, M.M. Hagerott and A.V. Nurmikko, Appl. Phys. Lett. 63 (1993) 1812.

Farrell, H.H., M.C. Tamargo, J.L. De Miguel, F.S. Turco, D.M. Hwang and R.E. Nahory, J. Appl. Phys. 69 (1991) 7021.

Fasolino, A., E. Molinari and J.C. Maan, Phys. Rev. B 39 (1989) 3923.

Faurie, J.P., A. Million and J. Piaguet, Appl. Phys. Lett. 41 (1982) 713.

Faurie, J.P., C. Hsu and T.M. Duc, J. Vac. Sci. Technol. A 5 (1987) 3074.

Fitzgerald, E.A., Y.-H. Xie, D. Monroe, P.J. Silverman, J.M. Kuo, A.R. Kortan, F.A. Thiel and B.E. Weir, J. Vac. Sci. Technol. B 10 (1992) 1807.

Flores, F., A. Muñoz and J.C. Duran, Appl. Surf. Sci. 41/42 (1989) 144.

Flores, F., R. Perez, R. Rincon and R. Saiz-Pardo, Phil. Trans. 344 (1993) 567.

Forrest, S.R., in: Heterojunction Band Discountinuities: Physics and Device Applications, Eds. F. Capasso and G. Margaritondo (North-Holland, Amsterdam, 1987) ch. 8.

Fountain, G.G., S.V. Hattangady, D.J. Vitkavage, R.A. Rudder and R.J. Markunas, Electron. Lett. 24 (1988) 1134.

Fowler, R.H., Phys. Rev. B 38 (1931) 45.

Franciosi, A., L. Sorba, G. Bratina and G. Biasiol, J. Vac. Sci. Technol. B 11 (1993) 1628.

Franciosi, A., L. Vanzetti, A. Bonanni, L. Sorba, G. Bratina and G. Biasiol, in: II-VI Blue/Green Laser Diodes, Eds. R.L. Gunshor and A.V. Nurmikko, Proc. SPIE 2346 (1994) 100.

Freeouf, J.L. and J.M. Woodall, Surf. Sci. 168 (1986) 518.

Freeouf, J.L., D.A. Buchanan, S.L. Wright, T.N. Jackson and B. Robinson, Appl. Phys. Lett. 57 (1990) 1919 (a).

Freeouf, J.L., D.A. Buchanan, S.L. Wright, T.N. Jackson, J. Batey, B. Robinson, A. Callegari, A. Paccagnella and J.M. Woodall, J. Vac. Sci. Technol. B 8 (1990) 860 (b).

Frensley, W.R. and H. Kroemer, Phys. Rev. B 16 (1977) 2642.

Freundlich, A., J.C. Grenet, G. Neu, A. Leycuras and C. Verie, Appl. Phys. Lett. 52 (1988) 1976.

Furdyna, J.K., J. Appl. Phys. 64 (1988) R29.

Furdyna J.K. and J. Kossut, Eds., Diluted Magnetic Semiconductors, Vol. 25 of Semiconductors and Semimetals (Academic Press, New York, 1988).

Gaines, J.M., R.R. Drenten, K.W. Haberern, T. Marshall, P. Mensz and J. Petruzzello, Appl. Phys. Lett. 62 (1993) 2462.

Gillespie, H.J., G.E. Crook and R.J. Matyi, Appl. Phys. Lett. 60 (1992) 721.

Gozzo, F., C. Coluzza, G. Margaritondo and F. Flores, Solid State Commun. 81 (1992) 553.

Gozzo, F., H. Berger, I.R. Collins, G. Margaritondo, W. Ng, A.K. Ray-Chaudhuri, S. Liang, S. Singh and F. Cerrina, Phys. Rev. B 51 (1995) 5024.

Grant, R.W., J.R. Waldrop, S.P. Kowalczyk and E.A. Kraut, J. Vac. Sci. Technol. B 3 (1985) 1295.

Grant, R.W., J.R. Waldrop, E.A. Kraut and W.A. Harrison, J. Vac. Sci. Technol. B 8 (1990) 736.

Grunthaner, F.J. and P.J. Grunthaner, Mater. Sci. Rep. 1 (1986) 65.

Gualtieri, G.J., G.P. Schwartz, R.G. Nuzzo and W.A. Sunder, Appl. Phys. Lett. 49 (1986) 1037.

Gualtieri, G.J., G.P. Schwartz, R.G. Nuzzo, R.J. Malik and J.F. Walker, J. Appl. Phys. 61 (1987) 5337.

Guha, S., J.M. DePuydt, J. Qiu, G.E. Höfler, M.A. Haase, B.J. Wu and H. Cheng, Appl. Phys. Lett. 63 (1993) 3023 (a).

Guha, S., J.M. DePuydt, M.A. Haase, J. Qiu and H. Cheng, Appl. Phys. Lett. 63, (1993) 3107 (b).

Guldner, Y., G. Bastard, J.P. Vieren, M. Voos, J.P. Faurie and A. Million, Phys. Rev. Lett. 51 (1983) 907.

Gunshor, R.L. and L.A. Kolodziejski, IEEE J. Quantum Electron. 24 (1988) 1744.

Haase, M., M.A. Emanule, S.C. Smith, J.J. Coleman and G.E. Stillman, Appl. Phys. Lett. 50 (1987) 404.

Haase, M.A., J. Qiu, J.M. DePuydt and H. Cheng, Appl. Phys. Lett. 59 (1991) 1272.

Haase, M.A., P.F. Baude, M.S. Hgedorn, J. Qiu, J.M. DePuydt, H. Cheng, S. Guha, G.E. Höfler and B.J. Wu, Appl. Phys. Lett. 63 (1993) 2315.

Haight, R. and J.A. Silberman, Appl. Phys. Lett. 57 (1990) 1548.

Hamann, D.R., M. Schlüter and C. Chiang, Phys. Rev. Lett. 43 (1979) 1494 for norm-conserving pseudopotentials.

Harrison, W.A., J. Vac. Sci. Technol. 14 (1977) 1016.

Harrison, W.A., E.A. Kraut, J.R. Waldrop and R.W. Grant, Phys. Rev. B 18 (1978) 4402.

Harrison, W.A., J. Vac. Sci. Technol. 16 (1979) 1492.

Harrison, W.A., J. Vac. Sci. Technol. A 1 (1983) 1672.

Harrison, W.A. and J. Tersoff, J. Vac. Sci. Technol. B 4 (1986) 1068.

Harrison, W.A., J. Vac. Sci. Technol. B 6 (1988) 1295.

Harrison, W.A. and E.A. Kraut, Phys. Rev. B 37 (1988) 8244.

Harrison, W.A., W.J. Walecki, A.V. Nurmikko, N. Samarth, H. Luo, J.K. Furdyna and N. Otsuka, Appl. Phys. Lett. 57 (1990) 466.

Hasegawa, H., M. Akazawa, H. Ishii and K. Matsuzaki, J. Vac. Sci. Technol. B 7 (1989) 870.

Hashimoto, Y., K. Hirakawa and T. Ikoma, Appl. Phys. Lett. 57 (1990) 2555.

Hashimoto, Y., K. Hirakawa, K. Harada and T. Ikoma, J. Cryst. Growth 111 (1991) 393.

Hashimoto, Y., G. Tanaka and T. Ikoma, J. Vac. Sci. Technol. B 12 (1994) 125.

Heiblum, M., M.I. Nathan and M. Eizenberg, Appl. Phys. Lett. 47 (1985) 503.

Heiblum, M., M.I. Nathan and M. Eizenberg, Surf. Sci. 174 (1986) 312 (a).

Heiblum, M., M.I. Nathan and M. Eizenberg, Surf. Sci. 174 (1986) 318 (b).

Heinemann, M. and M. Scheffler, Appl. Surf. Sci. 56–58 (1992) 628.

Henisch, H.K., Semiconductor Contacts (Oxford, New York, 1984) p. 301.

Herman, M.A. and H. Sitter, Molecular Beam Epitaxy, Fundamentals and Current Status, Springer Series in Materials Science, Vol. 7 (Springer, Berlin, 1989), and references therein.

Hiei, F., M. Ikeda, M. Ozawa, T. Miyajima, A. Ishibashi and K. Akimoto, Electron. Lett. 29 (1993) 878.

Hirakawa, K., Y. Hashimoto and T. Ikoma, Appl. Phys. Lett. 57 (1990) 2555.

Hirakawa, K., Y. Hashimoto, K. Harada and T. Ikoma, Phys. Rev. B 44 (1991) 1734.

Hohenberg, P. and W. Kohn, Phys. Rev. 136 (1964) B864.

Huang, Y., P.Y. Yu, M.N. Charasse, Y. Lo and S. Wang, Appl. Phys. Lett. 51 (1987) 192.

Hwang, J., P. Pianetta, G.D. Kubiak, R.H. Stulen, C.K. Shih, Y.-C. Pao, P.A.P. Lindberg and R. Chow, J. Vac. Sci. Technol. B 6 (1988) 1234.

Hwang, J., P. Pianetta, C.K. Shih, W.E. Spicer, Y.-C. Pao and J.S. Harris, Jr., Appl. Phys. Lett. 51 (1987) 1632.

Hybertsen, M.S., J. Vac. Sci. Technol. B 8 (1990) 773 (a).

Hybertsen, M.S., Phys. Rev. Lett. 64 (1990) 55 (b).

Hybertsen, M.S., private communication (1991).

Ihm, J., A. Zunger and M.L. Cohen, J. Phys. C 12 (1979) 4409.

Ihm J. and M.L. Cohen, Phys. Rev. B 20 (1979) 729.

Jeon, H., J. Ding, W. Patterson, A.V. Nurmikko, W. Xie, D.C. Grillo, M. Kobayashi and R.L. Gunshor, Appl. Phys. Lett. 59 (1991) 3619.

Johnson, N.F., P.M. Hui and H. Ehrenreich, Phys. Rev. Lett. 61 (1988) 1993.

Jusserand, B. and M. Cardona, in: Light Scattering in Solids V, Eds. M. Cardona and G. Güntherodt (Springer, Berlin, 1989) p. 49.

Kahn, A., C.R. Bonapace, C.B. Duke and A. Paton, J. Vac. Sci. Technol. B 1 (1983) 613.

Kaiser, W.J., M.H. Hecht, R.W. Fathauer, L.D. Bell, E.Y. Lee and L.C. Davis, Phys. Rev. B 44 (1991) 6549.

Kane, E., Phys. Rev. 147 (1966) 335.

Kassel, L., J.W. Garland, P.M. Raccah, M.A. Haase and H. Cheng, Semicond. Sci. Technol. 6 (1991) A146 (a).

Kassel, L., J.W. Garland, P.M. Raccah, M.C. Tamargo and H.H. Farrel, Semicond. Sci. Technol. 6 (1991) A152 (b), and references therein.

Katnani, A.D. and G. Margaritondo, Phys. Rev. B 28 (1983) 1944.

Katnani, A.D., P. Chiaradia, J.H.W. Sang and R.S. Bauer, J. Vac. Sci. Technol. B 2 (1984) 471.

Katnani, A.D., P. Chiaradia, J.H.W. Sang, P. Zurcher and R.S. Bauer, Phys. Rev. B 31 (1985) 2146.

Katnani, A.D. and R.S. Bauer, Phys. Rev. B 33 (1986) 1106.

Kawanaka, M. and J. Sone, J. Electron. Mater. 19 (1990) 575.

Kelly, M.K., D.W. Niles, E. Colavita, G. Margaritondo and M. Henzler, Appl. Phys. Lett. 46 (1985) 768.

Kendelewicz, T., M.D. Williams, W.G. Petro, I. Lindau and W.E. Spicer, Phys. Rev. B 31 (1985) 6503.

Kendelewicz, T., R. Cao, K. Miyano, I. Lindau and W.E. Spicer, J. Vac. Sci. Technol. B 7 (1989) 997.

Kleinman, L., Phys. Rev. B 24 (1981) 7412.

Kley, A. and J. Neugebauer, Phys. Rev. B 50 (1994) 8616.

Kohn, W. and L.J. Sham, Phys. Rev. 140 (1965) A1133.

Kowalczyk, S.P., E.A. Kraut, J.R. Waldrop and R.W. Grant, J. Vac. Sci. Technol. 21 (1982) 482. In a later paper [Waldrop et al., 1987] the same authors modified the values of the Ga 3d and Zn 3d binding energies in bulk standards. It is with such modifications that the reported valence band offsets become 1.08 ± 0.04 eV for ZnSe deposition at room temperature on GaAs(110) followed by annealing at 300°C, and 0.94 ± 0.04 eV for ZnSe deposition at 300°C.

Kowalczyk, S.P., R.W. Grant, J.R. Waldrop and E.A. Kraut, J. Vac. Sci. Technol. B 1 (1983) 684.

Kowalczyk, S.P., J.T. Cheung, E.A. Kraut and R.W. Grant, Phys. Rev. Lett. 56 (1986) 1605.

Kraut, E.A., R.W. Grant, J.R. Waldrop and S.P. Kowalczyk, Phys. Rev. Lett. 44 (1980) 1620.

Kraut, E.A., R.W. Grant, J.R. Waldrop and S.P. Kowalczyk, Phys. Rev. B 28 (1983) 1965.

Kroemer, H., in: Molecular Beam Epitaxy and Heterostructures, Eds. L.L. Chang and K. Ploog, NATO ASI Series (Nijhoff, Dordrecht, 1985), and references therein.

Kroemer, H., J. Polasko and S.J. Wright, Appl. Phys. Lett. 36 (1980) 763.

Kuech, T.F., M. Mäenpää and S.S. Lau, Appl. Phys. Lett. 39 (1981) 245.

Kunc, K. and R.M. Martin, Phys. Rev. B 24 (1981) 3445.

Kuo, L.H., L. Salamanca-Riba, B.J. Wu, J.M. DePuydt, G.M. Haugen, S. Guha and M.A. Haase, Appl. Phys. Lett. 65 (1994) 1230.

Laks, D.B. and A. Zunger, Phys. Rev. B 45 (1992) 14177.

Lambrecht, W.R. and B. Segall, Phys. Rev. B 41 (1990) 2832 (a).

Lambrecht, W.R. and B. Segall, Phys. Rev. B 41 (1990) 8353 (b).

Lambrecht, W.R., C. Amador and B. Segall, Mater. Res. Soc. Symp. Proc. 253 (1992) 381.

Landa, G., R. Carles, C. Fontaine, E. Bedel and A. Munoz-Yague, J. Appl. Phys. 66 (1989) 196.

Lastras-Martinez, A., V. Lee, J. Zehnder and P.M. Raccah, J. Vac. Sci. Technol. 21 (1982) 157.

Lee, H.P., X. Liu, H. Lin, J.S. Smith, S. Wang, Y.H. Huang, P. Yu and Y.Z. Huang, Appl. Phys. Lett. 53 (1988) 2394.

LeGoues, F.K., B.S. Meyerson and J.F. Morar, Phys. Rev. Lett. 66 (1991) 2903.

Leopold, D.J., J.G. Broerman, D.J. Peterman and M.L. Wroge, Appl. Phys. Lett. 52 (1988) 969.

Ley, L., S. Kowalczyk, R. Pollak and D.A. Shirley, Phys. Rev. Lett. 29 (1972) 1088.

Li, D., J.M. Gonsalves, N. Otsuka, J. Qiu, M. Kobayashi and R.L. Gunshor, Appl. Phys. Lett. 57 (1990) 449.

List, R.S., P.H. Mahowald, J. Woicik and W.E. Spicer, J. Vac. Sci. Technol. A 4 (1986) 1391.

List, R.S., J.C. Woicik, I. Lindau and W.E. Spicer, J. Vac. Sci. Technol. B 5 (1987) 1279.

List, R.S. and W.E. Spicer, J. Vac. Sci. Technol. B 6 (1988) 1228.

Liu, D.G., J.C. Fan, C.P. Lee, C.M. Tsai, K.H. Chang, D.C. Liou, T.L. Lee and L.J. Chen, Appl. Phys. Lett. 60 (1992) 2628.

Lucas, N., H. Zabel, H. Morkoç and H. Ünlü, Appl. Phys. Lett. 52 (1988) 2117.

Ludeke R. and A. Bauer, Phys. Scr. T 55 (1994) 90, and references therein.

Mahowald, P.H., R.S. List, W.E. Spicer, J. Woicik and P. Pianetta, J. Vac. Sci. Technol. B 3 (1985) 1252.

Mahowald, P.H., R.S. List, J. Woicik, P. Pianetta and W.E. Spicer, Phys. Rev. B 34 (1986) 7069.

Maierhofer, Ch., S. Kulkarni, M. Alonso, T. Reich and K. Horn, J. Vac. Sci. Technol. B 9 (1991) 2238.

Malik, R.J., L.M. Lunardi, J.F. Walker and R. Ryan, IEEE Electron Device Lett. EDL-9 (1988) 7.

Margaritondo, G., A.D. Katnani, N.G. Stoffel, R.R. Daniels and T.-X. Zhao, Solid State Commun. 43 (1982) 163.

Margaritondo, G. and A. Franciosi, Annu. Rev. Mater. Sci. 14 (1984) 67.

Margaritondo, G., C. Quaresima, F. Patella, F. Sette, C. Capasso, A. Savoia and P. Perfetti, J. Vac. Sci. Technol. A 2 (1984) 508.

Margaritondo, G. and P. Perfetti, in: Heterojunction Band Discontinuites: Physics and Device Applications, Eds. F. Capasso and G. Margaritondo (North-Holland, Amsterdam, 1987) ch. 2.

Margaritondo, G., J. Vac. Sci. Technol. 11 (1993) 1362.

Marsi, M., S. La Rosa, Y. Hwu, F. Gozzo, C. Coluzza, A. Baldereschi, G. Margaritondo, J.T. McKinley, S. Baroni and R. Resta, J. Appl. Phys. 71 (1992) 2048 (a).

Marsi, M., S. La Rosa, Y. Hwu and G. Margaritondo, J. Vac. Sci. Technol. A 10 (1992) 741 (b).

Marsi, M., R. Houdre', A. Rudra, M. Ilegems, F. Gozzo, C. Coluzza and G. Margaritondo, Phys. Rev. B 47 (1993) 6455.

Martin, R.M., J. Vac. Sci. Technol. 17 (1980) 978.

Martin, R.M., Band Structure Engineering in Semiconductor Microstructures, Vol. 189 of NATO Advanced Study Institute, Series B: Physics, Eds. R.A. Abram and M. Jaros (Plenum, New York, 1989).

Massidda, S., B.I. Min and A.J. Freeman, Phys. Rev. B 35 (1987) 9871, and references therein.

Matthews, J.W. and A.E. Blakeslee, J. Cryst. Growth 27 (1974) 118.

Matthews, J.W. and A.E. Blakeslee, J. Cryst. Growth 29 (1975) 273.

Matthews, J.W. and A.E. Blakeslee, J. Cryst. Growth 32 (1976) 265.

Mazuruk, K.M. Benzaquen, D. Walsh, B. Makuc, H. Jayatirtha and H. Aharoni, Can. J. Phys. 67 (1988) 339.

McCaldin, J.O., T.C. McGill and C.A. Mead, Phys. Rev. Lett. 36 (1976) 56.

McCaldin, J.O. and T.C. McGill, Appl. Phys. Lett. 61 (1992) 2243.

McKinley, J.T., Y. Hwu, D. Rioux, A. Terrasi, F. Zanini, G. Margaritondo, U. Debska and J.K. Furdyna, J. Vac. Sci. Technol. A 8 (1990) 1917.

McKinley, J.T., Y. Hwu, B.E.C. Koltenbah, G. Margaritondo, S. Baroni and R. Resta, J. Vac. Sci. Technol. A 9 (1991) 917.

McKinley, J.T., Y. Hwu, B.E.C. Koltenbah, G. Margaritondo, S. Baroni and R. Resta, Appl. Surf. Sci. 56–58 (1992) 762.

McKinley, J.T., R.G. Albridge, A.V. Barnes, A. Ueda, N.H. Tolk, C. Coluzza, F. Gozzo, G. Margaritondo, D. Martin, F. Morier-Genoud, C. Dupuy, A. Rudra and M. Ilegems, J. Vac. Sci. Technol. B 11 (1993) 1614.

McLean, A.B., I.T. McGovern, C. Stephens, W. Wilke, H. Haak, K. Horn and W. Braun, Phys. Rev. B 38 (1988) 6330.

Meng, Y., M.M. Nelson, J. Anderson and G.J. Lapeyre, J. Vac. Sci. Technol. A 8 (1990) 2667.

Mensz, P.M., S. Herko, K.W. Haberern, J. Gaines and C. Ponzoni, Appl. Phys. Lett. 63 (1993) 2800.

Miles, R.H., J.O. McCaldin and T.C. McGill, J. Cryst. Growth 85 (1987) 188.

Milnes, A.G. and D.L. Feucht, Heterojunctions and Metal–Semiconductor Junctions (Academic Press, New York, 1972).

Mönch, W., R.S. Bauer, H. Gant and R. Murschall, J. Vac. Sci. Technol. 21 (1982) 498.

Moore, K.J., P. Dawson and C.T. Foxon, J. Phys. Colloq. (Paris) 48 (1987) 525.

Morar, J.F. and M. Wittmer, Phys. Rev. B 37 (1988) 2618.

Morar, J.F. and P.E. Batson, J. Vac. Sci. Technol. B 10 (1992) 2022.

Morar, J.F., P.E. Batson and J. Tersoff, Phys. Rev. B 47 (1993) 4107.

Morris, I.L., R.H. Williams, J.I. Davies and G.J. Clarke, Appl. Phys. Lett. 62 (1993) 291.

Mujica, A., R. Perez, F. Flores and A. Muñoz, Phys. Rev. B 46 (1992) 9641.

Müller, G., A. Zrenner, F. Koch and K. Ploog, Appl. Phys. Lett. 55 (1989) 1564.

Muñoz, A., J.C. Duran and F. Flores, Surf. Sci. 181 (1987) L200.

Muñoz, A., R. Perez, J.C. Duran and F. Flores, Surf. Sci. 211/212 (1989) 503.

Muñoz, A., N. Chetty and R.M. Martin, Phys. Rev. B 41 (1990) 2976.

Muñoz, A. and P. Rodriguez-Hernandez, Phys. Rev. B 45 (1992) 4502.

Nakayama, N., S. Itoh, H. Okuyama, M. Ozawa, T. Ohata, K. Nakano, M. Ikeda, A. Ishibashi and Y. Mori, Electron. Lett. 29 (1993) 2194.

Neave, J.H., P.K. Larsen, B.A. Joyce, J.P. Growers and J.F. van der Veen, J. Vac. Sci. Technol. B 1 (1983) 668.

Ni, W.-X., J. Knall and G.V. Hansson, Phys. Rev. B 36 (1987) 7744.

Nicolini, R., L. Vanzetti, Guido Mula, G. Bratina, L. Sorba, A. Franciosi, M. Peressi, S. Baroni, R. Resta, A. Baldereschi, J.E. Angelo and W.W. Gerberich, Phys. Rev. Lett. 72 (1994) 294.

Niedermann, P., L. Quattropani, K. Solt, I. Maggio-Aprile and O. Fischer, Phys. Rev. B 48 (1993) 8833.

Niles, D.W., E. Colavita, G. Margaritondo, P. Perfetti, C. Quaresima and M. Capozi, Appl. Phys. Lett. 47 (1985) 1092.

Niles, D.W., E. Colavita, G. Margaritondo, P. Perfetti, C. Quaresima and M. Capozi, J. Vac. Sci. Technol. A 4 (1986) 962.

Niles, D.W., M. Tang, J. McKinley, R. Zanoni and G. Margaritondo, Phys. Rev. B 38 (1988) 10949.

Niles, D.W., M. Tang, J. McKinley, R. Zanoni and G. Margaritondo, J. Vac. Sci. Technol. A 7 (1989) 2464.

Niles, D.W. and H. Höchst, Phys. Rev. B 44 (1992) 10965.

Nitz, H.M., O. Granschow, V. Kaiser, L. Wiedmann and A. Benninghoven, Surf. Sci. 104 (1981) 365.

Northern, J.E., R.D. Bringans, R.I.G. Uhrberg, M.A. Olmstead and R.Z. Bachrach, Phys. Rev. Lett. 61 (1988) 2957.

Ohata, K., H. Hida and H. Miyamoto, IEEE Int. MTT-S Microwave Symp. Dig. (1984) 434.

Okuyama, H., Y. Kishita, T. Miyajima, A. Ishibashi and K. Akimoto, Appl. Phys. Lett. 64 (1994) 904.
Olego, D.J., J.P. Faurie and P.M. Raccah, Phys. Rev. Lett. 55 (1985) 328.
Olego, D.J. and J.P. Faurie, Phys. Rev. B 33 (1986) 7357.
Olego, D.J., Phys. Rev. B 39 (1989) 12743.
Okuyama, H., K. Nakano, T. Miyajima and K. Akimoto, J. Cryst. Growth 117 (1992) 139.
Orlowski, B., W.E. Spicer and A.D. Baer, AIP Conf. Proc. 20 (1974) 241.
Osbourn, G.C., J. Appl. Phys. 53 (1982) 1586.
Otsuka, N., Y.E. Ihm, K.A. Harris, J.W. Cook and J.F. Schetzina, J. Vac. Sci. Technol. A 5 (1987) 3129.
Ourmazd, A., D.W. Taylor, J. Cunningham and C.W. Tu, Phys. Rev. Lett. 62 (1989) 933.
Palm, H., M. Arbes and M. Schulz, Phys. Rev. Lett. 71 (1993) 2224.
Palmstrøm, C.J., Annu. Rev. Mater. Sci. 25 (1995) 389, and private communication.
Park, Y.S. and B.K. Shin, in: Topics in Applied Physics, Vol. 17 (Springer, Berlin, 1977) p. 133.
People, R., Phys. Rev. B 34 (1986) 2508.
People, R. and J.C. Bean, Appl. Phys. Lett. 48 (1986) 538.
Peressi, M., S. Baroni, A. Baldereschi and R. Resta, Phys. Rev. B 41 (1990) 12106.
Peressi, M., S. Baroni, R. Resta and A. Baldereschi, Phys. Rev. B 43 (1991) 7347. Note that the authors have used theoretical (calculated) values of the dielectric constant in their predictions.
Peressi, M., L. Colombo, A. Baldereschi, R. Resta and S. Baroni, Phys. Rev. B 48 (1993) 12047.
Perez, J.M., R.J. Wagner, J.R. Meyer, J.W. Han, J.W. Cook and J.F. Schetzina, Phys. Rev. Lett. 61 (1988) 2261.
Perez, R., A. Muñoz and F. Flores, Surf. Sci. 226 (1990) 371.
Perfetti, P., D. Denley, K.A. Mills and D.A. Shirley, Appl. Phys. Lett. 33 (1978) 667.
Perfetti, P., C. Quaresima, C. Coluzza, C. Fortunato and G. Margaritondo, Phys. Rev. Lett. 57 (1986) 2065.
Perfetti, P., Surf. Sci. 189/190 (1987) 362.
Petruzzello, J., J. Gaines, P. van der Sluis, D. Olego and C. Ponzoni, Appl. Phys. Lett. 62 (1993) 1496.
Petruzzello, J., J. Gaines and P. van der Sluis, J. Appl. Phys. 75 (1994) 63.
Pinczuk, A., J. Phys. Colloq. (Paris) C 5 (1984) 477.
Pollak, F.H. and M. Cardona, Phys. Rev. 172 (1968) 816.
Pollmann, J. and S.T. Pantelides, Phys. Rev. B 21 (1980) 709.
Priddy, K.L., D.R. Kitchen, J.A. Grzyb, C.W. Litton, T.S. Henderson, C.-K. Peng, W.F. Kopp and H. Morkoç, IEEE Trans. Electron Devices ED-34 (1987) 175.
Qian, Q.-D., J. Qiu, M. Kobayashi, R.L. Gunshor, M.R. Melloch and J.A. Cooper, Jr., J. Vac. Sci. Technol. B 7 (1989) 793.
Qiu, J., Q.-D. Quian, R.L. Gunshor, M. Kobayashi, D.R. Menke, D. Li and N. Otsuka, Appl. Phys. Lett. 56 (1990) 1272.
Qiu, J., D.R. Menke, M. Kobayashi, R.L. Gunshor, Q.-D. Quian, D. Li and N. Otsuka, J. Cryst. Growth 111 (1991) 747 (a).
Qiu, J., J.M. DePuydt, H. Cheng and M.A. Haase, Appl. Phys. Lett. 59 (1991) 2992 (b).
Qteish, A. and R.J. Needs, Phys. Rev. B 43 (1991) 4229.
Raisanen, A., S. Chang, P. Philip, N. Troullier, A. Franciosi and D.J. Peterman, J. Vac. Sci. Technol. A 6 (1988) 2741.
Raisanen, A., G. Haugstad, X. Yu and A. Franciosi, J. Appl. Phys. 70 (1991) 3115, and references therein.
Raisanen, A., L.J. Brillson, A. Franciosi, R. Nicolini, L. Vanzetti and L. Sorba, J. Electron. Mater. 24 (1995) 163 (a).
Raisanen, A., L.J. Brillson, L. Vanzetti, L. Sorba and A. Franciosi, J. Vac. Sci. Technol. A 13 (1995) 690 (b).
Raisanen, A., L.J. Brillson, L. Vanzetti, L. Sorba and A. Franciosi, Appl. Phys. Lett. 66 (1995) 3301 (c).
Ramsteiner, M., J. Wagner, H. Ennen and M. Maier, Phys. Rev. B 38 (1988) 10669.
Ray-Chaudhuri, A.K., W. Ng, S. Liang, S. Singh, J.T. Welnak, J.P. Wallace, C. Capasso, F. Cerrina, G. Margaritondo, J.H. Underwood, J. Kortright and R. Perera, J. Vac. Sci. Technol. A 11 (1993) 2324.
Reno, J. and J.P. Faurie, Appl. Phys. Lett. 49 (1986) 409.
Reno, J., I.K. Sou, J.P. Faurie, J.M. Berroir, Y. Guldner and J.P. Vieren, Appl. Phys. Lett. 49 (1986) 106.
Reno, J., I.K. Sou, J.P. Fauire, J.M. Berroir and Y. Guldner, J. Vac. Sci. Technol. A 5 (1987) 3107.
Resta, R., L. Colombo and S. Baroni, Phys. Rev. B 41 (1990) 12358.
Resta, R., L. Colombo and S. Baroni, Phys. Rev. B 43 (1991) 14273.
Ribbing, C.G., D.T. Pierce and W.E. Spicer, Phys. Rev. B 4 (1971) 4417.
Rioux, D. and H. Höchst, Phys. Rev. B 47 (1993) 1434.
Ripamonti, G., F. Capasso, A.L. Hutchinson, D.J. Meuhlner, J.F. Walker and R.J. Malik, Nucl. Instr. Meth. A 288 (1990) 99.

Rodriguez-Hernandez, P. and A. Muñoz, Physica B 185 (1993) 546.

Russo, B., C. Quaresima, M. Capozi, E. Paparazzo, P. Perfetti, G. Margaritondo, and C. Coluzza, in: Proc. 14th Int. Symp. on GaAs and Related Compounds (IOP, Bristol, 1988) p. 593.

Saito, T. and T. Ikoma, Superlatt. Microstruct. 12 (1992) 81.

Saito, T., Y. Hashimoto and T. Ikoma, Solid State Electron. 37 (1994) 743.

Saito, T., Y. Hashimoto and T. Ikoma, Phys. Rev. B 50 (1994) 17242.

Sambell, A.J. and J. Wood, IEEE Trans. Electron Devices ED-37 (1990) 88.

Sanderson, R.T., Inorganic Chemistry (Reinhold, New York, 1967).

Sanderson, R.T., Chemical Bonds and Bond Energy (Academic, New York, 1971).

Sands, T., C.J. Palmstrøm, J.P. Harbison, V.G. Keramidas, N. Tabatabaie, T.L. Cheeks, R. Ramesh and Y. Silberberg, Mater. Sci. Rep. 5 (1990) 99.

Satpathy, S. and R.M. Martin, Phys. Rev. B 39 (1989) 8494.

Scamarcio, G., V. Spagnolo, E. Molinari, L. Tapfer, L. Sorba, G. Bratina and A. Franciosi, Phys. Rev. B 46 (1992) 7296 (a).

Scamarcio, G., V. Spagnolo, E. Molinari, L. Tapfer, L. Sorba, G. Bratina and A. Franciosi, Superlatt. Microstruct. 12 (1992) 429 (b).

Schmiedeskamp, B., private communication (1993).

Schuermeyer, F.L., P. Cook, E. Martinez and J. Tantillo, Appl. Phys. Lett. 55 (1989) 1877.

Schulman, J.N. and T.C. McGill, Appl. Phys. Lett. 34 (1979) 663.

Schulman, J.N. and Y.-C. Chang, Phys. Rev. B 33 (1986) 2594.

Schwartz, G.P., M.S. Hybertsen, J. Bevk, R.G. Nuzzo, J.P. Mannaerts and G.J. Gualtieri, Phys. Rev. B 39 (1989) 1235.

Shahzad, K., D.J. Olego and C.G. Van de Walle, Phys. Rev. B 38 (1988) 1417.

Shannon, J., Solid-State Electron. 19 (1976) 537.

Sharan, S. and J. Narayan, J. Appl. Phys. 66 (1989) 2376.

Shay, J.L., S. Wagner and J.C. Phillips, Appl. Phys. Lett. 28 (1976) 31.

Shen, T.-H., M. Elliott, R.H. Williams and D. Westwood, Appl. Phys. Lett. 58 (1991) 842 (a).

Shen, T.-H., M. Elliott, A.E. Fowell, A. Cafolla, B.E. Richardson, D. Westwood and R.H. Williams, J. Vac. Sci. Technol. B 9 (1991) 2219 (b).

Shen, T.-H. and C.C. Matthai, Appl. Surf. Sci. 56–58 (1992) 746.

Shen, T.-H., A.C. Ford, M. Elliott, R.H. Williams, D.I. Westwood, D.A. Woolf, J.P. Marlow, J.E. Aubrey and G. Hill, J. Vac. Sci. Technol. 10 (1992) 1757 (a).

Shen, T.-H., M. Elliott, R.H. Williams, D.A. Woolf, D.I. Westwood and A.C. Ford, Appl. Surf. Sci. 56–58 (1992) 749 (b).

Shevchik, N.J., AIP Conf. Proc. 20 (1974) 72, and references therein.

Shibli, S.M., M.C. Tamargo, B.J. Skromme, S.A. Schwartz, R.E. Nahory and R.J. Martin, J. Vac. Sci. Technol. B 8 (1990) 187.

Shih, C.K. and W.E. Spicer, Phys. Rev. Lett. 58 (1987) 2594.

Shihong, X., L. Xianming, M. Maosheng, Z. Jingsheng, Z. Yuheng, X. Pengshou, and X. Zhenjia, Mod. Phys. Lett. B 7 (1993) 459.

Simon, A., D. Bertho, D. Boiron and C. Jouanin, Phys. Rev. B 42 (1990) 5221.

Smith, D.L. and C. Mailhiot, Phys. Rev. Lett. 58 (1987) 1264.

Sobiesierski, Z., D.A. Woolf, D.I. Westwood and R.H. Williams, Appl. Phys. Lett. 58 (1991) 628.

Sorba, L., G. Bratina, G. Ceccone, A. Antonini, J.F. Walker, M. Micovic and A. Franciosi, Phys. Rev. B 43 (1991) 2450.

Sorba, L., G. Bratina, A. Antonini, A. Franciosi, L. Tapfer, A. Migliori and P. Merli, Phys. Rev. B 46 (1992) 6834 (a).

Sorba, L., G. Bratina, A. Franciosi, L. Tapfer, G. Scamarcio, V. Spagnolo and E. Molinari, Appl. Phys. Lett. 61 (1992) 1570 (b).

Sorba, L., G. Bratina, A. Franciosi, L. Tapfer, G. Scamarcio, V. Spagnolo, A. Migliori, P. Merli and E. Molinari, J. Cryst. Growth 127 (1993) 121 (a).

Sorba, L., G. Biasiol, G. Bratina, R. Nicolini and A. Franciosi, J. Cryst. Growth 127 (1993) 93 (b).

Spicer, W.E., J.A. Silberman, I. Lindau, A.-B. Chen, A. Sher and J.A. Wilson, J. Vac. Sci. Technol. A 1 (1983) 1735.

Spicer, W.E., D.J. Friedman and G.P. Carey, J. Vac. Sci. Technol. A 6 (1988) 2746.

Spindt, C.J., R. Cao, K.E. Miyano, I. Lindau, W.E. Spicer and Y.-C. Pao, J. Vac. Sci. Technol. B 8 (1990) 974.

Sporken, R., S. Sivananthan, J.P. Faurie, J.J. Pireaux and R. Caudano, J. Vac. Sci. Technol. A 7 (1989) 427.

Stampfl, A., X.D. Zhang, G. Kemister, R.C.G. Leckey, J.D. Riley, B. Usher, P.T. Orders, R. Denecke, J. Faul and L. Ley, Phys. Rev. B 45 (1992) 4181.

Stephens, C., D.R.T. Zahn, K. Fives, R. Cimino, W. Braun and I.T McGovern, J. Vac. Sci. Technol. B 8 (1990) 674.
Stolz, W., F.E.G. Guimares and K. Ploog, J. Appl. Phys. 63 (1988) 492.
Störmer, H.L., R. Dingle, A.C. Gossard, W. Wiegmann and M.D. Sturge, Solid State Commun. 29 (1979) 705.
Strite, S., M.S. Ünlü, K. Adomi, G.-B. Gao and H. Morkoç, IEEE Electron Device Lett. EDL-11 (1990) 233 (a).
Strite, S., M.S. Ünlü, K. Adomi, G.-B. Gao, A. Agarwal, A. Rockett, H. Morkoç, D. Li, Y. Nakamura and N. Otsuka, J. Vac. Sci. Technol. B 8 (1990) 1131 (b).
Strite, S., M.S. Ünlü, K. Adomi and H. Morkoç, Appl. Phys. Lett. 56 (1990) 1673 (c).
Sudersena Rao, T., Y. Horikoshi, C. Jagadish, R.G. Elliman and J.S. Williams, Jpn. J. Appl. Phys. 31 (1992) 3282.
Sze, S.M., Physics of Semiconductor Devices (Wiley, New York, 1981).
Talwar, D.N. and M. Vandevyver, Phys. Rev. B 40 (1989) 9779.
Tamargo, M.C., J.L. de Miguel, D.M. Hwang and H.H. Farrell, J. Vac. Sci. Technol. B 6 (1988) 784.
Tapfer, L., M. Ospelt and H. von Känel, J. Appl. Phys. 67 (1990) 1298.
Tapfer, L. and K. Ploog, Phys. Rev. B 33 (1986) 5565.
Tapfer, L. and K. Ploog, Phys. Rev. B 40 (1989) 9802.
Tapfer, L., Phys. Scri. T 25 (1989) 45.
Tapfer, L., G.E. Crook, O. Brandt and K. Ploog, Appl. Surf. Sci. 56–58 (1992) 597.
Tejedor, C., F. Flores and E. Louis, J. Phys. C 10 (1977) 2163.
Tersoff, J., Surf. Sci. 168 (1984) 275 (a).
Tersoff, J., Phys. Rev. Lett. 52 (1984) 465 (b).
Tersoff, J., Phys. Rev. B 30 (1984) 4874 (c).
Tersoff, J., in: Heterojunction Band Discontinuities: Physics and Device Applications, Eds. F. Capasso and G. Margaritondo (North-Holland, Amsterdam, 1987) p. 1.
Tersoff, J. and C.G. Van de Walle, Phys. Rev. Lett. 59 (1987) 946.
Tersoff, J., private communication (1993).
Thorne, R., S. Su, R. Fischer, W. Kopp, W. Lyons, P. Miller and H. Morkoç, IEEE Trans. Electron Devices ED-30 (1983) 212.
Tit, N., M. Peressi and S. Baroni, Phys. Rev. B 48 (1993) 17607.
Tiwari, S., S.L. Wright and J. Batey, IEEE Electron Device Lett. EDL-9 (1988) 488.
Tiwari, S. and D.J. Frank, Appl. Phys. Lett. 60 (1992) 630 (a).
Tiwari, S. and D.J. Frank, Appl. Phys. Lett. 61 (1992) 2244 (b).
Tran, T.T. and S.A. Chambers, J. Vac. Sci. Technol. B 11 (1993) 1459 (a).
Tran, T.T. and S.A. Chambers, Phys. Rev. B 47 (1993) 13023 (b).
Ukita, M., H. Okuyama, M. Ozawa, A. Ishibashi, K. Akimoto and Y. Mori, Appl. Phys. Lett. 63 (1993) 2082.
Ünlü, M.S., S. Strite, G.B. Gao, K. Adomi and H. Morkoç, Appl. Phys. Lett. 56 (1990) 842.
Van der Merwe, J.H., J. Appl. Phys. 34 (1963) 123.
Van der Merwe, J.H. and N.G. Van der Berg, Surf. Sci. 32 (1972) 1.
Van der Ziel, J.P., N. Chand and J.S. Weiner, J. Appl. Phys. 66 (1989) 1195.
Van de Walle, C.G. and R.M. Martin, J. Vac. Sci. Technol. B 4 (1986) 1055 (a).
Van de Walle, C.G. and R.M. Martin, Phys. Rev. B 34 (1986) 5621 (b).
Van de Walle, C.G. and R.M. Martin, Phys. Rev. B 35 (1987) 8154.
Van de Walle, C.G. and R.M. Martin, Phys. Rev. B 37 (1988) 4801.
Van de Walle, C.G., Phys. Rev. B 39 (1989) 1871.
Van de Walle, C.G. and R.M. Martin, Phys. Rev. Lett. 62 (1989) 2028.
Van Vechten, J.A., J. Vac. Sci. Technol. B 3 (1985) 1240.
Vanzetti, L., X. Yu, A. Raisanen, L. Sorba, G. Haugstad, G. Bratina and A. Franciosi, J. Cryst. Growth 117 (1992) 573.
Vanzetti, L., A. Bonanni, L. Sorba, A. Franciosi, M. Lomascolo, D. Greco and R. Cingolani, in: Proc. 22th Int. Conf. on the Physics of Semiconductors, Ed. D.J. Lockwood (World Scientific, Singapore, 1995) p. 767.
von Ortenberg, M., Phys. Rev. Lett. 49 (1982) 1041.
Wagner, S., J.L. Shay, K.J. Bachmann and E. Bueheler, Appl. Phys. Lett. 26 (1975) 229.
Wagner, R.J., J.M. Perez, J.R. Meyer, J.W. Han, J.W. Cook, Jr. and J.F. Schetzina, J. Vac. Sci. Technol. A 7 (1989) 411.
Waldrop, J.R. and R.W. Grant, Phys. Rev. Lett. 43 (1979) 1686.

Waldrop, J.R., E.A. Kraut, S.P. Kowalczyk and R.W. Grant, Surf. Sci. 132 (1983) 513.

Waldrop, J.R., R.W. Grant, S.P. Kowalczyk and E.A. Kraut, J. Vac. Sci. Technol. A 3 (1985) 835.

Waldrop, J.R., R.W. Grant and E.A. Kraut, J. Vac. Sci. Technol. B 5 (1987) 1209.

Waldrop, J.R., R.W. Grant and E.A. Kraut, J. Vac. Sci. Technol. B 7 (1989) 815.

Waldrop, J.R., E.A. Kraut, C.W. Farley and R.W. Grant, J. Vac. Sci. Technol. B 8 (1990) 768.

Waldrop, J.R., G.J. Sullivan, R.W. Grant, E.A. Kraut and W.A. Harrison, J. Vac. Sci. Technol. B 10 (1992) 1773.

Wall, A., A. Raisanen, S. Chang, P. Philip, N. Troullier, A. Franciosi and D.J. Peterman, J. Vac. Sci. Technol. A 5 (1987) 3193.

Wall, A., Y. Gao, A. Raisanen, A. Franciosi and J.R. Chelikowsky, Phys. Rev. B 43 (1991) 4988.

Wang, W.I., E.E. Mendez and F. Stern, Appl. Phys. Lett. 45 (1985) 639.

Wang, M.W., J.O. McCaldin, J.F. Swenberg and T.C. McGill, Appl. Phys. Lett. 66 (1995) 1974.

Watkins, G.D., in: Defect Control in Semiconductors: Proceedings of International Conference on Science and Technology of Defect Control in Semiconductors, Ed. K. Sumino (North-Holland, Amsterdam, 1990).

Wearie, D. and E. O'Reilly, in: Noncrystalline Semiconductors, Vol. I, Ed. M. Pollak (CRC Press, Boca Raton, FL, 1987) p. 1.

Weber, J. and M.I. Alonso, Phys. Rev. B 40 (1989) 5683.

Wei, S. and A. Zunger, Phys. Rev. Lett. 59 (1987) 144.

Weinberg, Z.A. and A. Harstein, J. Appl. Phys. 54 (1983) 2517.

Wilke, W.G. and K. Horn, J. Vac. Sci. Technol. B 6 (1988) 1211.

Wilke, W.G., R. Seedorf and K. Horn, J. Vac. Sci. Technol. B 7 (1989) 807.

Wilke, W.G., R. Seedorf and K. Horn, J. Cryst. Growth 101 (1990) 620 (a).

Wilke, W.G., Ch. Maierhofer and K. Horn, J. Vac. Sci. Technol. B 8 (1990) 760 (b).

Wilks, S.P. and R.H. Williams, J. Electron Spectrosc. Rel. Phen. 72 (1995) 49.

Williams, R., Phys. Rev. 140 (1965) A 569.

Williams, R. and M.H. Woods, J. Appl. Phys. 43 (1972) 4142.

Williams, M.D. and T.H. Chiu, J. Vac. Sci. Technol. B 8 (1990) 758.

Wilson, B.A., IEEE J. Quantum Electron. QE-24 (1988) 1763.

Wolford, D.J., T.F. Kuech, J.A. Bradley, M.A. Gell, D. Ninno and M. Jaros, J. Vac. Sci. Technol. B 4 (1986) 1043.

Wolford, D.J., T.F. Kuech and M. Jaros, in: Heterojunction Band Discontinuities: Physics and Device Applications, Eds. F. Capasso and G. Margaritondo (North-Holland, Amsterdam, 1987) ch. 6.

Wolford, D.J., in: Proc. 18th Int. on the Physics of Semiconductors, Ed. O. Engstrom (World Scientific, Singapore, 1987) p. 1115.

Woodall, J.M., R.T. Hodgson and R.L. Gunshor, Appl. Phys. Lett. 58 (1991) 379.

Wright, A.C. and J.O. Williams, J. Cryst. Growth 114 (1991) 99.

Wu, G.Y., D.L. Smith, C. Mailhiot and T.C. McGill, Appl. Phys. Lett. 49 (1986) 1551.

Xing, Y.R., R.W. Devenish, T.B.F. Joyce, C.J. Kiely, T.J. Bullough and P.J. Goodhew, Appl. Phys. Lett. 60 (1992) 616.

Xu, F., M. Vos, J.P. Sullivan, Lj. Atanasoska, S.G. Anderson, J.H. Weaver and H. Cheng, Phys. Rev. B 39 (1988) 7831.

Yang, Z., K.A. Bowers, J. Ren, Y. Lansari, J.W. Cook, Jr. and J.F. Schetzina, Appl. Phys. Lett. 62 (1992) 2671.

Yu, E.T., D.H. Chow and T.C. McGill, Phys. Rev. B 38 (1988) 12764.

Yu, E.T., D.H. Chow and T.C. McGill, J. Vac. Sci. Technol. B 7 (1989) 391.

Yu, E.T., E.T. Croke, D.H. Chow, D.A. Collins, M.C. Phillips, T.C. McGill, J.O. McCaldin and R.H. Miles, J. Vac. Sci. Technol. B 8 (1990) 908.

Yu, E.T., J.O. McCaldin and T.C. McGill, Solid State Phys. 46 (1992) 1 (a).

Yu, E.T., M.C. Phillips, D.H. Chow, D.A. Collins, M.W. Wang, J.O. McCaldin and T.C. McGill, Phys. Rev. B 46 (1992) 13379 (b).

Yu, X., PhD Thesis, University of Minnesota (1992).

Yu, X., A. Raisanen, G. Haugstad, N. Troullier and A. Franciosi, Phys. Rev. B 48 (1993) 4545.

Zahn, D.R.T., W. Richter, A.B. McLean, R.H. Williams, C. Stephens, I.T. McGovern, R. Cimino, W. Braun and N. Esser, Appl. Surf. Sci. 41/42 (1989) 179.

Zahn, D.R.T., Ch. Maierhofer, A. Winter, M. Reckzügel, R. Srama, A. Thomas, K. Horn and W. Richter, J. Vac. Sci. Technol. B 9 (1991) 2206.

Zanio, K. and T. Massopust, J. Electron. Mater. 15 (1986) 103.

Zanio, K., J. Vac. Sci. Technol. A 4 (1986) 2106.
Zhang, S.B., M.L. Cohen, S.G. Louie, D. Tomanek and M.S. Hybertsen, Phys. Rev. B 41 (1990) 10058.
Zhu, J.G. and C.B. Carter, Phil. Mag. A 62 (1990) 319, and references therein.
Zhu, X. and S.G. Louie, Phys. Rev. B 43 (1991) 14142.
Zou, J., Z. Abid, H. Dong and A. Gopinath, Appl. Phys. Lett. 58 (1991) 2411.
Zurcher, P. and R.S. Bauer, J. Vac. Sci. Technol. A 1 (1983) 695.